ABSTRACT

Title of Dissertation: EXPERIMENTAL AND THEORETICAL INVESTIGATION OF INTEGRATED ENGINE GENERATOR – LIQUID DESICCANT SYSTEM

Sandeep M. Nayak, Doctor of Philosophy, 2005

Directed By: Professor Reinhard Radermacher, Ph.D.
Department of Mechanical Engineering

Combined heat and power (CHP) involves on-site generation of electricity by using gas-fired equipment along with utilization of waste heat available from the power generation process. This research focuses on the design, installation and analysis of integration options of a modular CHP system involving the integration of a natural gas fired reciprocating engine generator with a liquid desiccant dehumidification system in a medium sized commercial office building. The engine generator provides 75 kW of electrical power fed parallel to the grid while the combined waste heat from the exhaust gases and jacket water from the engine is used to regenerate the liquid desiccant. The liquid desiccant unit dehumidifies the outdoor air and supplies it to the mixed air section of the roof top unit of the building. The experimental part of the research discusses the various aspects involved in the design and installation of the system such as the mechanical design of the structure, the heat

recovery loop design and the electrical interconnection with the grid. Extensive testing and data analysis was conducted to characterize the performance of the integrated system and compare the performance with a traditional power plant as well as conventional HVAC systems.

A comprehensive steady state thermodynamic model of the integrated CHP system was coded in Visual Basic .Net. After validation with experimental results, an economic and climate model was integrated into the thermodynamic model with actual electricity and gas prices as well as the climate data for different representative states in the United States to demonstrate the feasibility of the system under different scenarios. This research addresses and assesses the different integration opportunities and issues encountered during the integration of the engine generator – liquid desiccant system with the existing electrical grid and the roof top unit. Based on the hands-on experience gained during the design, installation, operation and maintenance of the integrated system as well as the results obtained from extensive simulation of the system, this research develops valuable design guidelines on the integration and operation of the packaged engine generator-liquid desiccant system in commercial office buildings for future designers and system integrators.

EXPERIMENTAL AND THEORETICAL INVESTIGATION OF INTEGRATED ENGINE GENERATOR – LIQUID DESICCANT SYSTEM

By

Sandeep M. Nayak

Dissertation submitted to the Faculty of the Graduate School of the
University of Maryland, College Park, in partial fulfillment
of the requirements for the degree of
Doctor of Philosophy
2005

Advisory Committee:
Professor Reinhard Radermacher, Chair/Advisor
Professor Avram Bar-Cohen
Associate Professor Tien-Mo Shih
Assistant Professor Bao Yang
Professor Henry King

Dedication

This dissertation is lovingly dedicated to my parents for their endless love and support that made this work possible

Acknowledgements

My thanks and sincere appreciation goes to Dr. Radermacher for giving me the opportunity to study and conduct research at University of Maryland and helping me, realize my goals. Without his encouragement, wisdom and advice this work would not have been complete. I would also like to thank Dennis Moran and Vikrant Aute for their guidance at crucial moments throughout the research process.

Special thanks go to all my colleagues at CEEE, both past and present – Aris Marantan, Matt Cowie, Hans Huff, Layla Monajemi, Lorenzo Cremaschi, Amr Gado, Jun Pyo-Lee, Eric Xuan, Lucia Liao and Anna Bahn for their continuous cooperation and friendship. It was a pleasure working with each and every one of you.

Finally I would like to express my deepest gratitude to my parents, my brother and my sister whose encouragement, devotion and love always motivated me to do my best and without whom this research would not have seen the light of this day.

Table of Contents

List of Tables

List of Figures

Nomenclature

Abbreviations

ARES	Advanced Reciprocating Engine System
ASHRAE	American Society of Heating, Refrigeration and Air-Conditioning Engineers
ATS	Auto Transfer Switch
BCHP	Building Cooling, Heating and Power
CC	Combined Cycle
CHP	Combined Heating and Power
COP	Coefficient of Performance
CT	Current Transducer
DAS	Data Acquisition System
DSS	Dynamic Search Strategy
DX	Direct Expansion
EIA	Energy Information Administration
EES	Engineering Equation Solver
EX	Exhaust Gas
GHV	Gross Heating Value
HHV	Higher Heating Value
HP VEE	Hewlett Packard Visual Engineering Environment
HRL	Heat Recovery Loop
HV	High Voltage

HVAC	Heating, Ventilation and Air-Conditioning
HX	Heat Exchanger
IAQ	Indoor Air Quality
IEEE	Institution of Electronic and Electrical Engineers
IES	Integrated Energy Systems
JW	Jacket Water
LDU	Liquid Desiccant Unit
LHV	Lower Heating Value
LV	Low Voltage
MILP	Mixed Integer Linear Programming
NG	Natural Gas
PEC	Primary Energy Consumption
PT	Power Transducer
RH	Relative Humidity
RPM	Revolutions Per Minute
ROI	Return On Investment
RTU	Roof Top Unit
SHF	Sensible Heat Factor
SI	Spark Ignition
SOC	Systems Operations Center
TMY	Typical Meteorological Year
UPS	Uninterrupted Power Supply
US DOE	United States Department Of Energy

UV	Under Voltage
VAV	Variable Air Volume
VB	Visual Basic

Symbols

C_p	Specific Heat at Constant Pressure
C_v	Specific Heat at Constant Volume
F	Function
h	Enthalpy
L_v	Latent Heat of Evaporation
m	Mass
P	Pressure
Q	Heat Exchange Capacity
T	Temperature
u	Internal Energy
V	Volume
w	Humidity Ratio
x	Lithium Chloride Salt Concentration
η	Efficiency

Subscripts

a	Air
c	Conditioner

elec	Electrical
eng	Engine
f	Fuel
glycol	50:50 Ethylene Glycol-Water Solution
grid	Electrical Grid
in	Inlet
ip	Input
lat	Latent
n	Number of Variables
oa	Outdoor Air
op	Operational
out	Outlet
pa	Process Air
r	Regenerator
rem	Removal
ret	Return
s	Lithium Chloride-Water Solution
sat	Saturation
sen	Sensible
sup	Supply
vent	Ventilation
w	Water
wh	Waste Heat

Units

A	Amps
Btu	British Thermal Unit
C	Celsius
cfm	Cubic Feet Per Minute
F	Fahrenheit
ft	Feet
hr	Hour
Hz	Hertz
kW	Kilowatt
kWh	Kilowatt-hour
lb	Pound
MW	Megawatt
psia	Pounds Per Square Inch Absolute
psig	Pounds Per Square Inch Gauge
V	Volts
$	Dollars

Chapter 1: Introduction

1.1 CHP – The Basic Concept

Combined heat and power, or CHP, refers to generating electricity at or near the place where it is used. The waste heat from the electricity generation can be used for space heating, water heating, process steam for industrial steam loads, humidity control, air conditioning, water cooling, product drying, or for nearly any other thermal energy need. Higher overall system efficiencies can be achieved with CHP systems as compared to conventional power plants because of the utilization of thermal energy, that would otherwise be wasted, and the reduction of transmission, distribution and energy conversion losses.

CHP has several acronyms and is sometimes referred by other related terms such as cogeneration, Building Cooling, Heating, and Power (BCHP), Integrated Energy Systems (IES), trigeneration etc in the literature. Though most of the CHP systems typically run on natural gas, recent developments have made it possible to use methane which is also known as biogas produced from landfills, wastewater treatment plants, concentrated livestock operations, food and beverage processing waste, wood, or other organic products, making CHP a renewable energy resource. They can also run on traditional fuels such as propane, diesel, or most other liquid or gaseous fossil fuels.

Some of the prime movers used by CHP systems to generate electricity are reciprocating engines, micro turbines, combustion turbines, and fuel cells. There are many possible uses for the waste heat depending upon the application, geographic location and the energy cost structures of both fuel and grid electricity. Possible waste heat technologies include absorption chillers, humidifiers, desiccant dehumidifiers, steam generators, hot water heating, space heating and thermal storage.

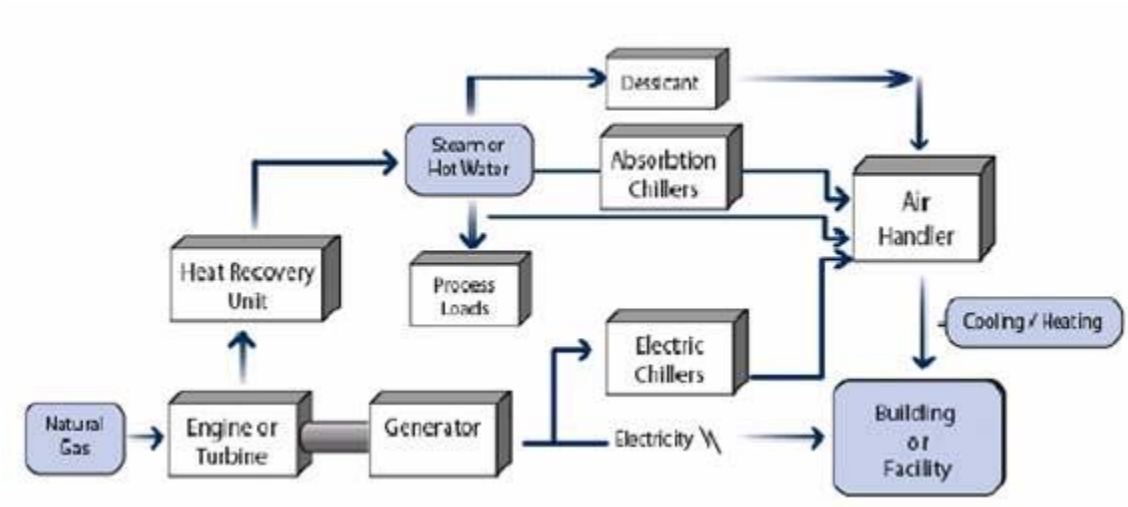

Figure 1: Typical Layout of a CHP System

Figure 1 shows the schematic of a typical CHP system that can be integrated for a building or any facility. Here, the fuel shown is natural gas which is combusted in a reciprocating engine generator or a turbine to generate electricity. This electricity is fed to the main grid of the building or a facility or can be used to take care of a certain part of the load such as the electric chillers. The waste heat from the prime mover is recovered and used to generate hot water or steam that can then be used to handle process loads or used in an absorption chiller to provide cooling or can be used to regenerate a desiccant dehumidification unit that would handle the latent load of the building.

1.2 Benefits of CHP

Deployment of CHP systems offers several advantages that have been enumerated below:

1. **Lower energy costs:** CHP offers significant cost savings on energy costs, especially during peak times.

2. **Higher reliability power:** Having CHP systems installed onsite result in fewer power outages and reduced downtime. Table 1 shows the economic losses that some of the businesses suffer in the event of a blackout.

Table 1: Economic Loss to Businesses in U.S.A. due to Power Outage

Industry	Average Cost of Power Outage ($/hr)
Brokerage operations	6,480,000
Credit card operations	2,580,000
Airline reservations	90,000
Telephone ticket sales	72,000
Cellular communications	41,000

(Source: www.bchp.org)

3. **Improved power quality:** CHP systems provide high power quality without any surges and dips in electric power supply that can otherwise wreak havoc

on computer systems and sensitive manufacturing processes in fields such as bio-tech, pharmaceutical, plastics manufacturing etc.

4. **Improved environmental quality:** CHP is much more efficient than the conventional power plant using less fossil fuel, has fewer greenhouse gas emissions and lesser smog-forming emissions for the same amount of energy resulting in improved environmental quality.

5. **Improved indoor air quality:** CHP can be used to run a desiccant dehumidification unit and better control of humidity reduces total air conditioning loads, prevents mold, mildew, and rot damage, and protects moisture-sensitive manufacturing processes.

6. **Reduced transmission and distribution losses:** An average of 5-10% of electricity generated at a power plant is lost during transmission and distribution to the site. Since CHP is located right near where the electricity is used, it doesn't have any line losses.

7. **Lower overall fuel use:** Conventional systems that generate electricity and thermal energy separately require about 65% more energy input than integrated CHP systems. Using CHP prolongs the availability of limited fuel.

1.3 CHP Market Potential

The significant benefits offered by CHP systems such as improved power reliability and quality, reduced energy costs and improved indoor air quality make it attractive in a wide variety of market sectors. The market potential of CHP can be broadly categorized into two sectors, viz., the commercial sector and the industrial sector.

Commercial Sector: The various markets that come under the commercial sector are:

- Hospitals
- Educational Facilities
- Office Buildings
- Data Centers
- Nursing Homes
- Hotels
- Supermarkets
- Retail Stores
- Restaurants

Industrial Sector: The different markets that come under the industrial sector are:

- Petroleum refining
- Chemical process plants

- Food processing
- Glass industry
- Steel industry
- Metal Casting
- Forest products
- Paper manufacturing

Chapter 2: Background

2.1 Literature Review

The literature review focuses on Combined Heat and Power (CHP) research in the industrial and commercial sector, liquid desiccant analysis and desiccant dehumidification systems involving liquid desiccants.

2.1.1 CHP in Industrial Sector

Extensive research and development has been conducted in Combined Heat and Power for large-scale industrial applications as compared to the commercial sector resulting in higher number of CHP systems installed in the industrial sector, making CHP an established technique within the industrial sector for simultaneously meeting power and process steam requirements. Available literature shows that CHP is utilized to a greater extent by certain industries such as the paper and pulp industry, chemicals, refining and steel owing to certain characteristics like high and relatively constant steam and electric demands and access to byproduct or waste fuels [Onsite, 2000]. The CHP systems are typically sized to meet the base load thermal demand and produce electricity as a byproduct. A large percentage of these systems are based on combined cycle consisting of large combustion turbines, boilers or heat recovery steam generators and steam turbines. The very low power to heat ratio of these systems ensured that electricity generated would not exceed plant demand and

resulted in very high overall fuel utilization. Though reciprocating engine systems can provide higher electrical efficiencies than combustion turbines in smaller sizes, one of the main reasons for not using them in large scale plants is because a significant portion of the waste heat from engine systems is rejected in the jacket water at a temperature generally too low to produce high-quality steam. Steam can be produced from the engine's exhaust heat in the same manner as from the exhaust of a combustion turbine, though the volume of exhaust per unit of electrical output is generally much lower. The jacket water for most systems is suitable only for production of hot water. While engine systems may not serve the needs of some process industries with high-pressure steam requirements, they can be a good candidate for many food and manufacturing industries that do not require high-pressure steam but use large quantities of wash water and low-pressure steam.

Mansour and Davidson, (1996) provide an overview of a 118 MVA cogeneration application for a large pulp mill in Canada with a connection to a 25 kV limited capacity utility distribution system. The research discusses in detail some of the unique challenges which were encountered in the installation and have addressed special application concerns which result from the interconnection of a large industrial plant cogeneration facility and a limited capacity utility tie system. Soares et al., (2001) assessed the economic performance of three natural gas-fired cogeneration systems at two specific industrial plants, one in the chemical sector and the other in the pulp and paper sector as these two sectors make intensive use of self-produced power. The study was done in the light of restructuring of Brazil's power sector and trying to address some of the main barriers to cogeneration development in

Brazil related to issues of buyback rate, backup energy contracts and transmission rates. The results showed that small and medium-size units, less than 20 MWe, were feasible for electric-intensive industrial plants, due to the high risk of power outages of the Brazilian electrical system. Large units were found to be feasible only with the adoption of incentive policies for selling off surplus power generated by the cogeneration system. Ashmore, (2003) describes a combined cycle cogeneration plant for a pharmaceutical industry that is designed around a 27.5 MW gas turbine, supplementary-fired heat recovery steam generator and a small existing steam turbine genset. At base load output, the cogeneration plant is capable of generating about 32 MW of power and process steam for pharmaceuticals production. Similar studies based on design and operation of industrial CHP plants has been discussed by many other researchers [Jansen, 1979], [Nash, 1983], [Chellini, 1984], [Stambler, 1985], [Fulton, 1996], [Mathis, 1996], [Varley, 1998] and [Hepbasli and Ozalp, 2002].

Although there is general agreement that CHP systems can save energy when compared with the separate generation of heat and electricity, the economics of such systems is a fertile ground for argument and dispute. In part this stems from the adoption of different criteria but it also arises from the complication of analysis and the introduction of socio political factors. Cleugh (1980) describes an approach to assess the various parameters affecting the economics of industrial CHP. Cleugh in his study has isolated important factors such as fuel prices, discount rates related to the cost of capital and the balance of heat and power loads to see how these factors affect industrial CHP plants. Illerhaus and Verstege (1999) implemented a new method with dynamic search strategy (DSS) based on mixed integer linear

programming (MILP) for calculating the optimal unit commitment and economic dispatch of industrial enterprises with its own energy supply system, mostly with CHP plants. In order to yield the most synergetic effects, both the marketplace and the demand of disposable industrial processes were taken into account. They were able to achieve a considerable acceleration of calculation time using the new optimization method. Similar research based on economics and optimization of industrial CHP systems has been reported by others [Rodrigues and Cavanna, 1979], [Stromberg and Franck, 1994], [Mohanty and Panda, 1995], [Liszka et al., 2003], [Cormio et al., 2003], [Uszkat and Szargut, 2004] and [Marbe et al., 2004].

CHP systems based on natural gas fuel have much reduced levels of greenhouse gases improving environmental quality compared to conventional power plants. Axelsson et al. (1999) present a method that identifies economically optimal combinations of enhanced heat recovery, integration of combined heat and power and fuel switching, in an existing industrial energy system at various emission levels. Novel types of composite curves based on pinch technology, representing the existing temperature levels for supplying heat and the possible ones that may be attained after retrofitting were used as tools for estimating the opportunities for CHP and the trade-off between improved heat exchanging and CHP in their study. The economic potential of industrial combined heat and power CHP in Netherlands and the associated reduction in CO_2 emissions were estimated by Blok and Turkenburg, (1994). They developed a computer model in which simulation and an economic optimization of possible CHP plants was carried out individually for each of the 300 largest energy-consuming industrial plants in Netherlands. The results of the

simulation showed that the reduced CO_2 emissions were equivalent to about 4% of the present CO_2 emissions in Netherlands. Mahi, (1993) conducted in his research an environmental assessment of the different industrial CHP systems in the United Kingdom and then discussed the relevant legislation in the United Kingdom along with emission control systems that were used to comply with these regulations.

2.1.2 CHP in Commercial Sector

The commercial sector is comprised of a broad range of markets that include private and government services but not including manufacturing, mining, or agriculture. Commercial applications, typically but not exclusively, are based on energy use in buildings. Unlike the industrial sector that, on balance, reflects an electric load limited environment for CHP, the commercial sector is predominantly thermal load limited. This limitation can occur in two ways; either the thermal load is inadequate or it is highly seasonal, i.e., non-coincident with the electric load – as in the thermal needs for space heating. Another limitation of commercial applications is the more limited hours of operation compared to an industrial process operation. An office building may operate 3,500 hours per year compared to a refinery that is operated continuously or 8,760 hours per year. High and fairly constant thermal loads and a high number of operating hours per year characterize the commercial applications that are favorable to CHP. CHP systems are also typically sized to operate on a base load basis and utilize the electric grid for supplementary and backup power.

One of the markets in commercial sector is hospitals which are basically large facilities with around-the-clock operation and characterized by large, steady thermal and electric requirements, making it an ideal candidate for a combined heat and power system. Jackson, (1987) describes a CHP system designed and operated in a hospital in UK. The CHP system consisted of a 13-liter Waukesha reciprocating engine driving an Artemis 86 kW generator. The engine was run on natural gas. The electricity from the generator was fed parallel to the hospital grid while the heat produced from the engine was passed through a series of heat exchangers into the hot water and heating systems of the hospital. The CHP system was found to have significant savings when run for a longer time of the year and the payback was less than five years. Leijendeckers et al., (1971), describe a completely self-contained CHP installation for a fully air-conditioned 420 bed hospital complete with operating theatres, X-ray rooms, polyclinic, kitchen, etc. The CHP system is comprised of four reciprocating gas engines, each driving a 700 kVA brushless generator. Heat recovery from engine jacket water and exhaust supplies steam for the absorption type air-conditioning and winter heating. Additional steam is supplied by four gas-fired boilers. The electric automatic 220/380 V switchgear and control system automatically start, stop and synchronize the gas engine generators in a predetermined sequence, and in response to electric demand load sensing. The study also describes the controls involved in the system. Economic analysis and feasibility of CHP systems for hospitals have also been reported by other researchers [Alton, 1987], [Lee, 1987], [Hanitsch and Bleyl, 1995], [Burdon, 1998], [Jafari, 2002] and [Szklo et al., 2004].

Supermarkets are one of the most energy-intensive types of commercial buildings in the commercial sector. Refrigeration is the largest component of supermarket energy use, accounting for half or more of the store total since large amount of energy is used to maintain chilled and frozen food in both product display cases and storage refrigerators. Compressors and condensers account for 60-70% of refrigeration energy consumption [Baxter, 2003]. The remainder is consumed by the display and storage cooler fans, display case lighting, evaporator defrosting, and for anti-sweat heaters used to prevent condensate from forming on doors and outside surfaces of display cases. Maidment et al., (2001) investigated the practical and economic viability of an integrated combined heating and cooling system in a supermarket. The system consisted of a direct-drive screw compressor, which was powered by a throttle controlled gas engine. The waste heat from the engine was used to provide hot water for space heating and for general usage within the catering and toilet facilities in the supermarket. In this study, the working principle of the novel system and the integration of the gas engine system into the typical supermarket are described in detail. A computer model was used to simulate the energy consumption of the supermarket and to calculate the energy consumed by the conventional system and that used by a number of alternative combined heating and cooling system configurations. The additional capital cost of each configuration was estimated and this was used to calculate the payback period. The results showed that a payback period of 4.2 years may be achieved with a system that used approximately 500,000 kWh per annum less primary energy than a conventional system. Maidment and Tozer, (2002) proposed that heat generated by the CHP primemover could be used to

power an absorption refrigeration system providing cooling for the refrigerated cabinets in a supermarket. The research initially described the cooling, heating and power requirements of a typical supermarket and then reviewed a number of combined cooling heating and power (CCHP) options involving the use of different cooling and engine technologies. The authors also calculated and compared the energy savings and capital costs of the different options against typical conventional supermarket technology.

The hotel industry is another energy and resource intensive section of the commercial sector. More than half of the electrical load for a hotel is consumed by the heating, air conditioning and ventilation systems for space conditioning. The other electrical loads are lighting, escalators, elevators etc. Other significant energy usages in a hotel are domestic hot water production, laundry facilities, swimming pools etc. Thus combined heat and power systems can be very energy efficient and help reduce the energy consumption of the hotels by producing electricity and using the waste heat from the primemover for production of hot water or low pressure steam. Babus'Haq et al., (1990) developed a software model to study the economics of using CHP systems in a two-storey hotel that would satisfy the power and heating demands of the hotel. Their results estimated a payback period of less than three years. Epler, (2004) describes a CHP system for a hotel in California consisting of a 60 kW microturbine. An air-to-water heat exchanger recovers the exhaust heat from the microturbine and is then fed to a series of hot water storage tanks that provide for domestic uses in the hotel such as showers. The CHP system on an average supplies 60% of the hotel's electricity load and 100% of its domestic hot water needs.

CHP penetration in commercial office buildings is limited as compared to other areas in the commercial sector such as the educational facilities and health care or hospitals. Some of the factors that drive the favorable economics of CHP in these sectors are higher occupancy levels, with students or patients occupying the facilities around the clock, creating high load factors that help amortize the investment in CHP systems and the balance between thermal and electric loads in these sectors is relatively high compared with office buildings. There are different types of prime movers that can be integrated with various thermally activated technologies to provide cooling, heating and power in a commercial office building. An example of one such integrated CHP system is a microturbine integrated with an absorption chiller. Marantan, A (2002) and Liao, X (2003) have described an integrated CHP system consisting of a microturbine that produces 60 kW of power that is supplied to the office building while the exhaust heat from the microturbine is used in a single effect absorption chiller that produces 18 tons of cooling which is provided to the building. The waste heat from absorption chiller is then utilized for regeneration of a solid desiccant dehumidification unit that dehumidifies 1.42 m3/s (3000 cfm) of outside air which is then supplied to the mixed air chamber of the roof top unit.

Smith et al., (1995) report the technical, economic and environmental performance of a 40 kWe CHP plant, located within the Queens Building at De Montfort University in United Kingdom. From thermodynamic analysis, they found that the CHP plant had an overall efficiency of 77% while the economic analysis showed a 7.1 year payback period. Environmental analysis showed that the CHP generated energy produces half the carbon dioxide emissions of separately imported

electricity and heat from a boiler plant. Schaaf, (1998) reports a reciprocating engine-based CHP system for a large bank building in Frankfurt, Germany. The system consists of a MAN B&W 8 liter spark ignited gas engine that generates an electrical output of 1.5 MW and a MAN B&W 6 liter dual fuel gas engine generating an electrical output of 2.3 MW. The gensets are connected via closed circuits and intermediate heat exchangers to the heating circuits of the building supplying heating temperatures of 90 ºC and 35 ºC. Two additional 4.5 MW boilers provide for peak load coverage at a supply temperature of 90 ºC. The CHP plant is designed to provide hot water in base load operation. The overall efficiency of this system was found to be around 79%.

2.1.3 Liquid Desiccant Dehumidification

Controlling humidity in a conditioned space can be important for a wide variety of reasons. Traditional concerns include moisture damage during marine transport, humidity damage for moisture-sensitive artifacts, process improvement for certain manufacturing sectors like electronics and pharmaceuticals, product protection from degradation and protection from corrosion. The dehumidification is not only useful for industrial purposes, but also for commercial and residential application. The humidity level in the ambient air also affects the comfort. The ASHRAE standard 55-92 for thermal environment conditions for human occupancy specifies conditions for the thermally acceptable environment. The ASHRAE Comfort Zone ranges for temperature and humidity in summer is 22.5 °C to 26 °C at relative humidity of 60 % and is 23.3 °C to 27.2 °C at relative humidity between 20 % and 25 % during winter.

In conventional cooling systems, dehumidification is achieved by cooling a moist air stream below its dew point so that liquid water condenses out of the air. In order to achieve design indoor conditions, the air is reheated before it is supplied to the conditioned space. Desiccant dehumidification systems on the other hand remove moisture from the air by forcing water vapor into a desiccant material. The driving force is the lower water vapor pressure of the desiccant than that of the humid air. Desiccants can either be solid or liquid, both behave in the same way, their water vapor pressure is a function of temperature and moisture content. The difference between solid and liquid desiccants is their reaction to moisture. Solid desiccants like silica gel mostly adsorb the moisture that means there is no chemical reaction. Liquid desiccant materials usually absorb the moisture by undergoing a chemical or physical change.

Peng and Howell, (1982) analyzed a liquid desiccant dehumidification system for a warehouse application. Flat plate solar collectors were installed on the roof of the warehouse to use solar energy for the regeneration of the liquid desiccant which was triethylene glycol-water solution in this case. A mathematical model was used to simulate the system consisting of the absorber, evaporator, regenerator and a collector/storage tank hot water loop. The simulation results showed that the proposed solar powered liquid desiccant system offered considerable savings in operating cost over a conventional dehumidification system for long term warehouse storage applications. In order to analyze the performance of the system using desiccant technology, the thermo physical properties of desiccants are essential. In particular, the vapor pressure of the liquid desiccant is one of the important properties in liquid

desiccant dehumidification. Ahmed et al., (1997) attempted to predict this property based on a classical thermodynamics approach and found that the predicted values for lithium chloride agreed very well with the experimental results. The authors also developed mixing rules to predict the properties such as vapor pressure, density and viscosity of desiccant mixtures formed by mixing lithium chloride and calcium chloride. By combining these two salts, improved characteristics can be expected as well as a considerable reduction in cost. The poor performance of calcium chloride is due to its high vapor pressure while on the other hand, lithium chloride possesses low vapor pressure and is stable, but its cost is high compared with calcium chloride. To stabilize calcium chloride and to decrease the high cost of lithium chloride, the two can be mixed in different combinations and the mixing rules can then be used to predict the thermo physical properties of the mixture. Martin and Goswami, (1999) conducted a detailed experimental investigation of the heat and mass transfer process between a liquid desiccant (triethylene glycol) and air in a packed bed regenerator using high liquid flow rates. Later a finite difference model was used to assess the effects of variables such as air and desiccant flow rates, air temperature and humidity, desiccant temperature and concentration and the area available for heat and mass transfer on the regeneration process. Good agreement was shown to exist between the experimental findings and the predictions from finite difference modeling. The design variables that were found to have the greatest impact on the performance of the regenerator were the air flow rate and the humidity ratio, the desiccant temperature and concentration and the packed bed height. The liquid flow rate and the inlet air temperature did not have a significant effect on the regenerator performance.

Lazzarin et al. (1999) investigated chemical dehumidification of air by a liquid desiccant in a packed tower both theoretically and experimentally for air conditioning and industrial applications. Furthermore, a parametric study was carried out considering the solutions H_2O/LiBr and $H_2O/CaCl_2$ to determine the optimum operative conditions. It was found that good tower efficiencies could be obtained using flow ratios (liquid/gas mass flow rates) in the range of 1 – 2.5. Jain et al, (2000) performed a design optimization of liquid desiccant cooling systems to minimize the life cycle costs under given constraints. The optimization was a mixed integer nonlinear programming problem that was solved by modified box's complex method. The total cost (capital + running) of the system over its life span was selected as the objective function to be minimized. The design variables were the length and number of tubes and mass flow rates of air and solution for the absorber, regenerator and different heat exchangers used in the liquid desiccant system. The optimization problem was subject to constraints arising due to the sensible and latent load capacity of the system and the necessity to keep the air velocities in the absorber and regenerator below the critical values for splash entrainment and flooding respectively. If the velocity of the air is very high, it would carry away the solution with it or block the flow of the solution. The design variables also had upper and lower bounds to prevent the variables from taking any arbitrary values during the optimization process. The optimization results were reported for a 20 TR unit and were found that if waste heat is available, then the initial and running costs of a liquid desiccant cooling system were one-fourth as compared to a conventional vapor compression system. Fumo and Goswami, (2002) studied the performance of a packed tower

absorber and regenerator for an aqueous lithium chloride desiccant dehumidification system. The rates of dehumidification and regeneration, as well as the effectiveness of the dehumidification and regeneration processes were assessed under the effects of variables such as air and desiccant flow rates, air temperature and humidity, and desiccant temperature and concentration. The water condensation rate in the conditioner was found to be increasing with the air flow rate since a high air flow rate will remove the dehumidified air more rapidly from the interface, thereby reducing the humidity gradient between the interface and bulk air and maintaining a higher potential for mass transfer. The water condensation rate in the conditioner was found to decrease with increase in desiccant temperature because a higher desiccant temperature gives a lower potential for mass transfer in the dehumidifier resulting in lower condensation rate. In the case of the regenerator, the water evaporation rate was found to increase with the air flow rate since a high air flow rate rapidly removes the higher moist air from the interface reducing the humidity gradient between the interface and bulk air maintaining a higher potential for mass transfer. On the other hand the water evaporation rate was found to increase with the inlet desiccant temperature because higher the temperature of the desiccant, higher is its vapor pressure and consequently higher is the potential for mass transfer.

2.2 Dehumidification Loads in an Office Building

The dehumidification requirements of commercial buildings vary significantly with the particular building application. However, for a typical office building, the general sources of latent loads are:

1. Infiltration

Outdoor air can enter a building through cracks in the building envelope due to pressure differences across the envelope. If the outdoor air is more humid than the indoor air, the infiltration air can bring dehumidification loads. However, good design practice dictates that commercial buildings should operate with positive pressure to prevent infiltration of unconditioned air from outdoors.

2. Internal Moisture Generation

Moisture is generated in buildings by human occupants, cooking activities and other activities that involve water use such as cleaning. In most commercial office buildings, the moisture generated by occupants is the main internal gain.

Table 2 shows the rate of moisture generation by average human occupants at a variety of activity levels. The moisture generation rates range from 0.1 lb/hr for the most sedentary activities to over 1.0 lb/hr for athletic activities. For most commercial office building occupants, though, the generation rate is between 0.10 – 0.25 lb/hr, giving latent loads of 100 – 250 Btu/hr per person.

Table 2: Moisture generated by human occupants (ASHRAE 1997)

Activity	Generation (lb/hr/person)	Latent Load (Btu/hr/person)	Sensible Load (Btu/hr/person)
Seated at theater	0.10	105	225
Seated, very light work	0.15	155	245
Moderately active office work	0.19	200	250
Standing, light work, walking	0.24	250	250
Light bench work	0.45	475	275
Moderate dancing	0.52	545	305
Athletics	1.04	1090	710

3. Ventilation

Like infiltration, mechanically-driven airflow from outdoor can bring humidity into the building. The magnitude of the ventilation load depends on the ventilation airflow rate and the difference between the indoor and outdoor conditions.

$$Q_{vent,sen} = \dot{m}vent\, C_p \left(T_{OA} - T_r\right)$$

$$Q_{vent,lat} = \dot{m}vent\, h_{fg} \left(W_{OA} - W_r\right)$$

where,

$Q_{vent,sen}$ = sensible ventilation load

$Q_{vent,lat}$ = latent ventilation load

m_{vent} = Mass flow rate of ventilation air

C_p = Specific heat of the air

T_{OA} = Outdoor air temperature

T_r = Building room temperature

h_{fg} = Heat of vaporization of water

W_{OA} = Outdoor air humidity ratio

W_r = Building room air humidity ratio

The ventilation or outdoor airflow rate is dictated by indoor air quality requirements or make-up air requirements. ASHRAE Standard 62 sets the design requirements to provide adequate indoor air quality. In most building applications, the standard specifies outdoor airflow based on occupancy. In some cases in which significant non-occupant related indoor contaminants are generated within the building, the ventilation rate is specified based on floor area. In hotels, ventilation is specified per room. Table 3gives the design ventilation rates from ASHRAE Standard 62.

Table 3: Design ventilation rates from ASHRAE Standard 62

Application	Estimated Max. Occupancy (people/1000 ft^2)	Outdoor Air Requirement (cfm/person)	Outdoor Air Requirement (cfm/ft^2)
Cafeteria, fast food	100	20	2.00
Office Space	7	20	0.14
Conference Room	50	20	1.00
Retail Store (street level)	30	-	0.30
Auditorium/Theater	150	15	2.25
Classroom	50	15	0.75
Hotel Room	8	30 cfm/room	0.12

Ventilation only imposes loads on the building when the outdoor conditions are different than the indoor conditions. Figure 2 shows the magnitude of the sensible and latent ventilation loads as a function of outdoor temperature and humidity for a building with indoor conditions of 75°F and 50% RH as calculated from the above equations. The loads are expressed per unit volumetric airflow rate as Btu/hr/cfm (Brandemuehl and Katejanekarn, 2000).

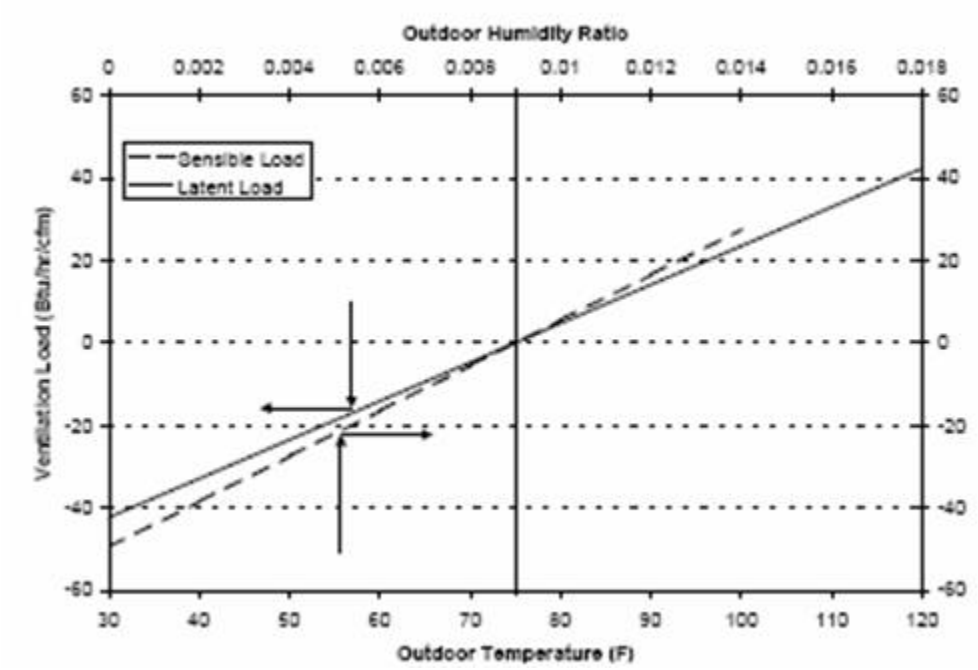

Figure 2: Ventilation loads at typical indoor conditions

Figure 2 in combination with Table 3 can be used to assess the size of ventilation cooling and dehumidification loads at a particular set of outdoor conditions. From Table 3 it can be seen that a commercial office building requires 0.14 cfm/ft^2 of outdoor air. When the outdoor air has a humidity ratio of 0.0133, corresponding to an outdoor condition of 80°F and 60% RH, it can be found from Figure 2 the latent ventilation load is 20 Btu/hr/cfm, giving a latent load in the office building of 2.8 Btu/hr/ft^2. At this outdoor condition, the ventilation latent load is twice that of occupants alone given in Table 3.

The calculations of dehumidification loads above indicate that, even at design occupancy, ventilation is the most important source of latent loads in commercial office buildings. Since the average occupancy of most buildings is significantly less than the design occupancy, the average moisture generation by occupants is an even

smaller fraction of the total latent load. The calculations also imply that dehumidification requirements can be a very large portion of overall building loads. Rooftop equipment is often estimated at about 400 ft^2/ton, or 2.5 tons/1000 ft^2, which corresponds to 30 Btu/hr/ft^2 (Brandemuehl and Katejanekarn, 2000). At the outdoor conditions of 80 F and 60% RH, the latent load due to ventilation air forms 20% of the total capacity estimate of the rooftop equipment. This percentage of latent load would be much higher at more humid conditions.

2.3 Conventional Air-Conditioning Process

Conventional air conditioning systems are typically controlled by a thermostat (or some similar receiver/controller combination). Controls are set to keep the space dry bulb temperature from exceeding the thermostat setpoint. Air from the space is drawn back to the air handling unit, where its temperature is again decreased before being supplied back to the space. The temperature decrease is accomplished by the returned air being drawn through (or blown through) a cooling coil within the air handling unit. The coil is typically a specially designed finned-tube heat exchanger that contains a relatively cold circulating fluid (usually chilled water or a refrigerant) into which heat from the air is transferred. This situation is often more complicated by the fact that some outside air is then mixed with the returned air from the space, and that mixture is cooled by the coil. The most common reason for introducing outside air is to provide ventilation for the occupants of the space. As the cooling coil reduces the dry bulb temperature of the air so that the air, in turn, will provide

sensible cooling for the space, the dry bulb temperature of the air is reduced almost to its dew point temperature. In fact, a considerable portion of the air actually reaches saturation due to its contact with, or proximity to, the cooling coil, which has a temperature considerably lower than the air's dew point temperature. As a result, water condenses from the air on to the coil. Judicious selection of airflow velocities will allow the condensate to drip into a collection pan from which it will drain instead of being blown through the ductwork. The described process, which began with the objective of keeping the dry bulb temperature of a space from exceeding a thermostatic setpoint, produces a condition where the air introduced is not only cooler, but also drier. One device, the cooling coil, performs dual service by both lowering the dry bulb temperature of the air and reducing its moisture content. The moisture removal is not incidental or accidental; the cooling coil is selected based on its capability to remove the space and outside air sensible and latent (moisture) loads estimated to occur on a design day. Figure 3 shows the conventional air conditioning and dehumidification process on a psychometric chart.

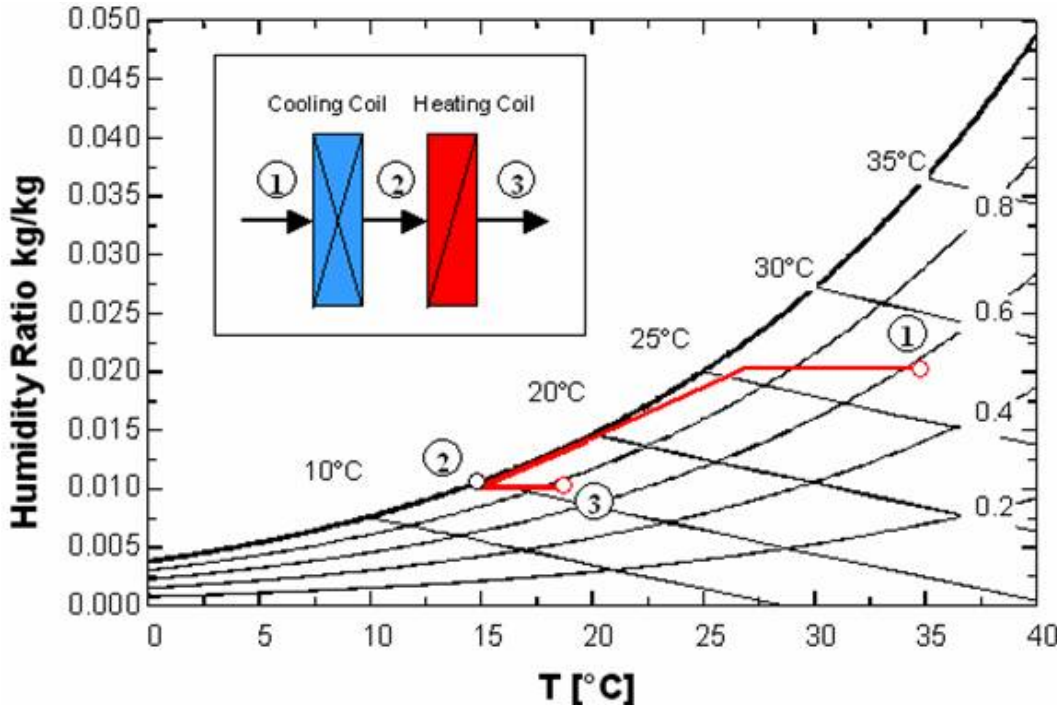

Figure 3: Conventional Dehumidification Process in a typical Roof Top Equipment

Initially the outdoor air enters the roof top unit at state 1 where the dry bulb temperature of the moist air decreases, while the moisture content remains constant. The dry bulb temperature continues to decrease as moisture begins to condense out of the air onto the cooling coil resulting in a simultaneous decrease in the moisture content. In order to deliver air at the desired dry condition of approximately 45% relative humidity, state point 2 has a lower temperature than needed to supply the space. In order to achieve design indoor conditions, some form of reheating is used from state point 2 to 3.

2.3.1 Disadvantages of Conventional Process

The relative humidity in the space is controlled only indirectly and it floats up and down as a result of changing match between the sensible and latent capacity of the equipment compared to the sensible and latent loads. The space thermostat controls HVAC system operation to meet the sensible load. That is, the equipment sensible capacity is controlled to meet the sensible load. If the latent capacity of the equipment is inadequate to meet the latent load, the indoor humidity increases. The conventional process can be modified, with some increase in control complexity and first cost to achieve improved indoor environmental conditions under off-design outdoor conditions. The modification essentially overcools the air in response to a call for dehumidification from a humidistat, then reheating the cold dry air as necessary to ensure that the thermostat dry bulb temperature setpoint is not exceeded. However, this scheme increases the controls complexity and first cost. The primary increase in cost, however, results from the cooling system running longer to dehumidify the air and the air subsequently requiring reheat. This type of modification is seldom employed due to the additional costs involved. Thus in an office building, off-design outdoor conditions may well result in a somewhat humid indoor environment. Alternatively, to address occupant complaints of discomfort, the thermostat setpoint may be lowered, reducing the indoor humidity level. Without reheat control, this action can lead to complaints because the space will feel too cold. Poor indoor environmental conditions often result in worker/occupant discomfort and decreased productivity.

Another potential problem with the conventional process is that of microbial and fungal growth in condensate drain pans. These can be carried into the ductwork and deposited where further growth can occur. Microbes and bacteria can be introduced into the space from breeding grounds in the pan or ductwork, causing occupant discomfort and possible allergic reactions or illness. Reheat will not solve this potential problem. Biological fouling of ducts may pose a serious problem in sensitive spaces such as operating rooms requiring a sterile environment. To summarize, potential problems with the conventional process are:

1. Difficulty in providing satisfactory indoor environmental conditions when off-design outdoor conditions are experienced
2. First cost and operating expense increase when the conventional system is modified with reheat control to provide satisfactory environmental conditions when off-design outdoor conditions
3. Difficulty in modifying existing conventional systems to handle additional outdoor air cooling load resulting from increased ventilation rates called for by ASHRAE Standard 62.
4. Indoor air quality problems due to microbial or fungal growth in condensate drain pans and ductwork.

2.4 Desiccant Dehumidification

Desiccant dehumidification equipment can address the problems cited above for the conventional process. Desiccant dehumidification technologies are based on the principles of sorption, which refers to the binding of one substance to another. Sorption occurs when a gas or liquid, the sorbate, binds to another liquid or solid, the sorbent. For dehumidification, the sorbate is water vapor and the sorbent is a liquid or solid desiccant that has an affinity to attract and hold water. The sorption can either be classified as absorption or adsorption. In adsorption, there is no change in the sorbent except for the added weight of the water. In absorption, there is a chemical change in the sorbent. For example, table salt is an absorbent that changes from a solid to a liquid as it absorbs moisture. By comparison, silica gel is a solid adsorbent that attracts water to its surface due to small electrical fields. In general, solid desiccant adsorb and liquid desiccants absorb.

Dehumidification with either solid or liquid desiccants is driven by a difference in water vapor pressure between the desiccant surface and that of the surrounding moist air. If the vapor pressure in the air is greater than that at the desiccant surface, moisture will be driven from the air to the desiccant surface. On the other hand, if the vapor pressure in the moist air is less than that at the desiccant surface, moisture will be driven from the desiccant into the air. Equilibrium occurs when the two vapor pressures are equal. Dehumidification is achieved by exploiting this behavior of desiccants through a cycle of moisture sorption and desorption by the desiccant. Moisture is removed from moist conditioned air with a high vapor pressure by exposing it to desiccants with low surface vapor pressure. The desiccant is then

exposed to air with a lower vapor pressure to drive the retained water from the desiccant.

Figure 4 shows illustratively the dehumidification and regeneration process that a desiccant material undergoes.

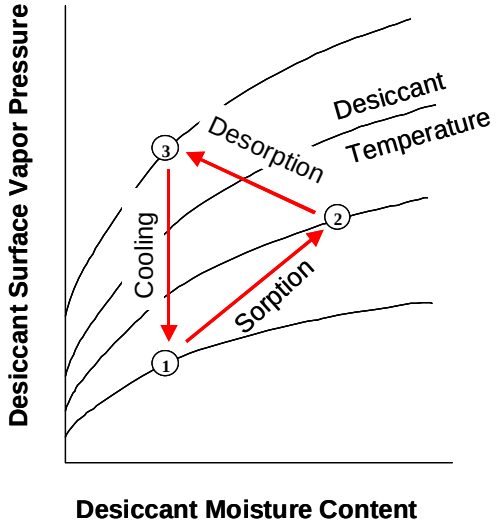

Figure 4: Desiccant Dehumidification and Regeneration Process

At point 1 the desiccant is dry and cold, so the partial vapor pressure is low. From 1 to 2 the cycle starts with the process called sorption. The desiccant picks up moisture from the air. The energy of evaporation is released and so the temperature increases. At point 2 the pressure is equal to the surrounding air, because the desiccant and the air get into equilibrium in the ideal case. The desiccant cannot collect more moisture because there is no more pressure difference to the air.

2.4.1 Advantages of desiccant dehumidification

A conventional roof top unit retrofitted with a desiccant dehumidification system offers several advantages as follows,

1. The desiccant unit itself is generally large and heavy, and will, if anything, result in increased first cost compared to adding reheat to a conventional system. However, installing a desiccant can result in reduced operating cost compared to a conventional system with reheat. This is more likely where the cost of electricity is high compared to natural gas if it is the fuel that is used as the energy source for desiccant regeneration. An electric bill typically has two components, an energy charge and a demand charge. The demand charge is usually a significant portion of the total cost for electricity. When an electrically powered water chiller or electrically powered direct expansion equipment would otherwise be used to provide latent cooling, a desiccant used for that purpose will reduce both electrical demand and electrical energy consumption, and the associated cost for each. Energy consumption for reheat would be eliminated.
2. Potential reduction in evaporator temperature to ensure adequate moisture removal would not be necessary. A dry cooling coil to enhance heat transfer may actually permit an increase in evaporator temperature without sacrificing sensible cooling capability. With the air in the space drier due to the desiccant's deep dehumidification capacity, it may also be possible to increase the dry bulb temperature set point for the space without sacrificing occupant comfort.

3. Latent cooling using desiccant dehumidification systems may be almost free in circumstances where waste heat, such as that from a natural gas driven engine generator or engine-driven chiller, may be used for desiccant regeneration.
4. Installing a desiccant unit may well be the least-expensive way to retrofit a facility to ensure compliance with ASHRAE Standard 62. Increasing the amount of ventilation air will generally increase the sensible and latent cooling loads imposed on the cooling coil. The exception, of course, would be when outside air conditions and a facility cooling load warrant air-side economizer operation. The latent cooling capacity of the desiccant can free-up equivalent capacity in the chiller or direct expansion equipment, allowing that equipment to possibly meet the additional sensible cooling loads arising from the increased ventilation air flow. Similarly, the cooling coil may well experience no increase in total load, with the increase in sensible load from the increased amount of outside air negated by the removal of most, if not all, of the outside air latent load it formerly had to remove plus the additional latent load due to the increased amount of ventilation air. Further, the cooling coil would perform more effectively since sensible heat ratios will invariably be high.
5. Microbial or fungal growth in the condensate drain pan and ductwork would be eliminated since the cooling coil will be a virtually dry coil for the vast majority of the time.

Chapter 3: Motivation and Objectives

3.1 Motivation

1. Combined heat and Power (CHP) systems have found lesser penetration in the commercial office buildings sector for the following reasons:
    - On an average, commercial office buildings are much smaller than industrial sites. Lack of research in integration of such systems has rendered the technology currently expensive.
    - Office buildings generally operate fewer hours per year and have lower load factors, providing fewer hours of operation per year resulting in longer payback periods.
    - Unlike the majority of industrial projects that can absorb the entire thermal output of a CHP system onsite, many commercial office buildings have either an inadequate thermal load or a highly seasonal load such as space heating. The best overall efficiency and economics come from a steady thermal load.
2. **Economic and Environmental Drivers for CHP:** Two key changes in the economic system are occurring that could make CHP more important economically and environmentally – the restructuring of the electric power industry may provide an enhanced economic driver and efforts to comply

with the Kyoto Protocol on global warming may provide an environmental driver for energy efficiency options such as CHP.

3. Research in desiccant dehumidification technology development has continued for several decades, however, commercial applications of desiccant dehumidification technology have been limited in the past by material and manufacturing considerations. Desiccant technology has been primarily used for industrial applications in niche markets such as the food industry, pharmaceuticals and others for accurate humidity control (Holzhauer [1979], Grosso et al. [1980], Griffiths [1996], Anon [2004]).
4. Indoor air quality (IAQ) problems related to humidity and ventilation can be improved using dehumidification systems. The Chesapeake building was designed to provide thermal comfort for its occupants, but does not provide direct humidity control. There have been complaints of high humidity in the summer months and very dry conditions during the winter months from building occupants. A desiccant regeneration CHP system can provide the needed humidity control directly and address some of the IAQ issues. Also, the control of outside air delivery to the building is limited by the centrally controlled outside air damper position. With only damper position control it is uncertain how much air is actually being provided because there is always a difference between building pressure and outside air pressure. Too much air leads to ineffective electricity use and too little air contributes to IAQ problems. These issues can be addressed during the integration of the liquid desiccant system.

5. The Chesapeake building energy consumption is primarily electric power, which makes it a good candidate for installing CHP technology. High electricity consumption during the heating season from distributed electric heaters (reheats) throughout the building can be reduced by using available heat from power generating equipment for space heating. Likewise, high electricity consumption during the cooling season from electric roof top units (RTU) can be offset by using waste heat activated desiccant dehumidification equipment, which can reduce energy consumption and eliminate high summertime electric demand charges. The demand charge is the price the utility company charges per kilowatt for the greatest amount of electric power supplied to a customer during on-peak weekday hours during the month.
6. Waste heat from the engine generator can be used for desiccant regeneration providing the thermal base load for the CHP system. This would allow increased use of CHP system resulting in improved economics and lower payback periods on the installed system.
7. Extensive research has been done on solar based regeneration of liquid desiccants. However detailed performance of regeneration through waste heat is not available.
8. Efficient operation of liquid desiccant system is possible at low regeneration temperatures (Ghaddar et al., 2003). The combined waste heat recovered from the exhaust gases and jacket cooling water from the engine generator is at a temperature ideal for regeneration of liquid desiccant.

9. Earlier research has focused on component level design and optimization. But the system level approach is missing wherein there is a need to address and resolve the integration challenges faced in the integration of the CHP system in a commercial office building.

3.2 Research Objectives

The research objectives of this study are grouped into three parts, experimental objectives, modeling objectives and system integration research:

3.2.1 Experimental Objectives

1. Design and install an integrated engine generator-liquid desiccant system in a commercial office building.
2. Characterize the performance of the integrated system through performance measurement and extensive data analysis.
3. Primary energy consumption (PEC) comparison with traditional power plant and conventional HVAC systems.
4. Address and assess the different integration challenges encountered during the integration of the engine generator – liquid desiccant system with the existing electrical grid and the roof top unit.

3.2.2 Modeling Objectives

1. Develop experimentally verified thermodynamic and economic simulation model with fluctuating electricity and gas prices
2. Provide a tool to assess the feasibility of the engine generator – liquid desiccant system under different scenarios
3. Formulate design guidelines for optimum operation of the engine generator – liquid desiccant system based on simulation results

3.2.3 System Integration Research

Analyze different integration options of the liquid desiccant system with the roof top unit together with the development of energy efficiency improvements and design guidelines.

Chapter 4: Experimental Setup Description

4.1 Chesapeake Building Test Bed

The Chesapeake Building is a representative commercial office building on the campus of the University of Maryland and is well suited to demonstrate the benefits of CHP technology. The building was constructed in 1991 and measures 128 ft in length, 96 ft in width and 50 ft in height. The physical size of the Chesapeake Building (52,700 square feet) puts it into a medium size office building category (10,000-100,000 square feet). This category represents 23% of all buildings and comprises 46% of the total floor space in the US. Since the building is administrative in nature, building occupancy for the majority of the employees is from 9am to 5pm Monday through Friday with only a few exceptions. There are approximately 200 employees in the building during normal operating hours and the work is generally light duty office work. The Chesapeake Building features some ideal characteristics that make it a good candidate to demonstrate CHP technology.

First, the building was built in a relatively remote location – on the edge of a very large university campus. The remote location helps to reinforce and demonstrate the idea of distributed on-site power generation. Since it is remotely located, the building is far away from the campus central heating and cooling plant, which makes it more difficult and more costly to provide steam or chilled water to the building. Therefore the building was designed to have cooling provided by electric Roof Top

Units (RTUs) and heating provided by variable air volume (VAV) electric reheat coils, thus making it an electric building. As discussed earlier, there is room for improved energy efficiency for electric buildings. The Chesapeake building also has a natural gas supply readily available, which makes the installation of BCHP components more feasible and less costly.

Indoor air quality (IAQ) problems related to humidity and ventilation can also be improved. The building was designed to provide thermal comfort for its occupants, but does not provide direct humidity control. There have been complaints of high humidity in the summer months and very dry conditions during the winter months from building occupants. A desiccant regeneration CHP system can provide the needed humidity control directly and address some of the IAQ issues. Also, the control of outside air delivery to the building is limited by outside air damper position. With only damper position control it is uncertain how much air is actually being provided because there is always a difference between building pressure and outside air pressure. Too much air leads to ineffective electricity use and too little air contributes to IAQ problems.

Finally, the building has basic-level HVAC controls. All of the VAVs are independently controlled by a space thermostat and do not have any higher-level energy management features. Controls such as this can be improved to include energy saving control strategies using programmable centrally controlled building energy management systems. Since the CHP concept applied to buildings involves integrating HVAC equipment, the opportunity to save additional energy exists when integration of all building HVAC components is done.

4.2 Existing Mechanical and Electrical Systems

The Chesapeake building is divided into two zones, the bottom two floors represent the first zone and the top two floors represent the second zone. The zones have equal space areas, similar occupancy distribution, similar heating/cooling loads, and is air-conditioned with a 90-ton direct expansion (DX) packaged roof top unit (RTU) which supplies 55º F air to each zone year-round. The supply air distribution is ducted to the Variable Air Volume (VAV) boxes, which modulate the volume of air that is distributed to the space. Driven by pressure differences, the air is collected in the suspended ceiling space and directed to the zones' mechanical shafts back to the roof top units as shown in Figure 5.

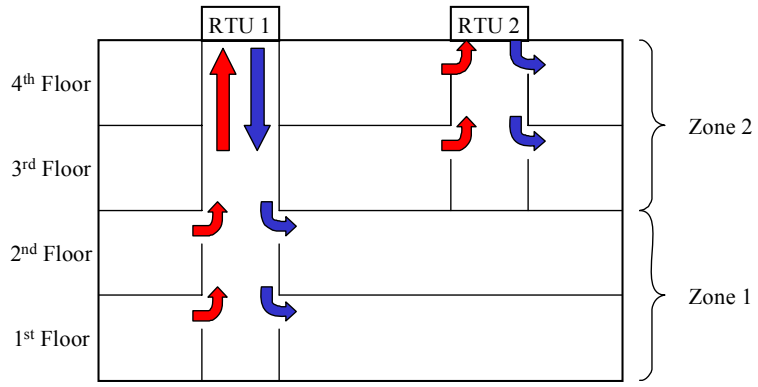

Figure 5: Air Distribution System at Chesapeake Building

The RTU is a commercial unit equipped with an economizer cycle. The schematic of the unit is provided in Figure 6. Outside air and return air are mixed in the mixed air section before being brought to the 90-ton DX interlaced evaporator

coil. The coil is part of two refrigeration systems of equal capacity and condenser units located at one end of the RTU.

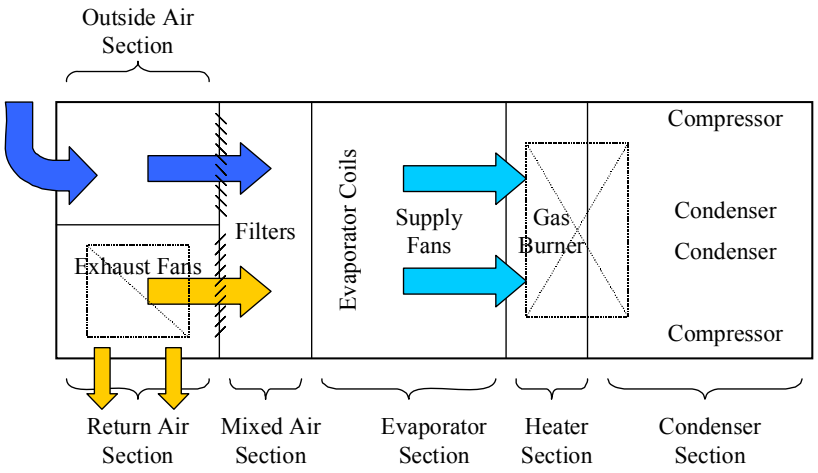

Figure 6: Schematic of Roof Top Unit (Top View)

Two supply fans operate in parallel to drive the air through the RTU and the building air distribution system. Variable frequency drives are used to modulate fan speeds, and thus, meet the amount of air required by the VAV distribution system by maintaining a set duct static pressure setting. The supply air temperature is controlled either with compressor stages in the refrigeration system or with the economizer cycle. The economizer cycle operates whenever the outside air temperature is below 55º F. The exhaust fans are used when larger quantities of outside air are brought into the building during economizer operation. If the outside air temperature is lower than the set supply air temperature of 55 ºF, the refrigeration system is not used to provide cooling.

The outside air and return air boxes are connected with a set of interlocked dampers, which modulate the amount of outside air. The exhaust dampers in the return air section in Figure 7 are used to vent excess return air. The interlocked

dampers have a minimum set position to ensure that a sufficient amount of outside air is supplied to the space during occupied hours.

The refrigeration system consists of two conventional R-22 vapor compression systems with reciprocating compressors. The refrigeration system has four stages of cooling for a coarse capacity control and hot gas bypasses for fine capacity control.

The RTUs are integrated with a VAV system, which includes VAVs with and without electric reheat. Each VAV box is locally controlled by a thermostat, which maintains a set temperature for the space it serves. The VAV boxes serving the core of the building can only modulate the volume of air delivered to the space, as the core requires cooling all year round. The fan powered VAV boxes with electric reheat serve the building perimeter and are shown in red in Figure 7. In addition to modulating the air volume, these boxes can re-circulate plenum air back to the space and use electric heaters to increase the supply air temperature. These boxes also provide the required heating for the building.

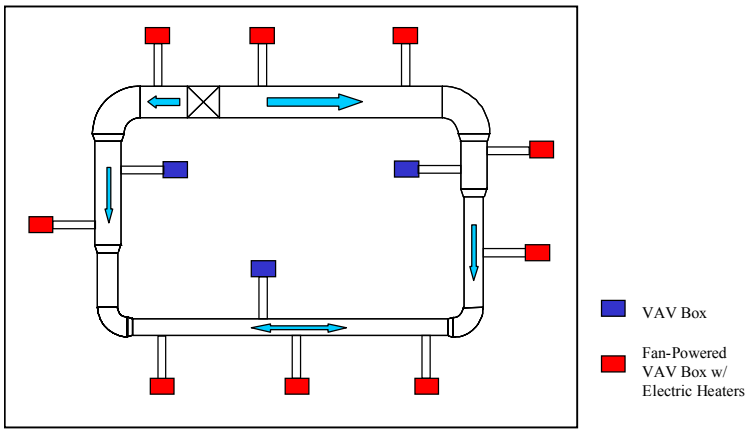

Figure 7: Typical Floor Level Air Distribution System

The variable frequency drives that modulate supply fan speeds maintain the static pressure difference between the VAV boxes and the RTUs. The VAV system has two modes of operation, occupied and unoccupied. The occupied mode of operation has been described above. In the unoccupied mode of operation, the RTU is turned off with the outside air damper completely closed. At the same time, the VAV boxes are turned off with their dampers set in the maximum open position. The RTU goes into a "night setback" mode of operation. If the building temperature drops below a set value, 65 ºF, the supply fans and the gas heater, indicated in Figure 6, energize to provide heating for the building. If the building temperature rises above the set limit, 85 ºF, the fans with the refrigeration system provide cooling. The VAV system has only basic controls without the capability of communication between the VAVs and RTU. The Central Control Management System of the campus has communication with the building mechanical system to monitor some of the performance parameters and to set the occupancy schedule.

The electrical system consists of low voltage and high voltage electrical panels on each floor, which tie into the building's main electrical panel in the ground-level electrical room. Each RTU has an individual circuit as well and ties into the main electrical panel. The low voltage circuits serve convenience outlets, dedicated circuits for kitchen appliances, office equipment, and lighting circuits. Lighting in the building is provided by fluorescent lighting fixtures, which use F40T12 type lamps. The high voltage circuits serve the VAV boxes, which include fans and electric heaters.

Natural gas usage in the building is very minimal. Natural gas is used for an emergency generator, a domestic hot water heater and burners in the RTUs. However, it has been observed from utility bills that the burners in the RTUs are seldom used. As a result, the largest consumer of natural gas on a regular basis is the domestic hot water heater.

4.3 Data Acquisition System

A Data Acquisition System (DAS) and measurement equipment were installed to determine the performance of the building in its existing condition as well as to measure the performance of the different CHP components installed at the building. The DAS utilizes state-of-the art equipment and is distinct and completely separate from the building's control system. The DAS is capable of providing high accuracy readings, and because all of the measurement routines and programs were custom programmed, the DAS is able to provide completely customized measurements.

The DAS consists of a C-size VXI mainframe with a command module, three 64-channel 5.5 digit multi-meter modules, and two counter/totalizer modules. The mainframe communicates through a GPIB interface card and is controlled by HP VEE 5.0 software. HP VEE 5.0 is a visual programming language specifically designed for instrument control, monitoring and data acquisition.

The DAS monitors and logs data for 180 instruments that were installed in the building and includes temperature probes, thermocouples, humidity sensors, hotwire anemometers, power meters, current transducers, building pressure transducers, gas

meters, equipment status sensors, fluid flow meters. In addition, a fully operational weather station was installed on the roof of the Chesapeake Building to record outside conditions. The weather station consists of outside air temperature and humidity sensors, a barometric pressure sensor, a solar intensity sensor, a wind vane and a wind anemometer.

The DAS takes readings continuously on a one-minute interval. To avoid any loss of data, the DAS was set up for remote access and control as well as remote data backup from a remote computer.

A screen capture of the DAS monitoring window is taken every 5 minutes and posted on the BCHP web page where it is available to the public. A sample screen capture is shown in Figure 8. The monitoring window is created to post readings collected from the sensors, as well as trends for several important parameters. Temperature, humidity, building pressure, supply airflow rates, and power consumption are presented on the left portion of the screen in Figure 8. Six graphs are constructed, shown in the middle of the screen in Figure 8, to indicate two-hour histories for temperatures, humidity, power readings, and flow rates. The right portion of the screen indicates the RTU operation status sensors, VAV status sensors, and the weather data (Marantan, 2002).

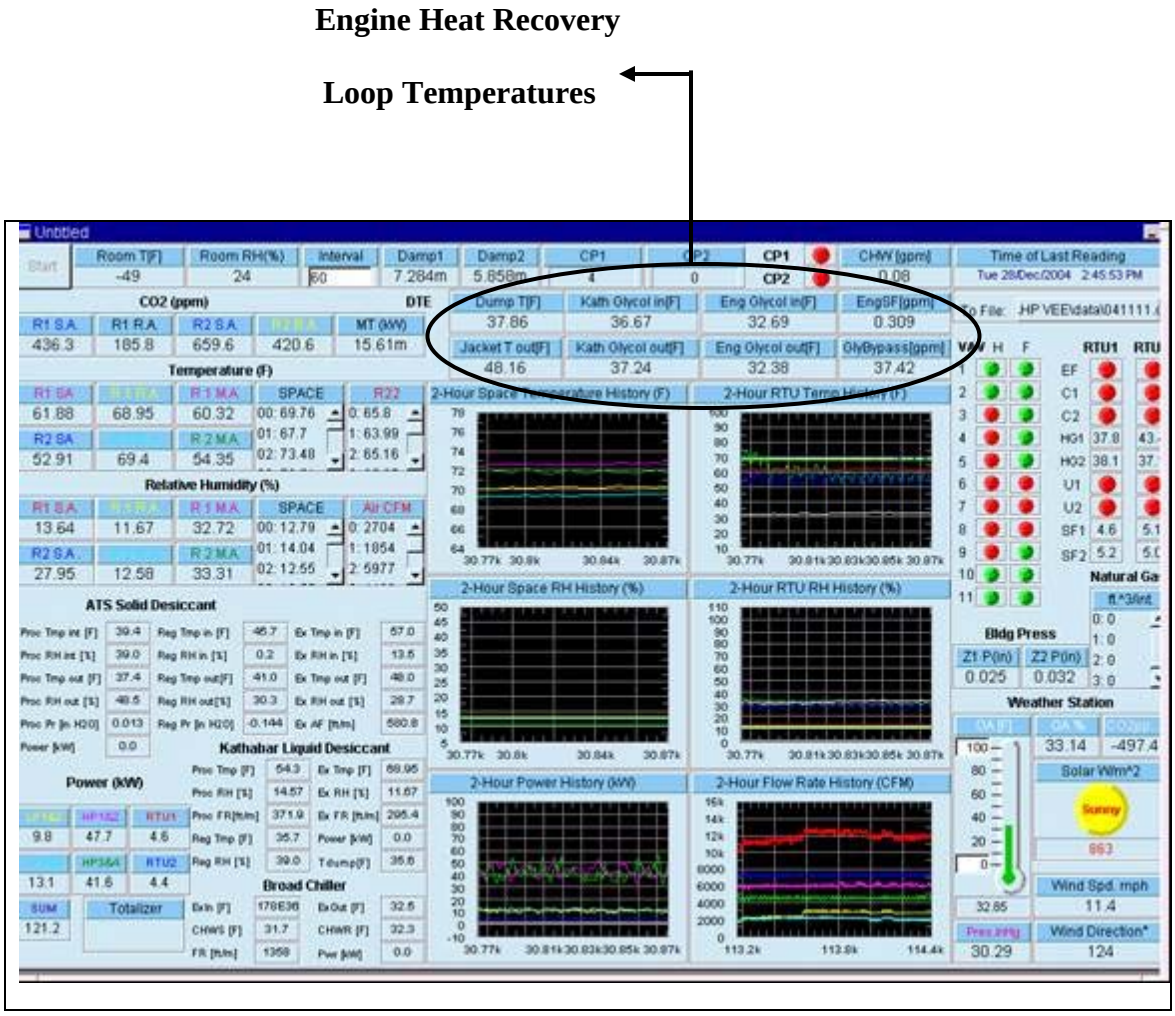

Figure 8: Data Acquisition System Monitoring Window

The data is collected in one-minute intervals by the DAS and is recorded in a file on the server. A custom developed Matlab program processes the log files, generates daily data files, and plots daily graphs as archives.

4.4 CHP System Description

As noted earlier, the four-storey Chesapeake building is divided into two heating, ventilating and air-conditioning (HVAC) zones facilitating operation of two different CHP systems for the two zones. This research focuses on the design and operation of the CHP system catering to zone 1 called as CHP system 1. Figure 9 shows the schematic layout of the system and its various components.

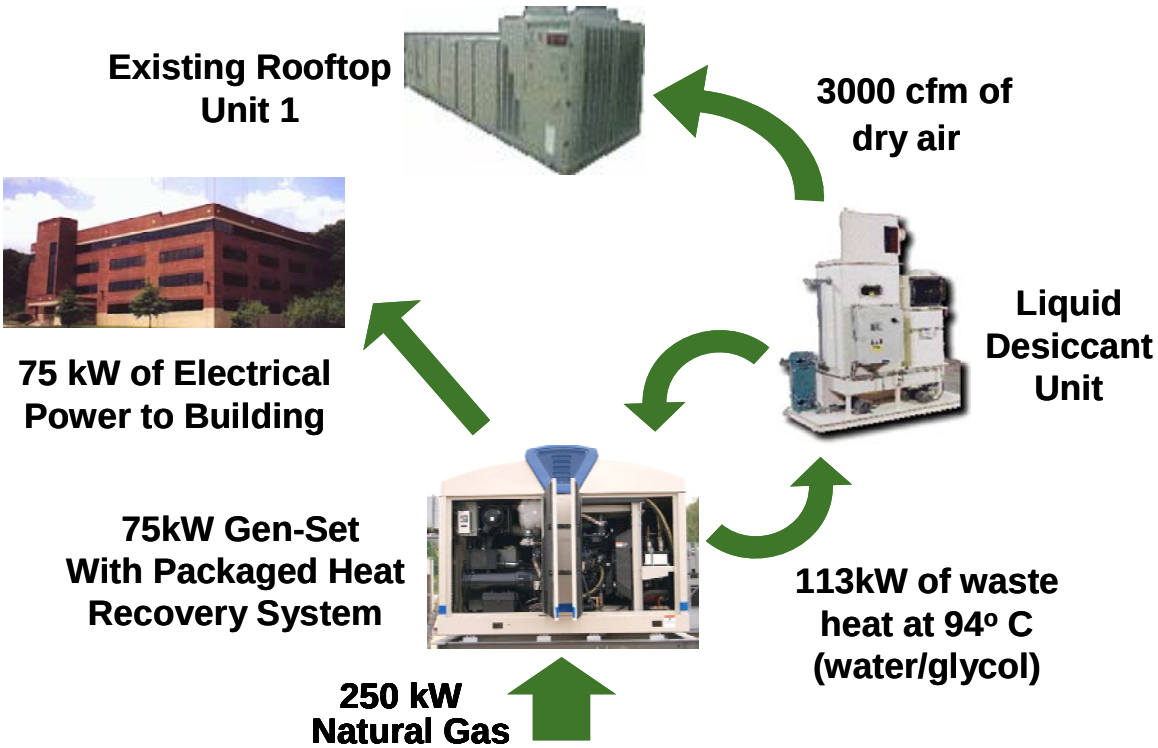

Figure 9: Schematic Layout of CHP System 1 at Chesapeake Building

Figure 9 shows a reciprocating engine generator that burns 250 kW of natural gas to produce 75 kW of electrical power that is fed parallel to the grid at the Chesapeake building. The combined waste heat from the exhaust gases and the jacket

cooling water from the engine amounting to around 113 kW is utilized in a liquid desiccant dehumidification system for regenerating the liquid desiccant. The liquid desiccant system dehumidifies 3000 cfm of moist outside air and supplies it to the mixed air chamber of the roof top unit 1 (RTU 1).

4.4.1 Reciprocating Engine Generator

The engine block, generator and the Woodward controller form the main components of the engine generator package. The engine block has eight cylinders arranged in a V shape with four cylinders in each bank. Starting at the front side of the engine block, the cylinders in the left bank are numbered 1-3-5-7 and cylinders in the right bank are numbered 2-4-6-8 (when viewed from the rear). The engine block is one piece cast iron with the cylinders encircled by coolant jackets. The engine system is cooled by capturing heat that would otherwise be wasted to the ambient air. A fluid to fluid heat exchanger and one exhaust gas to fluid heat exchanger in the engine unit capture waste heat from the unit and make that heat available for regeneration of the liquid desiccant. A load dump radiator module is employed to remove excess heat from the coolant system that is not used by the liquid desiccant system or to dissipate all the waste heat when the liquid desiccant system is not in operation.

The engine rpm of 2540 rpm is reduced to 1800 rpm to the generator by a mechanical device called the speed reducer. The speed reducer uses a duel gear drive to accomplish this reduction. Engine rpm turns an input shaft to the reducer, turning a gear that meshes to the second gear creating the reduction. Then through the output

shaft, the generator is turned. The speed reducer is connected between the engine flex plate and the generator flex plate. The generator is a 3 phase, 60 Hz, continuous duty synchronous type with output voltages of 120/208 volts and 277/480 volts. The generator is designed to produce a net electrical output of 75 kW at a power factor of 0.8 and has an electrical efficiency of 32%. The total package efficiency is around 75% when taking the thermal recovery into account.

The Woodward engine generator controller package is a microprocessor based complete generator load control and engine management package designed for use with an electronic engine speed control and a separate voltage regulator. The controller's functions include synchronizing, engine control, real and reactive load control, automatic generator sequencing and includes protective features for the engine such as over speed, high/low coolant temperature and oil pressure as well as for the generator over/under voltage and frequency, reverse power etc. Thus the controller monitors and governs the operations of the engine generator to assure consistent and efficient operation. Figure 10 shows the engine generator along with its different components.

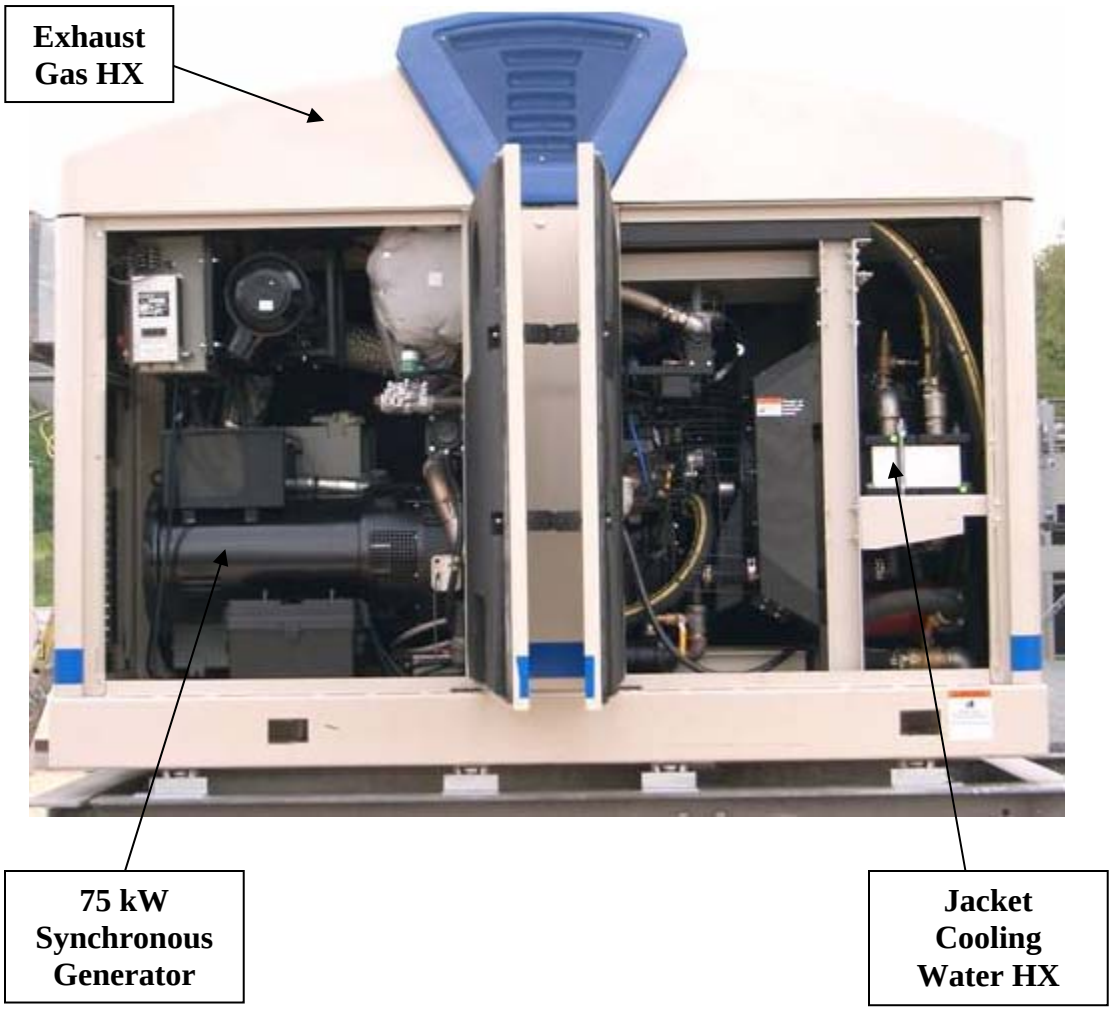

Figure 10: Engine Generator Package

4.4.2 Liquid Desiccant System

Liquid desiccants absorb moisture from or add moisture to the air, depending on the vapor pressure difference between the air and the solution. The equilibrium vapor pressure of the solution depends on its temperature and concentration. The higher the concentration and lower the temperature, higher would be the moisture absorbed.

The liquid desiccant system consists of an absorber, also called the conditioner, a regenerator, two pumps, and two heat exchangers as depicted in Figure 11. The

liquid desiccant unit uses lithium chloride (LiCl), a hygroscopic salt as its working fluid.

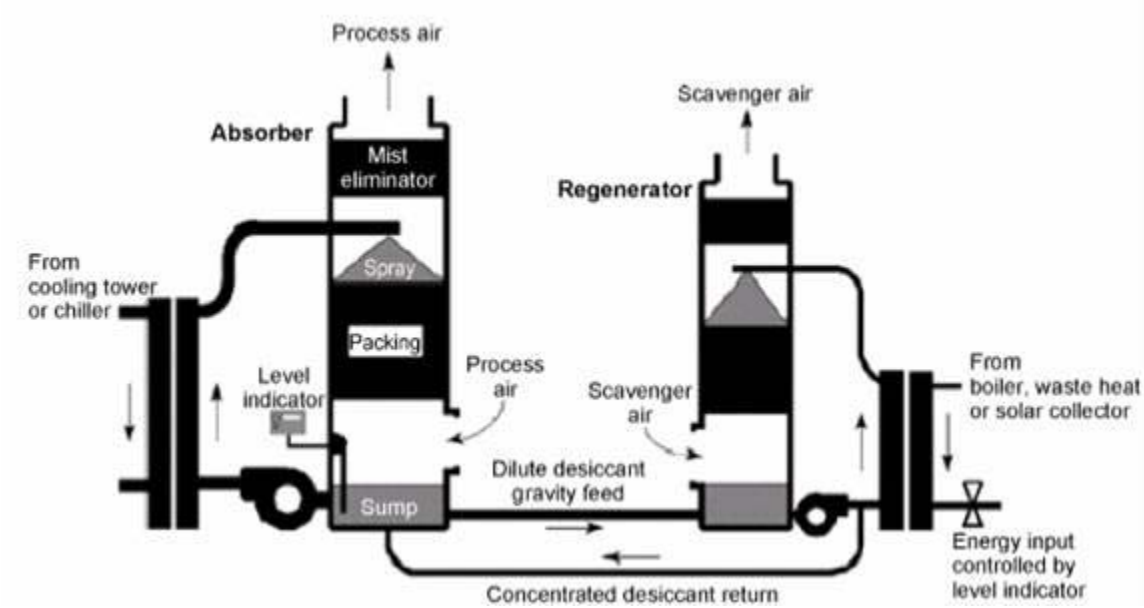

Figure 11: Configuration of Liquid Desiccant System

In the absorber, air is cooled and dried as it passes up through packing sprayed with chilled, concentrated liquid desiccant. This is called process or supply air because it is being supplied to the occupied space either directly or through the main air handler. The absorber has mist eliminators on its outlet to prevent droplets of desiccant from leaving with the process air. This is important to conserve desiccant and to prevent a corrosive or otherwise undesirable chemical from entering the ductwork.

In the regenerator, heated desiccant is sprayed down over another packing and scavenger air dries out the desiccant and carries the water, in the form of vapor, outside the building. The regenerator also has mist eliminators to conserve desiccant. In both absorber and regenerator, desiccant dripping from the packing is collected in a

sump. A gravity-feed line connects the sumps so water constantly collecting in the absorber sump naturally travels to the regenerator where it can be removed. The pumps are used to produce the sprays in the absorber and regenerator and drive the desiccant through the heat exchangers. The desiccant flow from the absorber sump to the absorber packing runs through a cooling heat exchanger. Either chillers or evaporative cooling towers can ultimately provide this cooling. The desiccant's ability to collect moisture is typically much greater than its ability to collect heat; therefore the absorber desiccant flow rate is determined by the amount of sensible cooling required by the process air. The regenerator pump serves the same purpose, but it pushes the desiccant through a heating heat exchanger. The desiccant must be heated before it will easily give up its moisture to the scavenger air. In the case of lithium chloride, 93 ºC (200 F) is a typical regeneration temperature. This is the main energy input driving the dehumidification process, and energy of this relatively low quality can be efficiently obtained from waste heat, natural gas, or solar collectors. A level indicator in the absorber sump controls this energy input. When the level in the absorber sump rises due to increased moisture load, the indicator calls for more energy input at the regenerator to maintain constant dehumidification performance. The regenerator desiccant flow rate is sized to satisfy the maximum expected dehumidification rate required by the process air. The regenerator pump also sends a small flow of concentrated desiccant to the absorber sump, completing the cycle.

An additional component that can be employed in the liquid desiccant system is the solution heat exchanger that is located between the conditioner and regenerator sections. The solution heat exchanger recovers heat from the hot, concentrated

desiccant solution leaving the regenerator for preheating the weak desiccant. Thus by using the solution heat exchanger the desiccant entering the regenerator heat exchanger would be warmer while the solution entering the conditioner heat exchanger would be a little cooler.

The waste heat activated liquid desiccant unit is attached to Roof Top Unit 1 (RTU 1) and supplies the treated outdoor air stream to RTU 1 in place of the unconditioned outdoor air originally drawn into the mixed air section. The processed desiccant air is added directly into the mixed air section while the damper from the outdoor air section of the RTU is completely closed.

The liquid desiccant system also utilizes the building air that is exhausted as the fresh outdoor air is drawn in for heat exchange since the return air is both cooler and drier than the outdoor air. This exhaust air is drawn from the return air section of the RTU through ducting that was retrofitted onto each RTU. Outdoor air could have been used for this application, but having an available stream of much cooler air allows the LiCl solution to be cooled down much further than would be possible with outdoor air. The end result is process air that is both cooler and less humid than outdoor air.

The use of building exhaust air in this desiccant unit is for heat exchange only – since the cooling tower runs on an open loop of water the building exhaust air does not come into direct contact with the desiccant material. This means that the reduced absolute humidity of the building exhaust air is not directly available to the system as it could be if it were able to be used in a direct contact heat exchange with the

working fluid, however it can be utilized indirectly since it has a lower wet bulb temperature as well.

Figure 12 shows the design parameters of the liquid desiccant system and its interconnection with the RTU1. The liquid desiccant unit consumes 9.5kW of electrical power to run pumps, fans as well as its associated cooling tower and controls.

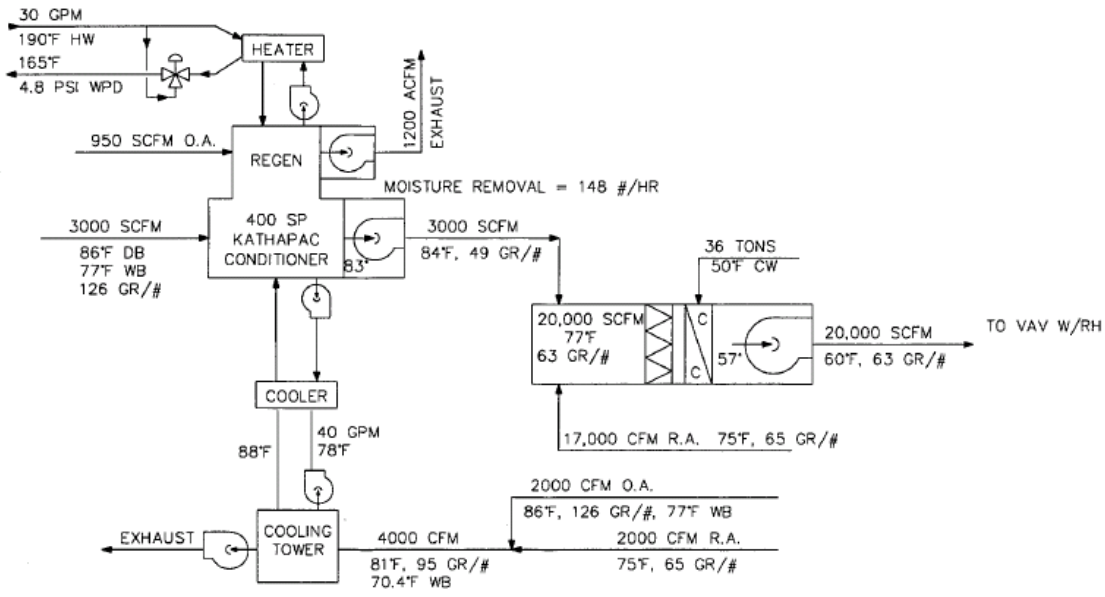

Figure 12: Design Parameters of the Liquid Desiccant System and RTU 1

4.5 Structural Platform Reinforcement

The engine generator along with the heat recovery loop consisting of the two heat exchangers and the pump comes in a single packaged unit. The weight of this unit is 2812 kg (6200 lbs) while the dump radiator module weighs around 907 kg (2000 lbs) which puts the total weight of the entire package at 3719 kg (8200 lbs)

making it quite heavy. Three different options existed for the installation of this engine generator package. The first option was to mount the engine generator and dump radiator module on the roof on an existing structural platform that were used for engine driven air conditioning units. This structural frame that was previously designed by a structural firm however was designed to handle a maximum load of 2268 kg (5000 lbs). Second option was to mount the engine generator package on the same structural platform as the liquid desiccant and solid desiccant systems. The combined weight of these two desiccant units is around 5443 kg (12000 lbs) while the structure was able to support a payload of 6804 kg (15000 lbs) at the most. Thus both the options required additional structural reinforcement to sustain the weight of the new engine generator package safely. The third and the last option were to install the engine generator and the dump radiator module on the ground. However this meant that the heat recovery piping for the ethyl glycol solution would have to be run through four floors to the roof since the liquid desiccant unit was already mounted on the roof. This would result in high heat loss in the long pipelines and the amount of heat finally supplied to the liquid desiccant unit might fall short of its design conditions. Moreover the ethylene glycol solution pump in the heat recovery loop of the engine generator is a two HP pump and can handle a maximum of 30 feet of head and hence would require a booster pump or another pump in series to pump the ethylene glycol solution all the way up to the roof.

Weighing all the three options, it was decided to go with the second option to reinforce the desiccant unit platform for the following reasons:

- The design cost of the desiccant unit platform was lower than the engine driven air conditioning unit structural frame.
- Since all the three components of the new CHP system 1 viz; engine generator, dump radiator and liquid desiccant system would on the same platform, the piping required between them would be at the minimum avoiding huge pipe heat losses as well as allowing to use single available solution pump.

The design analysis was done by a structural engineering consultant and nine additional beams were welded at locations specified in the design as part of the reinforcement.

4.6 Thermal Recovery Package of Engine Generator

As was previously mentioned, the engine generator consists of a plate and frame type heat exchanger to collect heat from the engine jacket cooling liquid as well as an air to fluid type heat exchanger to recover the heat from the exhaust gases. Figure 13 shows the thermal recovery package.

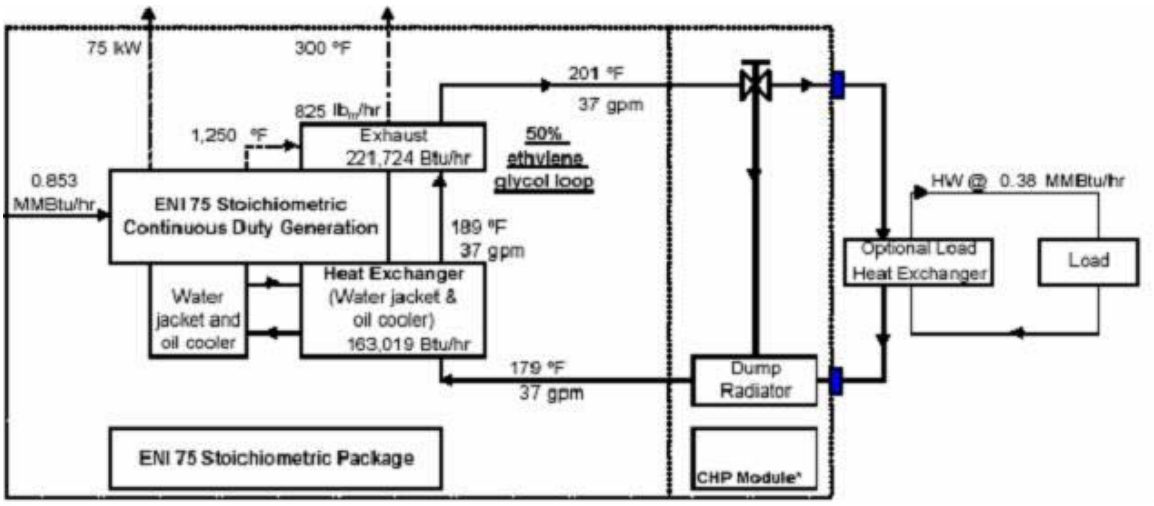

Figure 13: Thermal Recovery Package of Engine Generator

It can be seen from fig. 14 that the engine burns about 250 kW (853,000 Btu/hr) of natural gas to produce 75 kW of electrical power which is supplied to the Chesapeake building. The exhaust gas leaving the engine at a high temperature of 677 ºC (1250 ºF) then enters a heat exchanger where it exchanges heat with the ethylene glycol solution (50:50). The amount of heat recovered from the exhaust gases is around 65 kW (222,000 Btu/hr) while the waste heat recovered from the water jacket and oil cooler heat exchanger is about 48 kW (163,000 Btu/hr). Thus the ethylene glycol solution gets heated to 87 ºC (189 ºF) when it first passes through the water jacket and oil cooler heat exchanger and is finally heated to 94 ºC (201 ºF) after utilizing the exhaust gas heat. This heat is then used in the regenerator of the liquid desiccant system (this part is shown as optional load heat exchanger in fig.14) before it is returned back to the engine at 82 ºC (179 ºF). A three-way control valve directs any excessive heat to the dump radiator which though a separate heat exchanger module, is a part of the heat recovery loop.

Thus comparing with the design heat requirement of the liquid desiccant unit of 104 kW (355,000 Btu/hr), the total waste heat recovered from both the exhaust gases and jacket water heat exchangers of the engine generator is around 113 kW (385,000 Btu/hr). Also this heat is supplied to the liquid desiccant system at 94 ºC (201 ºF). Hence it can be seen that there exists a pretty good thermal match between the engine generator and the liquid desiccant system.

4.7 Design of Heat Recovery Loop

This section discusses the design of the heat recovery loop which is critical to the safe operation of the engine generator as well as the liquid desiccant system. It can be seen from Figure 13 that the flow rate of the ethyl glycol solution supplied from the engine generator is 2.3 x 10^{-3} m^3/s (37 gpm). However, the regenerator plate and frame heat exchanger of the existing liquid desiccant system is designed to handle a flow rate of only 1.9 x 10^{-3} m^3/s (30 gpm). This would have required modifying the liquid desiccant system to cope with more flow by increasing the number of plates of the plate and frame heat exchanger of the regenerator section. Also, the current pressure drop on the glycol side of the plate and frame heat exchanger of the regenerator is 33 kPa (4.8 psi) while according to the requirements specified by the engine generator manufacturer, the maximum pressure drop needs to be within 19 kPa (2.7 psi). To keep the modifications to the existing equipment at a minimum and at the same time achieve the desired performance, a new heat recovery loop scheme was designed. The schematic diagram of this heat recovery loop

between the engine generator and the liquid desiccant unit is shown in Figure 14. It can be seen that the return temperature of the ethyl glycol solution to the engine is set at 82ºC (179ºF). This is a critical parameter and this temperature should never go below 82ºC (179ºF), otherwise there is a possibility of running the engine too cold and eventually damaging the engine. On the other hand the liquid desiccant unit accepts or rejects heat based on the level of LiCl solution in the regenerator. At reduced moisture loads the regenerator cannot use all the heat that the engine supplies it with and care needs to be taken to see that the unit does not over regenerate, otherwise it would result in crystallization of the LiCl solution when the outside air humidity falls below design. Hence the controls of the heat recovery loop are based on the liquid level in the regenerator and the inlet temperature of the ethylene glycol solution to the dump radiator. This temperature would always be maintained at 83ºC (182ºF) since the solution would suffer some temperature drop as it passes through the dump radiator and the return temperature can still be maintained at 82ºC (179ºF).

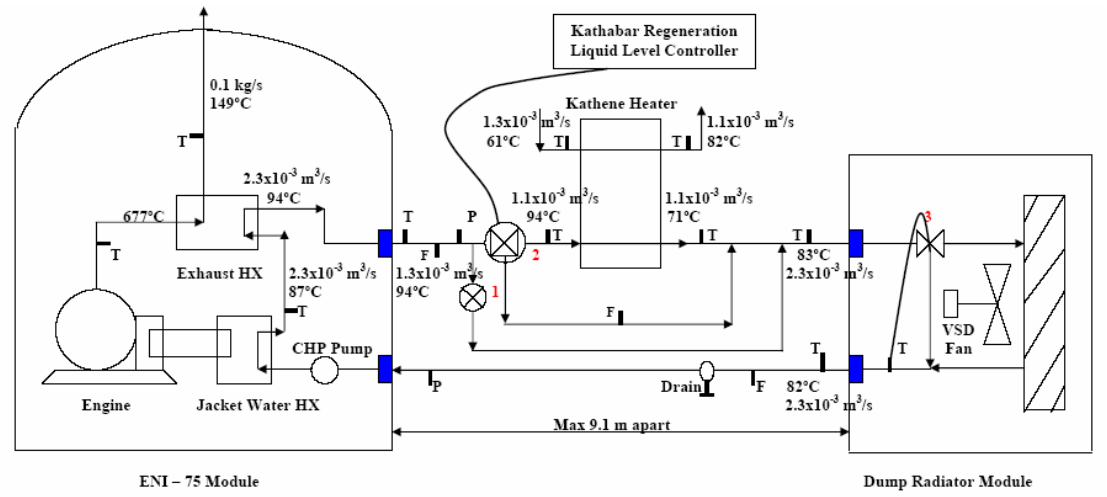

Figure 14: Process and Instrumentation Diagram for CHP System 1

The heat recovery loop schematic in Figure 14 shows three valves that are used to control the two control points described above. Valve 1 is a manual ball type valve that is adjusted to bypass 1.3 x 10^{-3} m^3/s (20 gpm) flow to the dump radiator, whenever the liquid desiccant system is in operation. Valve 2 is a 3-way control valve already installed for the liquid desiccant system. It modulates the flow through the regenerator heat exchanger based on the regeneration liquid level. So when the liquid desiccant unit does not require heat, this valve bypasses the regenerator and all the flow goes to the dump radiator. When the liquid desiccant requires heat, valve 2, at maximum opening will allow 1.1 x 10^{-3} m^3/s (17 gpm) at 94ºC (201ºF) to flow through the regenerator heat exchanger while the remaining 1.3 x 10^{-3} m^3/s (20 gpm) of flow at 94ºC (201ºF) passes through a bypass line to the inlet of the dump radiator where it combines with the 1.1 x 10^{-3} m^3/s (17 gpm) solution leaving the liquid desiccant unit at 70.5ºC (159ºF) during steady state conditions. Thus 2.3 x 10^{-3} m^3/s

(37 gpm) of flow is maintained to the dump radiator at 83ºC (182ºF). Valve 3 is the 3-way control valve, which modulates the flow across the dump radiator based on the return temperature to the engine and maintaining it at 179ºF and is supplied with the dump radiator module. Thus with this design, the maximum pressure drop in regenerator heat exchanger on glycol side is 9 kPa (1.3 psi) under the above conditions which is well within the specified requirements of the engine manufacturer of 19 kPa (2.7 psi). Figure 14 also shows the locations of the different temperature (T), pressure (P) and flow (F) sensors in the heat recovery loop.

4.8 Electrical Interconnection

Though the engine generator model can be either connected parallel to the grid or used as a stand alone generator, independent of the grid, for the CHP system designed, it was connected parallel to the grid at the Chesapeake building. Figure 15 shows the electrical layout in the electrical room of the Chesapeake building prior to the integration of the new 75 kW engine generator. The building receives 13.8 kV from the main campus sub-station and is dropped down to 480 V through a transformer that's situated outside the electrical room. In the electrical room, the main switch board distributes the voltage to the different loads of the building such the RTU's high voltage panels and low voltage panels.

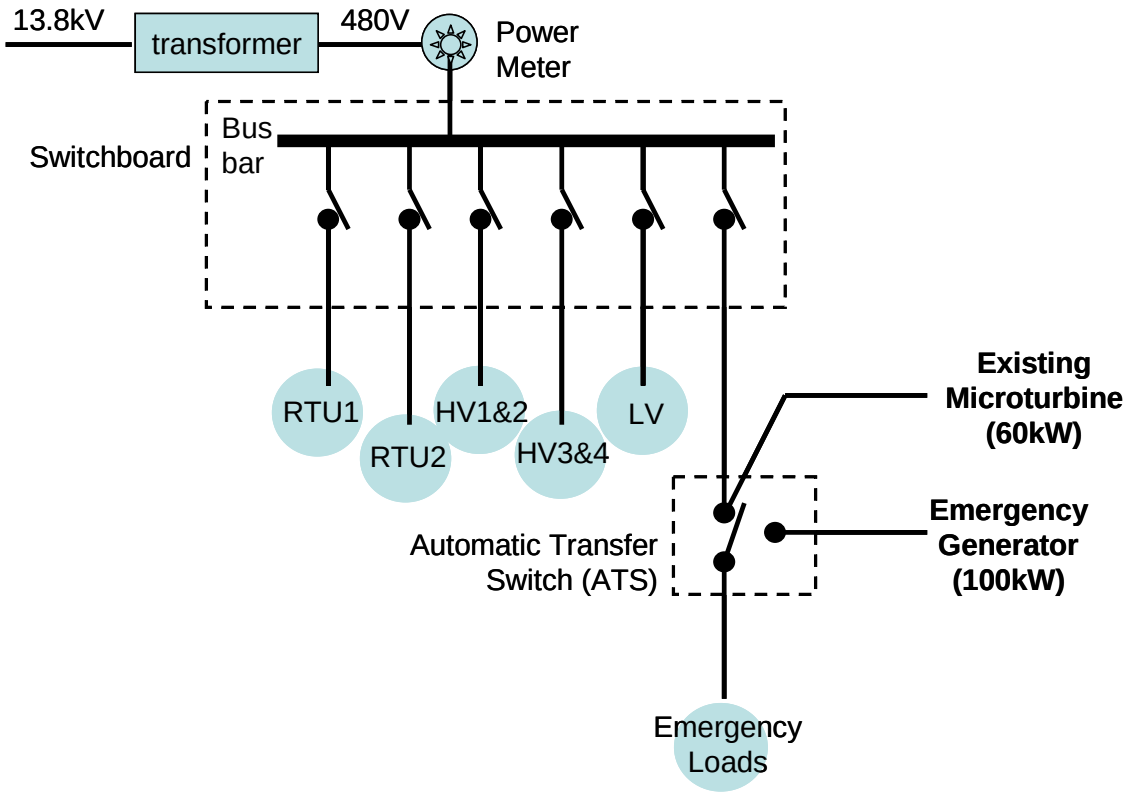

Figure 15: Previous Electrical Layout at Chesapeake Building

The building also has a 100 kW emergency engine generator that handles life safety loads in case of a power outage. The emergency loads are connected to the main bus bar via an Auto Transfer Switch (ATS). Whenever the grid goes down, the ATS gets disconnected from the main grid and the emergency generator kicks in to handle the emergency life safety loads of the building. Also CHP system 2 operating for zone 2 of the building has a 60 kW Capstone microturbine that was connected parallel to the grid through the ATS in the earlier configuration.

During the integration of the new 75 kW engine generator, several issues were raised by the facilities management and Trigen Cinergy Solutions that operates the campus 27 MW cogeneration plant at University of Maryland that warranted

changing the existing electrical connections of CHP system 2. One of the main concerns raised was the direct connection of the 60 kW Capstone microturbine on the normal side inside the ATS. There cannot be two generators operated in the same auto transfer switch. Figure 16 shows the new electrical layout that was designed according to electrical codes and standards laid down at the University of Maryland, College Park.

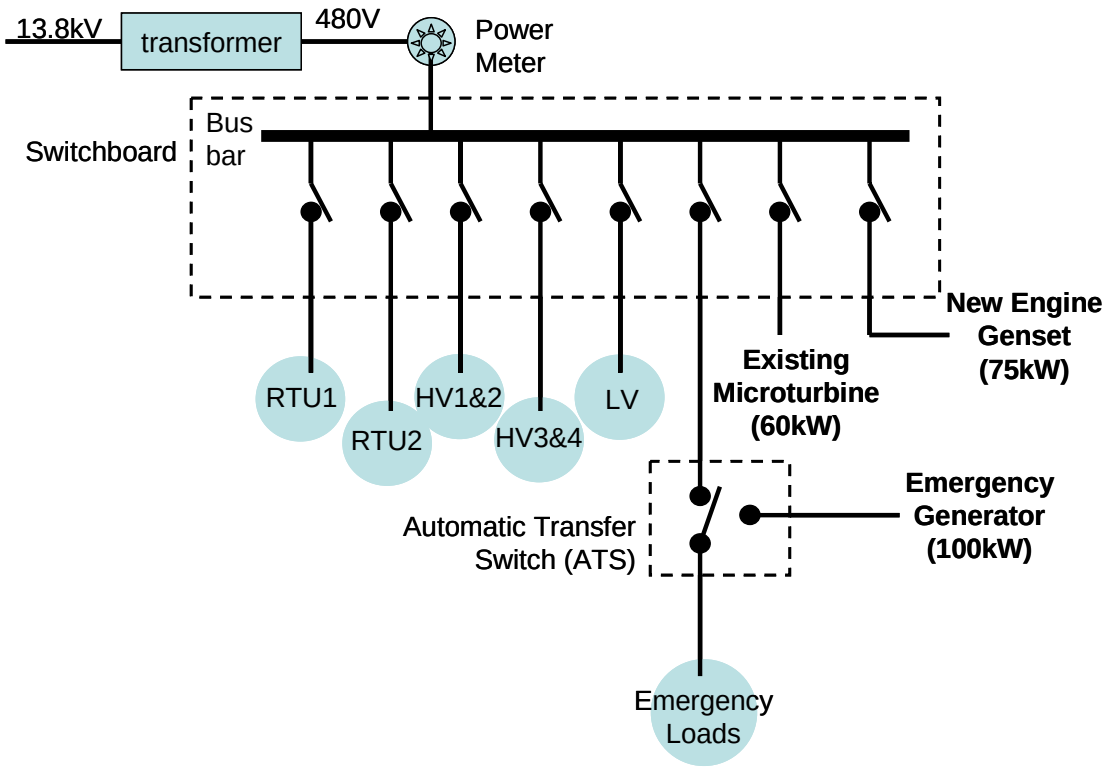

Figure 16: New Design of Electrical Layout at Chesapeake Building

It can be seen from Figure 16 that in the new design the 60 kW microturbine was disconnected completely from the auto transfer switch and connected to the main bus bar directly through a 110 Ampere circuit breaker. The new 75 kW engine

generator was connected to the switchgear using a 125 Ampere circuit breaker. Both the breakers are equipped with Under Voltage (UV) shunt trips.

Figure 17 shows the schematic design of the utility interface panel and its electrical connections to the main switchgear. The utility interface panel consists of the Sepam relay that provides protective functions to monitor and protect the engine generator from over and under voltage, over and under frequency and reverse power or back - feeding the grid. The power to the utility interface panel is drawn directly from the main switchgear.

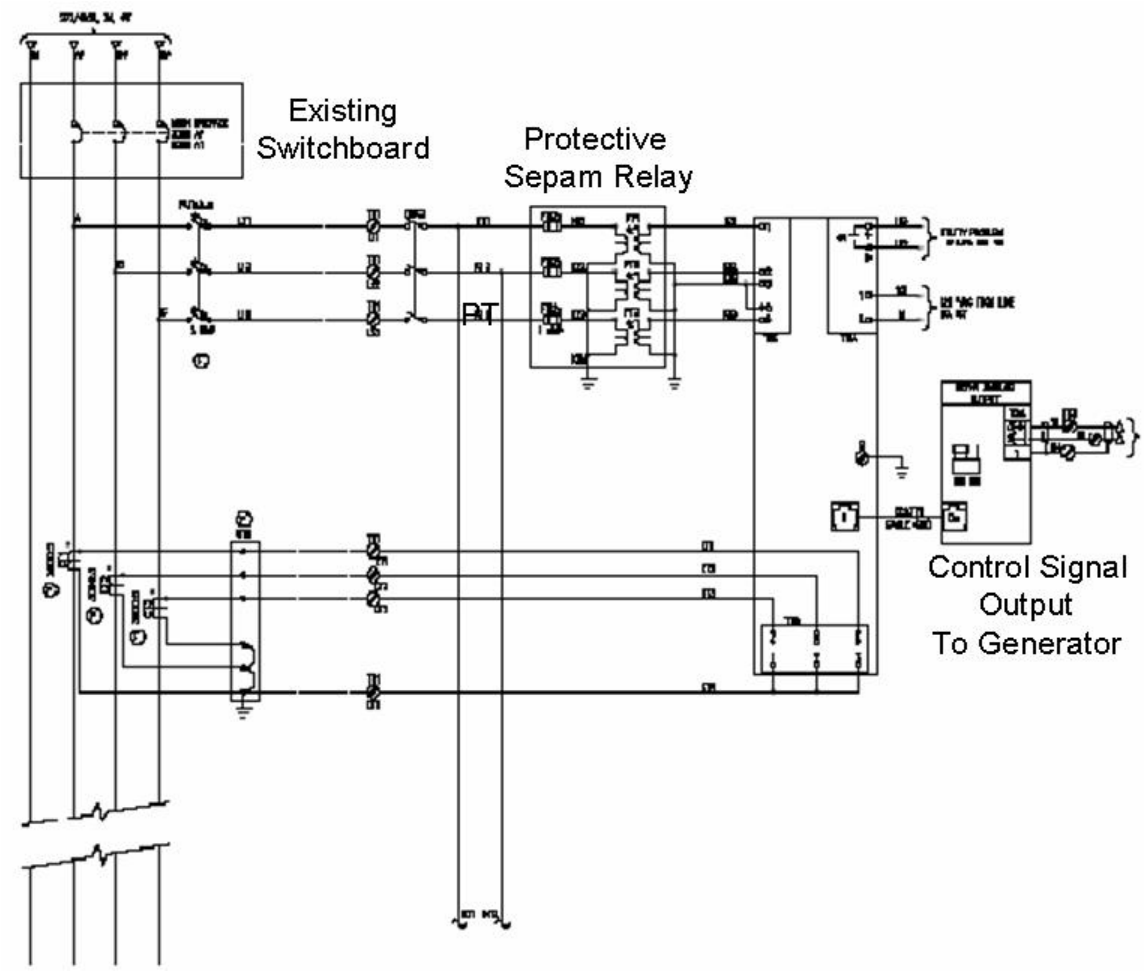

Figure 17: Design of Utility Interface Panel

The control signals from the utility interface panel are in turn sent to the microprocessor based wood ward controller inside the engine generator. Thus when the utility grid is present, at full load or base load, the engine generator would be supplying 75 kW and the microturbine 60 kW of electrical power to the grid. Hence the building will be drawing 135 kW less power from the utility, thus saving in utility electrical costs. However when the grid goes down as would happen in a power outage scenario, the trip signal would be sent from the Sepam relay in the utility interface controller to the package circuit breaker inside the generator on the roof that would disconnect the generator from the building. Also at the same instant, the protective relay opens the 110 A and 125 A circuit breakers for the microturbine and engine generator respectively in the electrical room resulting in shutdown of the two prime movers. As the electrical power for the utility interface panel is provided through the main grid, an uninterrupted power supply (UPS) is housed inside the utility panel that charges as long as the grid is present. In the event of grid failure the UPS supplies the power to the Sepam relay so that it is capable of sending the signals to the circuit breakers in the electrical room and on the roof.

In a real world scenario, a CHP system is meant to be operating in the case of power outages. However for this research project, it was required to have such detailed and complex electrical interconnection for the following reasons:

- The engine generator and the microturbine are not designed to support the entire electrical load of the building which is around 200 kW on an average.

- Secondly as this is a research project, the CHP system needs to be shutdown for maintenance purposes and the building shouldn't suffer during the time the systems are not working.
- Last but the most important reason is safety. In the event of a grid failure the microturbine and engine generator shouldn't be energizing the grid when an electrical operator is working on it.

In the earlier electrical connection the power wires from the microturbine to the ATS in the electrical room were enclosed in an underground conduit that was a spare conduit for the 100 kW emergency generator which was objected to by the facilities management and hence was taken out during the installation of new conduits. Figure 18 shows the plan of the electrical room along with different conduits.

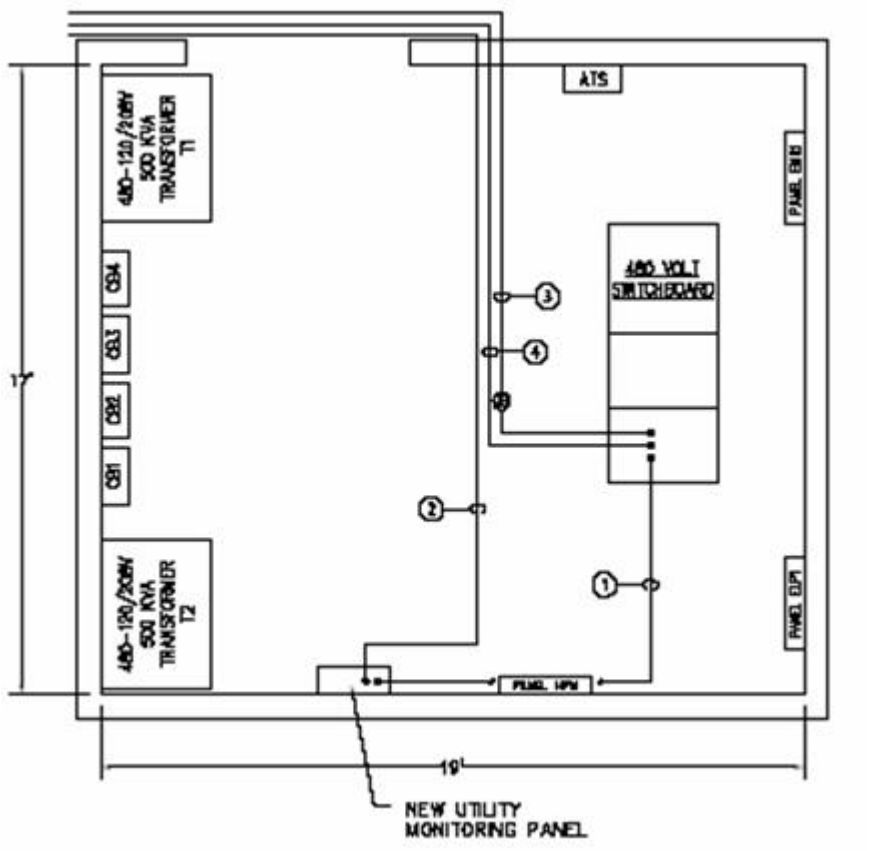

Figure 18: Conduit Layout in the Electrical Room

The various wires in the conduits and their purpose are explained in Table 4 along with the respective size of the conduits.

Table 4: Different Conduits and Wires Installed in the Electrical Room of Chesapeake Building

Conduit No.	From	To	Wires	Conduit Size
1	Switchboard	Utility Interface Panel	PT and CT Leads, UV Trips	1”
2	Utility Interface Panel	75 kW Engine Generator	Utility fault and kW signal, Circuit breaker interlock, SOC panel communications	1”
3	Switchboard	60 kW Microturbine	Power wires	1.5”
4	Switchboard	75 kW Engine Generator	Power wires, Battery charger power	2”

Figure 19 shows the conduit layout on the roof for the engine generator. A 1” signal conduit consists of all the control wires pulled from the electrical room to the microprocessor based Woodward controller inside the engine generator. The power wires from the engine generator to the main switchgear in the electrical room are enclosed in a 2” conduit.

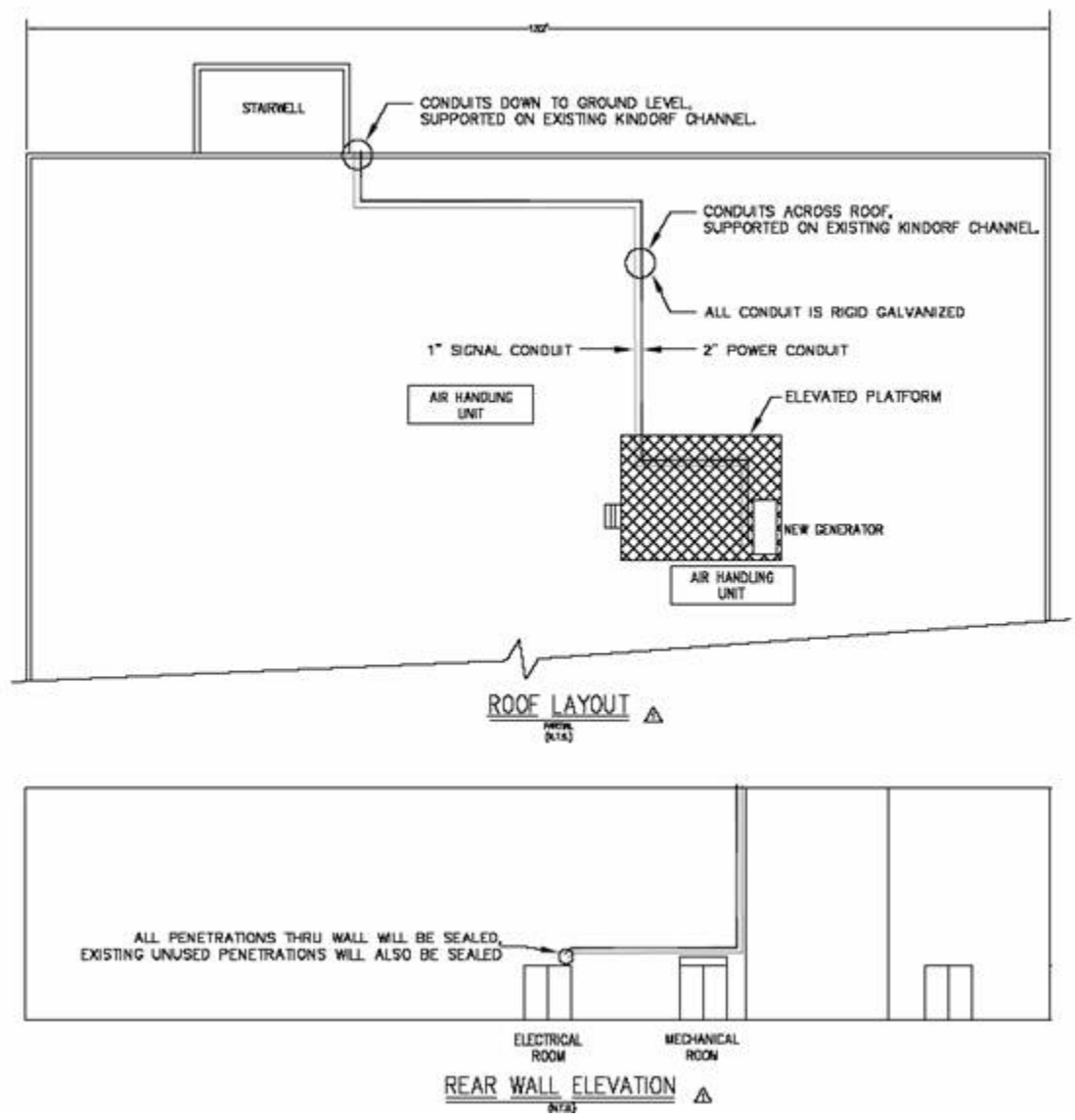

Figure 19: Conduit Layout on the Roof of the Chesapeake Building

Chapter 5: Experimental Results

5.1 Building Electrical Load

After finishing the electrical interconnection of the engine generator with the grid and the integration of the engine heat recovery loop with the liquid desiccant unit, the CHP system was operated and tested over a range of ambient temperature and humidity ratios as well as under full load and part load conditions. Figure 20 depicts the electrical load profile of the Chesapeake building for a typical weekday in the winter period (December 21, 2004). The minimum ambient air temperature on this day was -8.5 ºC. The data was sampled every minute. The maximum electrical load was around 225 kW on this day. The heating load is the major component of the total electrical demand of the building during winter times.

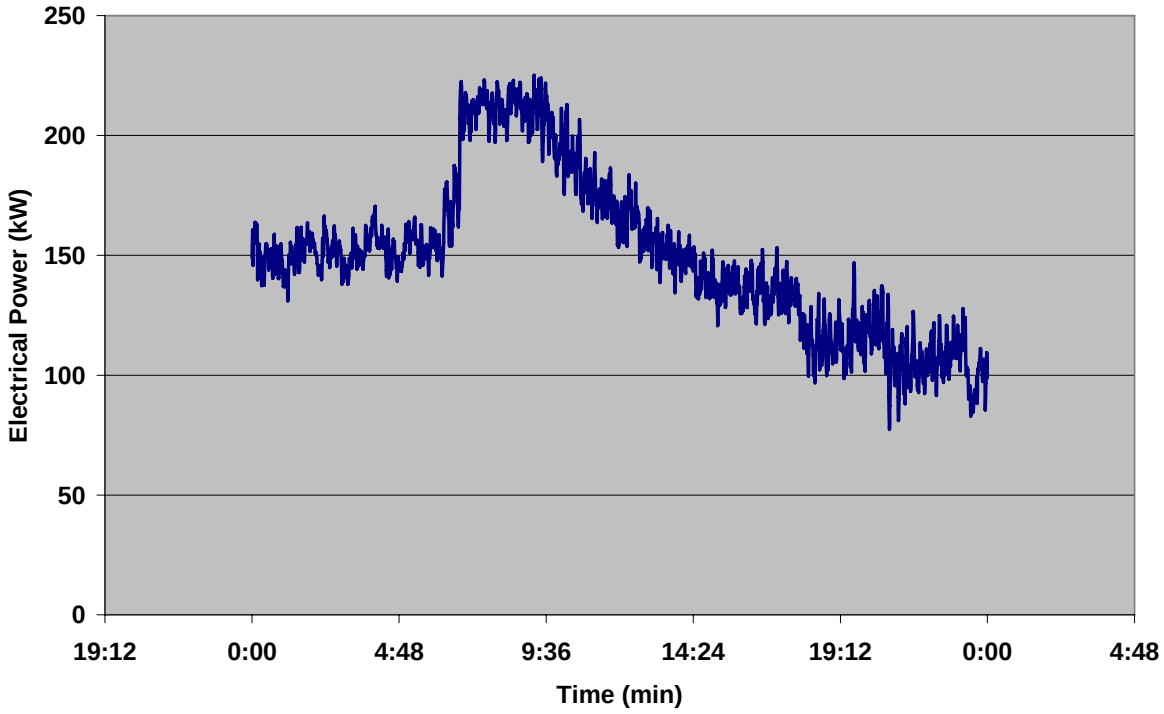

Figure 20: Electrical Load Profile of Chesapeake Building on a Typical Weekday in Winter

Figure 21 shows the 24 hour electricity load profile of the Chesapeake building for a weekday on a typical hot and humid day in summer (June 13, 2005). The maximum electrical demand was around 284 kW during the day while the minimum electrical load was about 59 kW at night. The maximum outdoor air temperature on this day was about 31 ºC while the maximum humidity ratio was around 16 g/kg.

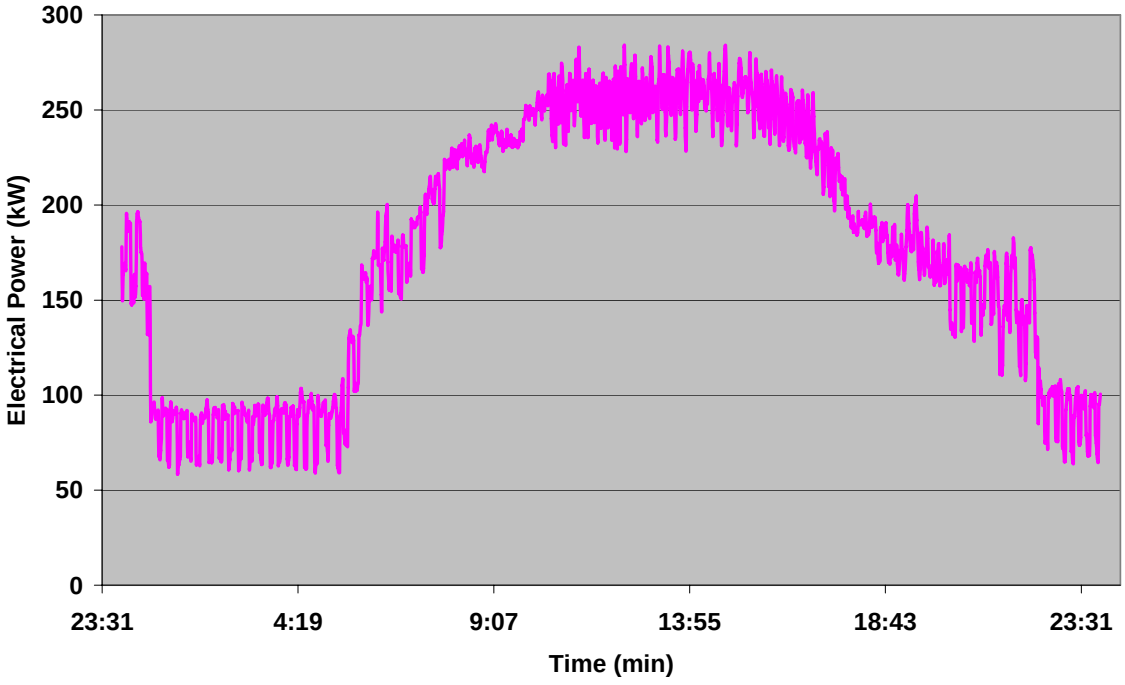

Figure 21: Electrical Load Profile of Chesapeake Building on a Typical Weekday in Summer

Figure 22 shows the sharing of the electrical power between the engine generator and the utility in order to satisfy the total electrical demand of the building. The data analyzed here was again on June 13, 2005. The engine was run at full load of 75 kW and it can be seen from Figure 22 that the power drawn from the utility decreases as a result of this proving that the controls for the electrical interconnection are working perfectly fine. The fluctuations in the graph occur due to the cycling of the compressors in the two roof top units. The amount of energy cost savings depend on the time of operation of the engine generator and the peak demand charges charged by the respective utility company.

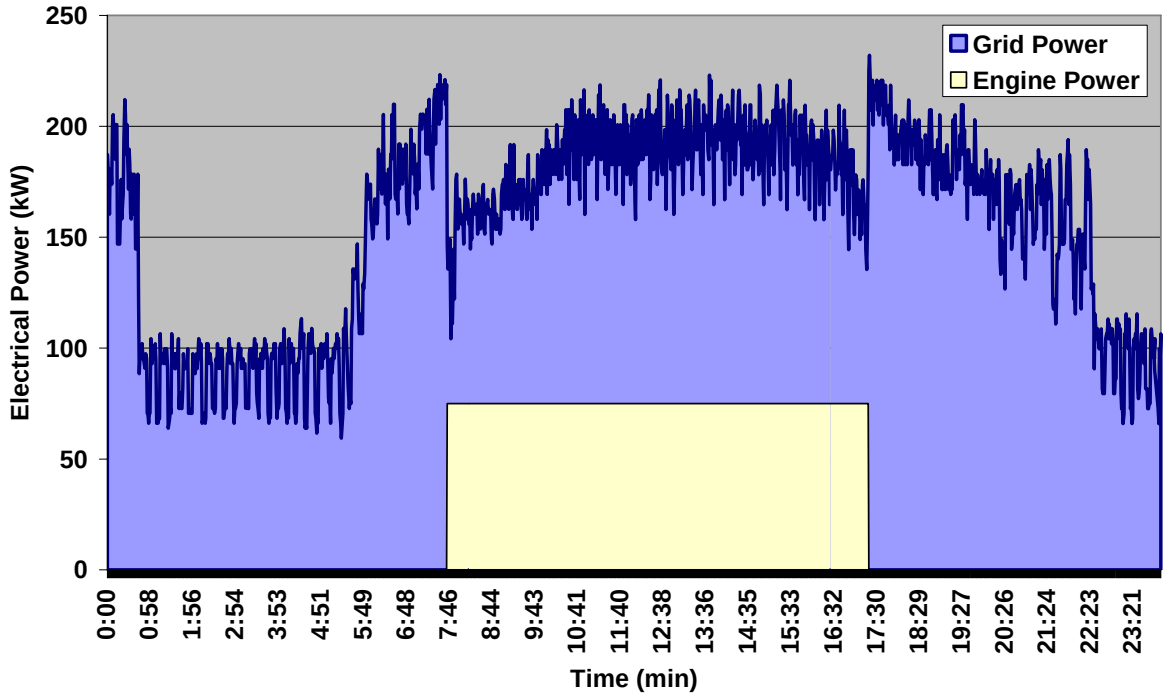

Figure 22: Utility and Engine Electrical Power Profiles

Power meters are located at various locations inside the electrical room to measure the total electrical power required by the building. High voltage power, low voltage power, RTU1 and RTU 2 power are measured and added to determine the total electrical load of the Chesapeake building. Figure 23 shows the total power measured in the above manner and the electrical power monitored by the building utility power meter on Tuesday, October 19, 2004. The engine generator was not run on this day. It is seen from Figure 23 that the power recorded from the building power meter is always greater than the total power measured by the different power meters. This difference is the power that is drawn by the emergency circuits to take care of life safety loads in the building including the elevator load that is fed by a different circuit than the ones monitored above.

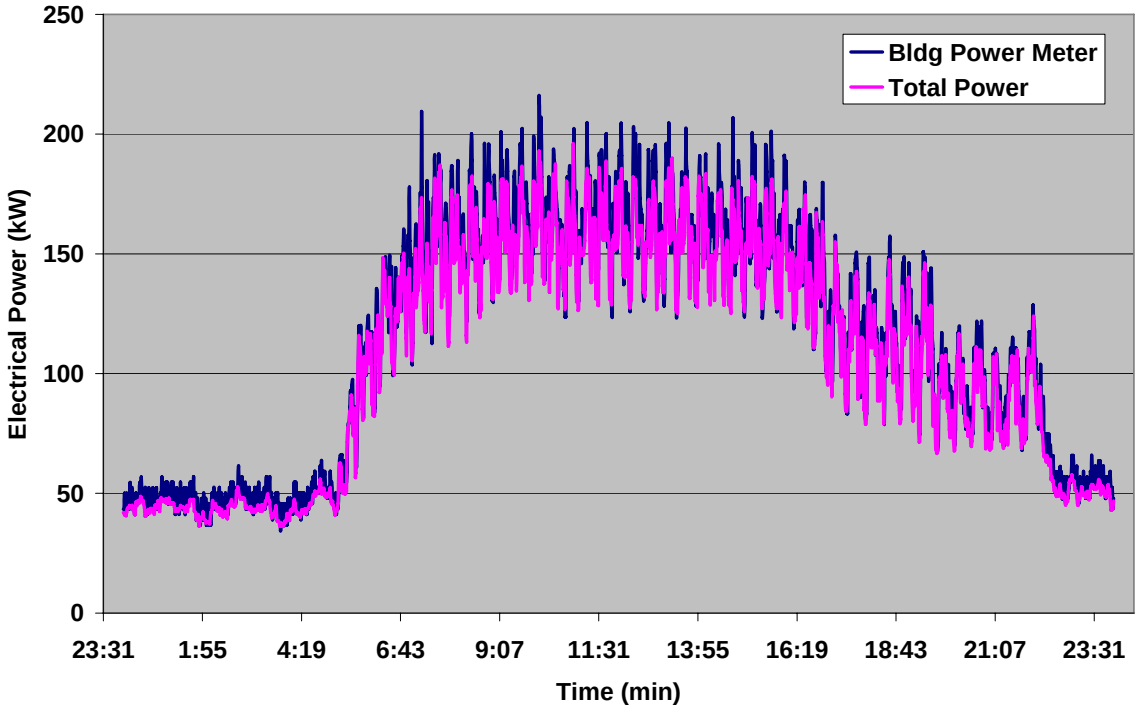

Figure 23: Comparison between Measured and Total Electrical Power

Figure 24 shows the average emergency electrical load on an hourly basis on October 19, 2004 at the Chesapeake building. The maximum emergency load (average per hour) was 10.3 kW while the average emergency load was 6.1 kW. However the peak emergency load calculated at an instant (on a minute basis) was around 50 kW.

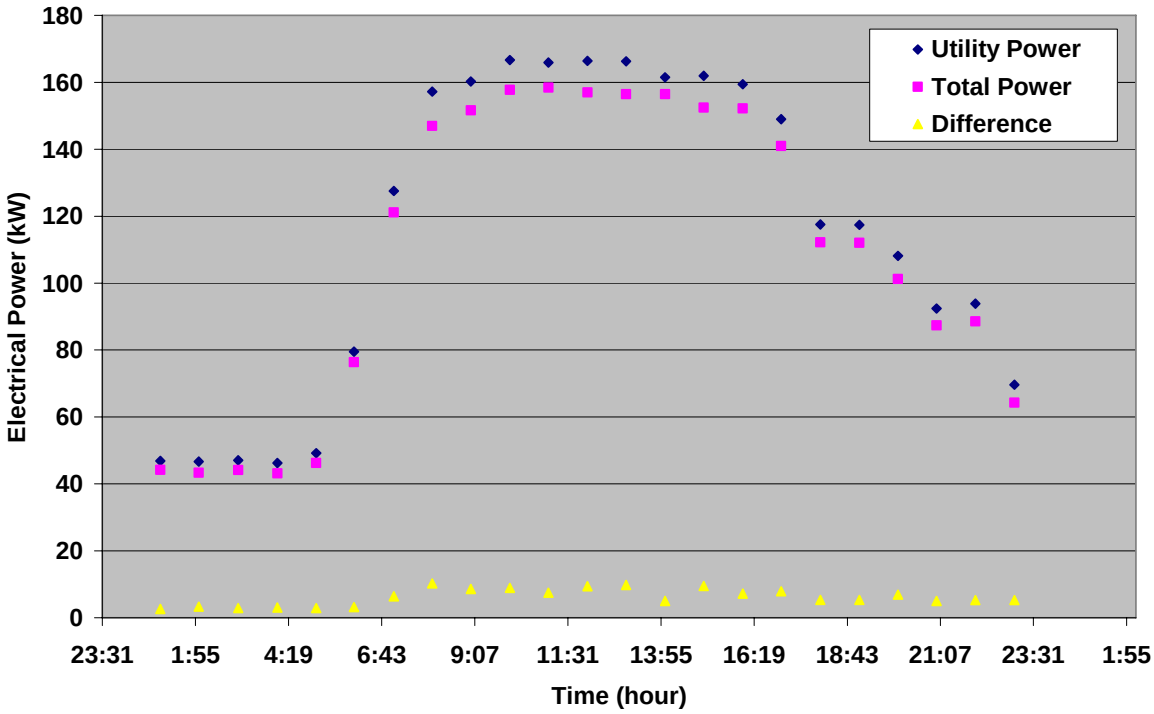

Figure 24: Hourly Emergency Electrical Load Profile of Chesapeake Building

5.2 Heat Recovery Loop Temperatures

The ethyl glycol heat recovery loop temperatures are measured at the inlet and outlet of the engine and liquid desiccant system respectively as well as at the inlet to the dump radiator module and outlet of the jacket water heat exchanger. Figure 25 shows the engine supply, engine return and jacket water heat exchanger outlet ethyl glycol temperatures when the engine was running at base load of 75 kW on August 03, 2005. It is seen from Figure 25 that the engine supply glycol temperature was around 93 ºC (200 F), while the engine return glycol temperature was about 86 ºC

(188 F) and the glycol temperature recorded at the outlet of the jacket water heat exchanger was around 82 ºC (180 F). These measured heat recovery loop temperature values are close to the design specifications of the engine generator provided by the manufacturer. Thus the experimental results are in good agreement to the design values of the engine generator heat recovery package.

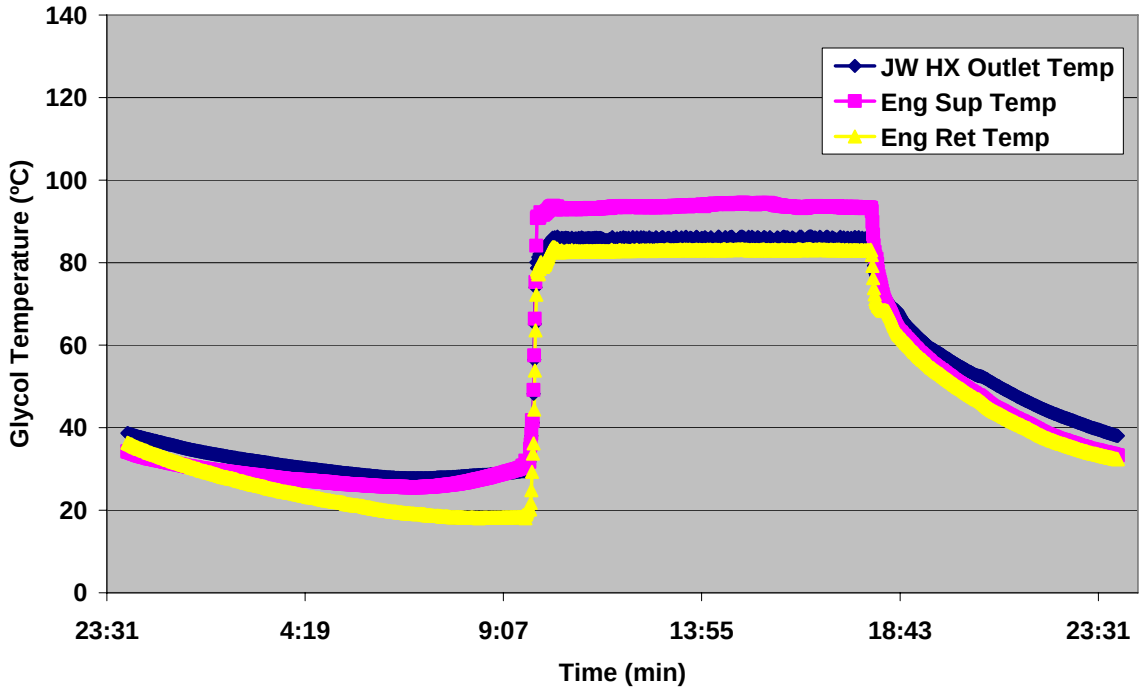

Figure 25: Engine Heat Recovery Loop Temperatures

In order to characterize the part load performance of the engine generator, it was run from 75 kW to 40 kW by reducing it in steps of 5 kW each time. The engine generator was not operated below 40 kW since it was recommended by the engine manufacturer not to do so. The engine generator was run at part load in both winter and the summer season to also determine the effect of outdoor air conditions on the engine generator performance. Figure 26 shows the engine return temperature at full load and part load conditions during winter. The engine return temperature refers to

the temperature of the 50:50 ethylene glycol – water solution that returns back to the engine after it has been cooled by the dump radiator module. For evaluation purposes only the steady state portion of the plot has been shown here rather than the entire 24 hour plot as was described in Figure 25. The fluctuations seen in the plots shown in Figure 26 and in all the figures discussed in this chapter are due to the constant changing in the ambient air conditions.

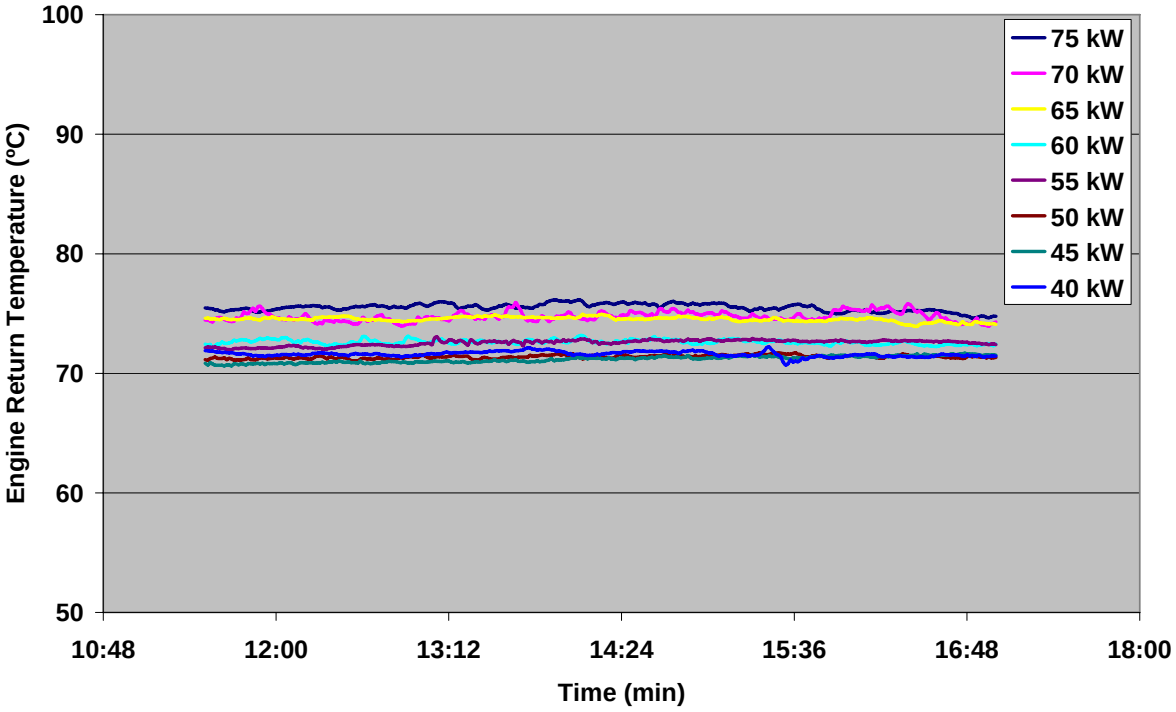

Figure 26: Engine Return Temperature at Different Engine Generator Loads during the Winter Season

Figure 27 shows the reduction in engine return temperature when the engine generator load was changed from 75 kW to 40 kW. It is observed from Figure 27 that the engine return temperature dropped from 75 ºC at 75 kW to about 71 ºC at 40 kW which is not a high temperature difference.

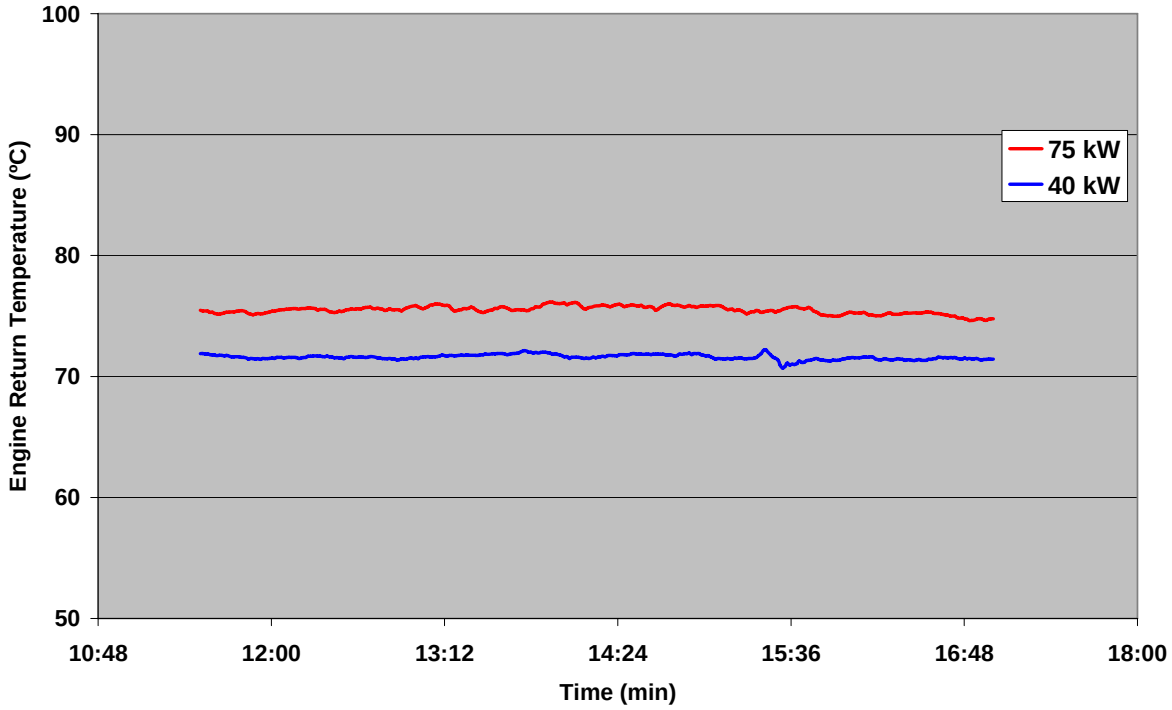

Figure 27: Comparison of Engine Return Temperature at 75 kW and 40 kW during the Winter Season

Table 5 summarizes the average engine return temperatures at different part loads during the winter time along with the ambient air conditions and the day when the data was analyzed.

Table 5: Engine Return Temperature and Outdoor Air Conditions at Part Load during Winter Season

Engine Generator Load (kW)	Day System was Run	Average Engine Return Temperature (°C)	Average Outdoor Air Temperature (°C)	Average Outdoor Air Enthalpy (kJ/kg)
75	11/30/2004	75	10	20
70	12/03/2004	74	8	14
65	12/10/2004	74	10	27
60	12/15/2004	72	1	5
55	12/16/2004	72	5	9
50	12/20/2004	71	-7	-6
45	12/21/2004	71	0.3	3
40	12/23/2004	71	13	34

Figure 28 shows the engine return temperature at full load and part load conditions during the summer season.

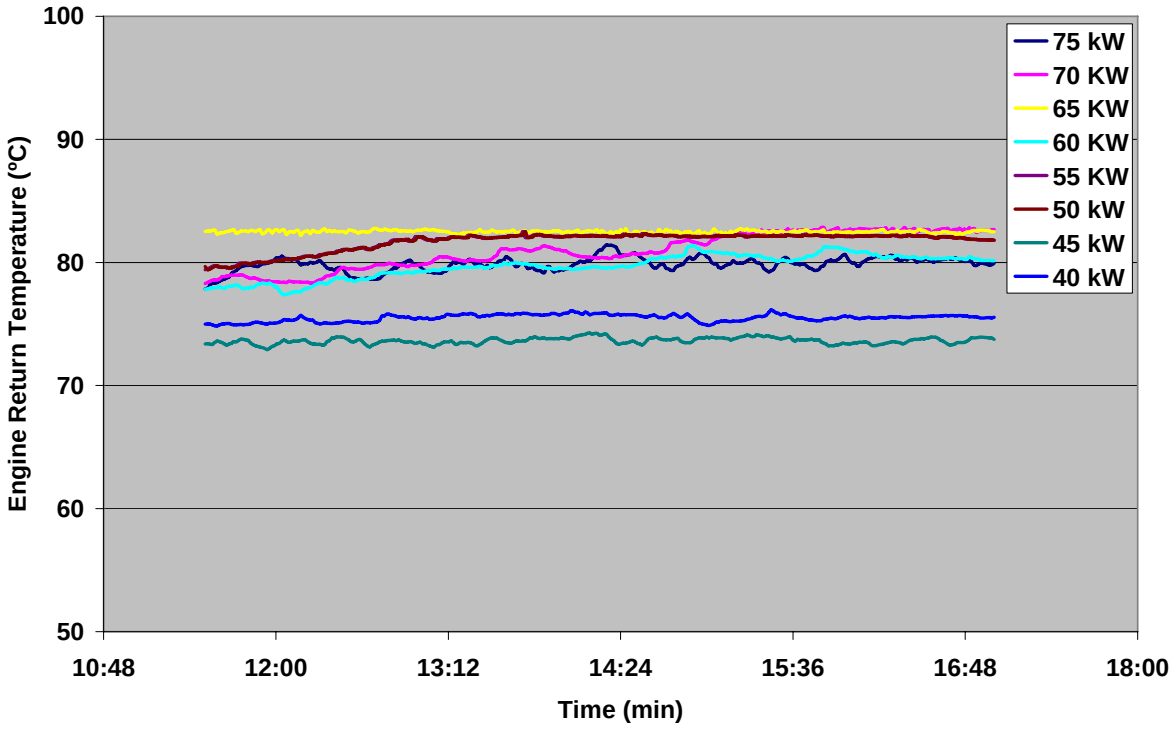

Figure 28: Engine Return Temperature at Different Engine Generator Loads during the Summer Season

Figure 29 shows the reduction in engine return temperature when the engine generator load was changed from 75 kW to 40 kW. It is observed from Figure 29 that the engine return temperature dropped from 80 ºC at 75 kW to about 75 ºC at 40 kW giving a temperature difference of 5 ºC. The engine return temperature for 40 kW is higher owing to a high outdoor air temperature of around 33 ºC compared to the full load condition where the outdoor air temperature was moderate and about 25 ºC.

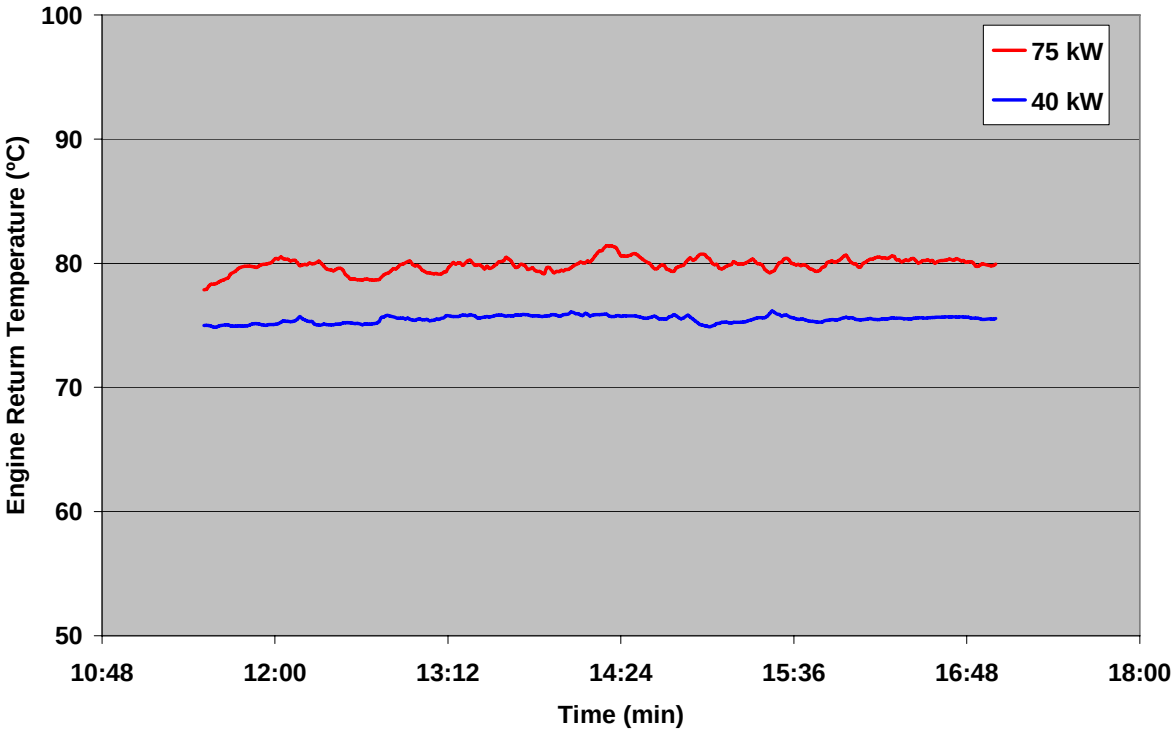

Figure 29: Comparison of Engine Return Temperature at 75 kW and 40 kW during the Summer Season

Table 6 summarizes the average engine return temperatures at different part loads during the summer time along with the ambient air conditions and the day when the data was analyzed.

Table 6: Engine Return Temperature and Outdoor Air Conditions at Part Load during Summer Season

Engine Generator Load (kW)	Day System was Run	Average Engine Return Temperature (°C)	Average Outdoor Air Temperature (°C)	Average Outdoor Air Enthalpy (kJ/kg)
75	06/01/2005	80	25	42
70	08/10/2005	81	28	61
65	08/05/2005	83	33	64
60	07/01/2005	80	31	63
55	07/27/2005	82	34	70
50	07/28/05	82	35	70
45	09/06/05	74	25	46
40	08/04/2005	75	33	62

It is observed from Table 5 and Table 6 that the outdoor air conditions do have an effect on the engine return temperature. It is also seen that the engine return temperature in some part load conditions is actually greater than the base load case because of higher outdoor air temperature.

Figure 30 shows the engine supply temperature at full load and part load conditions during winter. The engine supply temperature refers to the temperature of the 50:50 ethylene glycol – water solution that is supplied by the engine to the liquid desiccant unit or the dump radiator module after the solution has picked up the waste heat from both the jacket water heat exchanger and the exhaust gas heat exchanger.

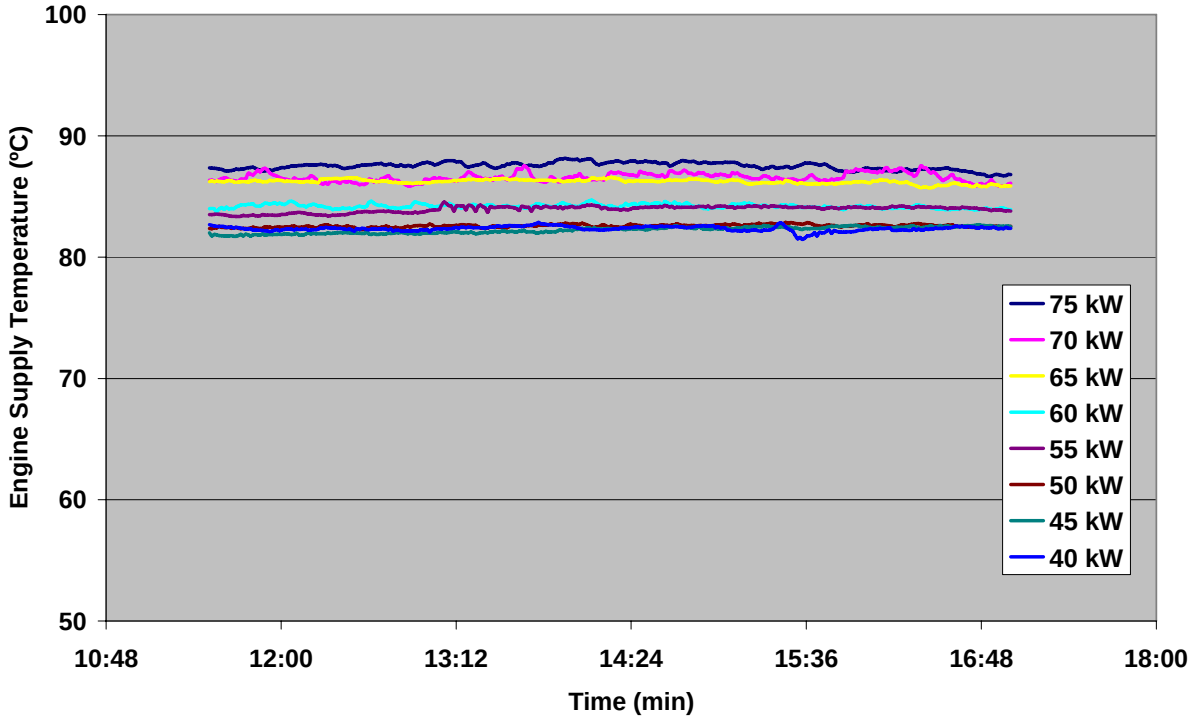

Figure 30: Engine Supply Temperature at Different Engine Generator Loads during the Winter Season

Figure 31 shows the reduction in engine supply temperature when the engine generator load was changed from 75 kW to 40 kW. It is observed from Figure 31 that the engine supply temperature dropped from 87 ºC at 75 kW to about 82 ºC at 40 kW.

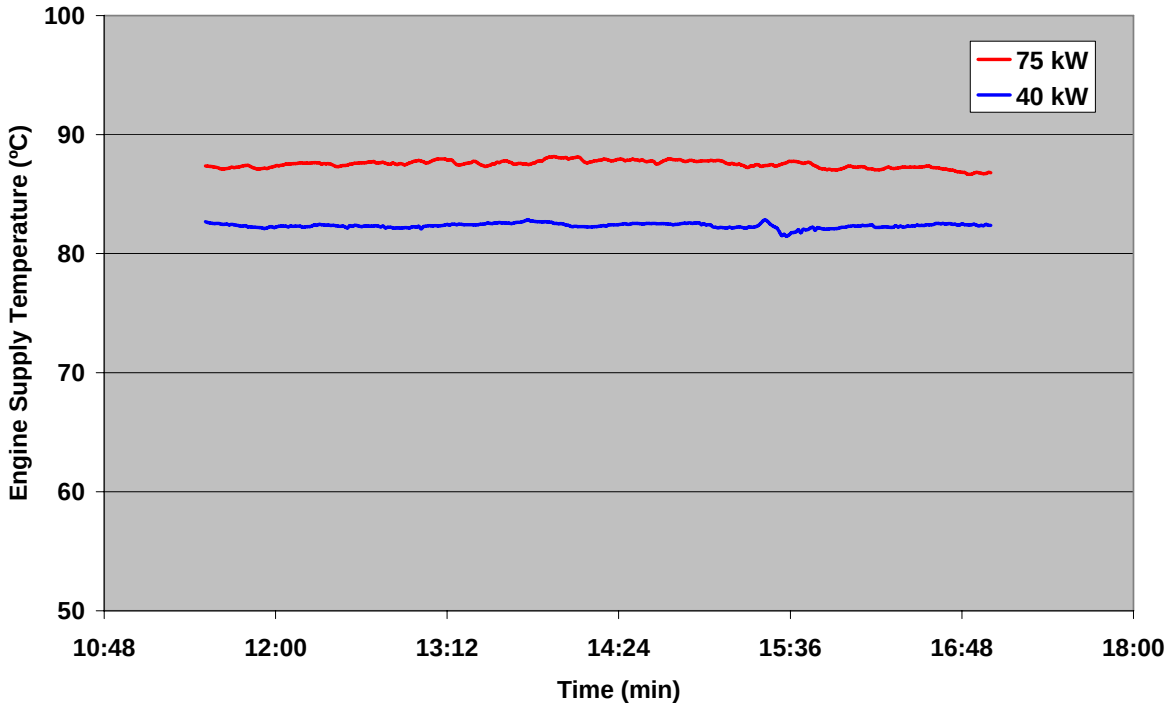

Figure 31: Comparison of Engine Supply Temperature at 75 kW and 40 kW during the Winter Season

Table 7 summarizes the average engine supply temperatures at different part loads during the winter time along with the ambient air conditions and the day when the data was analyzed.

Table 7: Engine Supply Temperature and Outdoor Air Conditions at Part Load during Winter Season

Engine Generator Load (kW)	Day System was Run	Average Engine Supply Temperature (ºC)	Average Outdoor Air Temperature (ºC)	Average Outdoor Air Enthalpy (kJ/kg)
75	11/30/2004	87	10	20
70	12/03/2004	86	8	14
65	12/10/2004	86	10	27
60	12/15/2004	84	1	5
55	12/16/2004	84	5	9
50	12/20/2004	82	-7	-6
45	12/21/2004	82	0.3	3
40	12/23/2004	82	13	34

Figure 32 shows the engine supply temperature at full load and part load conditions during the summer season.

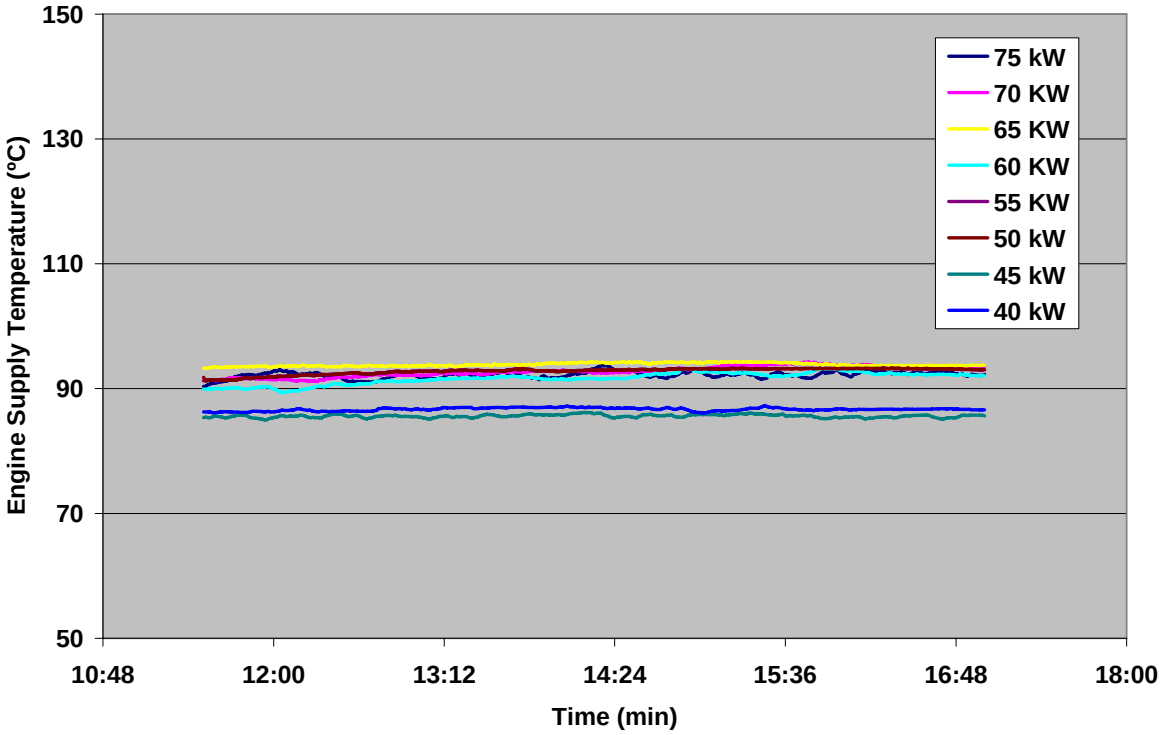

Figure 32: Engine Supply Temperature at Different Engine Generator Loads during the Summer Season

Figure 33 shows the reduction in engine supply temperature when the engine generator load was changed from 75 kW to 40 kW. It is observed from Figure 33 that the engine supply temperature dropped from 92 ºC at 75 kW to about 87 ºC at 40 kW giving a temperature difference of 5 ºC. The engine supply temperature for 40 kW is higher owing to a high outdoor air temperature of around 33 ºC compared to the full load condition where the outdoor air temperature was moderate and about 25 ºC.

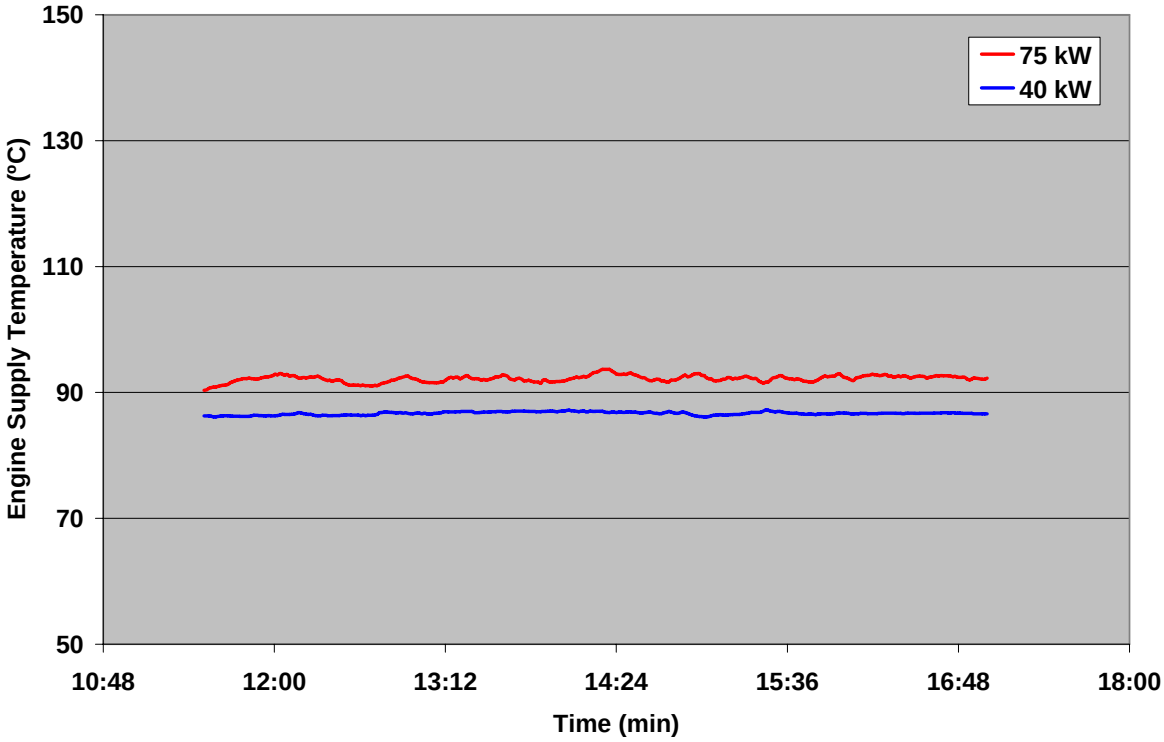

Figure 33: Comparison of Engine Supply Temperature at 75 kW and 40 kW during the Summer Season

Table 8 summarizes the average engine supply temperatures at different part loads during the summer time along with the ambient air conditions and the day when the data was analyzed.

Table 8: Engine Supply Temperature and Outdoor Air Conditions at Part Load during Summer Season

Engine Generator Load (kW)	Day System was Run	Average Engine Supply Temperature (ºC)	Average Outdoor Air Temperature (ºC)	Average Outdoor Air Enthalpy (kJ/kg)
75	06/01/2005	92	25	42
70	08/10/2005	93	28	61
65	08/05/2005	94	33	64
60	07/01/2005	91	31	63
55	07/27/2005	93	34	70
50	07/28/05	92	35	70
45	09/06/05	86	25	46
40	08/04/2005	87	33	62

It can be noted from Table 8 that engine supply temperature as high as 92 ºC was realized even at part load of 50 kW which was same as the one obtained at 75 kW owing to high outdoor air temperature resulting in higher exhaust gas temperature.

Figure 34 shows the jacket water heat exchanger (JW HX) outlet temperature at full load and part load conditions during winter. As the name suggests, the JW HX outlet temperature refers to the temperature of the 50:50 ethylene glycol – water solution after it has recovered the heat from the jacket water heat exchanger.

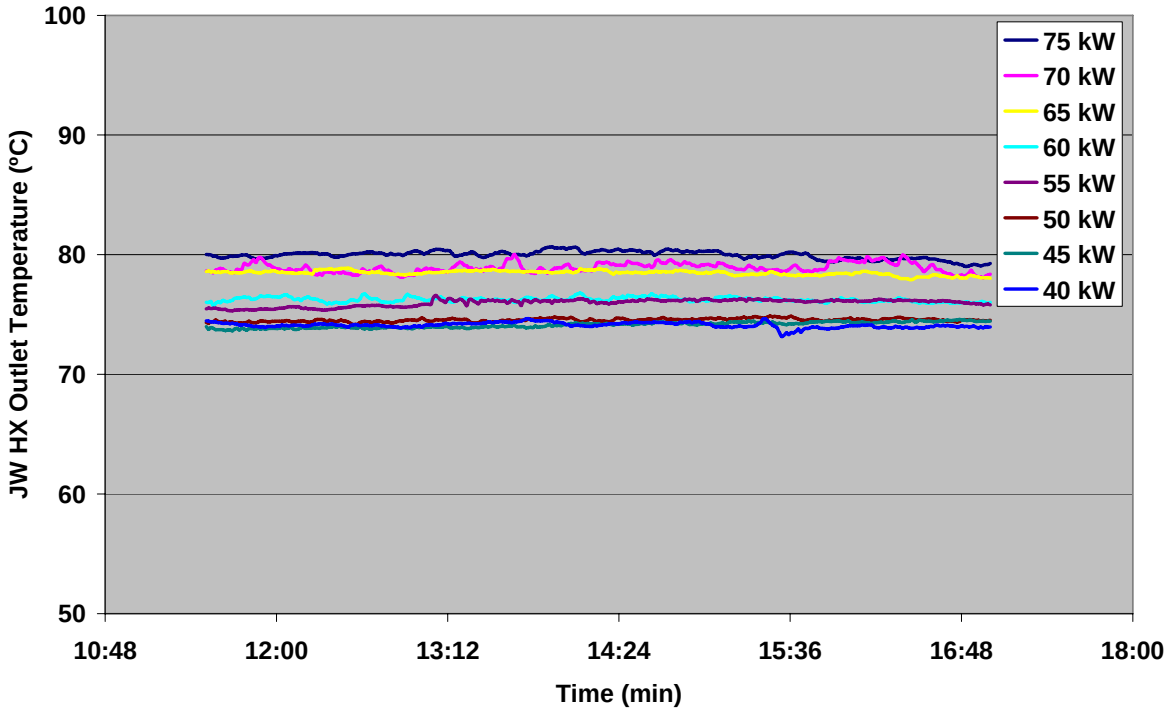

Figure 34: Jacket Water HX Outlet Temperature at Different Engine Generator Loads during the Winter Season

Figure 35 shows the reduction in JW HX outlet temperature when the engine generator load was changed from 75 kW to 40 kW. It is observed from Figure 35 that the JW HX outlet temperature dropped from 80 ºC at 75 kW to about 74 ºC at 40 kW.

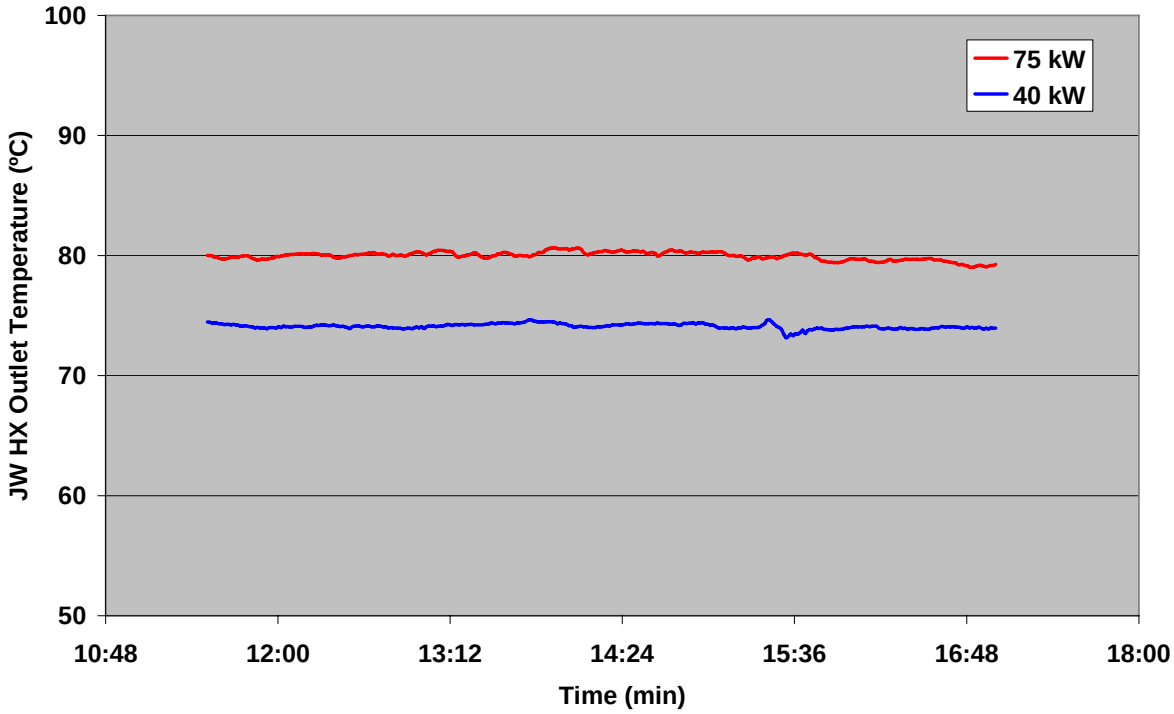

Figure 35: Comparison of Jacket Water HX Outlet Temperature at 75 kW and 40 kW during the Winter Season

Table 9 summarizes the average JW HX outlet temperatures at different part loads during the winter time along with the ambient air conditions and the day when the data was analyzed.

Table 9: JW HX Outlet Temperature and Outdoor Air Conditions at Part Load during Winter Season

Engine Generator Load (kW)	Day System was Run	Average JW HX Outlet Temperature (ºC)	Average Outdoor Air Temperature (ºC)	Average Outdoor Air Enthalpy (kJ/kg)
75	11/30/2004	80	10	20
70	12/03/2004	79	8	14
65	12/10/2004	78	10	27
60	12/15/2004	76	1	5
55	12/16/2004	76	5	9
50	12/20/2004	74	-7	-6
45	12/21/2004	74	0.3	3
40	12/23/2004	74	13	34

Figure 36 shows the JW HX outlet temperature at full load and part load conditions during the summer season.

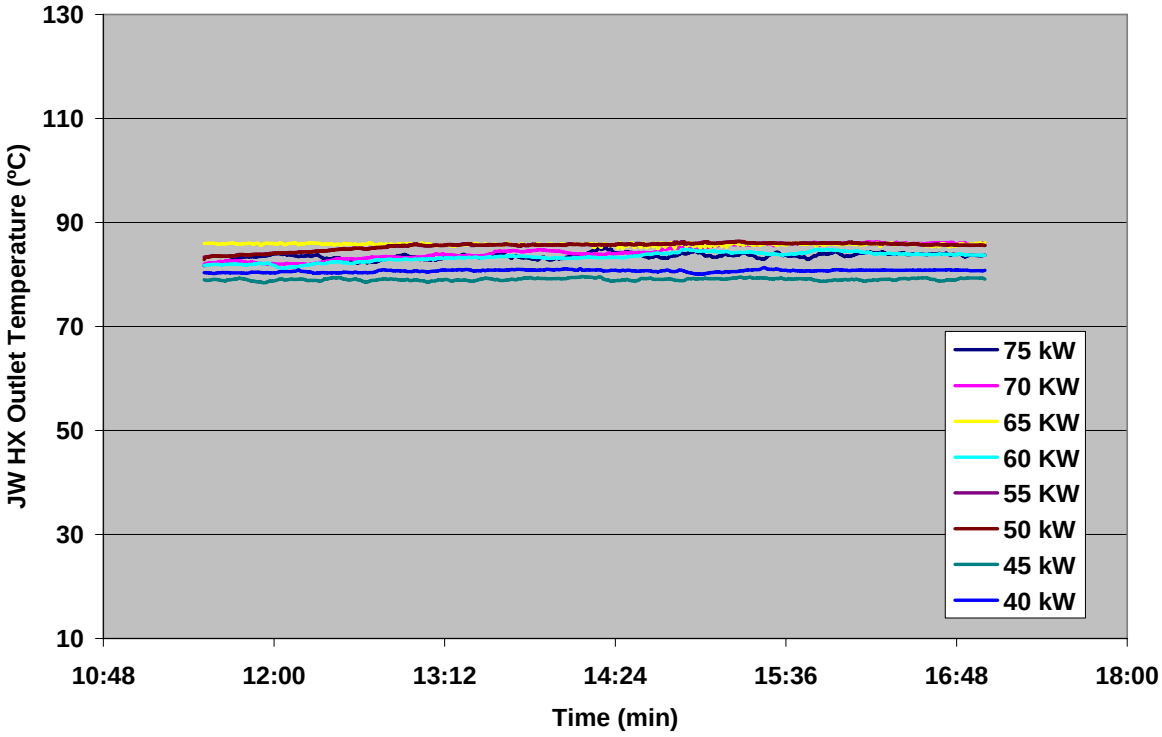

Figure 36: JW HX Outlet Temperature at Different Engine Generator Loads during the Summer Season

Figure 37 shows the reduction in JW HX outlet temperature when the engine generator load was changed from 75 kW to 40 kW. It is observed from Figure 37 that the JW HX outlet temperature dropped from 83 ºC at 75 kW to about 80 ºC at 40 kW giving a temperature difference of 3 ºC. The JW HX outlet temperature for 40 kW is higher owing to a high outdoor air temperature of around 33 ºC compared to the full load condition where the outdoor air temperature was moderate and about 25 ºC.

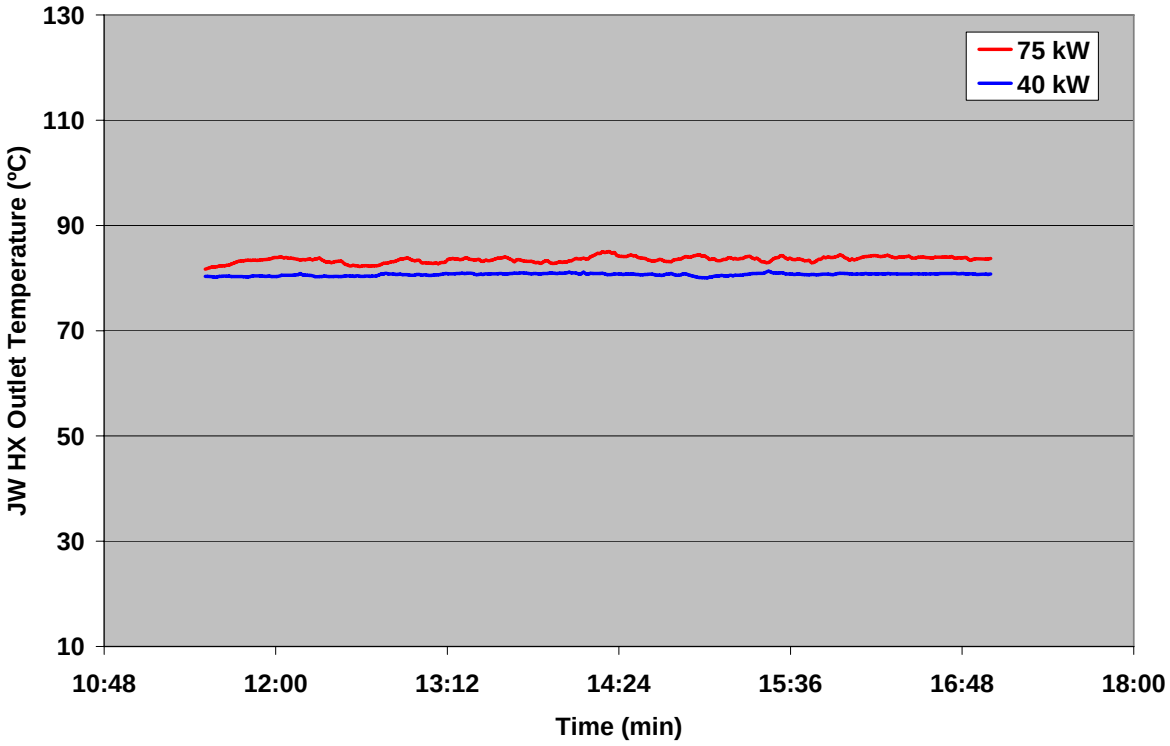

Figure 37: Comparison of JW HX Outlet Temperature at 75 kW and 40 kW during the Summer Season

Table 10 summarizes the average JW HX outlet temperatures at different part loads during the summer time along with the ambient air conditions and the day when the data was analyzed.

Table 10: JW HX Outlet Temperature and Outdoor Air Conditions at Part Load during Summer Season

Engine Generator Load (kW)	Day System was Run	Average JW HX Outlet Temperature (°C)	Average Outdoor Air Temperature (°C)	Average Outdoor Air Enthalpy (kJ/kg)
75	06/01/2005	83	25	42
70	08/10/2005	84	28	61
65	08/05/2005	82	33	64
60	07/01/2005	83	31	63
55	07/27/2005	85	34	70
50	07/28/05	85	35	70
45	09/06/05	79	25	46
40	08/04/2005	80	33	62

5.3 Performance of Engine Generator

This section deals with the detailed characterization of the performance of the engine generator over a range of ambient air temperature and relative humidity. Extensive analysis was carried out for base load as well as part load conditions during the summer and winter seasons. Based on the measured heat recovery loop temperatures and flow rates, various parameters of the engine generator such as

amount of waste heat recovered from jacket water and exhaust gas heat exchangers, electrical efficiency, CHP efficiency etc. have been calculated and explained in this section.

The amount of waste heat recovered from the jacket water heat exchanger is calculated using the following equation,

$$\dot{Q}_{JW} = \dot{m}_{glycol}\, Cp_{glycol} (T_{JWHXOut} - T_{Eng\,Ret})$$

Where,

$\dot{Q}_{JW}$ = amount of waste heat recovered by 50:50 ethylene glycol – water solution from the jacket water heat exchanger (kW).

$\dot{m}_{glycol}$ = mass flow rate of 50:50 ethylene glycol – water solution (kg/s).

Cp_{glycol} = specific heat of 50:50 ethylene glycol – water solution (kJ/kg K)

$T_{JWHXOut}$ = temperature of 50:50 ethylene glycol – water solution at the outlet of the jacket water heat exchanger (K).

$T_{Eng\,Ret}$ = temperature of 50:50 ethylene glycol – water solution at the inlet of the jacket water heat exchanger (K).

Figure 38 plots the waste heat recovered by the 50:50 ethylene glycol – water solution from the jacket water heat exchanger at full load as well as at different part loads for the winter season.

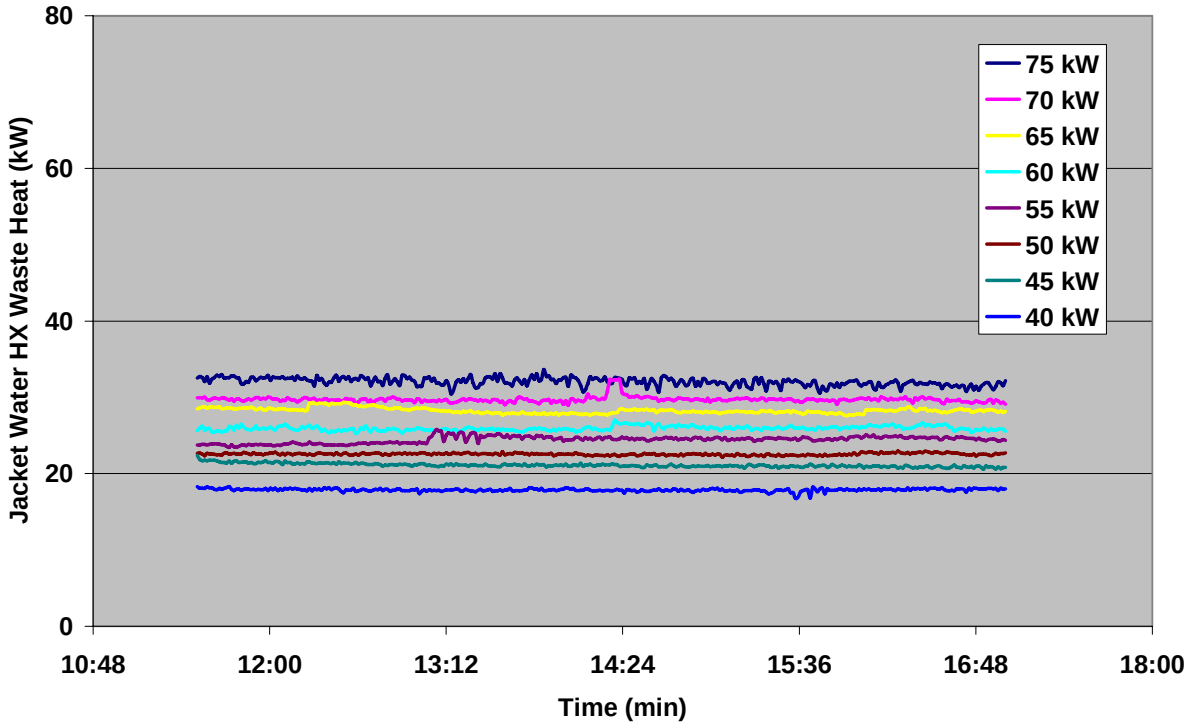

Figure 38: Jacket Water HX Waste Heat at Different Engine Generator Loads during the Winter Season

Figure 39 shows the reduction in JW HX waste heat when the engine generator load was changed from 75 kW to 40 kW. It is observed from Figure 39 that the JW HX waste heat dropped from around 32 kW at 75 kW to about 18 kW at 40 kW which is a difference of 14 kW.

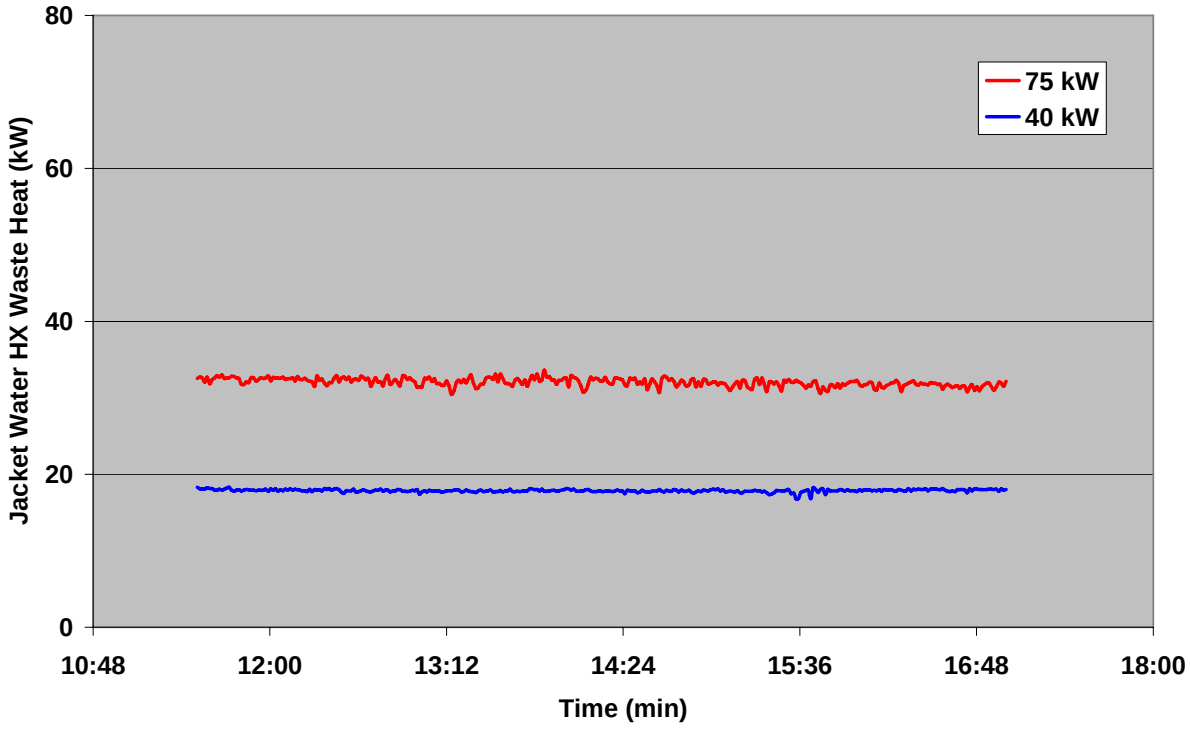

Figure 39: Comparison of JW HX Waste Heat at 75 kW and 40 kW during the Winter Season

Table 11 summarizes the average JW HX waste heat recovered at different part loads during the winter time along with the ambient air conditions and the day when the data was analyzed.

Table 11: JW HX Waste Heat and Outdoor Air Conditions at Part Load during Winter Season

Engine Generator Load (kW)	Day System was Run	Average JW HX Waste Heat (kW)	Average Outdoor Air Temperature (ºC)	Average Outdoor Air Enthalpy (kJ/kg)
75	11/30/2004	32	10	20
70	12/03/2004	30	8	14
65	12/10/2004	28	10	27
60	12/15/2004	26	1	5
55	12/16/2004	24	5	9
50	12/20/2004	22	-7	-6
45	12/21/2004	21	0.3	3
40	12/23/2004	18	13	34

Figure 40 shows the JW HX waste heat at full load and part load conditions during the summer season. The amount of waste heat recovered from the jacket water heat exchanger in some cases of part loads was found to be higher than that at 75 kW.

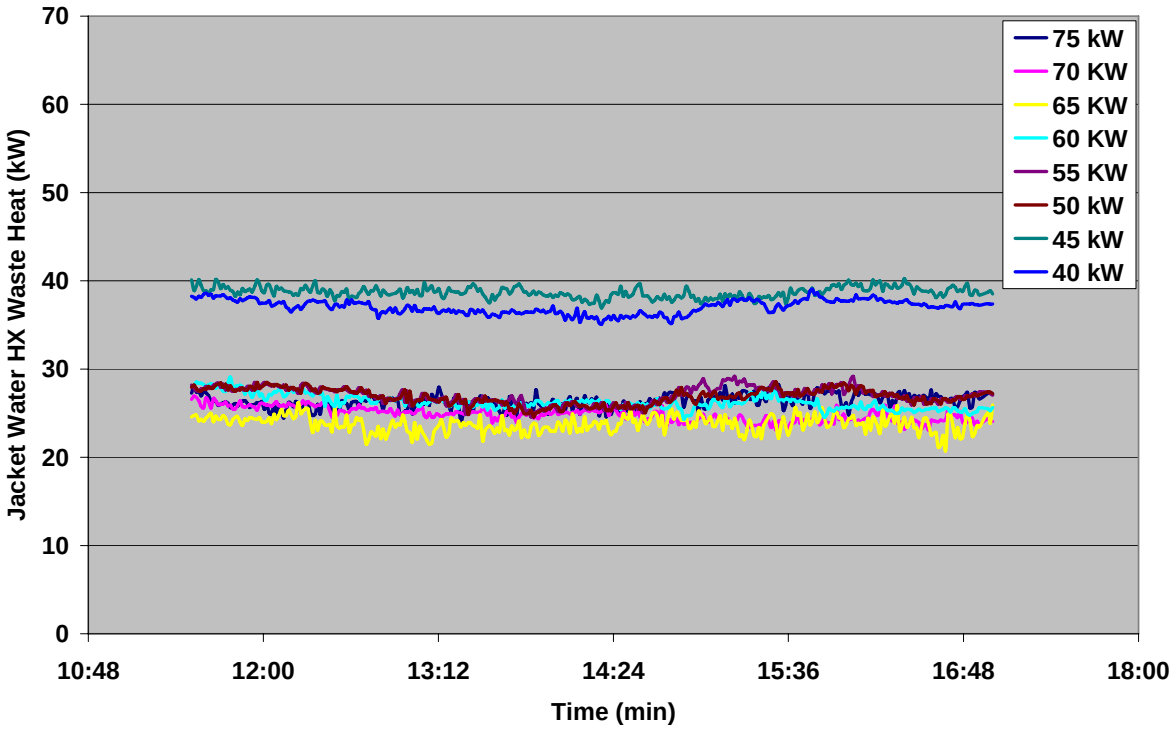

Figure 40: Jacket Water HX Waste Heat at Different Engine Generator Loads during the Summer Season

Figure 41 compares the amount of waste heat recovered by the ethylene glycol water solution from the jacket water heat exchanger at the full load of 75 kW and part load of 40 kW. It can be observed from Figure 41 that the JW HX waste heat at 40 kW is actually higher than that at 75 kW by about 11 kW. This is different than the results seen during the winter season where there was a reduction in the JW HX waste heat from 75 kW to 40 kW. This can be explained by the fact that the temperature difference of the 50:50 ethylene glycol – water solution across the jacket water heat exchanger was higher than that achieved at 75 kW. This temperature difference was higher at 40 kW since the engine supply temperature at the inlet of the dump radiator was lower than that at 75 kW and the dump radiator was able to cool it to a much lower temperature for the 40 kW case as compared to the 75 kW one.

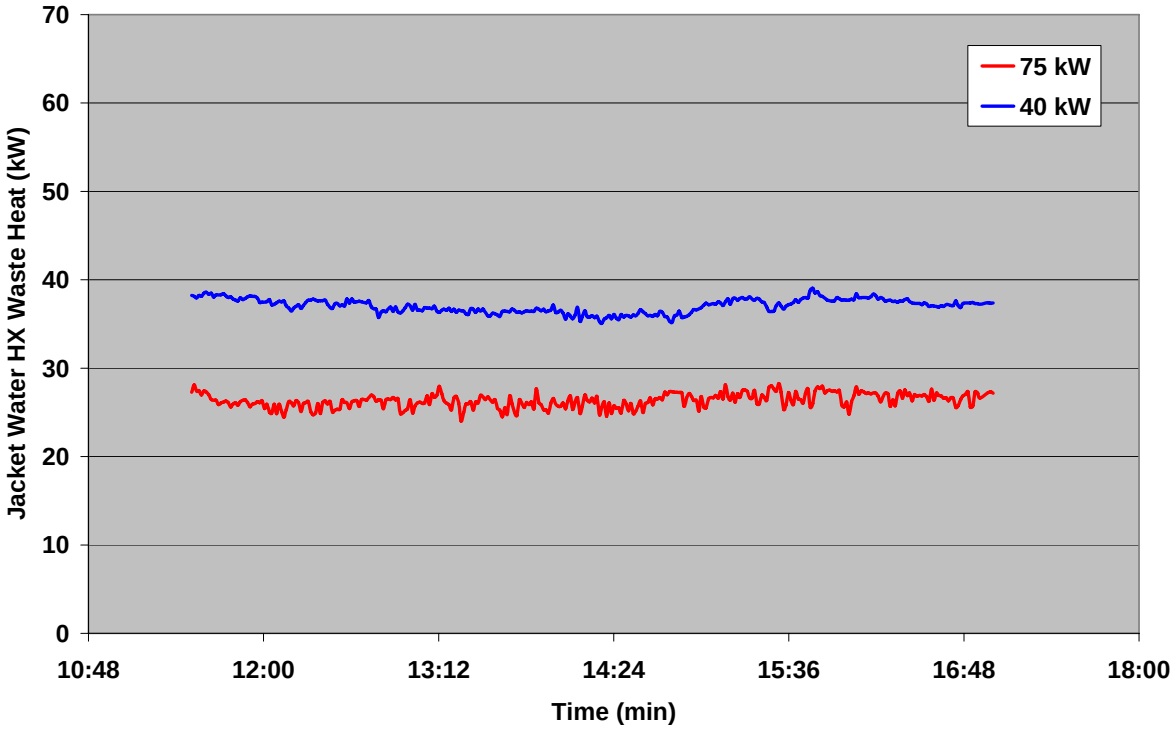

Figure 41: Comparison of JW HX Waste Heat at 75 kW and 40 kW during the Summer Season

Table 12 summarizes the average JW HX waste heat recovered at different part loads during the summer time along with the ambient air conditions and the day when the data was analyzed. It is seen from Table 12 that the JW HX waste heat was highest at 45 kW when the average ambient air temperature was around 25 ºC.

Table 12: JW HX Waste Heat and Outdoor Air Conditions at Part Load during Summer Season

Engine Generator Load (kW)	Day System was Run	Average JW HX Waste Heat (kW)	Average Outdoor Air Temperature (ºC)	Average Outdoor Air Enthalpy (kJ/kg)
75	06/01/2005	26	25	42
70	08/10/2005	25	28	61
65	08/05/2005	24	33	64
60	07/01/2005	26	31	63
55	07/27/2005	27	34	70
50	07/28/05	27	35	70
45	09/06/05	38	25	46
40	08/04/2005	37	33	62

The amount of waste heat recovered from the exhaust gas heat exchanger is calculated using the following equation,

$$\dot{Q}_{EX} = \dot{m}_{glycol}\, Cp_{glycol} (T_{EngSup} - T_{JWHXOut})$$

Where,

$\dot{Q}_{EX}$ = amount of waste heat recovered by 50:50 ethylene glycol – water solution from the jacket water heat exchanger (kW).

T_{EngSup} = temperature of 50:50 ethylene glycol – water solution at the outlet of the exhaust gas heat exchanger (K).

The specific heat of 50:50 ethylene glycol – water solution was calculated in EES at the average temperature which was found out for each time step by averaging the inlet and outlet temperatures to the exhaust gas heat exchanger. Figure 42 plots the waste heat recovered by the 50:50 ethylene glycol – water solution from the exhaust gas heat exchanger at full load as well as at different part loads for the winter season.

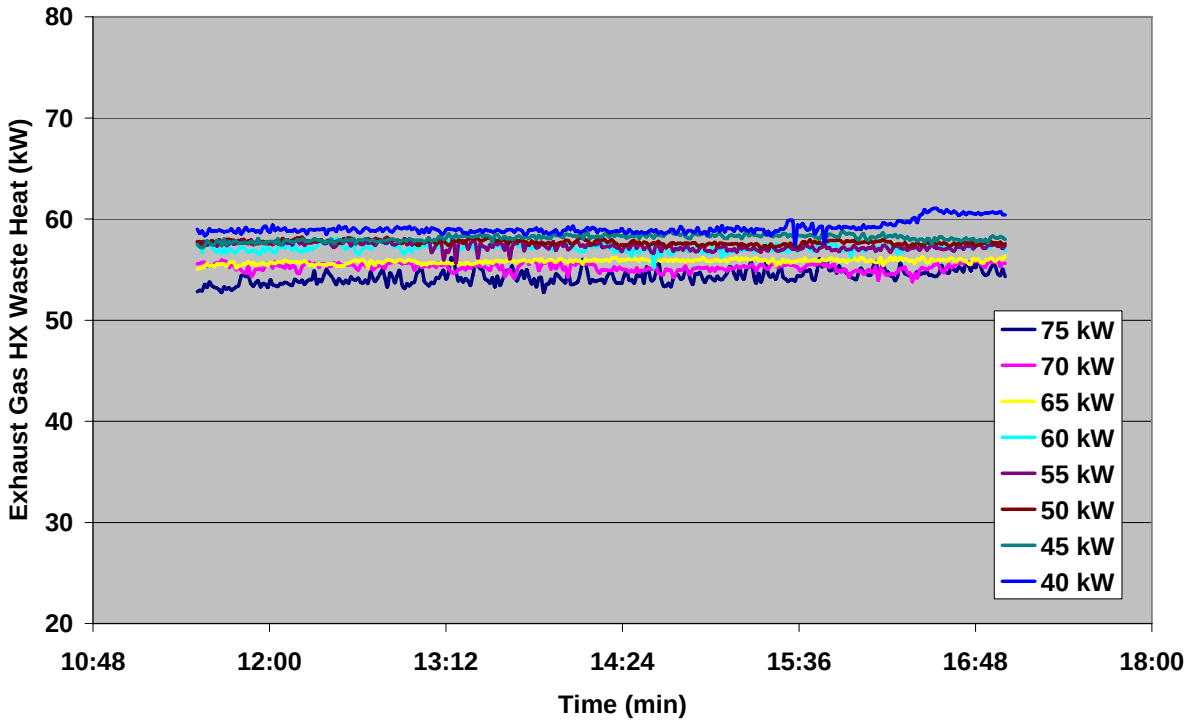

Figure 42: Exhaust Gas HX Waste Heat at Different Engine Generator Loads during the Winter Season

It can be seen from Figure 42 that the waste heat recovered by the ethylene glycol water solution from the exhaust gas heat exchanger is actually higher at part loads than at full load during the winter period while in case of the JW HX waste

heat, the amount of waste heat decreased at part loads. Figure 43 compares the exhaust gas HX waste heat recovered at 75 kW and 40 kW during winter.

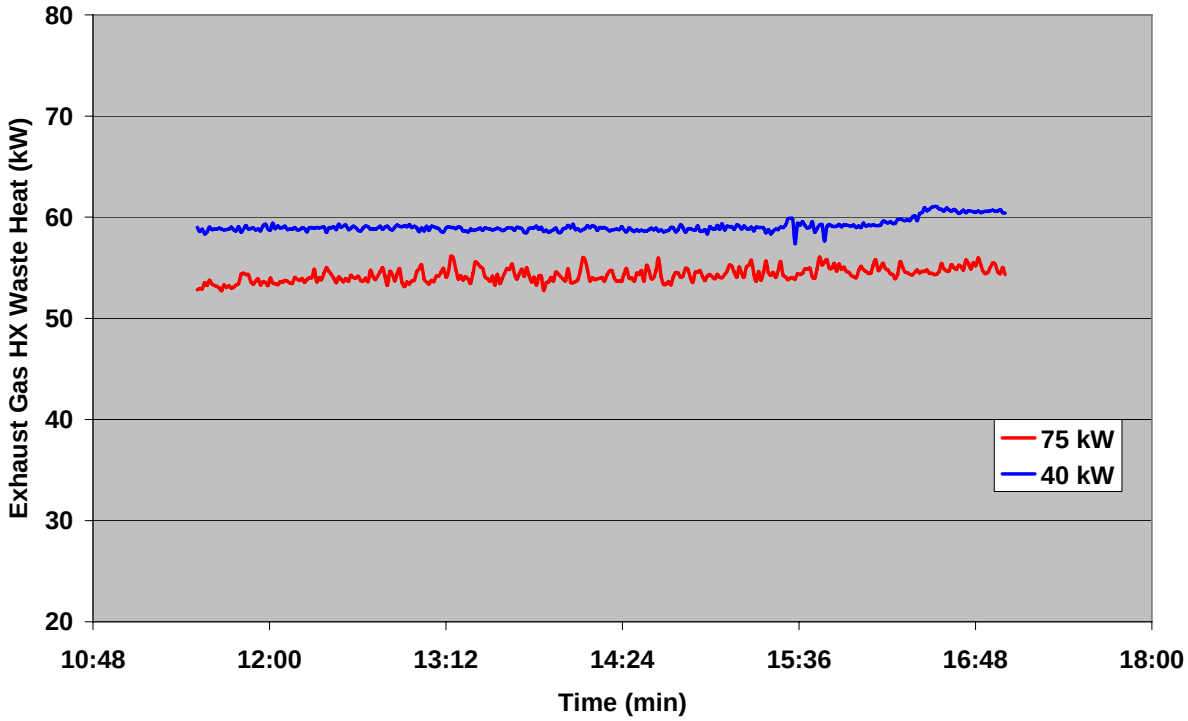

Figure 43: Comparison of Exhaust Gas HX Waste Heat at 75 kW and 40 kW during the Winter Season

The average exhaust gas HX waste heat at 75 kW was about 54 kW while at 40 kW; it was around 59 kW as shown in Figure 43. Table 13 summarizes the average exhaust gas HX waste heat recovered at different part loads during the winter time along with the ambient air conditions and the day when the data was analyzed.

Table 13: Exhaust Gas HX Waste Heat and Outdoor Air Conditions at Part Load during Winter Season

Engine Generator Load (kW)	Day System was Run	Average EX HX Waste Heat (kW)	Average Outdoor Air Temperature (ºC)	Average Outdoor Air Enthalpy (kJ/kg)
75	11/30/2004	54	10	20
70	12/03/2004	55	8	14
65	12/10/2004	56	10	27
60	12/15/2004	57	1	5
55	12/16/2004	57	5	9
50	12/20/2004	58	-7	-6
45	12/21/2004	58	0.3	3
40	12/23/2004	59	13	34

Figure 44 shows the exhaust gas HX waste heat at full load and part load conditions during the summer season. The wavy nature of the plots at part loads is due to the fluctuations in the outdoor air conditions especially the outdoor air temperature that varied quite a lot at times during the course of the day.

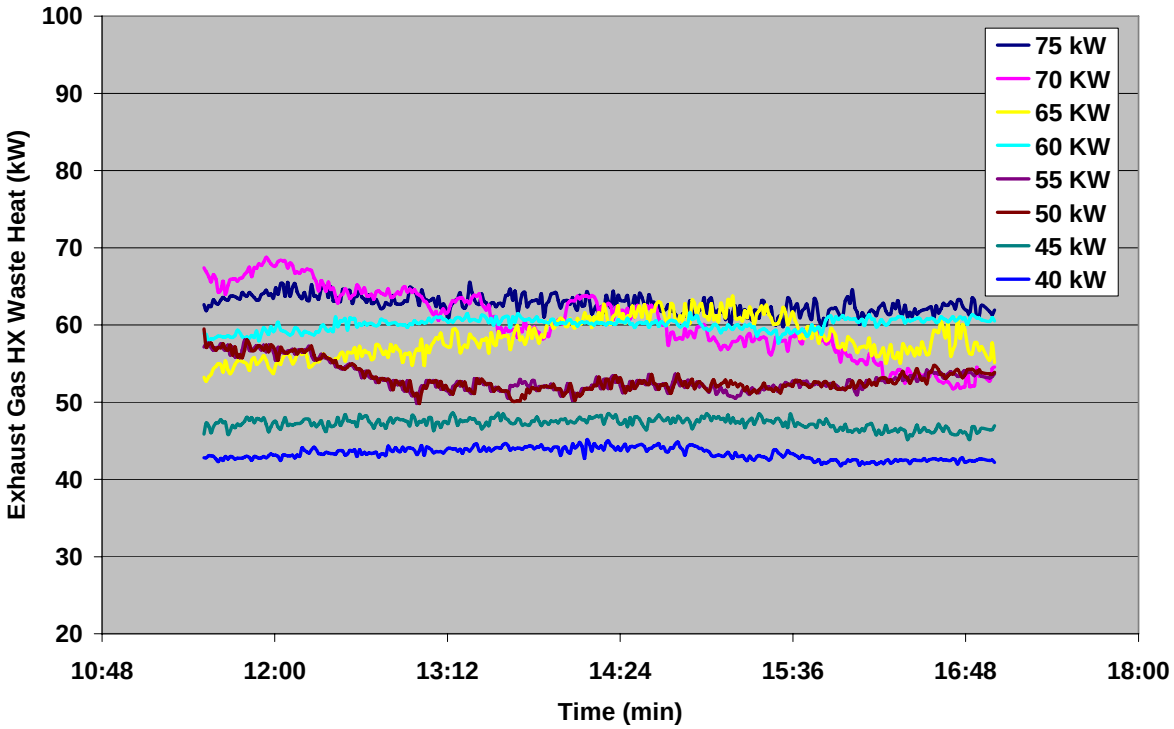

Figure 44: Exhaust Gas HX Waste Heat at Different Engine Generator Loads during the Summer Season

Figure 45 compares the exhaust gas HX waste heat recovered at full load of 75 kW and part load of 40 kW during the summer season. Figure 45 shows that there is a reduction of around 20 kW in the amount of waste heat recovered in the exhaust gas heat exchanger between the 75 kW and 40 kW engine generator loads.

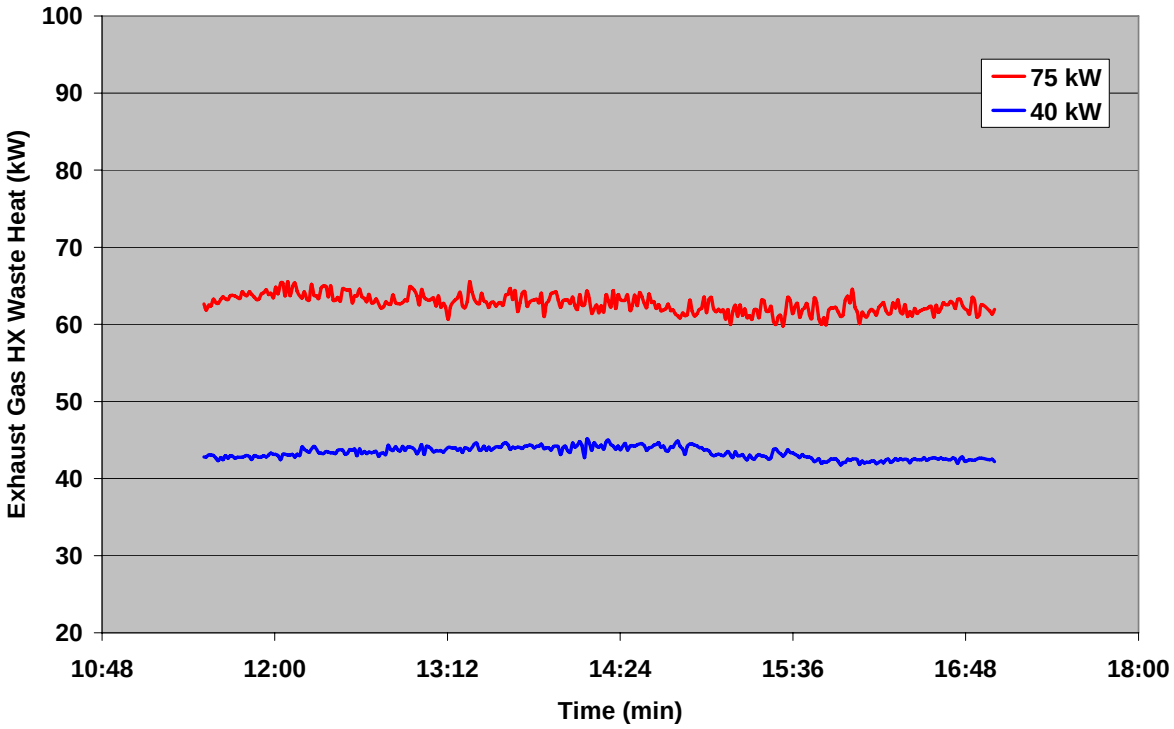

Figure 45: Comparison of Exhaust Gas HX Waste Heat at 75 kW and 40 kW during the Summer Season

Table 14 summarizes the average exhaust gas HX waste heat recovered at different part loads during the summer time along with the ambient air conditions and the day when the data was analyzed.

Table 14: Exhaust Gas HX Waste Heat and Outdoor Air Conditions at Part Load during Summer Season

Engine Generator Load (kW)	Day System was Run	Average EX HX Waste Heat (kW)	Average Outdoor Air Temperature (ºC)	Average Outdoor Air Enthalpy (kJ/kg)
75	06/01/2005	63	25	42
70	08/10/2005	60	28	61
65	08/05/2005	58	33	64
60	07/01/2005	60	31	63
55	07/27/2005	53	34	70
50	07/28/05	53	35	70
45	09/06/05	47	25	46
40	08/04/2005	43	33	62

The total amount of waste heat recovered from the engine generator heat recovery package is given by the equation below,

$$\dot{Q}_{Total} = \dot{Q}_{EX} + \dot{Q}_{JW}$$

Where,

$\dot{Q}_{Total}$ = Total amount of waste heat recovered from the engine generator heat recovery package.

Figure 46 plots the total waste heat recovered by the 50:50 ethylene glycol – water solution at full load as well as at different part loads for the winter season.

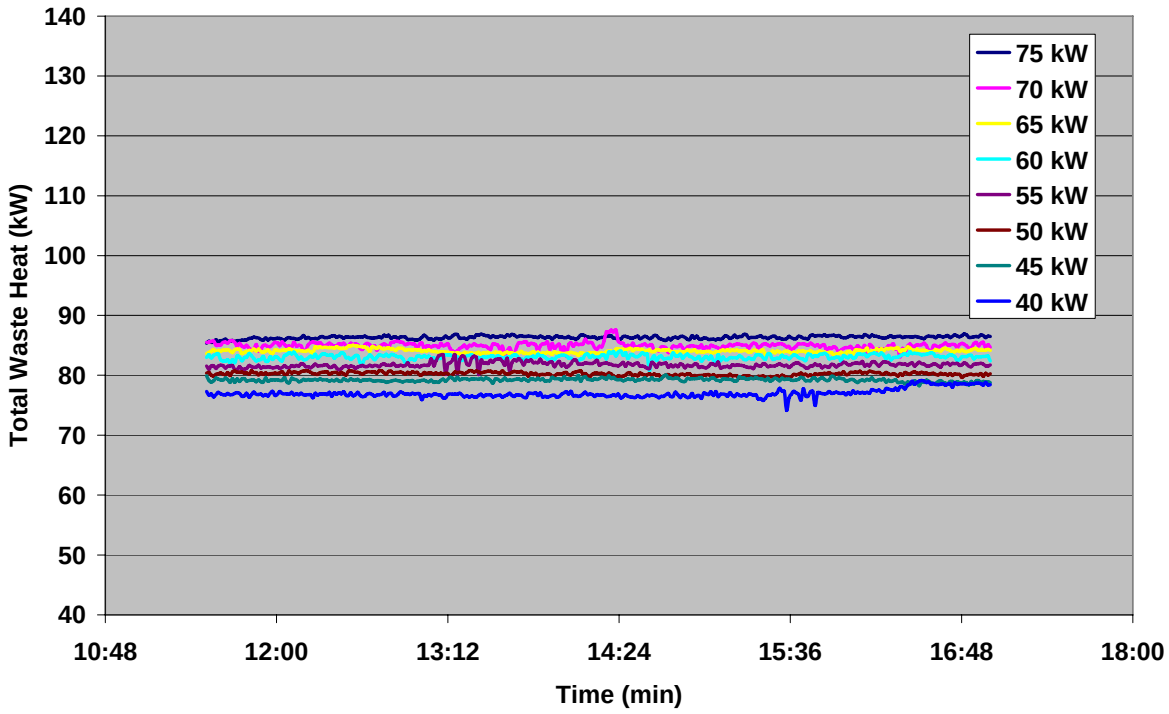

Figure 46: Total Waste Heat at Different Engine Generator Loads during the Winter Season

Figure 47 shows the reduction in the amount of total waste heat recovered as the engine load is dropped from 75 kW to 40 kW during the winter period. The total amount of waste heat decreased from about 86 kW at 75 kW load to around 77 kW at the engine load of 40 kW.

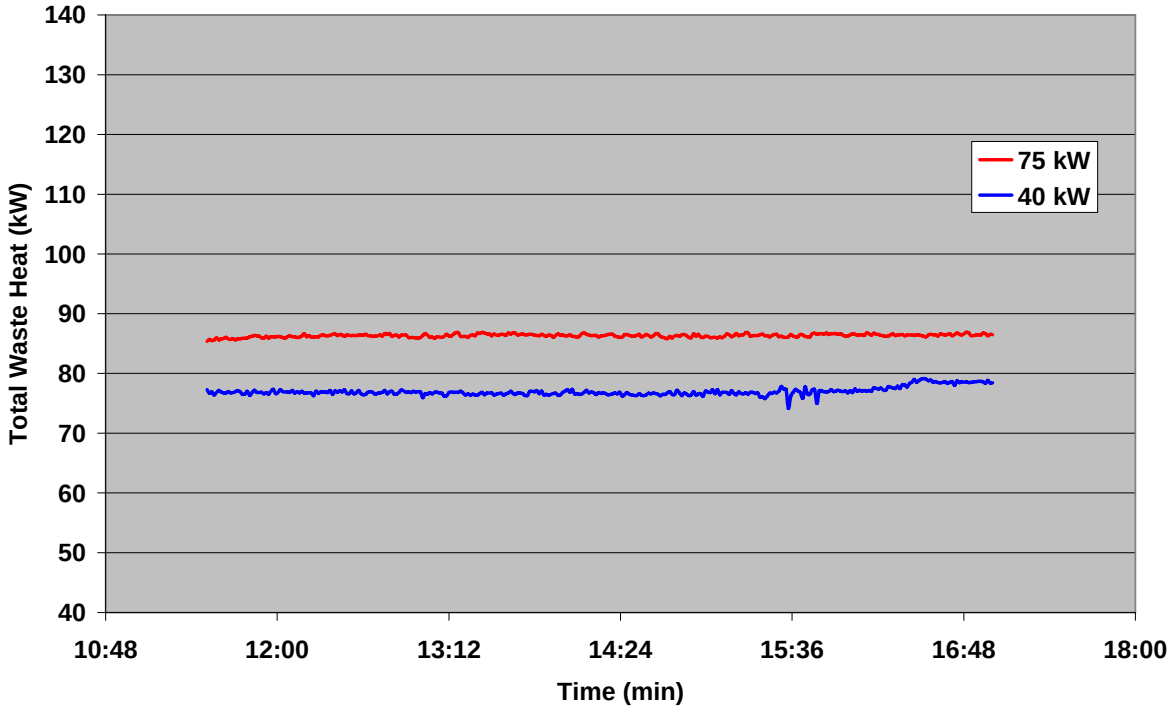

Figure 47: Comparison of Total Waste Heat at 75 kW and 40 kW during the Winter Season

Table 15 summarizes the average total waste heat recovered at different part loads during the winter time.

Table 15: Total Waste Heat and Outdoor Air Conditions at Part Load during Winter Season

Engine Generator Load (kW)	Day System was Run	Average Total Waste Heat (kW)	Average Outdoor Air Temperature (ºC)	Average Outdoor Air Enthalpy (kJ/kg)
75	11/30/2004	86	10	20
70	12/03/2004	85	8	14
65	12/10/2004	84	10	27
60	12/15/2004	83	1	5
55	12/16/2004	82	5	9
50	12/20/2004	80	-7	-6
45	12/21/2004	79	0.3	3
40	12/23/2004	77	13	34

Figure 48 shows the total waste heat recovered by the 50:50 ethylene glycol – water solution at full load as well as at different part loads during the summer season.

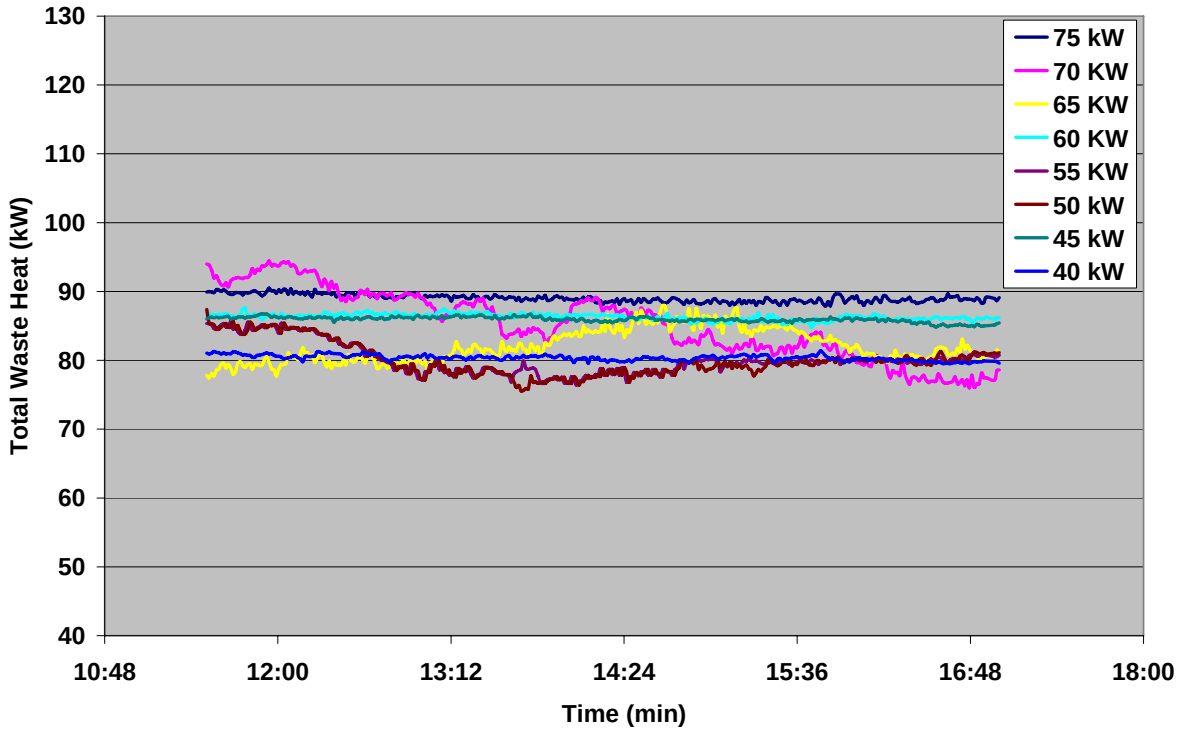

Figure 48: Total Waste Heat at Different Engine Generator Loads during the Summer Season

Figure 49 compares the amount of total waste heat recovered at 75 kW and 40 kW during the summer season. It is observed from Figure 49 that the total waste heat was about 89 kW at 75 kW while it was reduced to around 80 kW at 40 kW engine generator load.

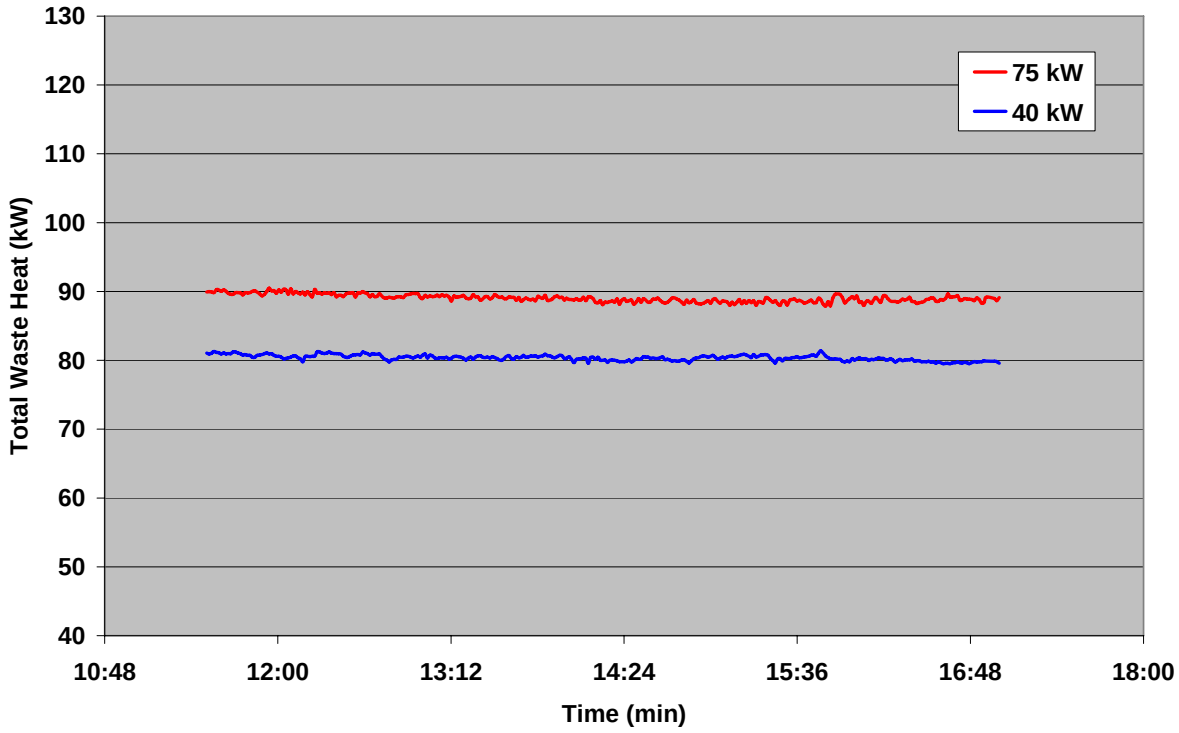

Figure 49: Comparison of Total Waste Heat at 75 kW and 40 kW during the Summer Season

The average total waste heat recovered by the engine generator heat recovery package at different loads during the summer period is given in Table 16. The total waste heat was actually a little higher at part loads of 60 kW and 45 kW due to higher amount of jacket water waste heat. The higher jacket water waste heat in these part load cases was because of the higher temperature difference across the jacket water heat exchanger which was discussed previously.

Table 16: Total Waste Heat and Outdoor Air Conditions at Part Load during Summer Season

Engine Generator Load (kW)	Day System was Run	Average Total Waste Heat (kW)	Average Outdoor Air Temperature (ºC)	Average Outdoor Air Enthalpy (kJ/kg)
75	06/01/2005	89	25	42
70	08/10/2005	85	28	61
65	08/05/2005	82	33	64
60	07/01/2005	86	31	63
55	07/27/2005	80	34	70
50	07/28/05	80	35	70
45	09/06/05	86	25	46
40	08/04/2005	80	33	62

The amount of natural gas consumed by the engine generator at base load of 75 kW and different part loads has been plotted in Figure 50. The data shown was recorded during the winter season.

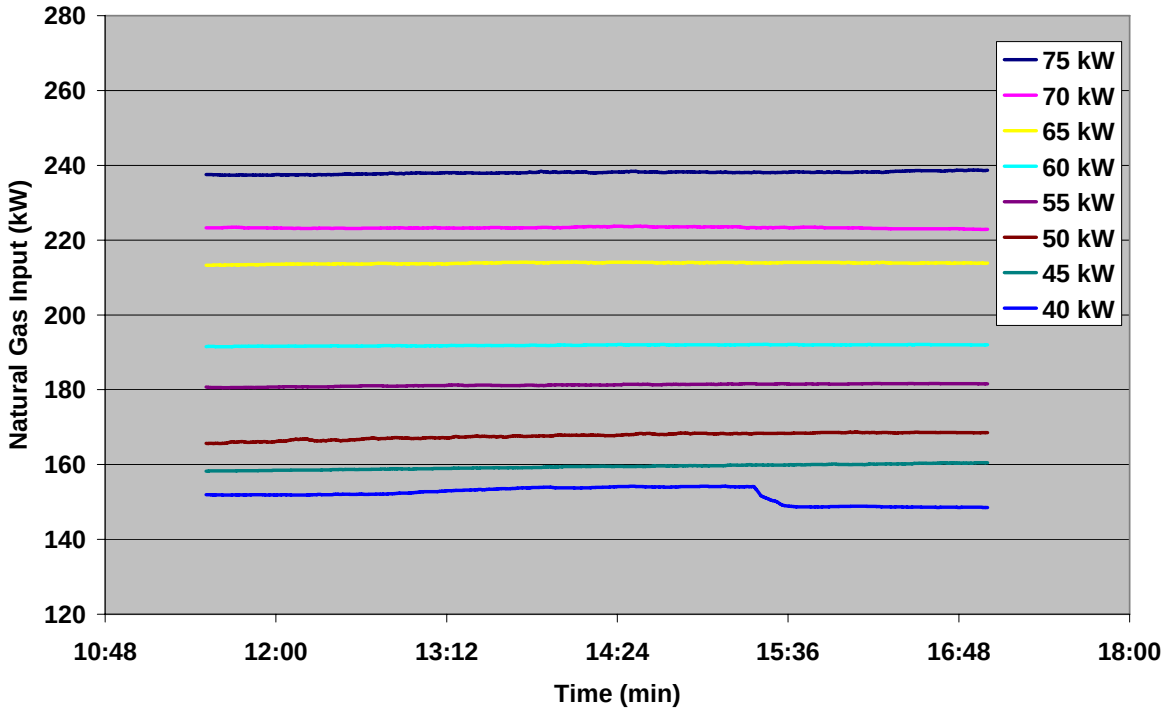

Figure 50: Natural Gas Consumption at Different Engine Generator Loads during the Winter Season

Figure 51 compares the natural gas consumption of the engine generator at 75 kW and 40 kW loads. The engine generator consumed about 238 kW of natural gas fuel at 75 kW as compared to around 152 kW of natural gas at 40 kW during the winter time. It is observed from Figure 51 that the natural gas consumption plot for 40 kW shows a decrease at around 3:20 pm. This was because of the sudden drop in outside air conditions, especially the ambient air temperature which can be seen from Figure 52 and Figure 53.

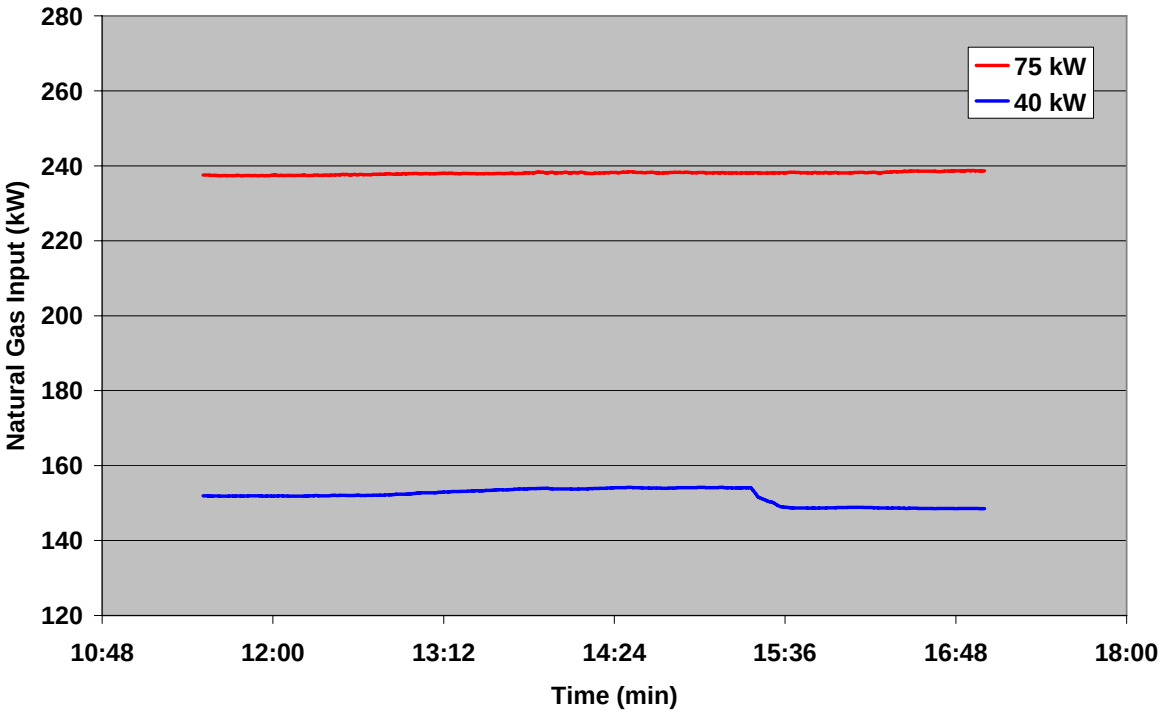

Figure 51: Comparison of Natural Gas Consumption at 75 kW and 40 kW during the Winter Season

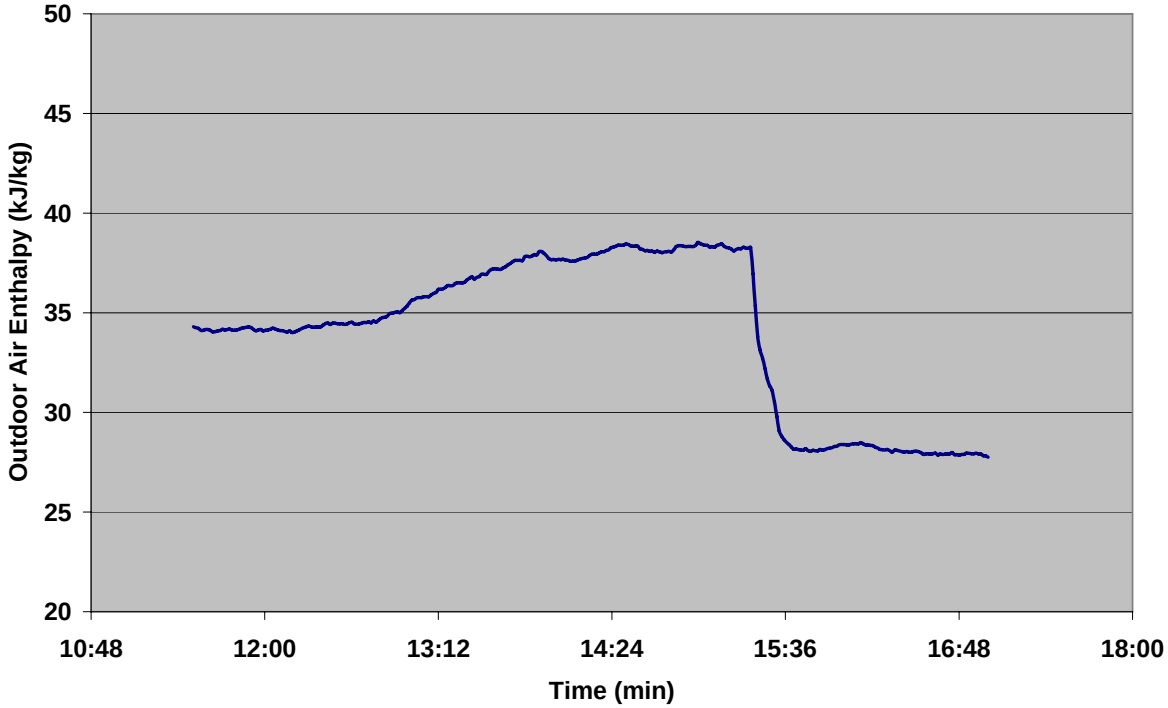

Figure 52: Variation of Outdoor Air Enthalpy for 40 kW Engine Load

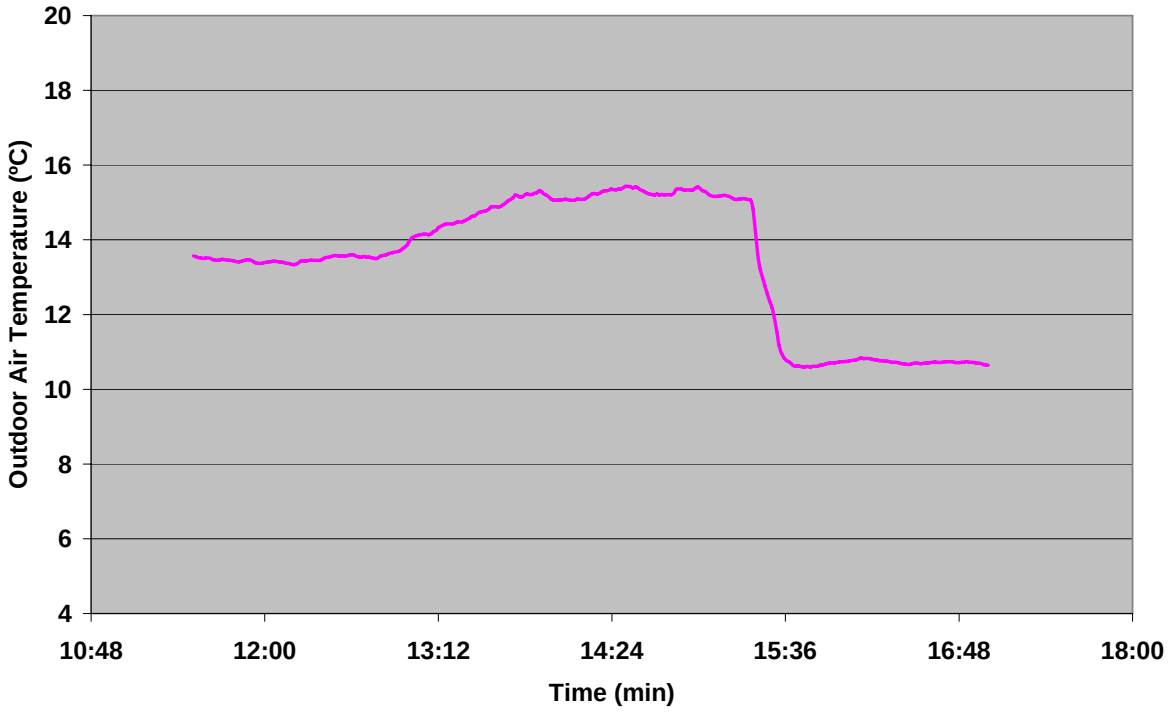

Figure 53: Variation of Outdoor Air Temperature for 40 kW Engine Load

Table 17 enumerates the average natural gas consumption of the engine generator at different part loads for the winter period.

Table 17: Natural Gas Consumption and Outdoor Air Conditions at Part Load during Winter Season

Engine Generator Load (kW)	Day System was Run	Average Natural Gas Consumption (kW)	Average Outdoor Air Temperature (°C)	Average Outdoor Air Enthalpy (kJ/kg)
75	11/30/2004	238	10	20
70	12/03/2004	223	8	14
65	12/10/2004	214	10	27
60	12/15/2004	192	1	5
55	12/16/2004	181	5	9
50	12/20/2004	168	-7	-6
45	12/21/2004	177	0.3	3
40	12/23/2004	152	13	34

The natural gas fuel consumption by the engine generator at different loads during the summer season is shown in Figure 54.

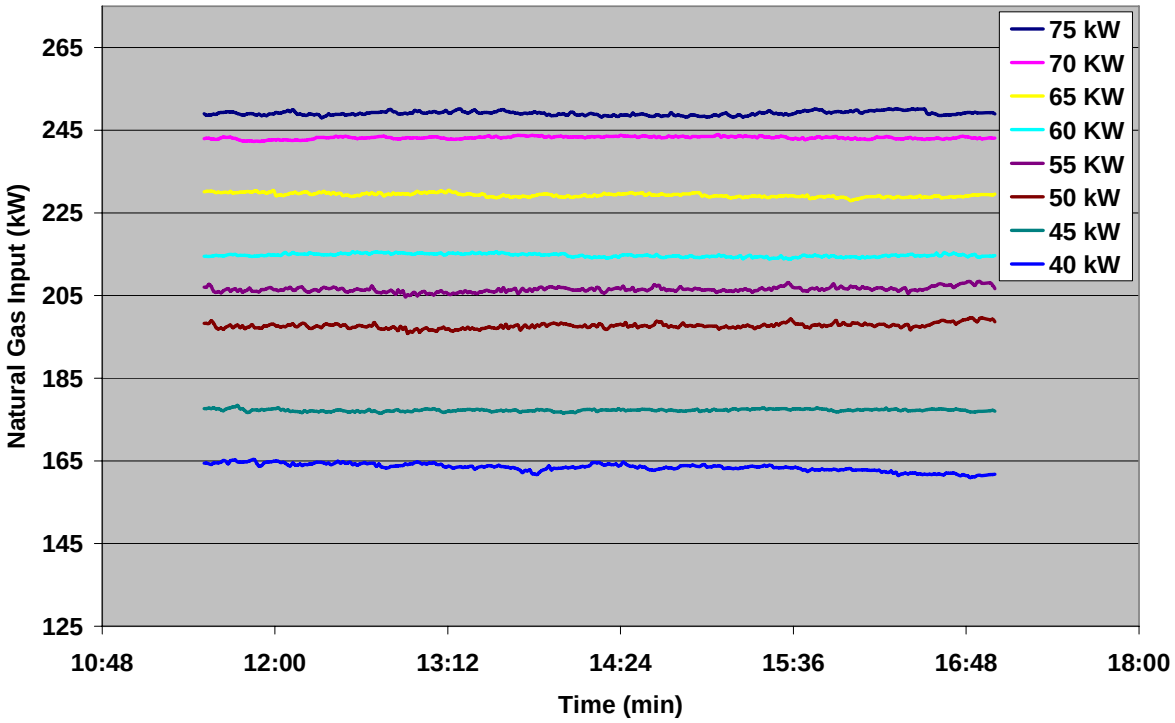

Figure 54: Natural Gas Consumption at Different Engine Generator Loads during the Summer Season

Figure 55 shows the reduction in the consumption of natural gas by the engine generator as the load on it was changed from 75 kW to 40 kW. It can be seen from Figure 55 that the natural gas consumption reduced by about 86 kW as the load on the engine dropped from 75 kW to 40 kW during the summer time which is incidentally same as that observed during the winter season.

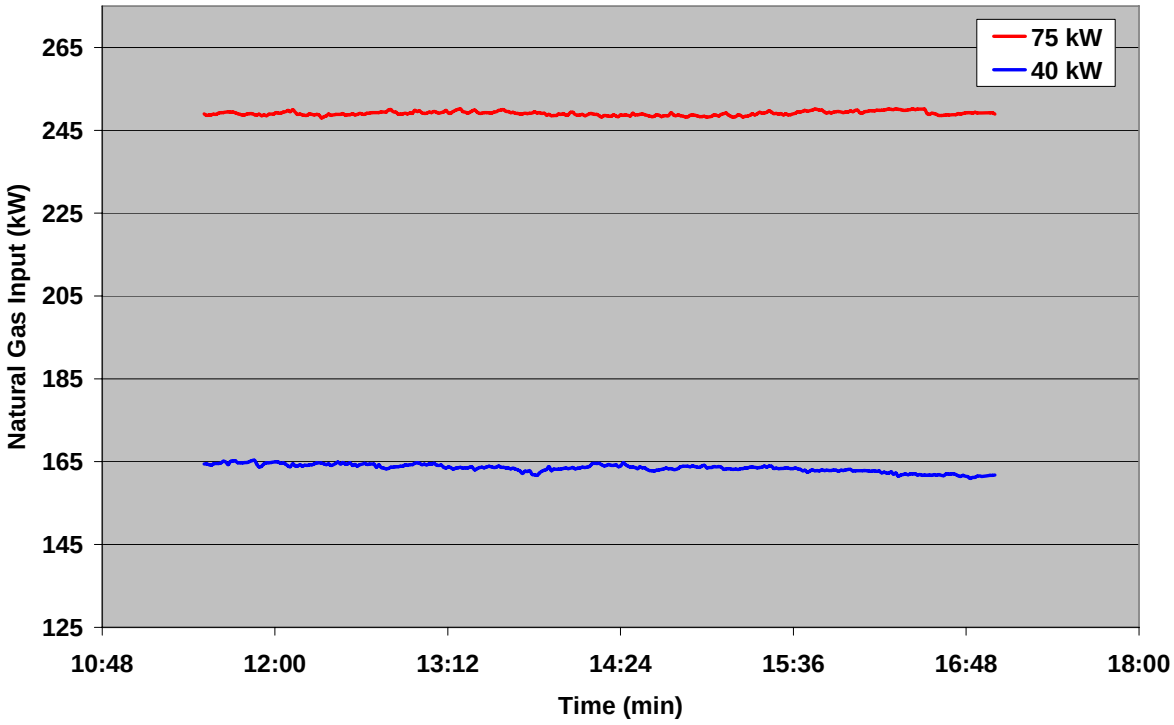

Figure 55: Comparison of Natural Gas Consumption at 75 kW and 40 kW during the Summer Season

Table 18 summarizes the natural gas fuel consumption by the engine generator at various loads during the summer period.

Table 18: Natural Gas Consumption and Outdoor Air Conditions at Part Load during Summer Season

Engine Generator Load (kW)	Day System was Run	Average Natural Gas Consumption (kW)	Average Outdoor Air Temperature (°C)	Average Outdoor Air Enthalpy (kJ/kg)
75	06/01/2005	249	25	42
70	08/10/2005	243	28	61
65	08/05/2005	229	33	64
60	07/01/2005	215	31	63
55	07/27/2005	207	34	70
50	07/28/05	198	35	70
45	09/06/05	177	25	46
40	08/04/2005	163	33	62

The heat of combustion is the energy released as heat when a compound undergoes complete combustion with oxygen. The chemical reaction is typically a hydrocarbon reacting with oxygen to form carbon dioxide, water and heat. The heat of combustion for fuels is expressed in different ways such as the HHV (Higher Heating value), LHV (Lower Heating Value), or GHV (Gross Heating Value). Lower heating value (LHV) accounts for water in the exhaust leaving as vapor. The energy required to vaporize the water therefore is not realized as heat. Gross heating value (GHV) accounts for water in the exhaust leaving as vapor, and includes liquid water

in the fuel prior to combustion. This value is important for fuels like wood or coal, which will usually contain some amount of water prior to burning. Higher heating value (HHV) is the same as the heat of combustion since the enthalpy change for the reaction assumes a common temperature of the compounds before and after combustion, in which case the water produced by combustion is liquid. To determine the electrical performance of the engine generator at full load and various part loads, the net electrical efficiency of the engine generator was calculated during both the winter and summer seasons. The lower heating value (LHV) of the fuel which in this case was natural gas was used in order to determine the energy content of the fuel input. The LHV of natural gas used in calculations was 33906 kJ/m^3 which was arrived at after consulting the engine manufacturer and Washington Gas Energy Services that supply natural gas to the Chesapeake building. The net electrical efficiency of the engine generator was calculated using the following equation,

$$\eta_{elec} = \frac{NetElectricalPower}{\dot{V}_f \, LHV_f}$$

Where,

η_{elec} = Net electrical efficiency of the engine generator

$\dot{V}_f$ = Volumetric flow rate of fuel (natural gas)

LHV_f = Lower heating value of fuel which for natural gas is 33906 kJ/m^3

Figure 56 shows the plots of the electrical efficiencies of the engine generator at full load as well as various part loads during the winter time.

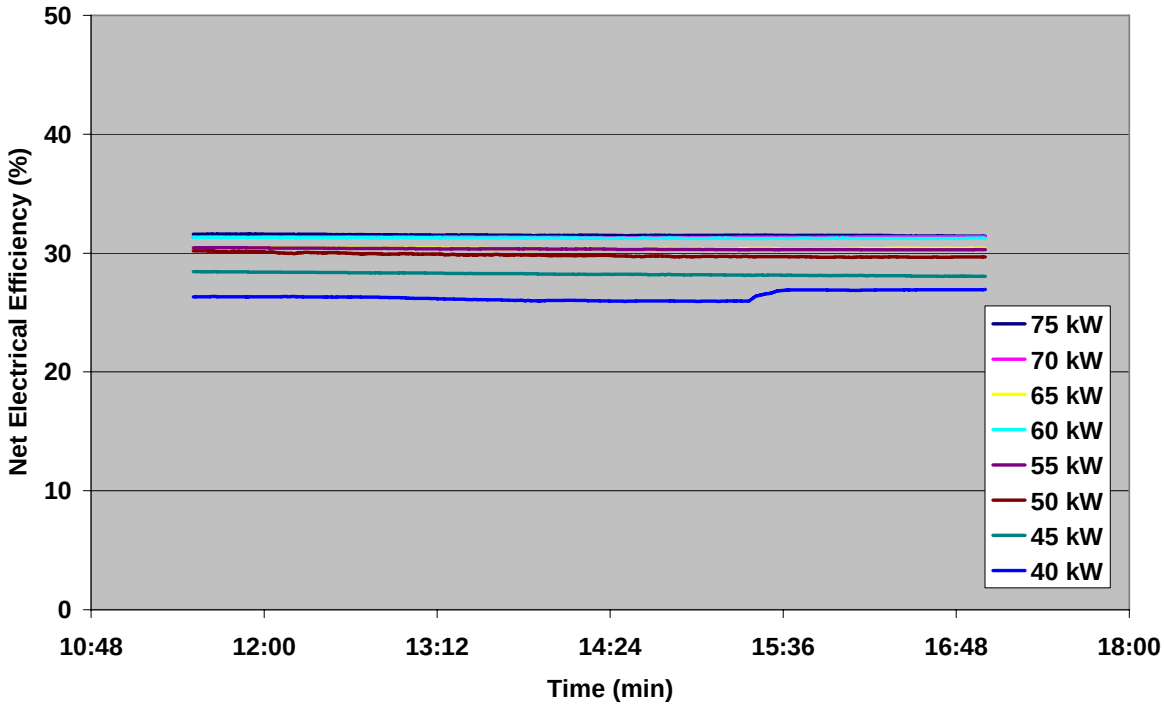

Figure 56: Net Electrical Efficiency at Different Engine Generator Loads during the Winter Season

The net electrical efficiency of the engine generator reduces as the load on it changes from 75 kW to 40 kW. This change in electrical efficiency at 75 kW and 40 kW during the winter period is shown in Figure 57. It is seen that the electrical efficiency of the engine generator increases slightly at around 3:20 pm. This is because of the sudden drop in outdoor air temperature as was explained previously in Figure 52 and Figure 53. The average electrical efficiency of the engine generator at 75 kW was about 32 % while it was around 26 % at 40 kW during the winter season.

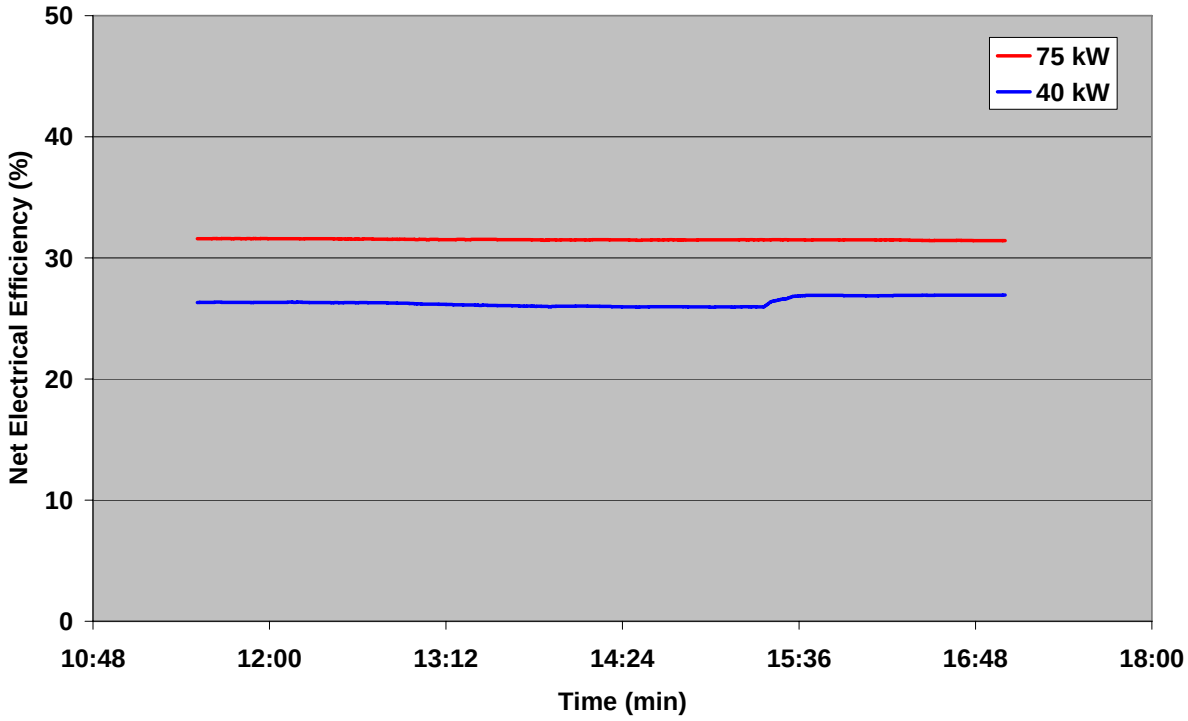

Figure 57: Comparison of Net Electrical Efficiency at 75 kW and 40 kW during the Winter Season

Table 19 enumerates the average electrical efficiencies of the engine generator at different loads for the winter period along with the outdoor air conditions for the different days the system was run.

Table 19: Net Electrical Efficiency and Outdoor Air Conditions at Part Load during Winter Season

Engine Generator Load (kW)	Day System was Run	Average Electrical Efficiency (%)	Average Outdoor Air Temperature (ºC)	Average Outdoor Air Enthalpy (kJ/kg)
75	11/30/2004	32	10	20
70	12/03/2004	31	8	14
65	12/10/2004	30	10	27
60	12/15/2004	31	1	5
55	12/16/2004	30	5	9
50	12/20/2004	30	-7	-6
45	12/21/2004	28	0.3	3
40	12/23/2004	26	13	34

Figure 58 shows the electrical efficiency of the engine generator at various loading conditions during the summer season.

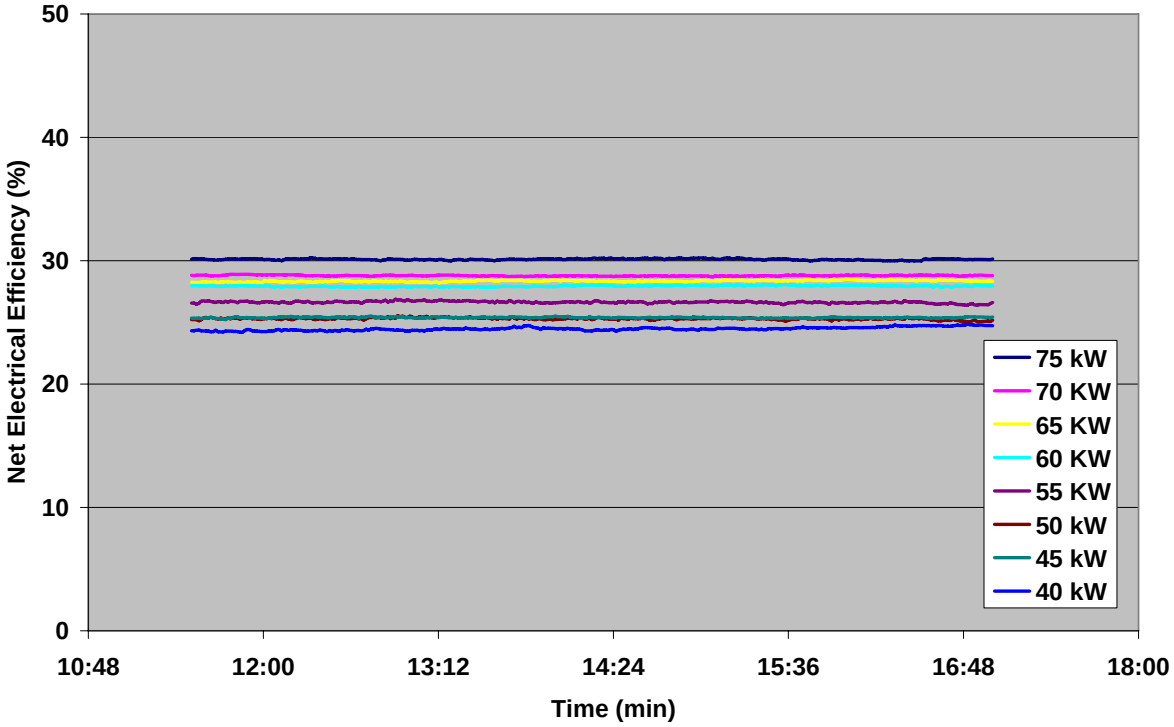

Figure 58: Net Electrical Efficiency at Different Engine Generator Loads during the Summer Season

Figure 59 compares the performance of the engine generator in terms of its net electrical efficiency between 75 kW and 40 kW for the summer period. It is observed from Figure 59 that the net electrical efficiency is around 30 % at 75 kW while it's about 24 % at 40 kW which is a reduction of 6 % from full load to the lowest part load that the engine was run at which was 40 kW.

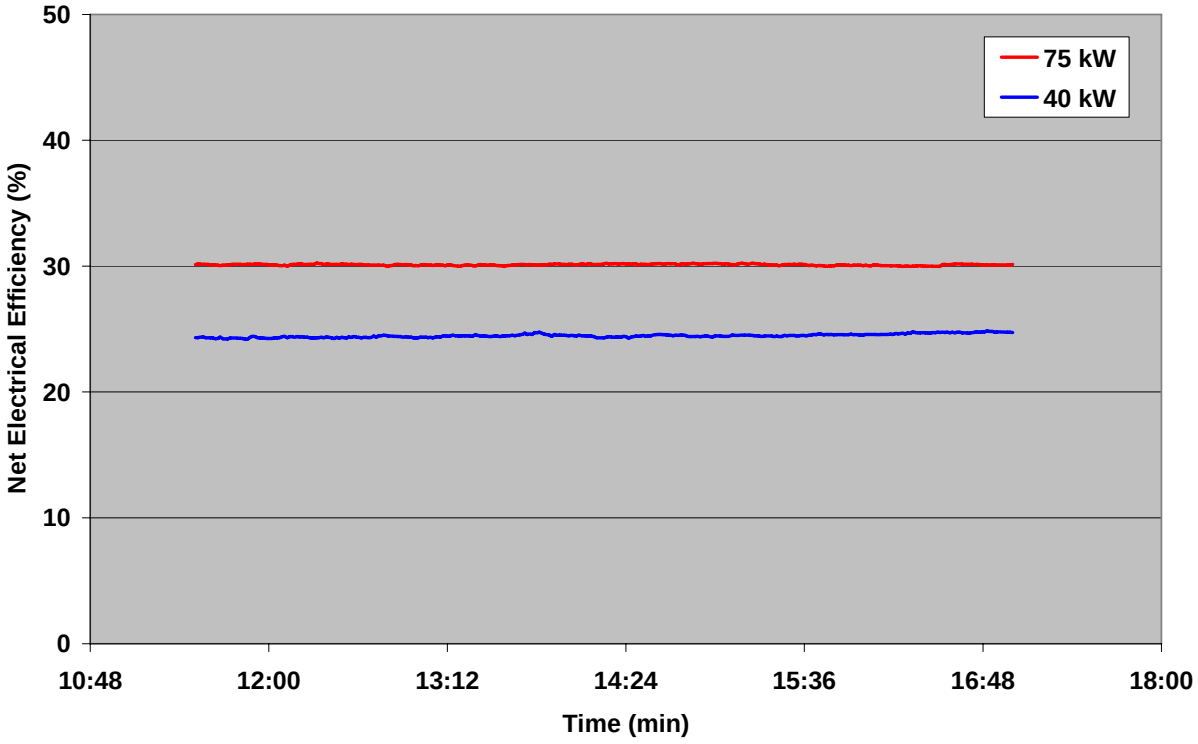

Figure 59: Net Electrical Efficiency at Different Engine Generator Loads during the Summer Season

The average electrical efficiency of the engine generator at full load and part load for the summer season is summarized in Table 20.

Table 20: Net Electrical Efficiency and Outdoor Air Conditions at Part Load during Summer Season

Engine Generator Load (kW)	Day System was Run	Average Electrical Efficiency (%)	Average Outdoor Air Temperature (°C)	Average Outdoor Air Enthalpy (kJ/kg)
75	06/01/2005	30	25	42
70	08/10/2005	29	28	61
65	08/05/2005	28	33	64
60	07/01/2005	28	31	63
55	07/27/2005	27	34	70
50	07/28/05	25	35	70
45	09/06/05	25	25	46
40	08/04/2005	24	33	62

The output of a spark-ignition engine depends largely on the quantity of energy liberated during the combustion of the fuel and the air. The volume of air utilized by the engine is many times the volume of the fuel used. Since the useful air-fuel mixture range is restricted, the output of the engine is pretty much limited by the amount of air which can be inducted. More air inducted permits the useful addition of more fuel, thus increasing the energy available to produce work. The ambient air conditions actually affect the volumetric efficiency of the engine. The volumetric efficiency is a measure of the success with which the air supply, and thus the charge,

is inducted into the engine. It is defined as the ratio of the actual weight of air drawn into the engine during a given period of time to the theoretical weight which should have been drawn in during that same period of time, based upon the total piston displacement of the engine, and the temperature and pressure of the surrounding atmosphere (Gill et al., 1959). Thus as outdoor air temperature increases, the density of air decreases resulting in less amount of charge admitted into the engine, resulting in lower volumetric efficiency. Similarly, the volumetric efficiency is higher in the winter season when the outside air temperatures are lower and the density of air is higher resulting in greater electrical efficiency of the engine generator since a greater weight of charge can be inducted into a given volume. Since in this case, the output of the engine generator is fixed at the start of each test, the effect of outside air conditions can be seen on the net electrical efficiency of the engine generator. Figure 60 plots the net electrical efficiency of the engine generator at 75 kW over a range of ambient air enthalpy. The data represents the average values of net electrical efficiency and outside air enthalpy for the days in both winter and summer when the engine was run. It is seen that for the same output power of 75 kW, the engine generator had higher electrical efficiency at lower air temperatures and enthalpies during winter as compared to summer conditions.

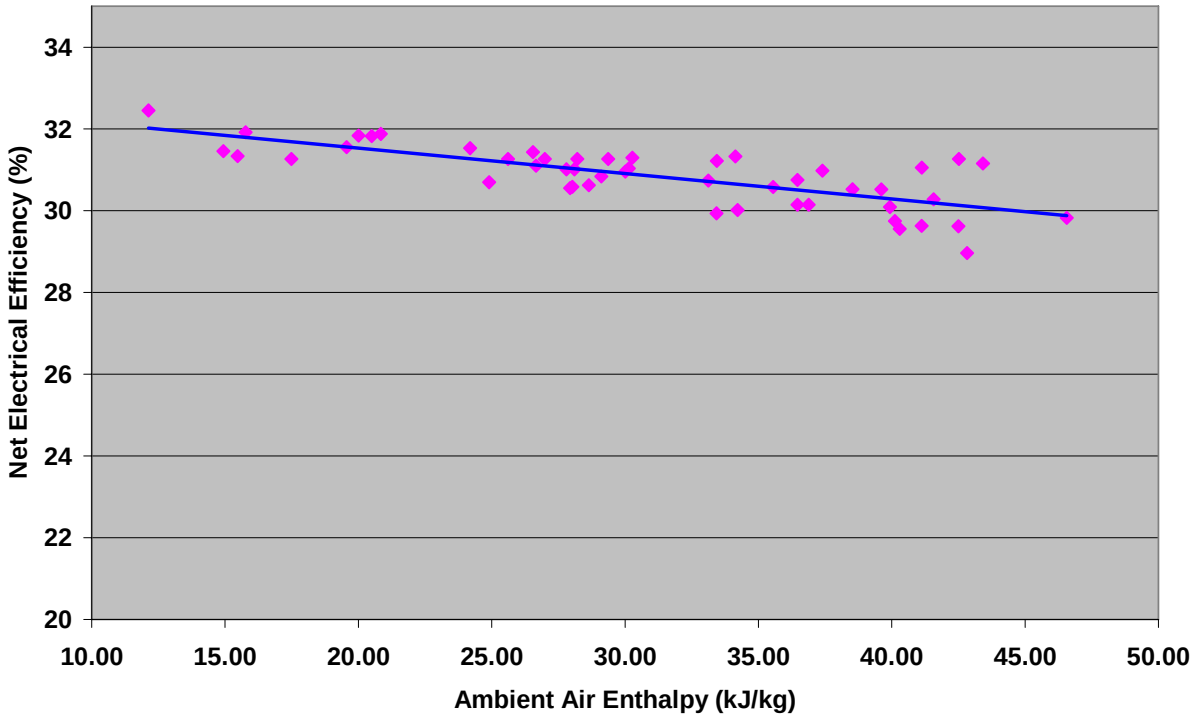

Figure 60: Effect of Ambient Air Enthalpy on Net Electrical Efficiency of Engine Generator

Figure 61 shows the engine performance curves which are plots of net electrical efficiencies Vs the electrical load of the engine generator. The engine performance curves have been plotted for both the winter and summer seasons. It is observed from Figure 61 that the net electrical efficiency of the engine generator at any load is higher in winter than in summer due to the effect of ambient air conditions on the volumetric efficiency of the engine that was explained in the previous section.

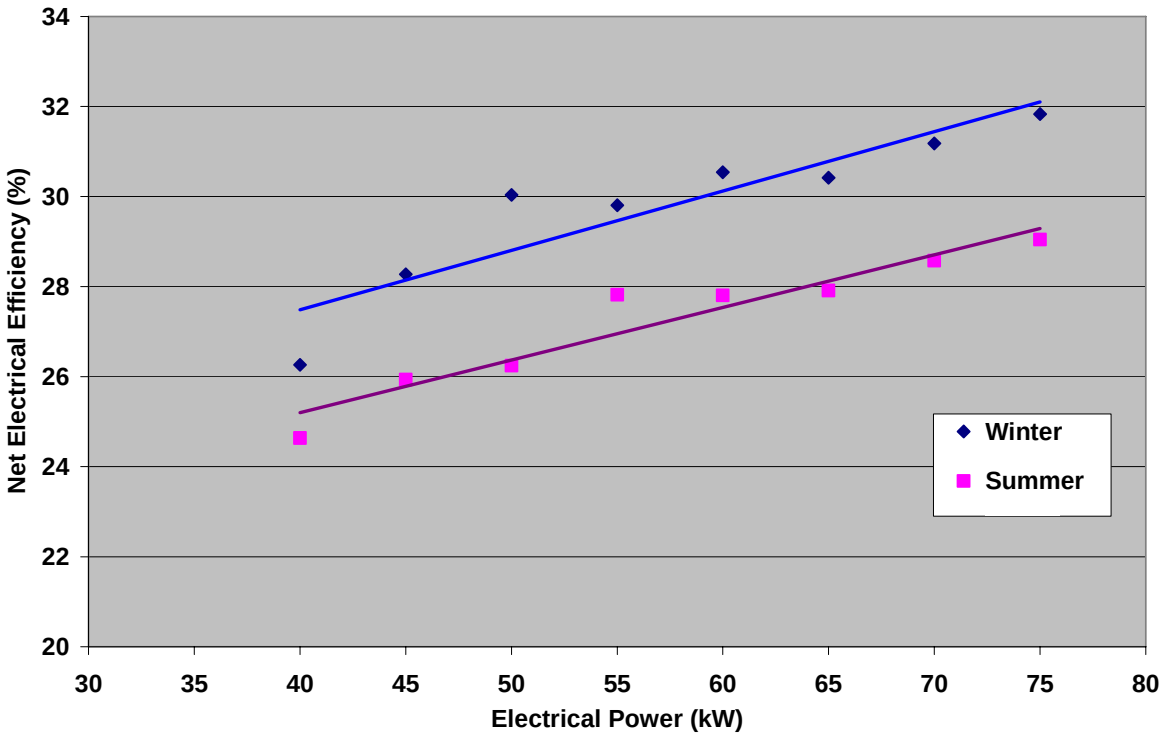

Figure 61: Engine Performance Curves of Engine Generator during Winter and Summer Seasons

Similar to the electrical efficiency, a packaged CHP efficiency of the engine generator was defined based on the net electrical power and the total waste heat recovered from the engine generator. To calculate the CHP efficiency of the engine generator, the following equation was used,

$$\eta_{CHP} = \frac{(NetElectricalPower + TotalWasteHeat)}{NaturalGasFuelInput}$$

Figure 62 shows the CHP efficiency of the engine generator at full load and different part load conditions for the winter season.

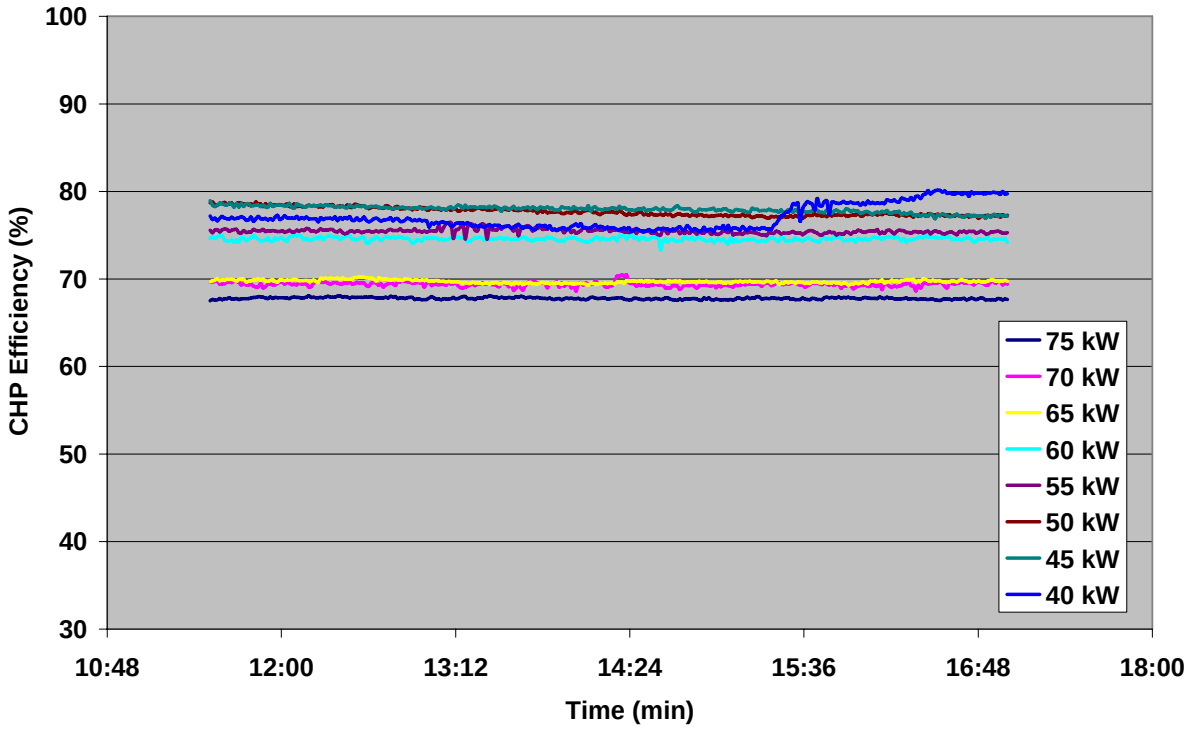

Figure 62: CHP Efficiency at Different Engine Generator Loads during the Winter Season

The comparison of CHP efficiency of the engine generator at 74 kW and 40 kW during the winter season is shown in Figure 63. The average CHP efficiency for 75 kW was around 68 % while for 40 kW, it was about 77 %. The CHP efficiency was actually found to higher at part load than at full load. This can be explained by the fact that though the amount of electrical power produced is lower at part load than full load, the total amount of waste heat recovered at part load is not very low in comparison to the base load condition which was discussed in Figure 47. This means that the numerator in the CHP efficiency equation is actually only a little less at part load than full load while the denominator which is the natural gas input is much lower at part load than full load since it has to produce less power. This translates into overall higher CHP efficiency at part load compared to full load condition.

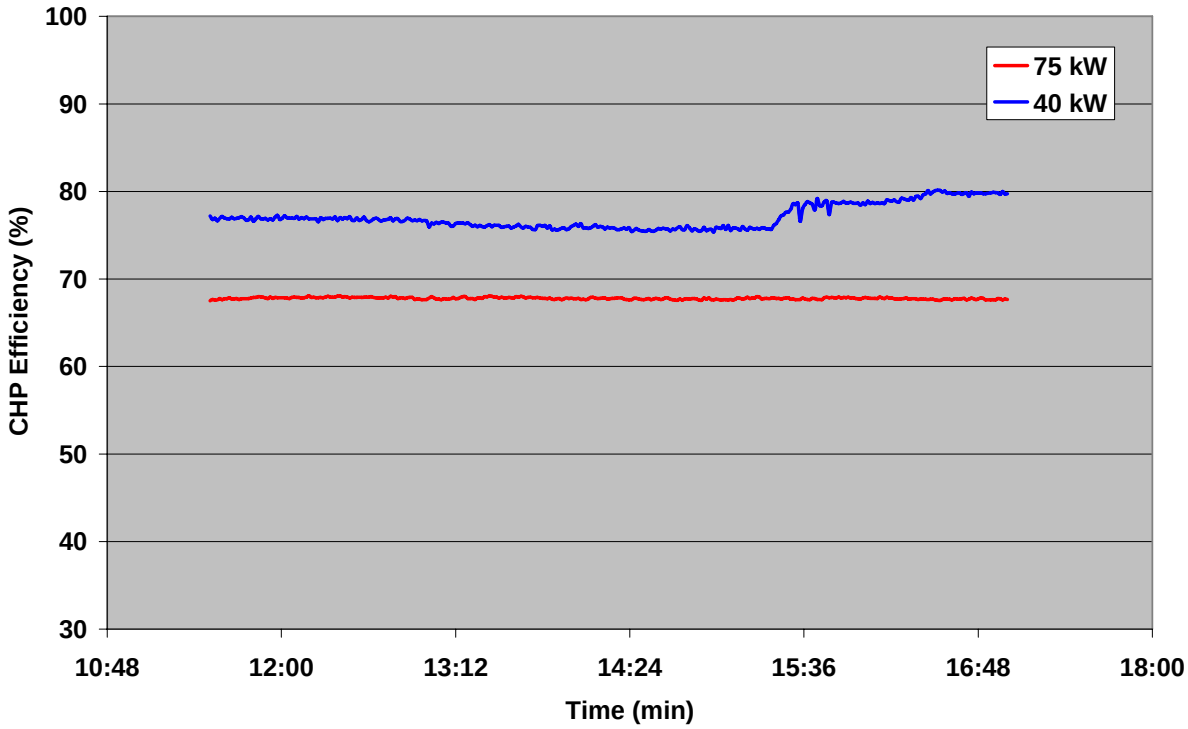

Figure 63: Comparison of CHP Efficiency at 75 kW and 40 kW during the Winter Season

It is also seen from Figure 63 that there is a sudden increase in the CHP efficiency for 40 kW. This was due to the sudden drop in outside air temperature that was shown in Figure 53. Table 21 summarizes the average CHP efficiency of the engine generator heat recovery package at different part loads during the winter season. It is seen from Table 21 that the CHP efficiency is actually a little higher at 50 kW and 45 kW than 40 kW owing to much colder air temperatures during these days.

Table 21: CHP Efficiency and Outdoor Air Conditions at Part Load during Winter Season

Engine Generator Load (kW)	Day System was Run	Average CHP Efficiency (%)	Average Outdoor Air Temperature (°C)	Average Outdoor Air Enthalpy (kJ/kg)
75	11/30/2004	68	10	20
70	12/03/2004	69	8	14
65	12/10/2004	70	10	27
60	12/15/2004	74	1	5
55	12/16/2004	75	5	9
50	12/20/2004	78	-7	-6
45	12/21/2004	78	0.3	3
40	12/23/2004	77	13	34

Figure 64 plots the CHP efficiency of the engine generator at different loads for the summer season.

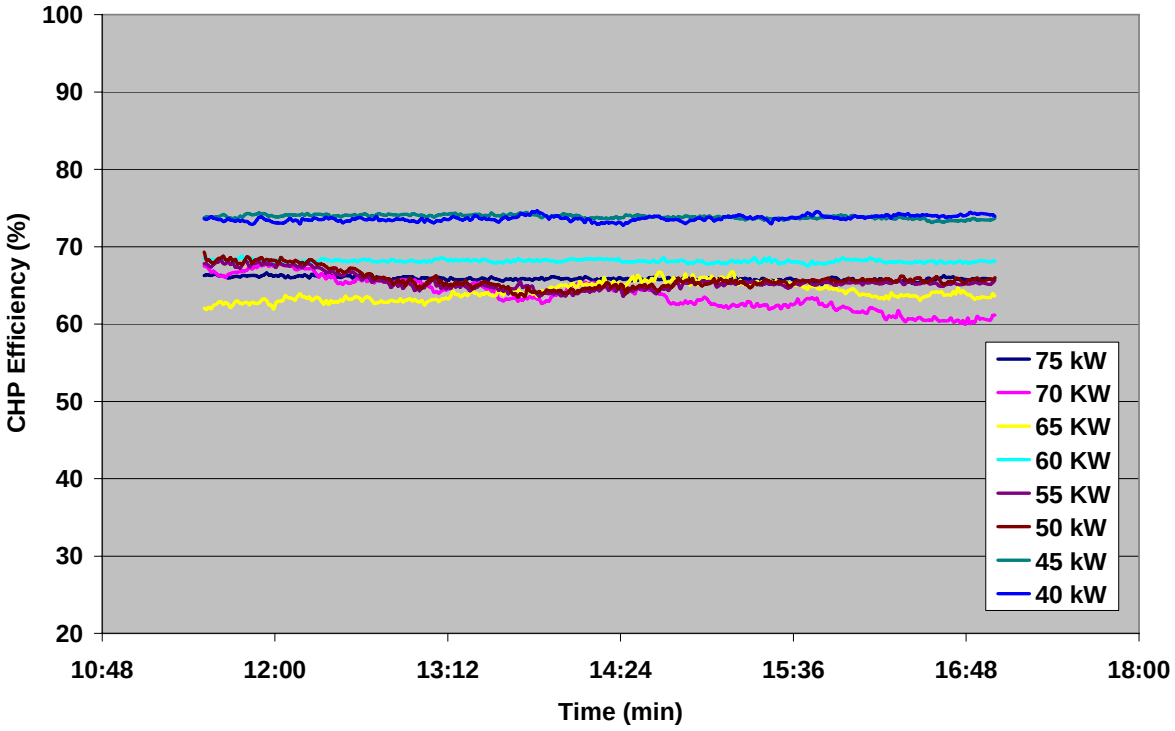

Figure 64: CHP Efficiency at Different Engine Generator Loads during the Summer Season

Figure 65 shows the comparison of CHP efficiency of the engine generator between 75 kW and 40 kW during the summer period. It is seen from Figure 65 that the average CHP efficiency increased from 66 % at 75 kW to around 74 % at 40 kW. This is similar to the situation seen in the winter time.

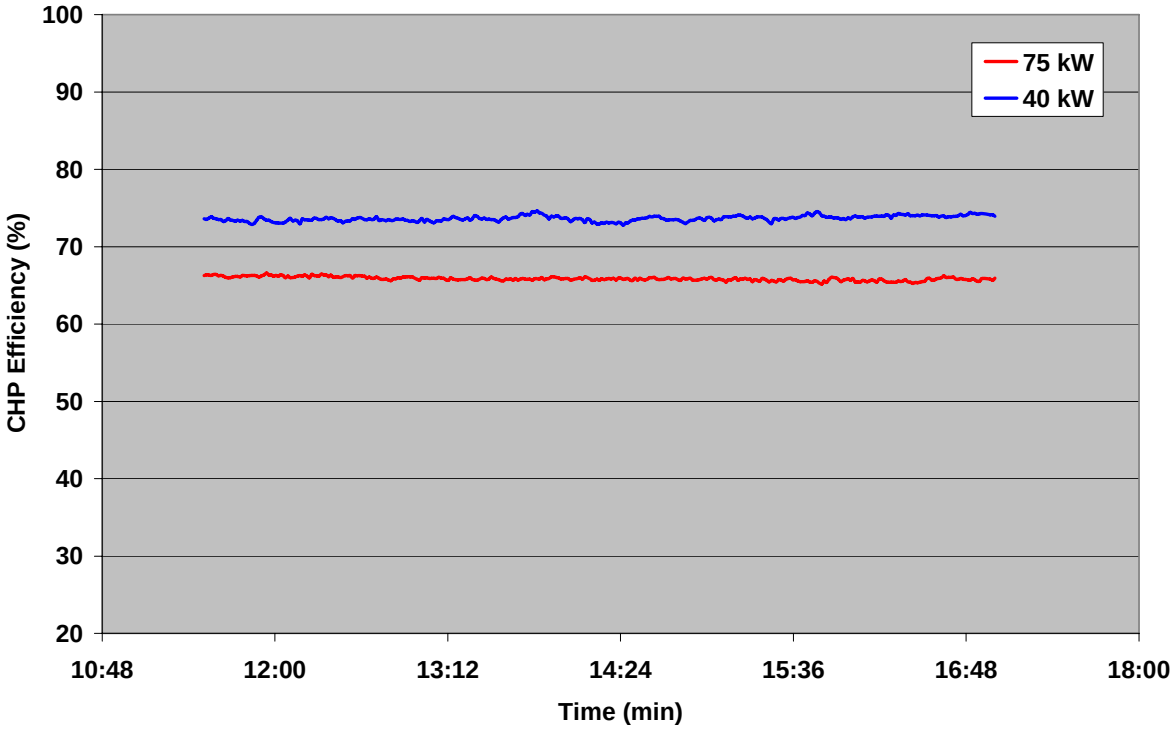

Figure 65: Comparison of CHP Efficiency at 75 kW and 40 kW during the Summer Season

Table 22 enumerates the average CHP efficiency of the engine generator at base load as well as various part loads during the summer season.

Table 22: CHP Efficiency and Outdoor Air Conditions at Part Load during Summer Season

Engine Generator Load (kW)	Day System was Run	Average CHP Efficiency (%)	Average Outdoor Air Temperature (°C)	Average Outdoor Air Enthalpy (kJ/kg)
75	06/01/2005	66	25	42
70	08/10/2005	64	28	61
65	08/05/2005	64	33	64
60	07/01/2005	68	31	63
55	07/27/2005	65	34	70
50	07/28/05	66	35	70
45	09/06/05	74	25	46
40	08/04/2005	74	33	62

5.4 Performance of Liquid Desiccant System

This section deals with the various aspects of the liquid desiccant system such as the latent and total cooling capacity, latent and total COP in order to determine its performance during the summer season. Figure 66 shows the process air and outdoor air temperatures on a hot and humid day in summer. The data was recorded on June 13, 2005 when the engine generator was running at 75 kW. The process air stream is

actually the outdoor air that passes through the conditioner section of the liquid desiccant system, is dehumidified and cooled and then supplied to the mixed air chamber of roof top unit 1 (RTU 1).

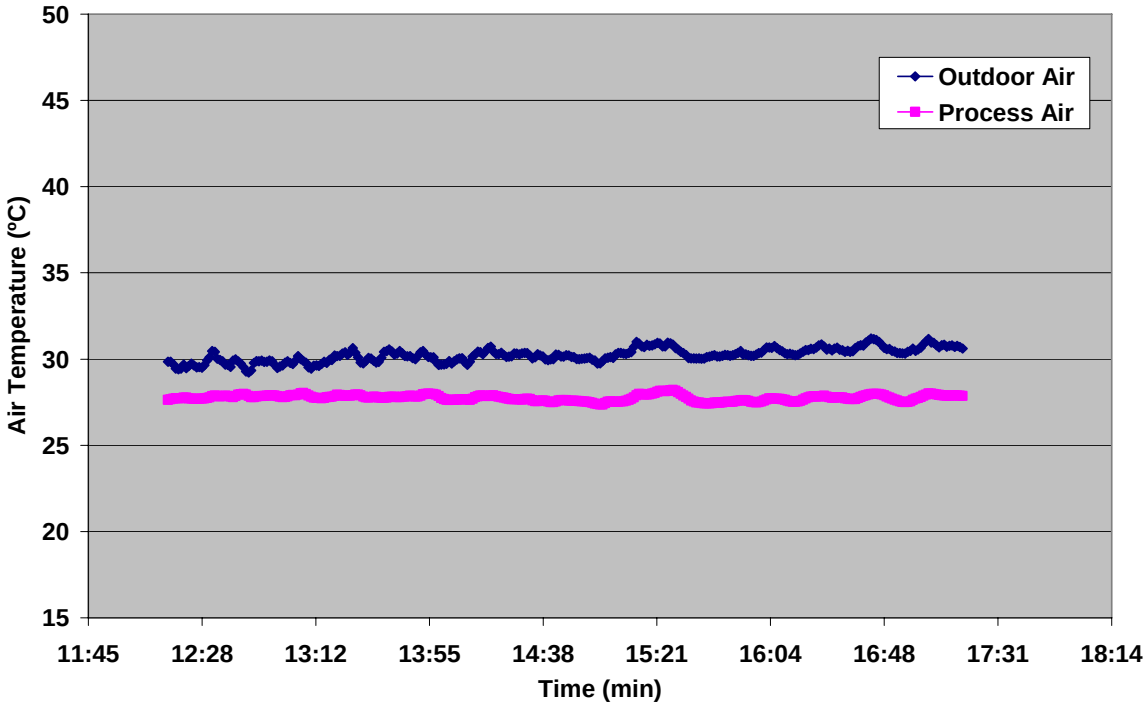

Figure 66: Outdoor and Process Air Temperatures for LDU on June 13, 2005 with 75 kW Engine Generator Load

It is seen from Figure 66 that the average outdoor air temperature was about 30 ºC while the process air temperature was around 27 ºC which shows that the liquid desiccant system also provides sensible cooling in addition to taking care of the dehumidification or latent load. Figure 67 shows the humidity ratio of the process air supplied to the mixed air chamber of RTU 1 along with the outdoor air humidity ratio. The temperature and relative humidity is actually measured in the experimental set up and the humidity ratio is calculated using psychometric routines in Engineering Equation Solver (EES) software.

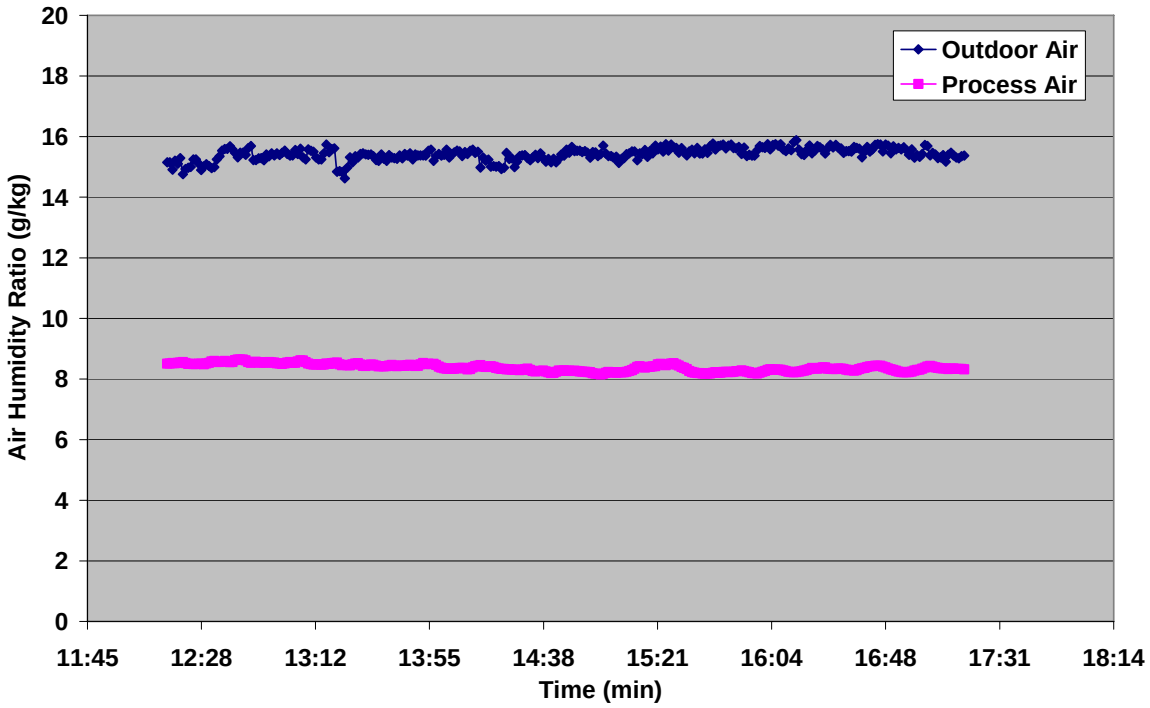

Figure 67: Outdoor and Process Air Humidity Ratios for LDU on June 13, 2005 with 75 kW Engine Generator Load

It can be observed from the humidity ratio plots of Figure 67 that the average reduction in outdoor air humidity achieved by the liquid desiccant system was around 7 g/kg.

The latent cooling capacity of the liquid desiccant system was found out by first calculating the amount of moisture removed from air using the following equation,

$$\dot{m}_{w,rem} = \dot{m}_{oa}(w_{oa} - w_{pa})$$

Where,

$\dot{m}_{w,rem}$ = moisture removal rate

$\dot{m}_{oa}$ = mass flow rate of outdoor air

w_{oa} = humidity ratio of outdoor air

w_{pa} = humidity ratio of process air

The latent cooling capacity was then calculated as below,

$$CoolCap_{latent} = \dot{m}_{w,rem} * L_v$$

Where,

$CoolCap_{latent}$ = latent cooling capacity of the liquid desiccant unit

L_v = latent heat of evaporation

The total cooling capacity provided by the liquid desiccant unit (LDU) is calculated by the equation below,

$$CoolCap_{total} = \dot{m}_{oa}\left(h_{oa} - h_{pa}\right)$$

Where,

$CoolCap_{total}$ = total cooling capacity of the LDU

h_{oa} = enthalpy of outdoor air

h_{pa} = enthalpy of process air

Figure 68 shows the latent and total cooling capacities of the liquid desiccant system for June 13, 2005 when the engine was running at full load of 75 kW. It is observed from Figure 68 that the latent cooling capacity was around 28 kW while the total cooling capacity of the LDU was about 34 kW on that particular day which was quite hot and humid as seen from Figure 66 and Figure 67. Also by comparing the latent and total cooling capacities of the liquid desiccant system from Figure 68, it is seen that the latent cooling is about 82 % of the total cooling capacity of the liquid desiccant unit.

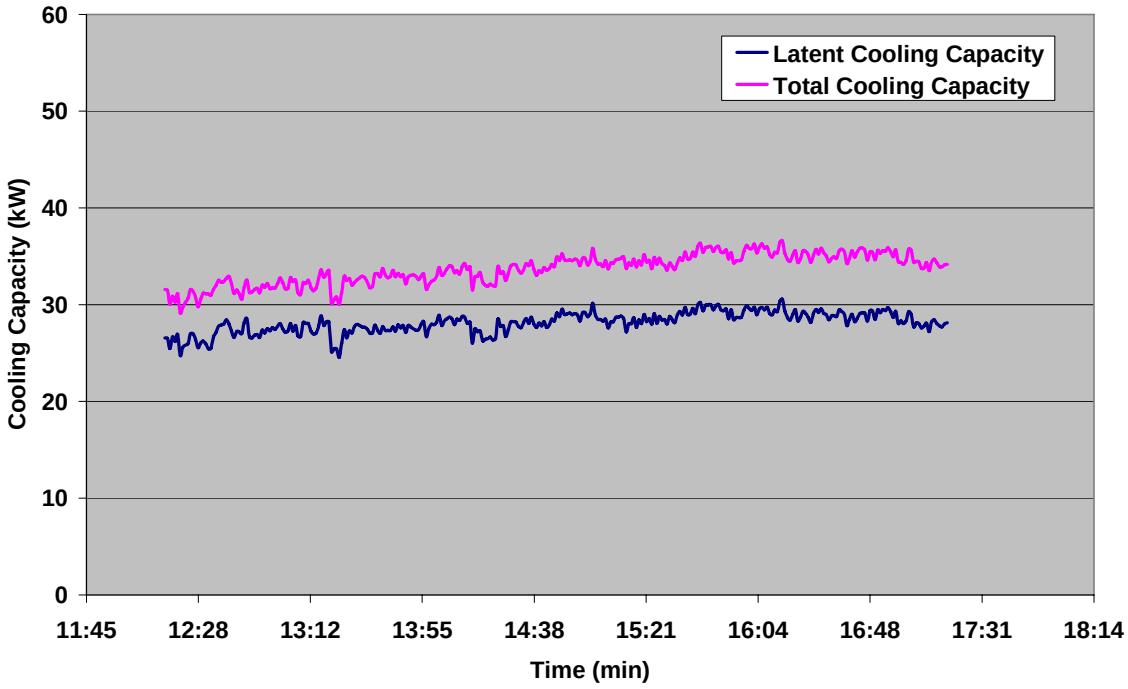

Figure 68: Latent and Total Cooling Capacity of LDU on June 13, 2005 with 75 kW Engine Generator Load

The performance of the liquid desiccant system can be characterized by using the coefficient of performance (COP) for the latent as well as total cooling. Both these COP's can be defined in different ways based on the type of input that is used to calculate them. This section discusses three definitions of COP in order to completely characterize the LDU performance and also know the difference in COP that results by using different definitions. The first one is defined by taking into account the waste heat supplied by the engine generator as the only input to the LDU. The data was analyzed for the day of June 13, 2005 with engine generator producing 75 kW power.

$$COP_{latent,wh} = \frac{CoolCap_{latent}}{WasteHeatInput}$$

$$COP_{total,wh} = \frac{CoolCap_{total}}{WasteHeatInput}$$

Where,

$COP_{latent,wh}$ = latent COP based on only waste heat as input

$COP_{total,wh}$ = total COP based on only waste heat as input

Figure 69 shows the plots of latent and total COP based on the first definition with waste heat as the only input to the liquid desiccant system. It is seen from Figure 69 that the average latent COP was 0.42 while the total COP was 0.5 in this case. The waste heat input supplied to the regenerator section of the LDU was around 68 kW.

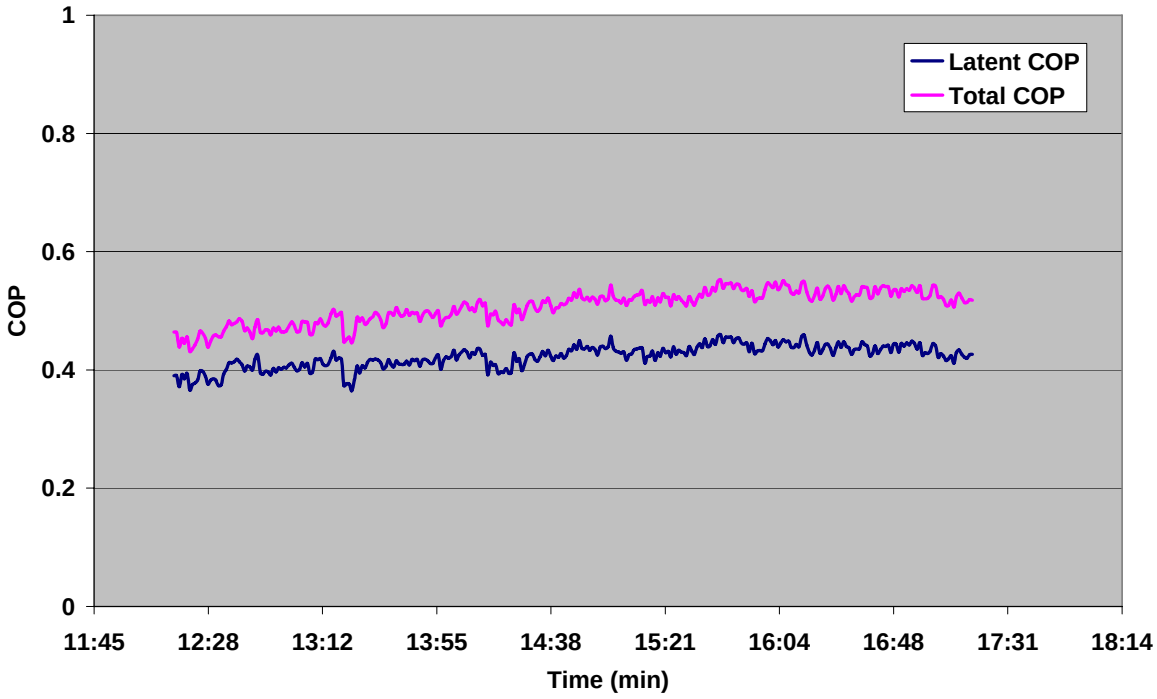

Figure 69: Latent and Total COP of LDU on June 13, 2005 with 75 kW Engine Generator Load based on Waste Heat Input Only

The liquid desiccant system uses electricity in order to run the desiccant pumps and fans. The second definition for the latent and total COP considers this parasitic electrical power as the only input to the LDU while disregarding the waste heat supplied by the engine.

$$COP_{latent,elec} = \frac{CoolCap_{latent}}{ParasiticElectricalPower}$$

$$COP_{total,elec} = \frac{CoolCap_{total}}{ParasiticElectricalPower}$$

Where,

$COP_{latent,elec}$ = latent COP based on only parasitic electrical power as input

$COP_{total,elec}$ = total COP based on only parasitic electrical power as input

The above definition is similar to the one used by chiller manufacturers to define the COP of a vapor compression chiller. The latent and total COP based on parasitic electrical power is plotted in Figure 70. The average latent COP was 2.9 while the total COP was 3.5 in this case which is similar to the COP of a vapor compression chiller. The average electrical power consumed by the pump and fans of the liquid desiccant system was around 9.7 kW.

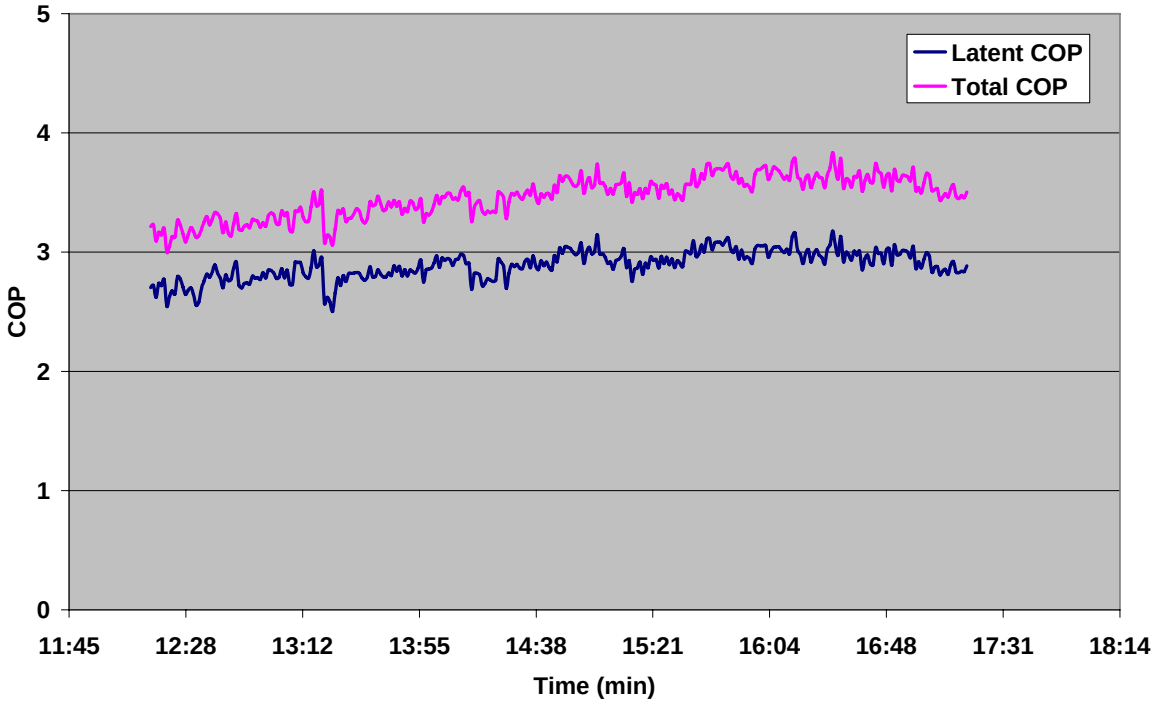

Figure 70: Latent and Total COP of LDU on June 13, 2005 with 75 kW Engine Generator Load based on Parasitic Electrical Power Only

The above results were analyzed when the engine generator was running at base load of 75 kW. Figure 71 shows the process air temperature supplied to the mixed air chamber of RTU 1 along with the outdoor air temperature when the engine generator was run at part load of 40 kW. The data was recorded on June 10, 2005 which was not a very hot day, however it was quite humid.

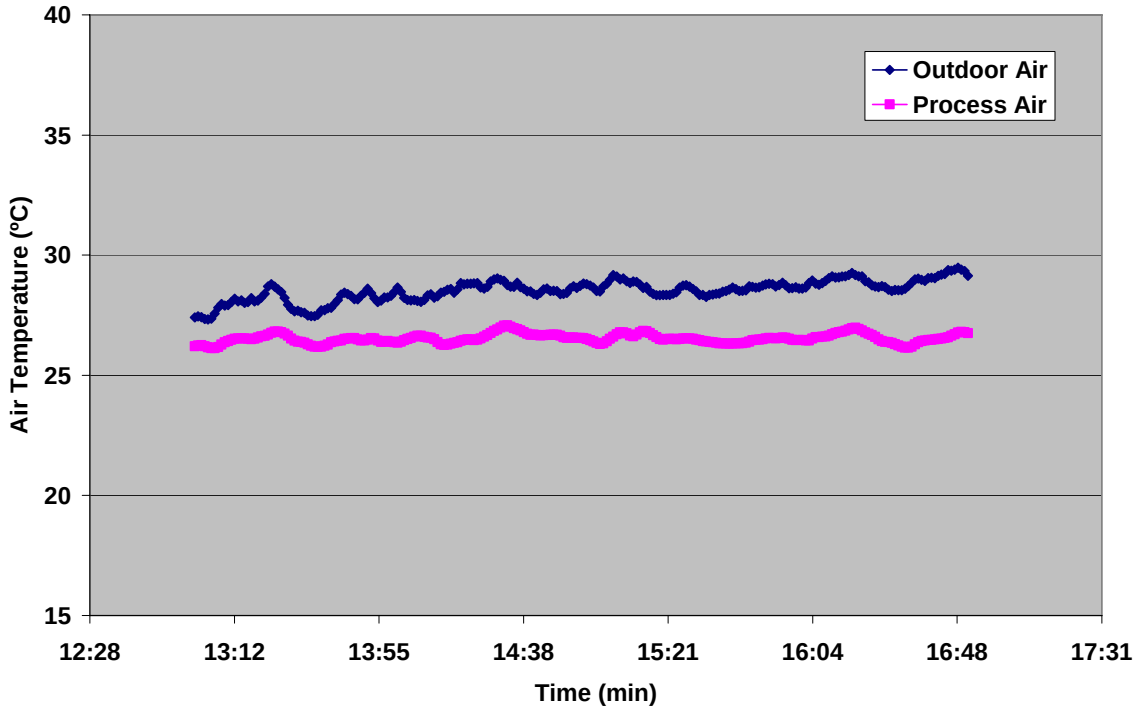

Figure 71: Outdoor and Process Air Temperatures for LDU on June 10, 2005 with 40 kW Engine Generator Load

It is observed from Figure 71 that the process air temperature is around 2 ºC cooler than the outdoor air temperature on this particular day. Figure 72 shows the outdoor air and process air humidity ratios for this day. The average reduction in humidity ratio between the process air and outdoor air was about 7g/kg.

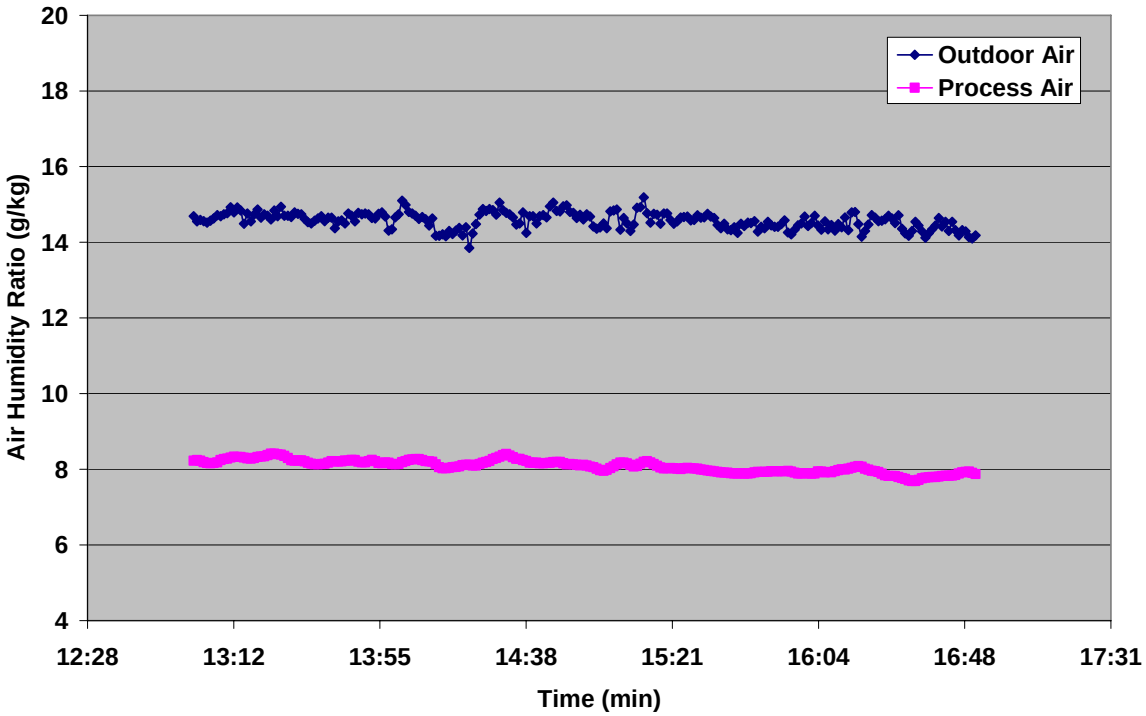

Figure 72: Outdoor and Process Air Humidity Ratios for LDU on June 10, 2005 with 40 kW Engine Generator Load

The latent and total cooling capacity of the liquid desiccant system on June 10, 2005 when the engine generator was being run at part load of 40 kW is shown in Figure 73. The average latent cooling capacity was around 26 kW while the total cooling capacity of the LDU was about 31 kW. In this case the latent cooling capacity was around 84 % of the total cooling capacity of the liquid desiccant system. Both the latent and total cooling capacities were slightly lower on this day as compared to the day of June 13, 2005 which was plotted in Figure 68 owing to different ambient conditions on the two days.

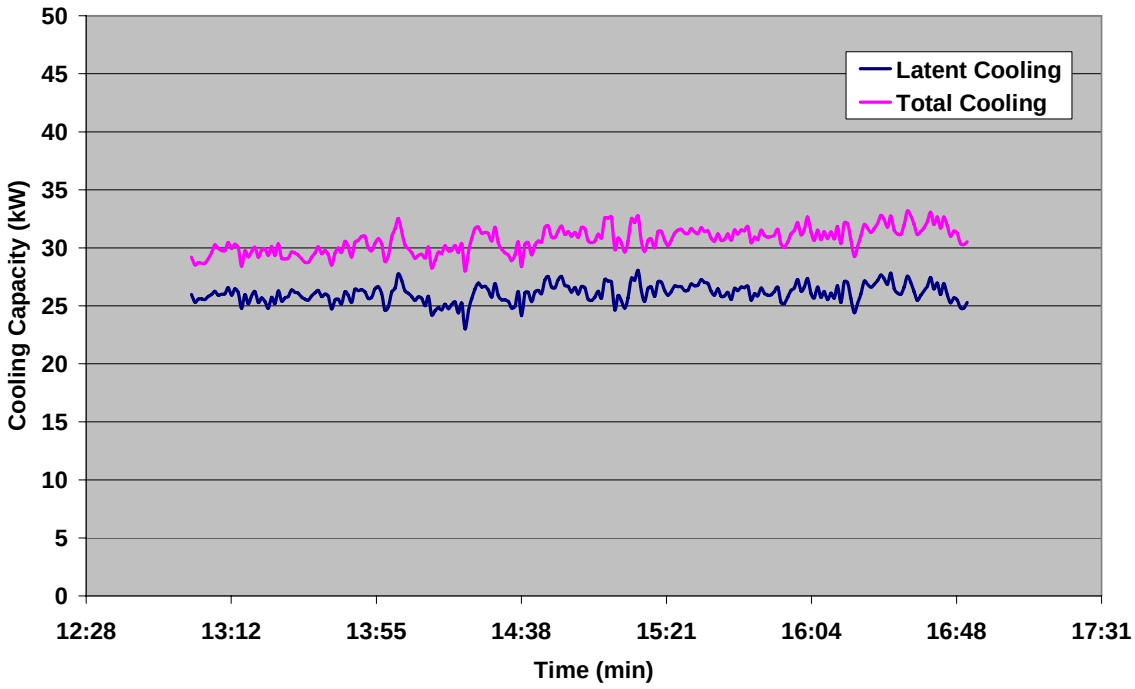

Figure 73: Latent and Total Cooling Capacity of LDU on June 10, 2005 with 40 kW Engine Generator Load

Figure 74 shows the plots of latent and total COP of the liquid desiccant system based on waste heat input only when engine was run at 40 kW. It is seen from Figure 74 that the latent COP was about 0.45 while the total COP was around 0.53 which is slightly higher than the latent and total COP achieved at 75 kW. Both the COP's are a little higher for 40 kW than at 75 KW because the waste heat input to the LDU at 40 kW was around 58 kW as compared to 67 kW at 75 kW.

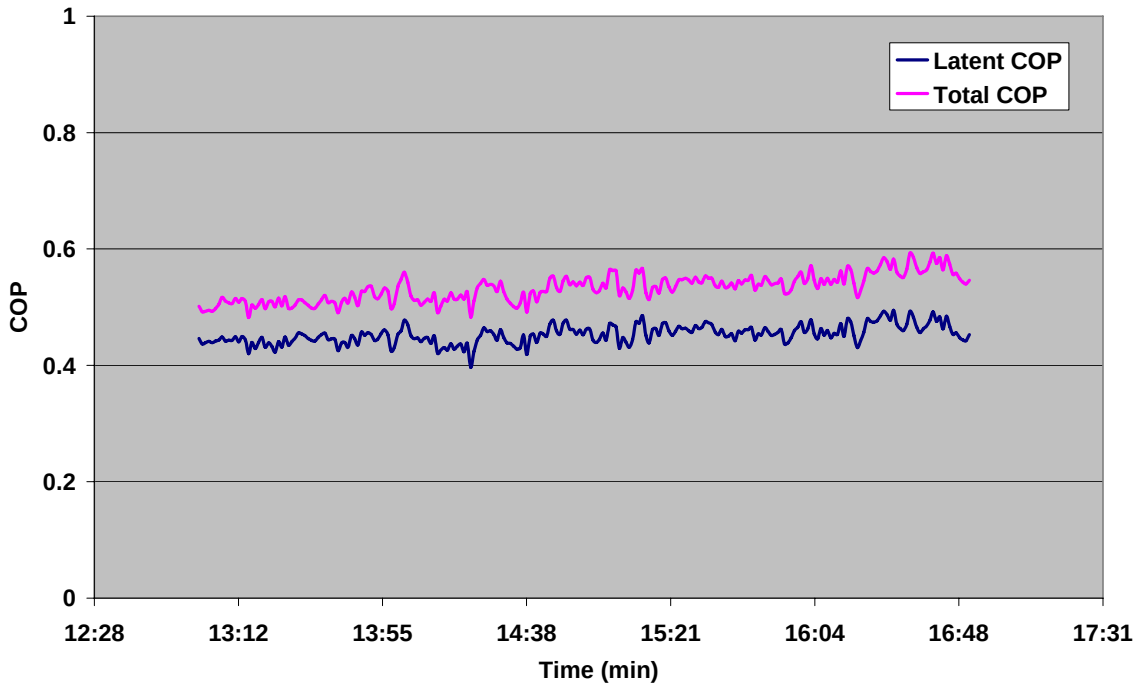

Figure 74: Latent and Total COP of LDU on June 10, 2005 with 40 kW Engine Generator Load based on Waste Heat Input Only

The latent and total COP based on the parasitic electrical power and neglecting the waste heat input at 40 kW is shown in Figure 75. The latent COP in this case was about 2.7 while the total COP was around 3.1 which are less than the COP values at 75 kW due to lower latent and total cooling capacities on the day the engine was run at 40 kW.

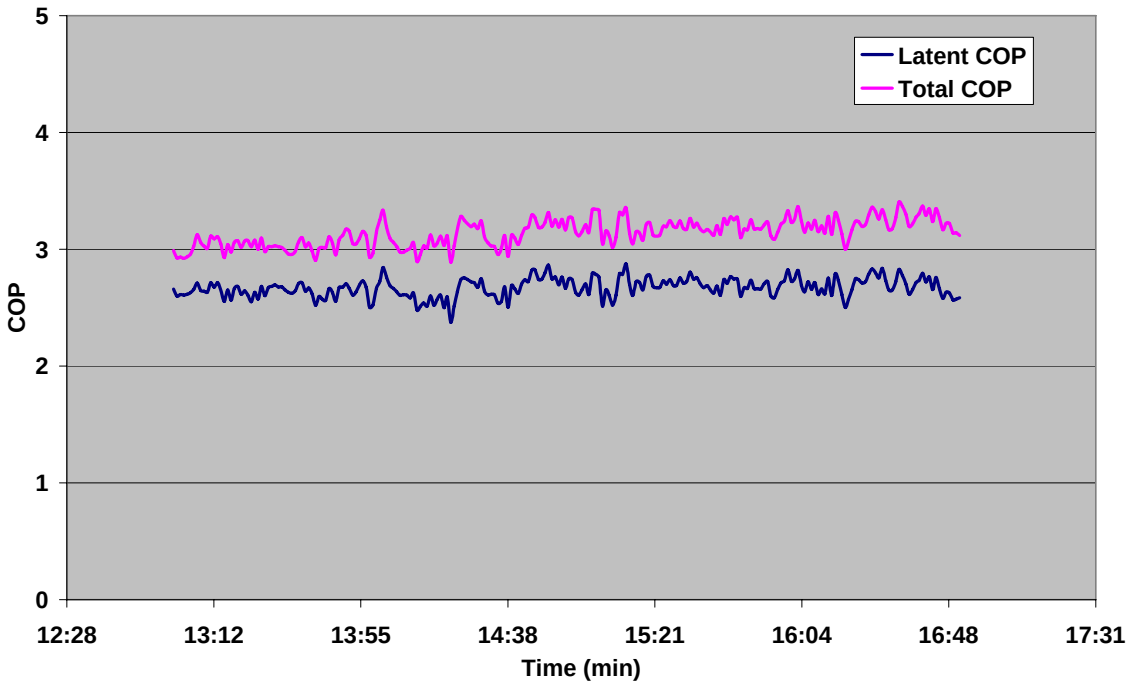

Figure 75: Latent and Total COP of LDU on June 10, 2005 with 40 kW Engine Generator Load based on Parasitic Electrical Power Only

Table 23 provides a comparison of the latent COP of the liquid desiccant system with the engine generator being run at full load of 75 kW and part load of 40 kW while Table 24 summarizes the average total COP of the LDU for these two engine generator loads.

Table 23: Comparison of Latent COP of LDU at 75 kW and 40 kW Engine Generator Loads

Input to LDU	Waste Heat	Parasitic Electrical Power
Engine Generator at 75 kW Load	0.42	2.9
Engine Generator at 40 kW Load	0.45	2.7

Table 24: Comparison of Total COP of LDU at 75 kW and 40 kW Engine Generator Loads

Input to LDU	Waste Heat	Parasitic Electrical Power
Engine Generator at 75 kW Load	0.5	3.5
Engine Generator at 40 kW Load	0.53	3.1

The above two definitions of COP based on waste heat or electrical power as input is what is the normal practice being followed in the industry. However, the coefficient of performance is actually defined as the ratio of the benefit that is obtained over what is paid for to achieve the benefit. So this research proposes a third definition of COP that is based on the primary energy consumption (PEC), which in this case would be natural gas fuel since the fuel is combusted to get electrical power and waste heat.

In defining this COP based on primary energy consumption it is considered that a smaller size engine generator is used that will supply all the parasitic electrical

power required to run the pumps and fans of the liquid desiccant system. The waste heat recovered from this small engine generator is used in the regeneration of the liquid desiccant. However this waste heat would not be enough to meet the heat requirements of the liquid desiccant system. So the additional heat is produced in a boiler that burns natural gas to produce hot water that is then combined with the hot water generated by the waste heat from the engine and this is provided to the regenerator section of the LDU. The latent and total coefficient of performance based on PEC is given by the following equation,

$$COP_{latent,PEC} = \frac{CoolCap_{latent}}{\left[\left(\frac{Power_{elec}}{\eta_{eng}}\right) + \left(\frac{\dot{Q}_{LDU} - \dot{Q}_{wh,eng}}{\eta_{boiler}}\right)\right]}$$

$$COP_{total,PEC} = \frac{CoolCap_{total}}{\left[\left(\frac{Power_{elec}}{\eta_{eng}}\right) + \left(\frac{\dot{Q}_{LDU} - \dot{Q}_{wh,eng}}{\eta_{boiler}}\right)\right]}$$

Where,

$COP_{latent,PEC}$ = Latent coefficient of performance of liquid desiccant system based on primary energy consumption

$COP_{total,PEC}$ = Total coefficient of performance of liquid desiccant system based on primary energy consumption

$Power_{elec}$ = Electrical power produced by the small engine generator

η_{eng} = Electrical efficiency of small engine generator

$\dot{Q}_{LDU}$ = Total heat requirement of the liquid desiccant unit

$\dot{Q}_{wh,eng}$ = Total waste heat recovered from the small engine generator

η_{boiler} = Efficiency of boiler

Based on the electrical power requirement of the liquid desiccant unit, a 10 kW engine generator was considered that has an electrical efficiency of 25 % based on LHV of the fuel and heat recovery efficiency of 75 % (BC Hydro, 2005). Considering the case presented before for the day of June 13, 2005, the latent cooling capacity was 28 kW while the total cooling capacity was around 34 kW. Thus the small engine generator supplies the 10 kW of electrical power to the liquid desiccant unit and also produces about 20 kW of waste heat based on the efficiencies stated above. The engine generator uses 40 kW of natural gas in this process. The remainder waste heat is then produced in the boiler at an efficiency of 80 % by combusting around 60 kW of natural gas. Hence using the above COP equations, the latent COP was found to be 0.28 while the total COP of the LDU was around 0.34 based on primary energy consumption. To compare this with the COP of the existing roof top unit, the COP based on primary energy consumption is used which is given by the following equation,

$$COP_{total,RTU,PEC} = \frac{CoolCap_{total}}{\left(\frac{Power_{elec,RTU}}{\eta_{grid}}\right)}$$

Where,

$COP_{total,RTU,PEC}$ = Total coefficient of performance of the roof top unit based on primary energy consumption

$Power_{elec,RTU}$ = Electrical power required by the roof top unit

η_{grid} = Electrical efficiency of the grid

The electrical efficiency of the grid was assumed to be 30.4 % (Energy Information Administration, US DOE). Thus to provide the 34 kW of total cooling, the primary energy consumption for the RTU works out to 31.94 kW and the total COP of the RTU is around 1.06 based on primary energy consumption as compared to the total COP of 3.5 obtained experimentally using only electrical power as input.

5.5 Performance of Integrated CHP System

The previous sections dealt with detailed characterization of the performance of the engine generator and liquid desiccant unit that formed the individual components of the CHP system. This section provides the efficiency of the integrated CHP system. The total integrated CHP system efficiency is defined as follows,

$$\eta_{CHPSystem} = \frac{Power_{eng} + Cooling_{LDU}}{Fuel_{ip}}$$

Where,

$\eta_{CHPSystem}$ = Efficiency of the integrated CHP system

$Power_{eng}$ = Net electrical power produced by the engine generator

$Cooling_{LDU}$ = Total amount of cooling provided by the liquid desiccant unit

$Fuel_{ip}$ = Amount of natural gas fuel supplied to the engine generator

Figure 76 compares the CHP system efficiencies between full engine load of 75 kW and part load of 40 kW based on the first definition. It is seen that the CHP system efficiency at 75 kW was around 42 % while it was about 43 % at 40 kW.

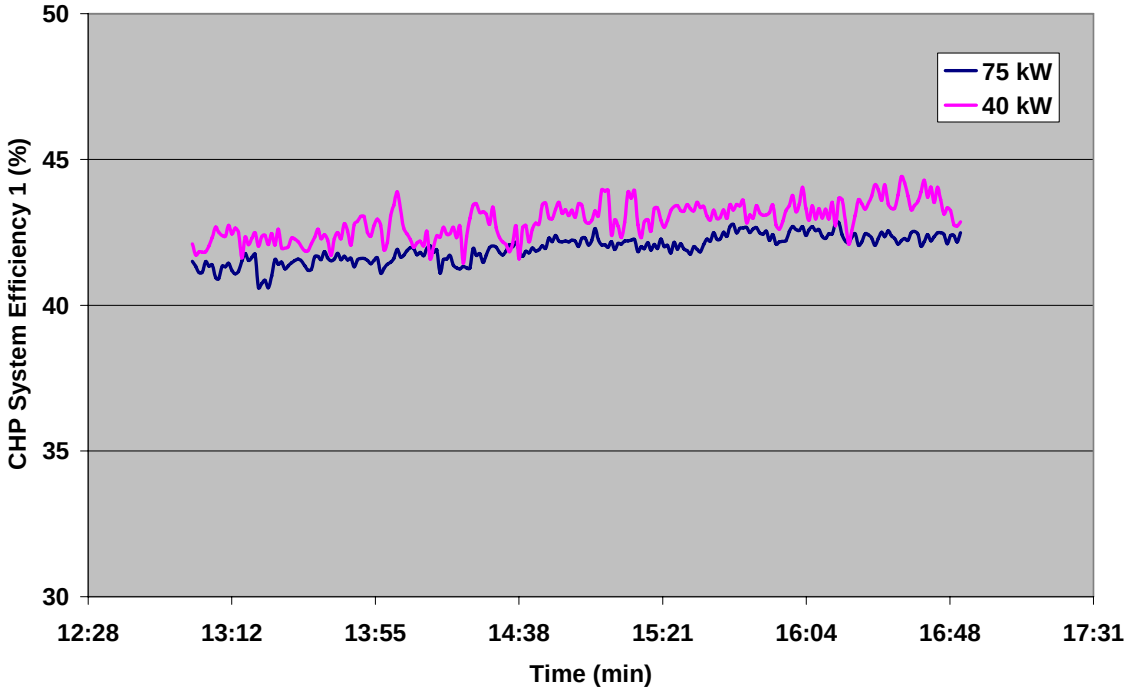

Figure 76: Comparison of CHP System Efficiency 1 between 75 kW and 40 kW

There are different ways of defining the overall CHP efficiency of an integrated CHP system and these different definitions have been explained in detail in Appendix B.

5.6 Performance of Roof Top Unit

The Chesapeake building is a four-storey, administrative building that is divided into two HVAC zones. Each zone has its own roof top unit; roof top unit 1 (RTU 1) caters to zone 1 which comprises of floors 1 and 2 while roof top unit 2 (RTU 2)

takes care of zone 2 which consists of floors 3 and 4. This gives a chance to actually test two different types of CHP systems in the same building at the same time. Thus CHP system 1 consisting of the engine generator and liquid desiccant unit is connected to RTU 1 while RTU 2 is associated with CHP system 2 that consists of a micro turbine, a single effect absorption chiller and a solid desiccant unit. Both the roof top units are identical in nature; each unit equipped with an economizer cycle. Outside air and return air are mixed in the mixed air section before being brought to the 90-ton DX interlaced evaporator coil which is part of two refrigeration systems of equal capacity and condenser units located at one end of the RTU. Detailed description of the roof top unit was provided in Chapter 4.

Figure 77 shows the electrical power consumed by the two roof top units on August 16, 2005. It is seen from Figure 77 that the electrical power consumption profiles of RTU 1 and RTU 2 are quite similar. On this day, the liquid desiccant system was not running and the CHP system 2 was also not in operation.

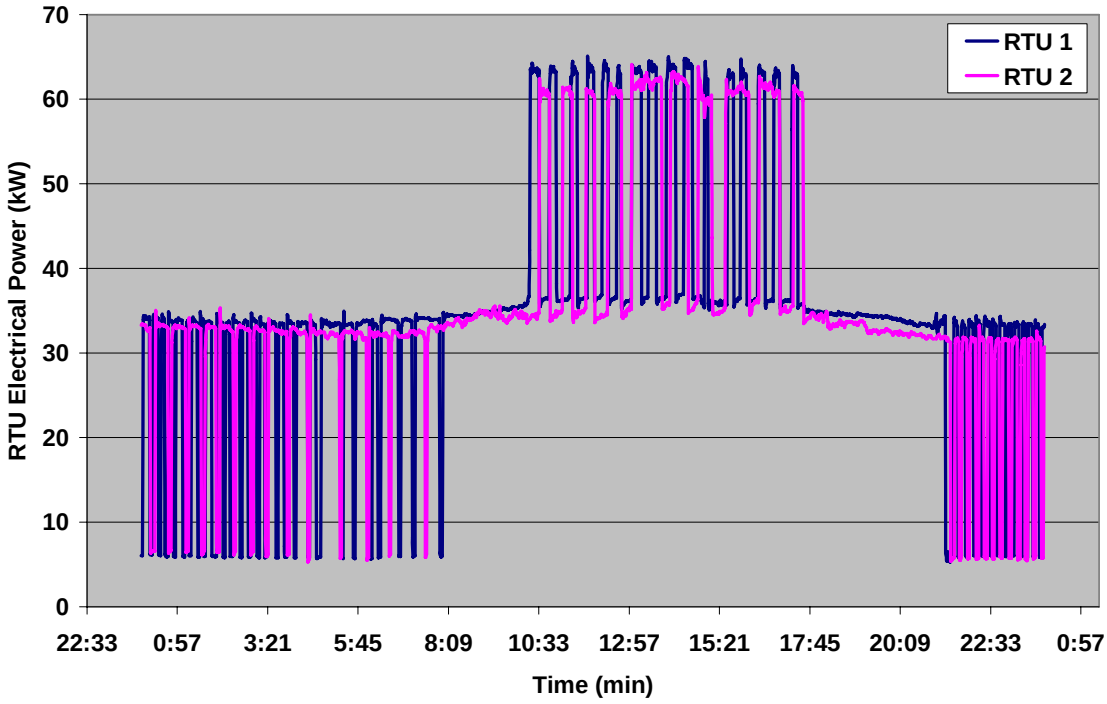

Figure 77: Electrical Power Consumption of RTU 1 and RTU 2 when LDU was Off

Figure 78 compares the electrical power consumption of RTU 1 with RTU 2 when the liquid desiccant unit was in operation on June 16, 2005. Figure 78 shows that there is a reduction in the total amount of electrical power required by the roof top unit 1 as compared to the electrical power requirement of RTU 2. This is because the liquid desiccant system cools and dehumidifies the outdoor air and supplies it to the mixed air section of RTU 1, thus reducing the cooling and dehumidification load on RTU 1, resulting in lower RTU 1 electrical power consumption. The CHP system 2 was also not operated on this day.

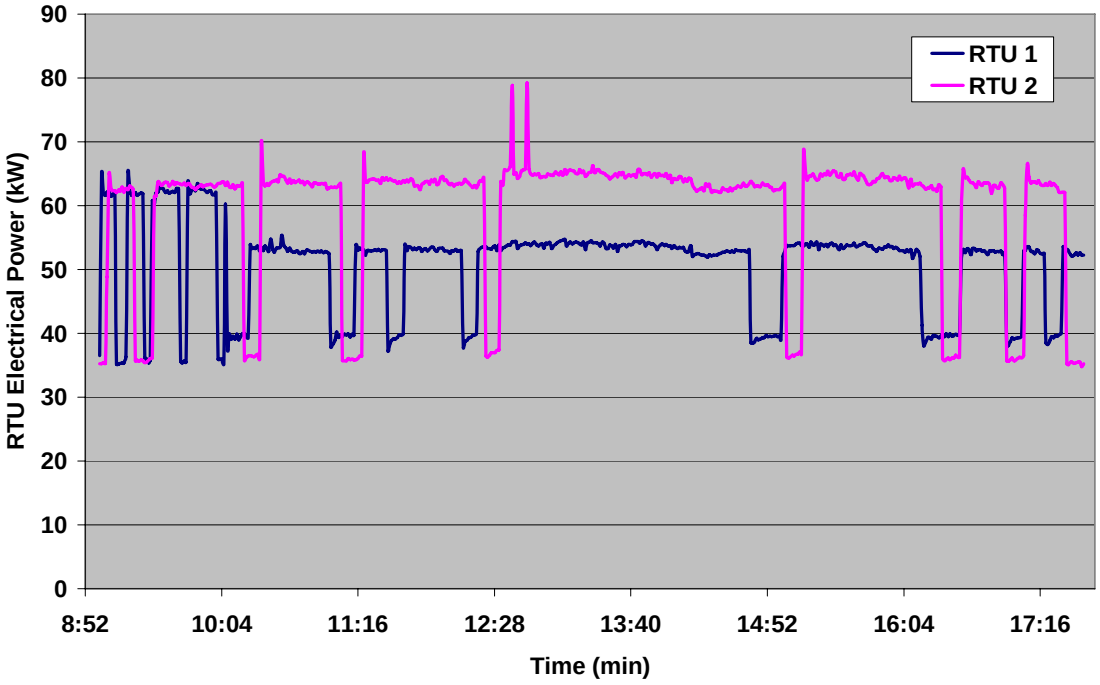

Figure 78: Electrical Power Consumption of RTU 1 and RTU 2 when LDU was On

5.7 Integrated CHP System Vs Conventional Systems

This section compares the integrated CHP system consisting of the engine generator and liquid desiccant unit with a traditional power plant and existing HVAC unit as well as with state of the art system consisting of combined cycle power plant and a new roof top unit in terms of the primary energy consumption (PEC). PEC is a measure of the fuel energy consumed in the provision of a set service, for example heating, heating and power or cooling, heating and power. A variety of different equipment can be used to convert fuel in one or many stages through into the final products. A measure of energy efficiency for systems that converts fuel into a mixture

of cooling, heating and power should recognize which system produces the greatest output for the same energy input, or, conversely, the smallest fuel input for the same outputs.

Figure 79 shows a traditional power plant that burns natural gas as fuel to produce electricity at around 30.4 % efficiency after accounting for transmission and distribution losses (EIA). The situation considered in Figure 79 is where the grid supplies 75 kW of electrical power to the building and also supplies 13 kW of electricity to run the roof top unit which in turn provides 45 kW of cooling to the building. The COP of the roof top unit was assumed to be 3.5, which is actually the average COP of RTU 1 found from analyzing experimental results. The primary energy consumption for this case turns out to about 289 kW.

Figure 80 shows the schematic of CHP system 1 with the engine generator providing 75 kW of electricity that is fed to the building while the waste heat recovered from the engine is used in the liquid desiccant unit which then supplies the 45 kW of cooling to the building. The electrical efficiency of the engine generator is assumed to be 31 % and the COP of the liquid desiccant unit is set at 0.5 that were obtained through experiments. It is seen that the primary energy consumption for this CHP system is around 242 kW.

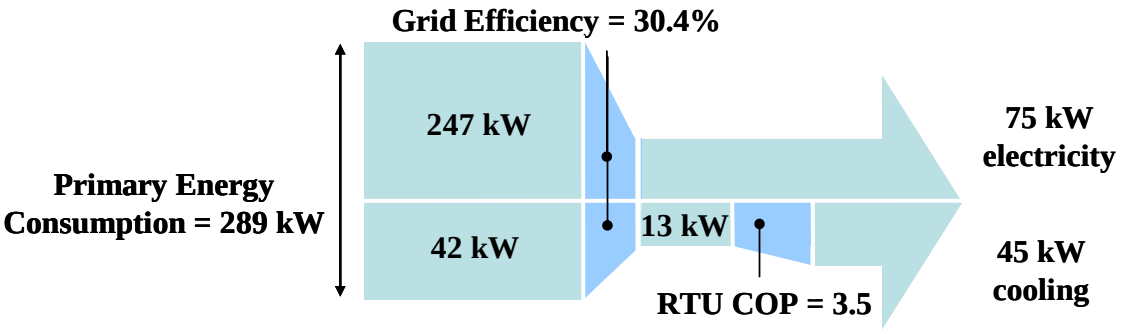

Figure 79: Schematic of Conventional System with Power Plant and Roof Top Unit

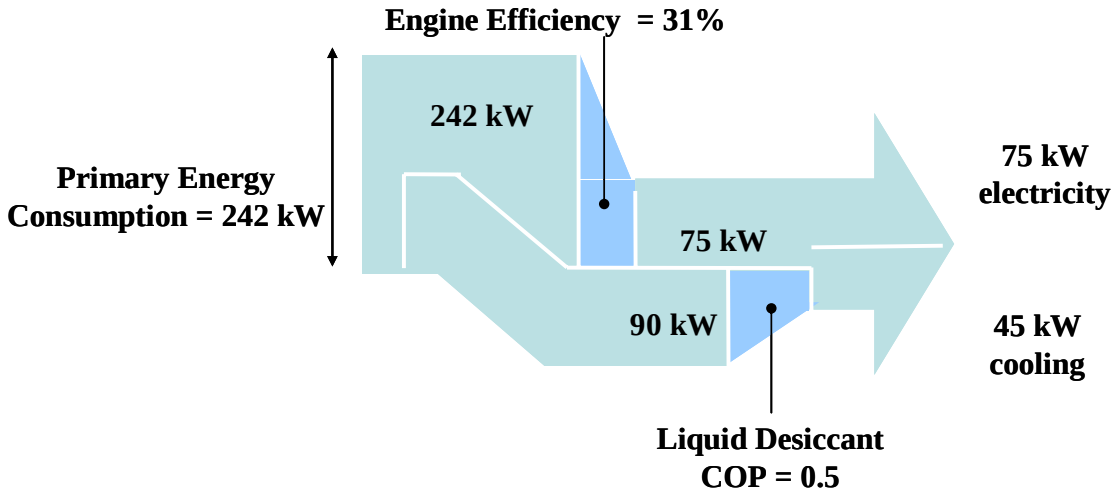

Figure 80: Schematic of Integrated CHP System with Engine Generator and Liquid Desiccant Unit

Thus comparing the integrated CHP system with the conventional system, it is observed that the designed CHP system consumes about 47 kW less of primary energy fuel which in this case is natural gas which translates to savings around 16.3 % in primary energy consumption over a traditional system. However the situation might be quite different when the above CHP system tries to compete with the state

of the art system, such as the University of Maryland campus combined cycle power plant that is operated by Trigen. Figure 81 shows the schematic of such a combined cycle power plant that supplies the 75 kW of electricity required by the building and also supplies the electricity to drive the new roof top unit which supplies the 45 kW of cooling required by the building. The electrical efficiency of the power plant used in the calculation of PEC was around 41 % based on the existing Trigen plant data while the COP of the new roof top unit was set at 5 which was obtained from the manufacturer's product catalog of packaged roof top air conditioners.

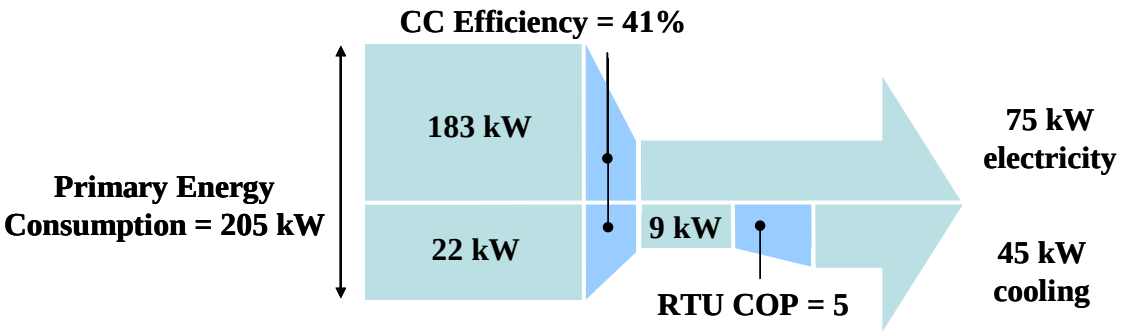

Figure 81: Schematic of Combined Cycle Power Plant and New Roof Top Unit

By comparing this state of the art system with the designed CHP system, it was found that the combined cycle power plant and new RTU system actually consumes about 37 kW less natural gas fuel than the CHP system saving around 15.3 % in primary energy consumption as compared to the CHP system.

Chapter 6: Thermodynamic and Economic Simulation

6.1 Introduction

After characterizing the performance of the system experimentally at base load as well as part load conditions, a theoretical evaluation of the CHP system was conducted through simulation. The modeling of the entire CHP system along with the control of the heat recovery loop was done in Microsoft.Net framework using Visual Basic.Net as the programming language.

The .NET framework is the programming model underlying .NET for developing, deploying, and running Web services and applications. .Net framework allows programs written in different programming languages and on different platforms to communicate and share data with one another through the common language runtime and class libraries that are at the center of the .NET framework. The common language runtime manages memory, security, and language integration. It also helps simplify code development and application deployment while improving application reliability. Using .Net framework would also facilitate code reuse or implementation in third party commercial application software such as Thermoflex, which is currently used to model large cogeneration facilities.

Some of the distinct features offered by Visual Basic.Net programming language are:

- All new, easy-to-use, powerful Integrated Development Environment (IDE)
- Full set of controls – ability to draw the application
- Response to mouse and keyboard actions
- Full array of mathematical, string handling, and graphics functions
- Can easily work with arrays of variables and objects
- Sequential file support
- Useful debugger and structured error-handling facilities
- Easy-to-use graphic tools
- Powerful database access tools
- Ability to develop both Windows and internet applications using similar techniques
- New common language runtime module makes distribution of applications a simple task

The simulation model consists of the following three major components:

1. **Thermodynamic Model:** Steady state thermodynamic models of the engine generator and liquid desiccant system were built based on conservation of energy and mass balance equations. After integration of the individual component models with the heat recovery loop, the thermodynamic model was validated with experimental results. The

inputs to the thermodynamic model are the ambient temperature and relative humidity and the power produced by the engine generator.

2. **Climate Model:** Following the validation of the thermodynamic model with the experimental results, weather data in the form of temperature and humidity ratio for different representative US states were incorporated into the model to assess the performance of the system under varying climate conditions. The US states were selected to cover the entire range of weather conditions ranging from mild to hot temperatures and dry to very humid weather. The inputs of the model in this case are the hourly profiles of outdoor air dry bulb temperature and relative humidity for each state.

3. **Economic Model:** Finally, an economic model consisting of average monthly electricity and natural gas prices for the above US states was integrated to quantify the energy savings and the payback period that is dependent on the capital cost as well as the operating cost. This is essential since the electricity and natural gas prices vary widely from region to region especially the cost of natural gas which is very volatile. The inputs to the model are the monthly electricity and natural gas prices for each state.

6.2 Need for Thermodynamic and Economic Model

The thermo-economic model of the CHP system combining the engine generator and a liquid desiccant system with built in weather information and electricity and gas prices will provide the building design engineers and system integrators with a powerful tool to assess the feasibility of the CHP system not only in terms of performance but also the economic viability of putting together such a CHP system. The different US states selected to conduct the assessment of the CHP system are Maryland, Arizona, Florida, California, New York, Georgia and Texas.

Figure 82 and Figure 83 show the humidity ratio and temperature respectively for Maryland along with their number of hours or frequency that they occurred in the year 2004 obtained from ASHRAE TMY data. Figure 84 and Figure 85 show the average monthly electricity and natural gas prices respectively for the annual year 2004 for Maryland that was obtained from Energy Information Administration (EIA) under US Department of Energy (DOE). The year 2004 was chosen for modeling purposes since all the data for the year 2005 was not yet available. It is observed that Maryland has moderate temperatures; however the humidity is high coinciding with the hottest part of the year making it a good candidate for the current CHP system since a liquid desiccant system provides both sensible cooling as well as dehumidification. Also the electricity is cheap while the natural gas prices are on the higher side.

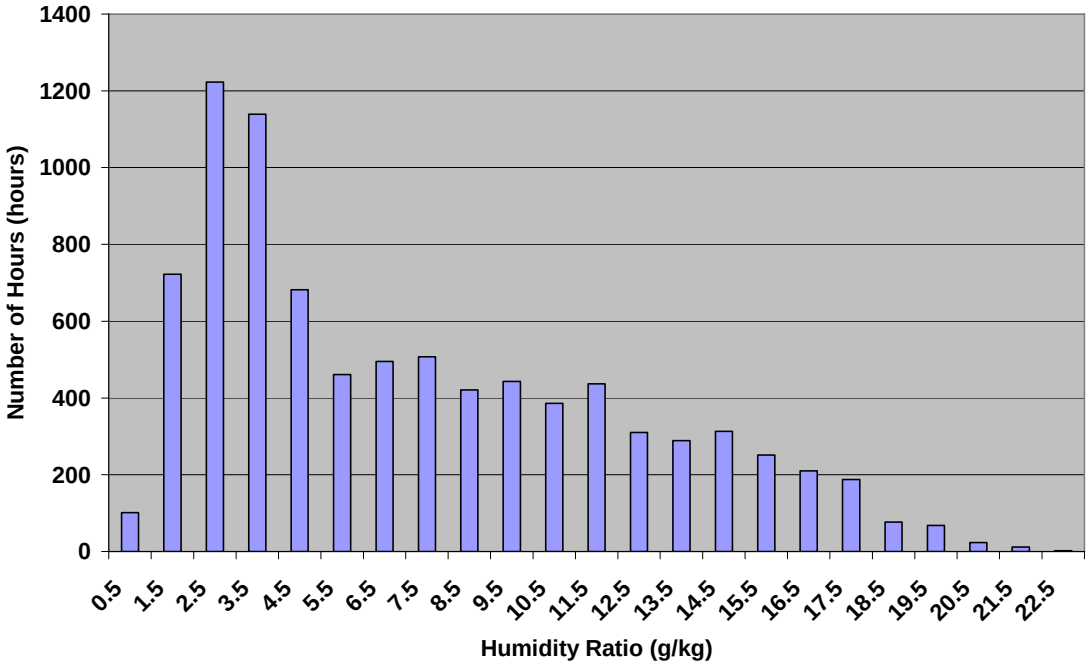

Figure 82: Humidity Levels in Maryland in 2004

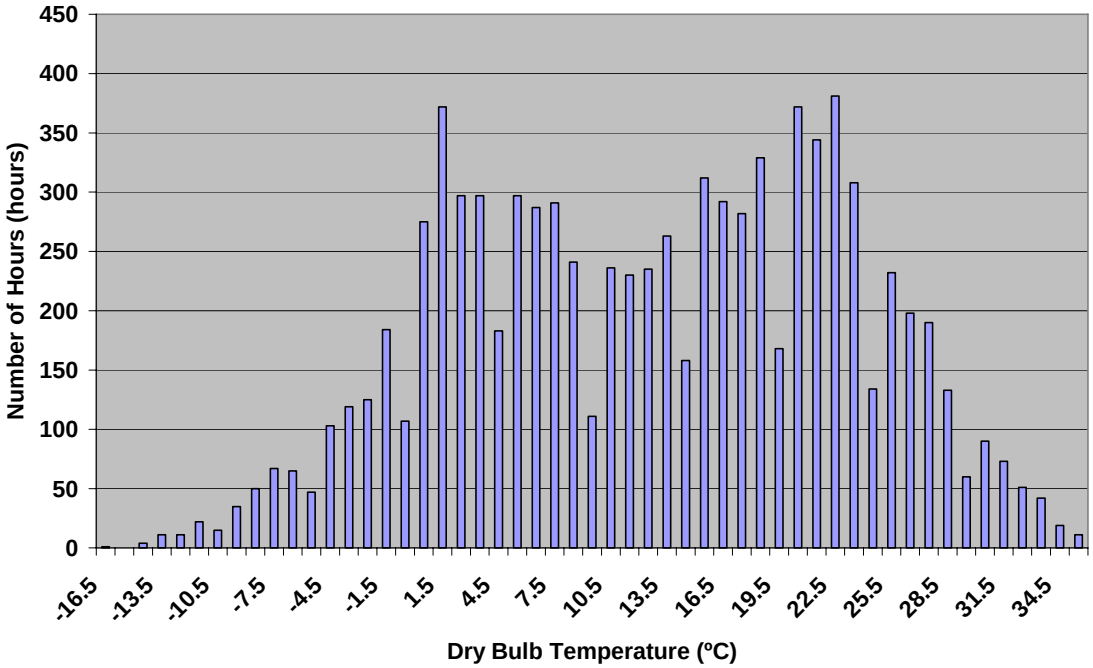

Figure 83: Temperature Profile for Maryland in 2004

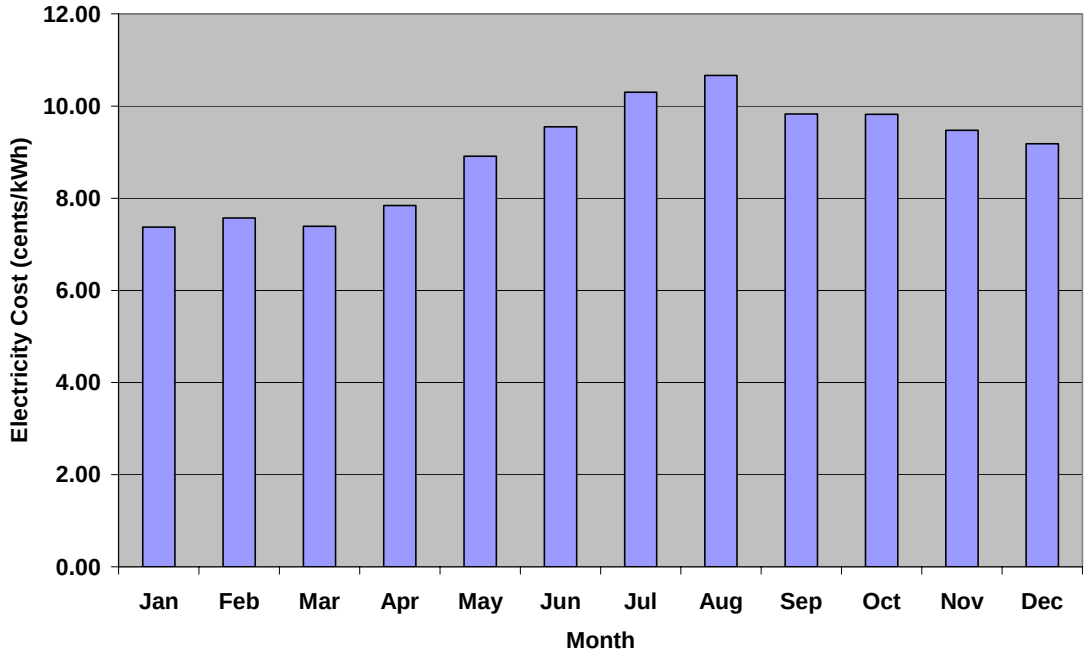

Figure 84: Monthly Electricity Prices for Maryland in 2004

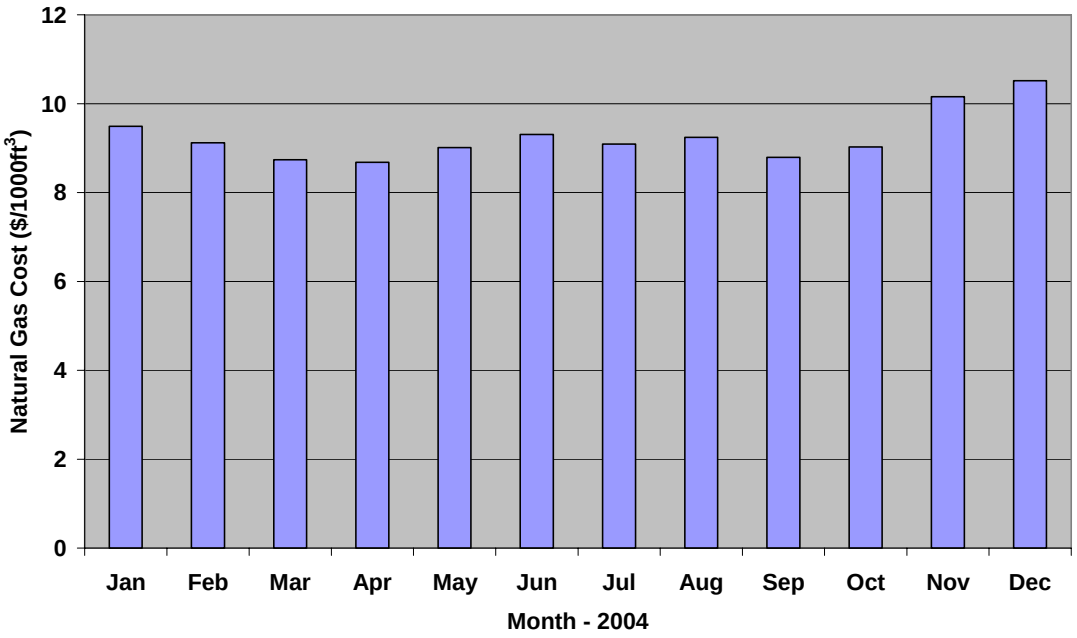

Figure 85: Monthly Natural Gas Prices for Maryland in 2004

Figure 86 and Figure 87 show the humidity ratio and temperature respectively for Arizona along with their number of hours or frequency that they occurred in the year 2004 obtained from ASHRAE TMY data. Figure 88 and Figure 89 show the average monthly electricity and natural gas prices respectively for the annual year 2004 for Arizona that was obtained from Energy Information Administration (EIA) under US Department of Energy (DOE). It can be seen that Arizona doesn't have too humid weather but is characterized by very high temperatures reaching up to 45 ºC. The electricity is again cheaper compared to natural gas prices.

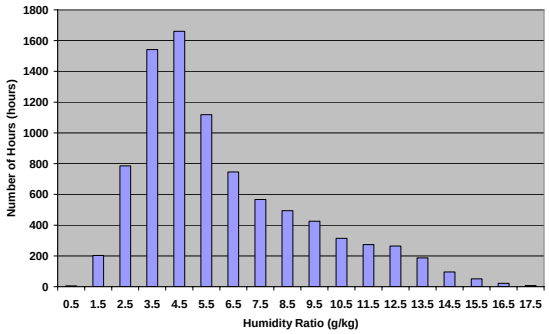

Figure 86: Humidity Levels in Arizona in 2004

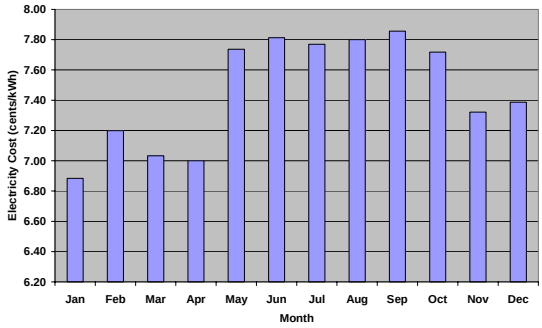

Figure 88: Monthly Electricity Prices for Arizona in 2004

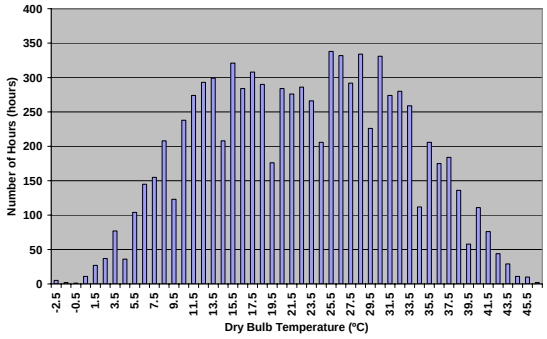

Figure 87: Temperature Profile for Arizona in 2004

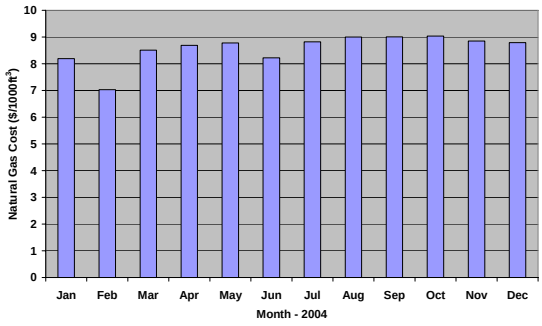

Figure 89: Monthly Natural Gas Prices for Arizona in 2004

Figure 90 and Figure 91 show the humidity ratio and temperature respectively for Florida along with their number of hours or frequency that they occurred in the year 2004. Figure 92 and Figure 93 show the average monthly electricity and natural gas prices respectively for the annual year 2004 for Florida. It is observed that Florida is different than Arizona, in that the weather is not too hot but is very humid. The natural gas prices are very high in the range of \$11 - \$12 per 1000 ft^3 of natural gas.

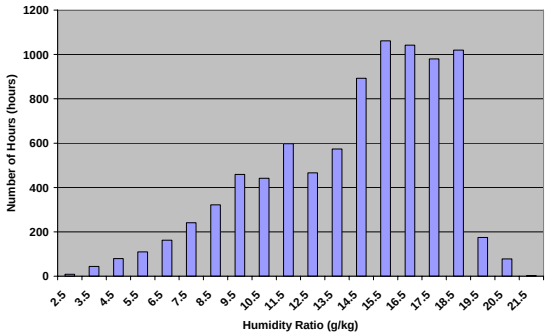

Figure 90: Humidity Levels in Florida in 2004

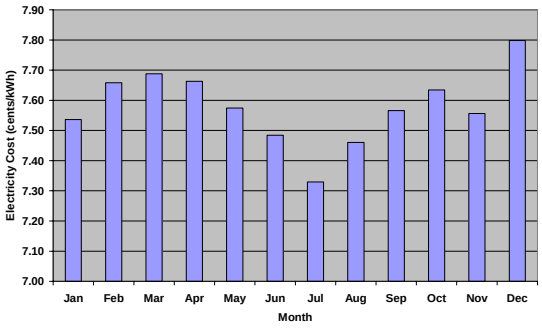

Figure 92: Monthly Electricity Prices for Florida in 2004

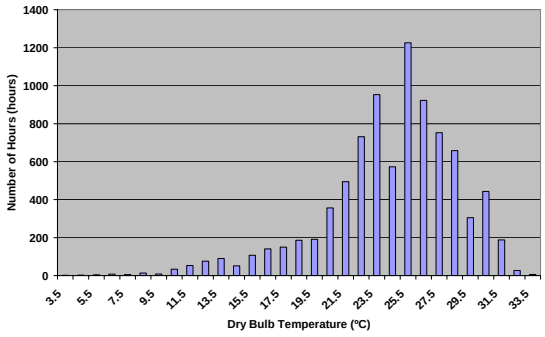

Figure 91: Temperature Profile for Florida in 2004

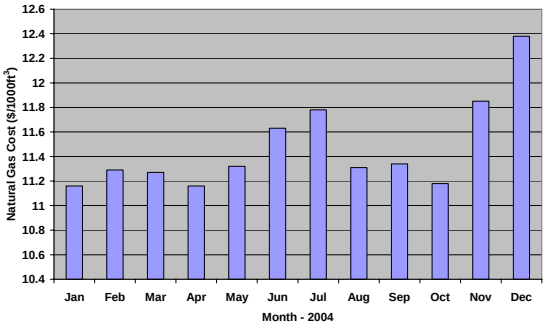

Figure 93: Monthly Natural Gas Prices for Florida in 2004

Figure 94 and Figure 95 show the humidity ratio and temperature respectively for California along with their number of hours or frequency that they occurred in the year 2004. Figure 96 Figure 97 and show the average monthly electricity and natural gas prices respectively for the annual year 2004 for California. It is found that California has a beautiful climate with regards to both temperature and humidity. The natural gas prices are in the range of $8 - $9 per 1000 ft^3 of natural gas on an average while the electricity prices are very high, over 13 cents/kWh for some months. The engine generator in this case can be used for peak shaving purposes or base loaded depending upon the demand charges.

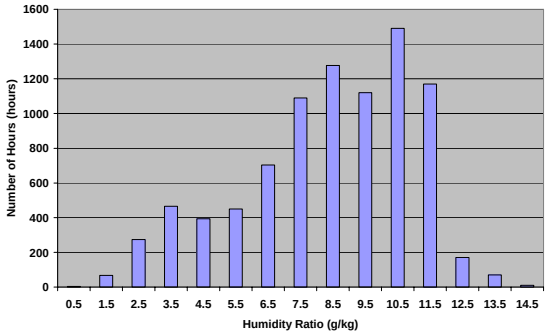

Figure 94: Humidity Levels in California in 2004

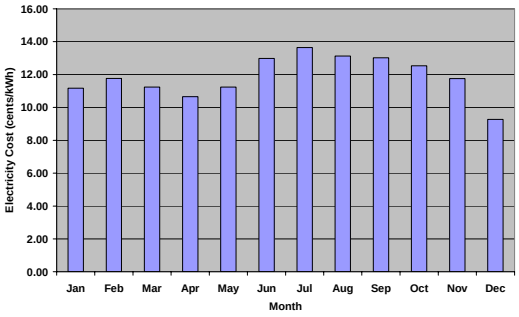

Figure 96: Monthly Electricity Prices for California in 2004

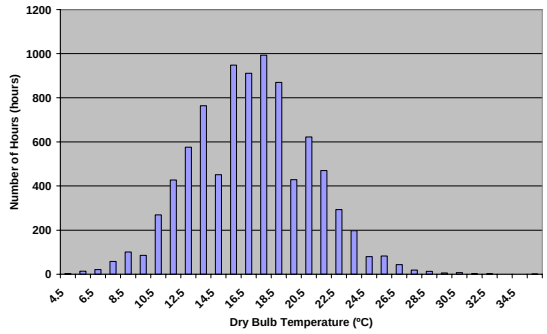

Figure 95: Temperature Profile for California in 2004

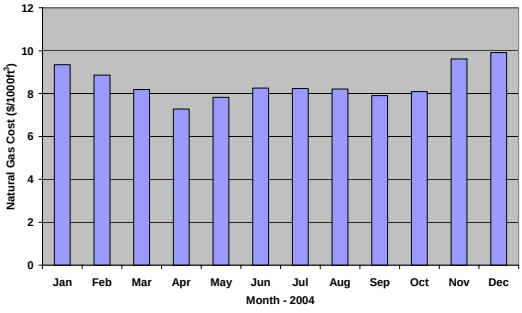

Figure 97: Monthly Natural Gas Prices for California in 2004

Figure 98 and Figure 99 show the humidity ratio and temperature respectively for New York along with their number of hours or frequency that they occurred in the year 2004. Figure 100 and Figure 101 show the average monthly electricity and natural gas prices respectively for the annual year 2004 for New York. It is found that compared to California, New York has somewhat higher temperature and humidity. The natural gas prices are in the range of \$9 - \$11/1000 ft^3 on an average while the electrical prices are in the range of 12 – 13 cents/kWh, but are spread over the year as compared to California.

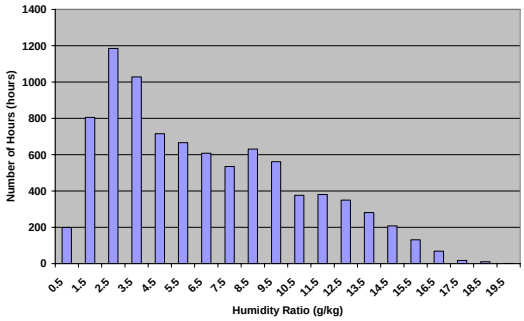

Figure 98: Humidity Levels in New York in 2004

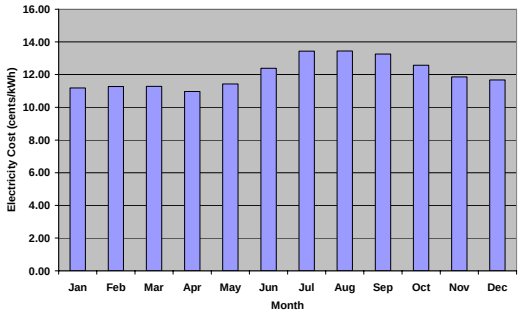

Figure 100: Monthly Electricity Prices for New York in 2004

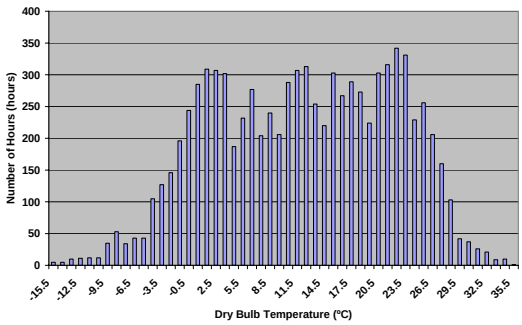

Figure 99: Temperature Profile for New York in 2004

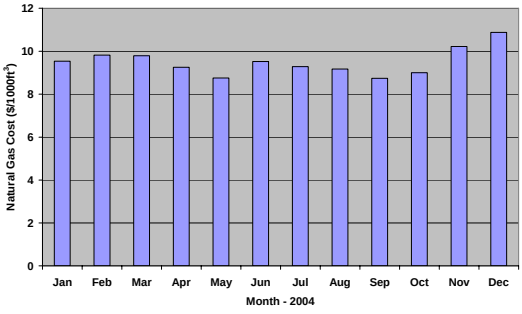

Figure 101: Monthly Natural Gas Prices for New York in 2004

Figure 102 and Figure 103 show the humidity ratio and temperature respectively for Georgia along with their number of hours or frequency that they occurred in the year 2004. Figure 104 and Figure 105 show the average monthly electricity and natural gas prices respectively for the annual year 2004 for Georgia. It can be observed that Georgia has higher temperatures and humidity though the number of hours is lesser than the other states. The gas prices are very high, around \$12/1000 ft^3, while the electricity prices fluctuate over the entire year.

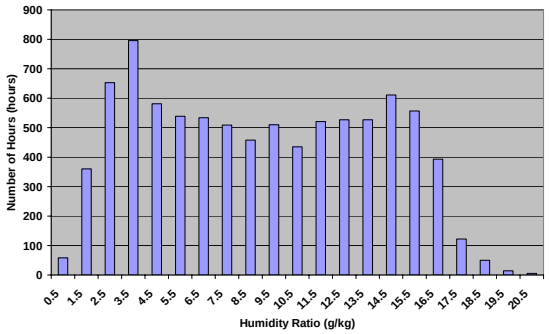

Figure 102: Humidity Levels in Georgia in 2004

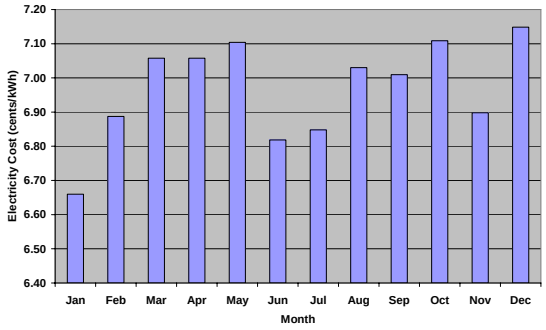

Figure 104: Monthly Electricity Prices for Georgia in 2004

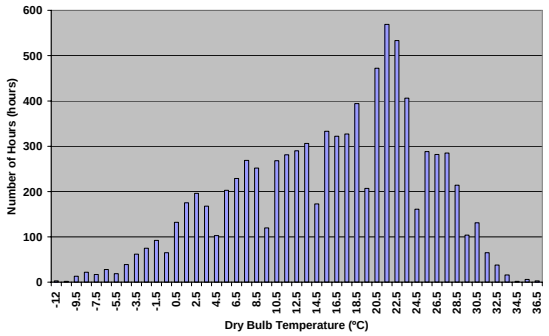

Figure 103: Temperature Profile for Georgia in 2004

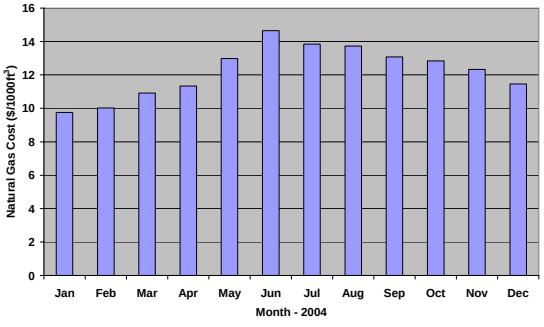

Figure 105: Monthly Natural Gas Prices for Georgia in 2004

Figure 106 and Figure 107 show the humidity ratio and temperature respectively for Texas along with their number of hours or frequency that they occurred in the year 2004. Figure 108 and Figure 109 show the average monthly electricity and natural gas prices respectively for the annual year 2004 for Texas. It is found that Texas has higher humidity with more number of hours than Georgia, while the temperature is higher than those in Florida, but the natural gas prices were lower in Texas in 2004 than the above mentioned states.

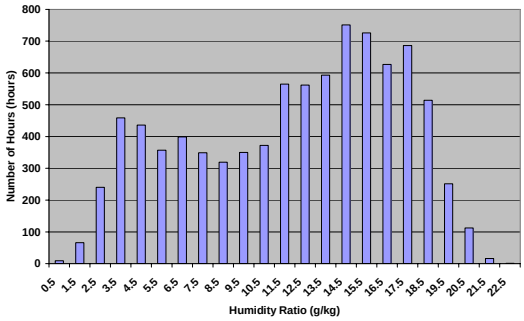

Figure 106: Humidity Levels in Texas in 2004

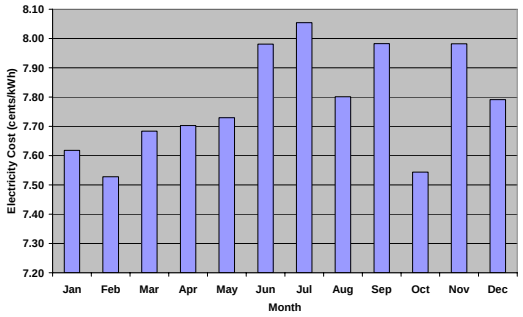

Figure 108: Monthly Electricity Prices for Texas in 2004

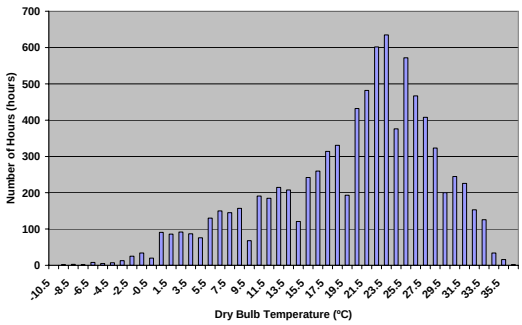

Figure 107: Temperature Profile for Texas in 2004

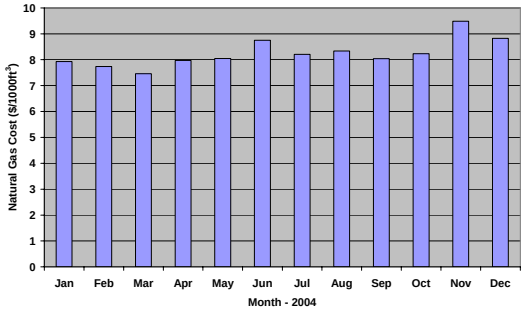

Figure 109: Monthly Natural Gas Prices for Texas in 2004

6.3 Liquid Desiccant Model

Desiccant air dehumidification involves heat and mass transfer at the same time between the air and the desiccant. Many design variables affect the performance of the packed bed dehumidifier and regenerator. For example, the difference between the vapor pressure of the desiccant and the partial pressure of water vapor in the air is the driving force for the mass transfer. The vapor pressure of the solution is a function of its concentration and temperature. The partial pressure in the air depends on the air temperature and humidity ratio.

Figure 110 shows a schematic representation of the liquid desiccant system with the different state points for air and the lithium chloride solution.

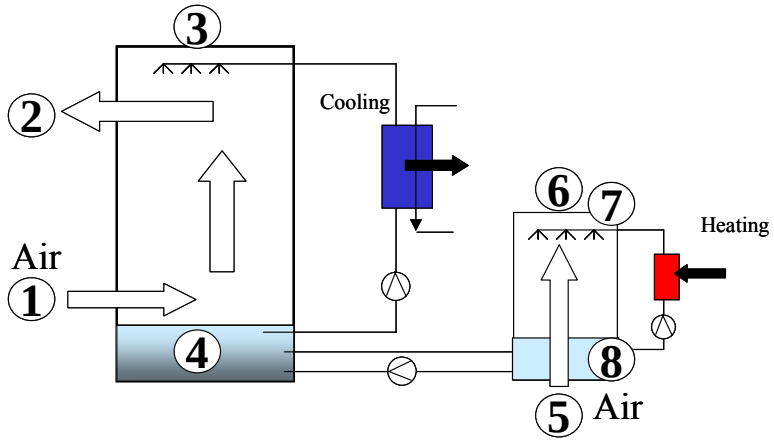

Figure 110: Schematic Representation of Liquid Desiccant System

The different state points mentioned in figure 29 are:

1. State point 1: Air inlet to conditioner

2. State point 2: Air outlet from conditioner
3. State point 3: LiCl solution inlet to conditioner
4. State point 4: LiCl solution outlet from conditioner
5. State point 5: Air inlet to regenerator
6. State point 6: Air outlet from regenerator
7. State point 7: LiCl solution inlet to regenerator
8. State point 8: LiCl solution outlet from regenerator

6.3.1 Conditioner Section

The efficiency of the heat and mass transfer process was assumed to be 90 % based on specifications from the liquid desiccant unit manufacturer. The energy balance for the conditioner between the air and the solution gives the following equations:

$$\dot{Q}_{12} = \dot{m}_{ac}\left(h_1 - h_2\right)$$

$$\dot{Q}_{34} = \dot{m}_{sc}\left(h_4 - h_3\right)$$

Where,

$\dot{Q}_{12}$ = heat transferred by air from state point 1 to 2

$\dot{Q}_{34}$ = heat transferred by solution from state point 3 to 4

$\dot{m}_{ac}$ = mass flow rate of outdoor air through the conditioner

$\dot{m}_{sc}$ = mass flow rate of solution in the conditioner

h_1 = enthalpy of air at inlet to conditioner

h_2 = enthalpy of air at outlet from conditioner

h_3 = enthalpy of solution at inlet to conditioner

h_4 = enthalpy of solution at outlet from conditioner

The mass balance of water in the conditioner is given by,

$$\dot{m}_{ac}\left(w_1 - w_2\right) = \dot{m}_{wc}$$

Where,

w_1 = humidity ratio of air entering the conditioner

w_2 = humidity ratio of air leaving the conditioner

$\dot{m}_{wc}$ = amount of moisture removed from air from point 1 to 2

The mass balance of solution in the conditioner is given by,

$$\left(1 - x_3\right)\dot{m}_3 + \dot{m}_{wc} = \left(1 - x_4\right)\dot{m}_4$$

Where,

$\dot{m}_3$ = mass flow rate of solution at inlet to the conditioner

x_3 = concentration of salt in the solution at inlet to conditioner

$\dot{m}_4$ = mass flow rate of solution at outlet from the conditioner

x_4 = concentration of salt in the solution at outlet from conditioner

6.3.2 Regenerator Section

The efficiency of the heat and mass transfer process between the outdoor air and lithium chloride water solution in the regenerator was assumed to be 85 %. The energy balance for the regenerator between the air and the solution gives the following equations:

$$\dot{Q}_{56} = \dot{m}_{ar}\left(h_6 - h_5\right)$$

$$\dot{Q}_{78} = \dot{m}_{sr}\left(h_7 - h_8\right)$$

Where,

$\dot{Q}_{56}$ = heat transferred by air from state point 5 to 6

$\dot{Q}_{78}$ = heat transferred by solution from state point 7 to 8

$\dot{m}_{ar}$ = mass flow rate of outdoor air through the regenerator

$\dot{m}_{sr}$ = mass flow rate of solution in the regenerator

h_5 = enthalpy of air at inlet to regenerator

h_6 = enthalpy of air at outlet from regenerator

h_7 = enthalpy of solution at inlet to regenerator

h_8 = enthalpy of solution at outlet from regenerator

The mass balance of water in the regenerator is given by,

$$\dot{m}_{ar}\left(w_6 - w_5\right) = \dot{m}_{wr}$$

Where,

w_5 = humidity ratio of air entering the regenerator

w_6 = humidity ratio of air leaving the regenerator

$\dot{m}_{wr}$ = amount of moisture transferred to air from point 5 to 6

The mass balance of solution in the regenerator is given by,

$$\left(1 - x_7\right)\dot{m}_7 - \dot{m}_{wr} = \left(1 - x_8\right)\dot{m}_8$$

Where,

$\dot{m}_7$ = mass flow rate of solution at inlet to the regenerator

x_7 = concentration of salt in the solution at inlet to regenerator

$\dot{m}_8$ = mass flow rate of solution at outlet from the regenerator

x_8 = concentration of salt in the solution at outlet from conditioner

The relation between humidity ratio (ω) and relative humidity (ϕ) is given by the following equation,

$$\phi = \frac{\omega P}{\left(0.622 + \omega\right)P_g}$$ (Cengel and Boles, 1994)

Where,

ϕ = relative humidity of air

ω = humidity ratio of air

P = total pressure of air

P_g = saturation pressure of water at the given temperature

The values of the various design variables and efficiencies obtained from the liquid desiccant unit manual provided by the manufacturer and used in the liquid desiccant system model are as follows,

$\dot{m}_{sr}$ = 1.631 kg/s

$\dot{m}_{ar}$ = 0.513 kg/s

$\dot{m}_{sc}$ = 3.08 kg/s

$\dot{m}_{ac}$ = 1.633 kg/s

$x_7 = 0.36$

$\eta_{conditioner} = 0.9$

$\eta_{regenerator} = 0.85$

The useful output variables obtained from the liquid desiccant model are the temperature and humidity ratio of the process air which are used in the roof top unit model described later in this chapter to calculate the cooling energy of the roof top unit.

6.4 Engine Model

The engine which constitutes the prime mover of CHP system 1 is a four-stroke, SI engine where the piston executes four complete strokes (two mechanical cycles)

within the cylinder and the crankshaft completes two revolutions for each thermodynamic cycle. A schematic of each stroke is shown in Figure 111 while Figure 112 depicts the different processes for a typical four-stroke SI engine on the P-v diagram.

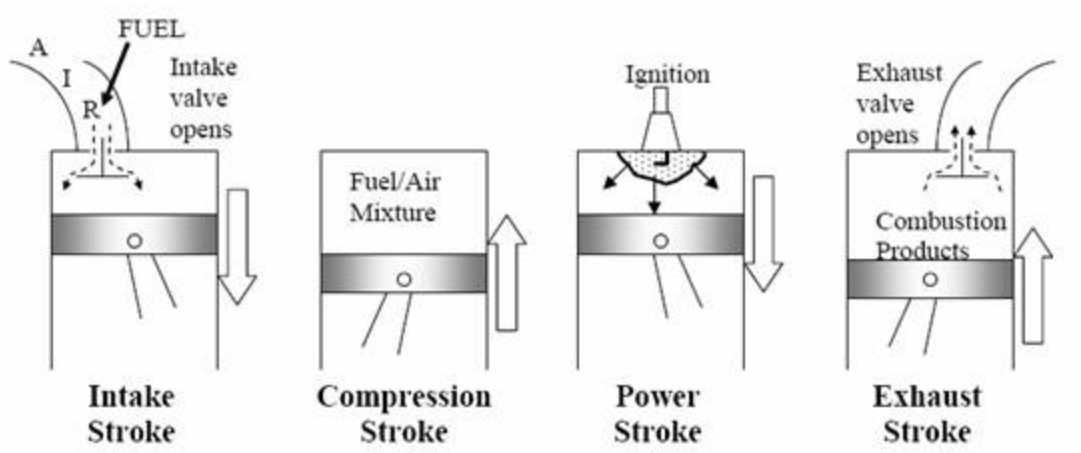

Figure 111: The Four Strokes in a Spark-Ignition Engine

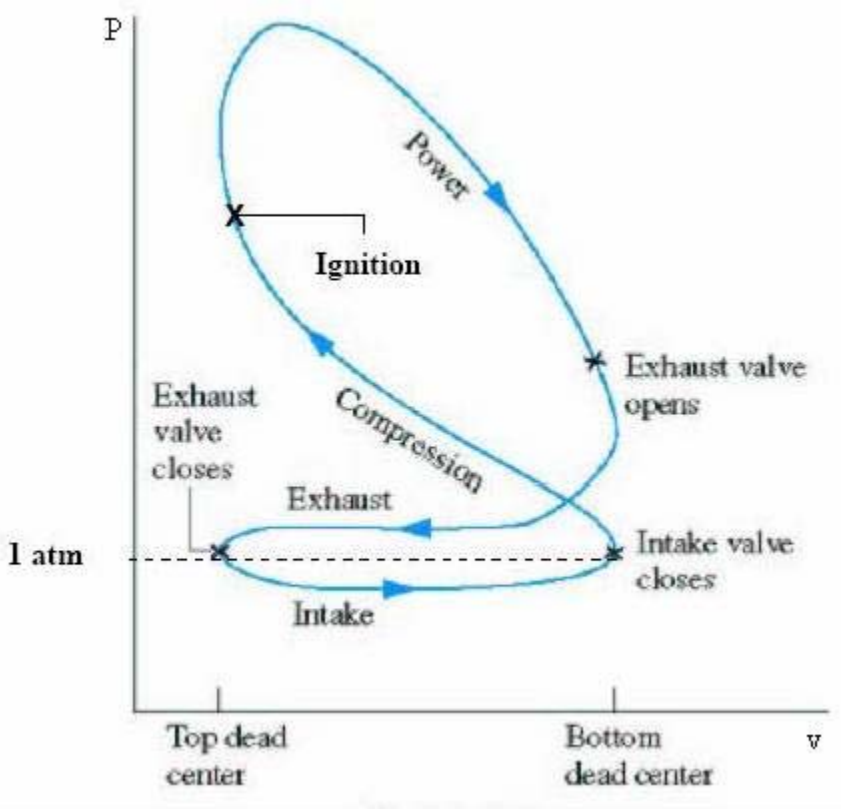

Figure 112: Representation of the Four Strokes of SI Engine on P-v Diagram

Initially, both the intake and the exhaust valves are closed and the piston is at its lowest position (BDC). During the compression stroke, the piston moves upward, compressing the air-fuel mixture. Shortly before the piston reaches its highest position (TDC), the spark plug fires and the mixture ignites, increasing the pressure and temperature of the system. The high pressure gases force the piston down, which in turn forces the crankshaft to rotate producing a useful work output during the expansion or power stroke. At the end of this stroke, the piston is at its lowest position and the cylinder is filled with combustion products. Now the piston moves upward one more time purging the exhaust gases through the exhaust valve in the

exhaust stroke and down a second time drawing in fresh air-fuel mixture through the intake valve during the intake stroke. The pressure in the cylinder is slightly above the atmospheric value during the exhaust stroke and slightly below during the intake stroke.

The Otto cycle is the ideal cycle that is used for the spark-ignition reciprocating engine. The thermodynamic analysis of the actual four-stroke cycle is very complicated and hence some standard assumptions (Cengel and Boles, 1994) are used to simplify the process in an ideal Otto cycle as follows,

1. The working fluid is air which continuously circulates in a closed loop and always behaves as an ideal gas.
2. All the processes which make up the cycle are internally reversible.
3. The combustion process is replaced by a heat addition process from an external source.
4. The exhaust process is replaced by a heat rejection process which restores the working fluid to its initial state.

Figure 113 and Figure 114 shows the different processes in an ideal Otto cycle on a Pressure-Volume (P-v) and Temperature-Entropy (T-s) diagram respectively.

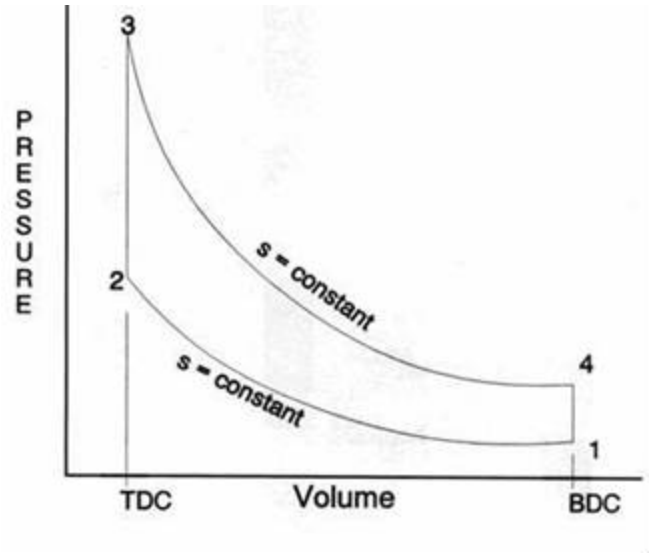

Figure 113: P-v Diagram of Ideal Otto Cycle

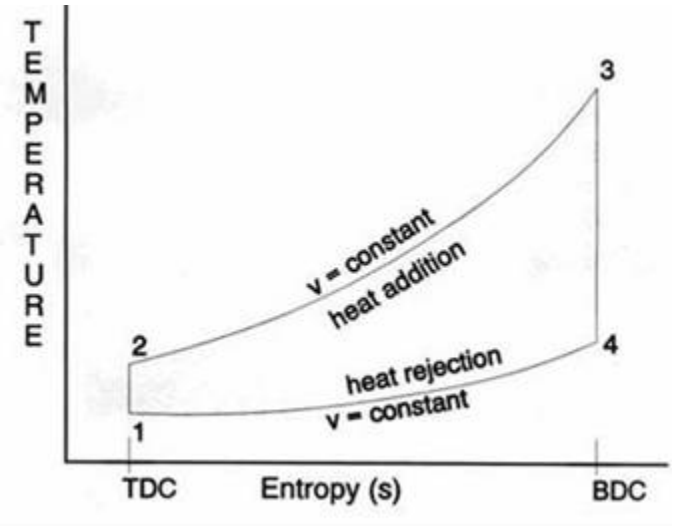

Figure 114: T-s Diagram of Ideal Otto Cycle

The different processes in the ideal Otto Cycle are:

Process 1→ 2 = Isentropic compression

Process 2 → 3 = Constant volume heat addition

Process 3 → 4 = Isentropic expansion

Process 4 → 1 = Constant volume heat removal

The Otto cycle is executed in a closed system and thus the first law of thermodynamics for any of the processes is expressed on a unit-mass basis as

$q - w = \Delta u$ (kJ/kg)

Applying the above first law relation to the isentropic compression process from 1 to 2,

$\cancel{q} - \left(-w_{in}\right) = u_2 - u_1$

$w_{in} = u_2 - u_1$

Where,

w_{in} = work input required for the compression process

u_2 = internal energy of the working fluid at point 2.

u_1 = internal energy of the working fluid at point 1.

However in a real SI engine the compression process is irreversible and is accounted by assigning an efficiency term to the process. The compression process efficiency was assumed to be 78 % (Gill, 1959).

$$w_{in,actual} = \frac{w_{in}}{\eta_c}$$

Where,

$w_{in,actual}$ = actual work input required for the compression process

η_c = compression process efficiency

The values of pressure, volume and temperature at the state points 1 and 2 can be found from the following equations,

$$\frac{v_{r_2}}{v_{r_1}} = \frac{v_2}{v_1} = \frac{1}{r}$$

$$\frac{P_2 v_2}{T_2} = \frac{P_1 v_1}{T_1} \rightarrow \frac{P_2}{P_1} = \frac{T_2}{T_1} \cdot \frac{v_1}{v_2}$$

Where,

v_{r_2} = reduced volume at point 2

v_{r_1} = reduced volume at point 1

v_2 = specific volume at point 2

v_1 = specific volume at point 1

r = compression ratio

P_2 = pressure at point 2

P_1 = pressure at point 1

T_2 = temperature at point 2

T_1 = temperature at point 1

Applying the first law relation to the combustion/constant volume heat addition process from 2 to 3,

$$(u_3 - u_2) = (+q_{in}) - \cancel{w}$$

$$q_{in} = (u_3 - u_2)$$

Where,

q_{in} = heat energy input obtained through combustion of air-fuel mixture

u_3 = internal energy of the working fluid at point 3.

The temperatures and pressures are found from,

$$\frac{P_3}{P_2} = \frac{T_3}{T_2}$$

Where,

P_3 = pressure at point 3

T_3 = temperature at point 3

Now using the first law for the expansion process from 3 to 4,

$$(u_4 - u_3) = \cancel{q} - (+w_{out})$$

$$w_{out} = (u_3 - u_4)$$

Where,

w_{out} = work output produced from the expansion process

u_4 = internal energy of the working fluid at point 4.

However in a real SI engine the expansion process is irreversible and hence the work output is less than the ideal one and is accounted by assigning an efficiency term to the process. The expansion process efficiency was set at 78 % (Gill, 1959).

$$w_{out,actual} = \eta_e w_{out}$$

Where,

$w_{out,actual}$ = actual work output produced by the expansion process

η_e = expansion process efficiency

The values of pressure, volume and temperature at the state points 3 and 4 can be found from the following equations,

$$\frac{v_{r_4}}{v_{r_3}} = \frac{v_4}{v_3} = r$$

$$\frac{P_4 v_4}{T_4} = \frac{P_3 v_3}{T_3} \rightarrow \frac{P_4}{P_3} = \frac{T_4}{T_3} \cdot \frac{v_3}{v_4}$$

Where,

v_{r_4} = reduced volume at point 4

v_4 = specific volume at point 4

P_4 = pressure at point 4

T_4 = temperature at point 4

Applying the first law to the constant volume heat removal or exhaust process from 4 to 1,

$$(u_1 - u_4) = (-q_{out}) - \cancel{w}$$

$$q_{out} = (u_4 - u_1)$$

Where,

q_{out} = heat rejected during the exhaust process

The temperatures and pressures are found from,

$$\frac{P_4}{T_4} = \frac{P_1}{T_1}$$

The thermal efficiency of the cycle is thus given by,

$$\eta_{cycle} = \frac{w_{cycle}}{q_{in}} = \frac{w_{out,actual} - w_{in,actual}}{q_{in}}$$

To account for other losses inside the engine as well as the generator, a correction factor of 0.85 was employed to calculate the net electrical efficiency of the engine generator.

$$\eta_{net,elec} = 0.85\eta_{cycle}$$

Where,

$\eta_{net,elec}$ = Net electrical efficiency of the engine generator

The values of various design variables obtained from the engine generator manual and input parameters used in the engine model are as follows,

P_1 = ambient air pressure = 101.325 kPa

r = compression ratio of engine = 9

T_1 = ambient air temperature

$\eta_e = \eta_c = 0.78$

W_{net} = Net power output from the engine

The different output variables or unknowns for the engine model that are obtained through the above equations and property routines are the temperature, pressure, volume and internal energy of the state points 2, 3 and 4 along with the net electrical efficiency of the engine generator.

6.5 Engine Heat Recovery

This section details the equations used to model the heat recovery of the engine generator package which consists of the jacket water and exhaust gas heat

exchangers. The efficiency of both the heat exchangers was assumed to be 75 % based on the specifications used by the engine manufacturer.

In the jacket water heat exchanger, there is heat transfer between the 50:50 ethylene glycol - water solution and engine coolant which is also a mixture of glycol and water in equal proportions. The energy balance equations in the jacket water heat exchanger is given by,

$$Q_{JW,eng} = \dot{m}_{eng} C_{p,glycol} \left(T_{eng,in} - T_{eng,out} \right)$$

$$Q_{JW,glycol} = \dot{m}_{glycol} C_{p,glycol} \left(T_{JW,out} - T_{JW,in} \right)$$

Where,

$Q_{JW,eng}$ = heat transferred from the engine coolant to ethylene glycol solution

$\dot{m}_{eng}$ = mass flow rate of engine coolant through the jacket water heat exchanger

$C_{p,glycol}$ = specific heat of glycol

$T_{eng,in}$ = temperature of engine coolant at inlet of jacket water heat exchanger

$T_{eng,out}$ = temperature of engine coolant at outlet of jacket water heat exchanger

$Q_{JW,glycol}$ = heat recovered by the ethylene glycol solution in the jacket water heat exchanger

$\dot{m}_{glycol}$ = mass flow rate of glycol solution through the jacket water heat exchanger

$T_{JW,out}$ = temperature of glycol solution at outlet of jacket water heat exchanger

$T_{JW,in}$ = temperature of glycol solution at inlet of jacket water heat exchanger

The energy balance equations governing the heat transfer in the exhaust gas heat exchanger between exhaust gases and 50:50 ethylene glycol solution is given by the following equations,

$$Q_{EX,air} = \dot{m}_{air} C_{p,air} \left(T_{air,in} - T_{air,out}\right)$$

$$Q_{EX,glycol} = \dot{m}_{glycol} C_{p,glycol} \left(T_{EX,out} - T_{JW,out}\right)$$

Where,

$Q_{EX,air}$ = heat transferred from air (exhaust gas) to ethylene glycol solution

$\dot{m}_{air}$ = mass flow rate of air

$C_{p,air}$ = specific heat of air

$T_{air,in}$ = temperature of air at inlet of the exhaust gas heat exchanger which is equal to the exhaust gas temperature from the engine.

$T_{air,out}$ = temperature of air at the outlet of exhaust gas heat exchanger that is vented to atmosphere.

$Q_{EX,glycol}$ = heat recovered by the glycol solution in the exhaust gas heat exchanger

$T_{EX,out}$ = temperature of glycol solution at outlet of exhaust gas heat exchanger that is supplied to the regenerator heat exchanger of the liquid desiccant unit.

The values of various design variables and efficiencies used in the engine heat recovery simulation are as follows,

$\dot{m}_{eng}$ = 3.15 kg/s

$\dot{m}_{glycol}$ = 2.43 kg/s

$\dot{m}_{air}$ = 0.1 kg/s

$\eta_{JWHX} = \eta_{EXHX} = 0.75$

The output variables obtained from the heat recovery loop model are the outlet temperature of glycol and the amount of waste heat recovered from the jacket water and exhaust gas heat exchangers.

6.6 Roof Top Unit

Many commercial buildings use conventional Roof Top Units (RTUs) to supply cooling and dehumidification. As described in Chapter 4, the Chesapeake Building has two 90 ton (316 kW) RTUs for each zone. Each RTU uses a conventional vapor compression cycle to cool air through a DX coil. Then the supply air is distributed via Variable Air Volume (VAV) boxes that modulate air volume distribution throughout each conditioned room based on wall-mounted thermostats, adjusted by the building occupants. Electric reheats within these VAV boxes provide localized heating when required. Figure 115 shows a schematic of the conventional roof top unit with the different state points for the air stream.

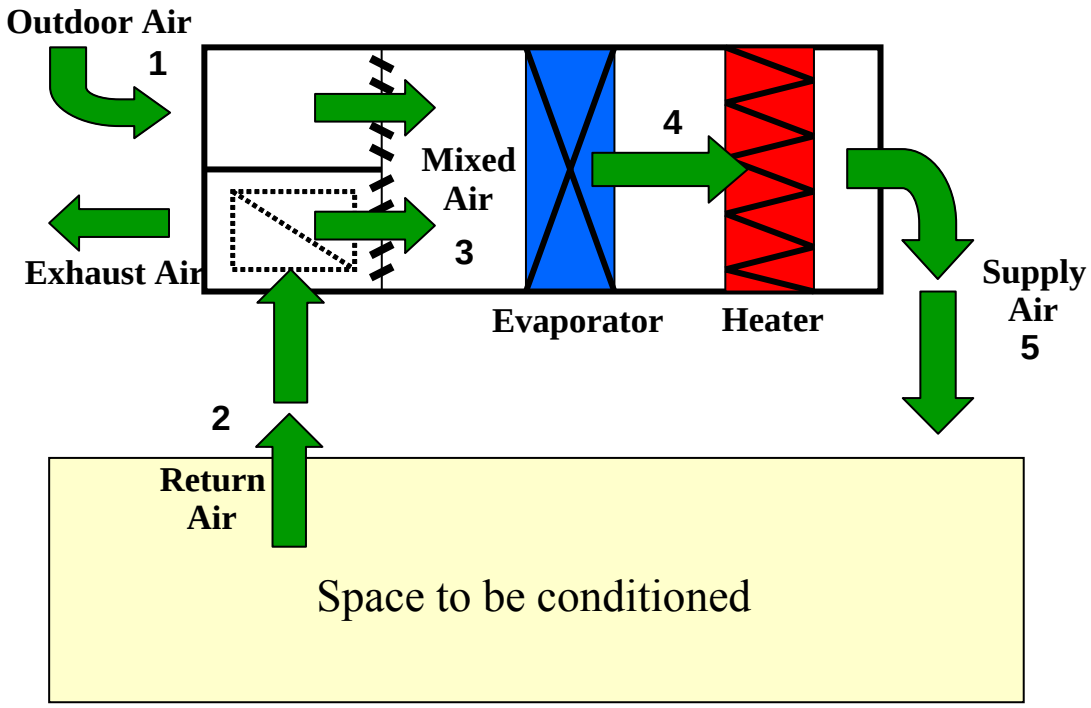

Figure 115: Schematic of Conventional Roof Top Unit

It can be seen from Figure 115 that the outdoor air at point 1 mixes with the return air (point 2) coming from the room and the mixed air at point 3 then passes over the evaporator coils where the air is cooled up to its dew point temperature to dehumidify which is given by point 4. The air is then heated back to the set point temperature and is supplied to the room which given by point 5. The volume flow rate of outdoor air is assumed to be 3000 cfm (1.42 m^3/s) while the return air flow rate was set at 17000 cfm (8.02 m^3/s) which is similar to RTU 1 at the Chesapeake building The conditions of the return air were fixed at 25 ºC and 50 % relative humidity while the conditions of the supply air to the room was assumed to be 18 ºC and humidity ratio of 8.5 g/kg of dry air based on ASHRAE comfort zone conditions (ASHRAE Fundamentals, 2001) and a sensible heat factor (SHF) of 0.7 (McQuiston et al., 1988).

The amount of cooling energy consumed by the roof top unit is given by the following equation,

$$Q_{cool} = \dot{m}_3 (h_3 - h_4)$$

Where,

Q_{cool} = Amount of cooling energy consumed by the roof top unit

$\dot{m}_3$ = mass flow rate of mixed air

h_3 = enthalpy of mixed air at inlet of the evaporator coil

h_4 = enthalpy of mixed air at outlet of the evaporator coil

The energy utilized in reheating the air back to the room set point temperature is calculated by the equation below,

$$Q_{reheat} = \dot{m}_3 (h_3 - h_4)$$

Where,

Q_{reheat} = Amount of energy consumed by the roof top unit to reheat the air back to the room set point temperature

Figure 116 shows the flow chart of the entire thermodynamic and economic simulation model. Each simulation run usually took around 15-18 minutes.

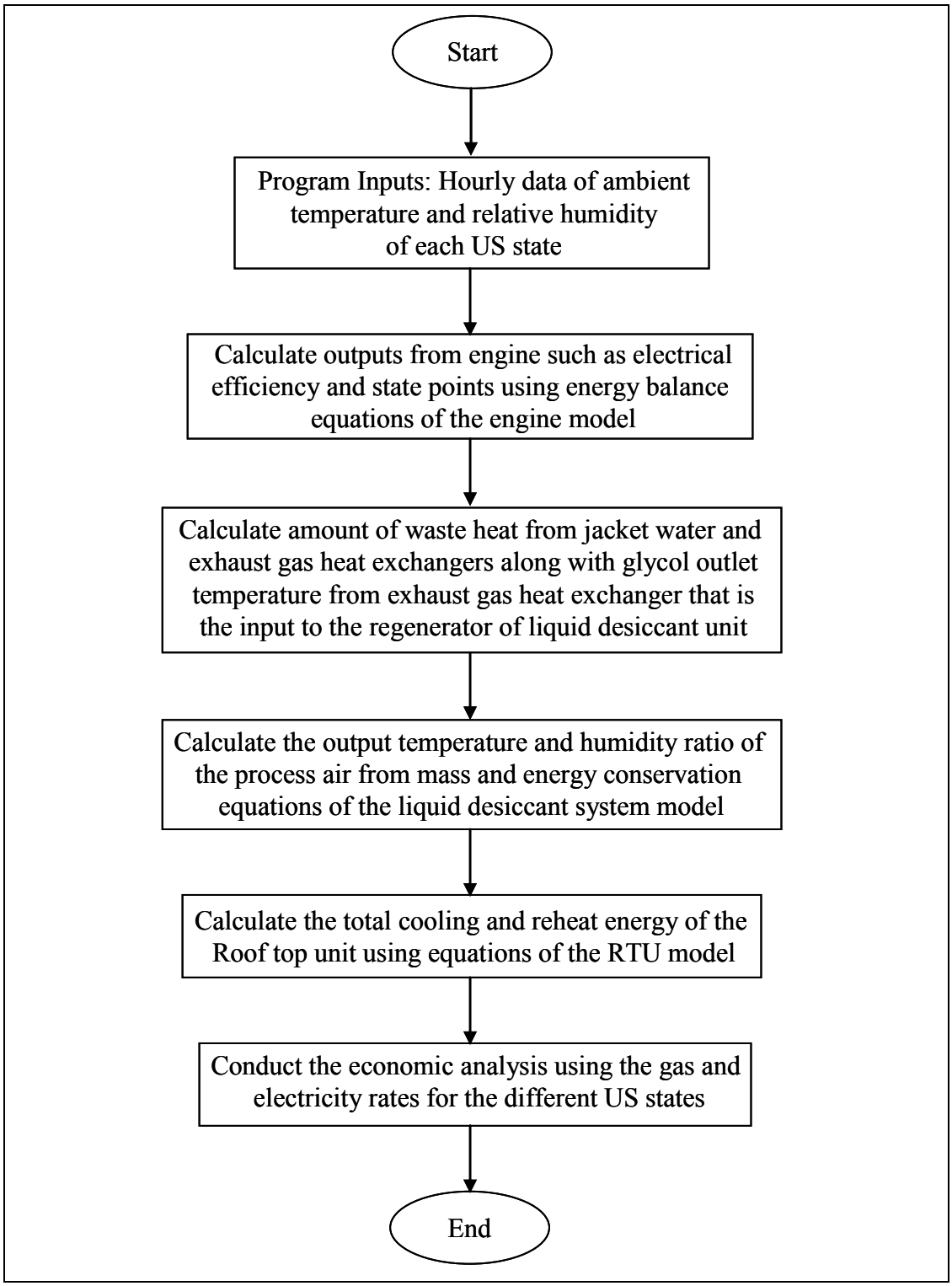

Figure 116: Flow Chart of Thermodynamic and Economic Model

6.7 Validation of Property Routines

Various property routines for ideal gas, moist air and lithium chloride – water solution have been explained and validated in this section

6.7.1 Ideal gas

The engine in the CHP system is modeled based on the Otto cycle and so the fluid used in the engine is assumed to be air that obeys the ideal gas laws. The property functions were built in Visual Basic.Net (VB.Net) using thermodynamic data from Cengel, Boles, McGraw Hill, 1994. These property functions were then compared with the thermodynamic functions in Engineering Equation Solver (EES) Version 7.183-3D. In EES the thermodynamic properties are based on data from Keenan, Chao, Keyes, Gas Tables, Wiley, 1983. Figure 117 shows the comparison of internal energy (u) over a range of temperature between the VB.Net function and EES.

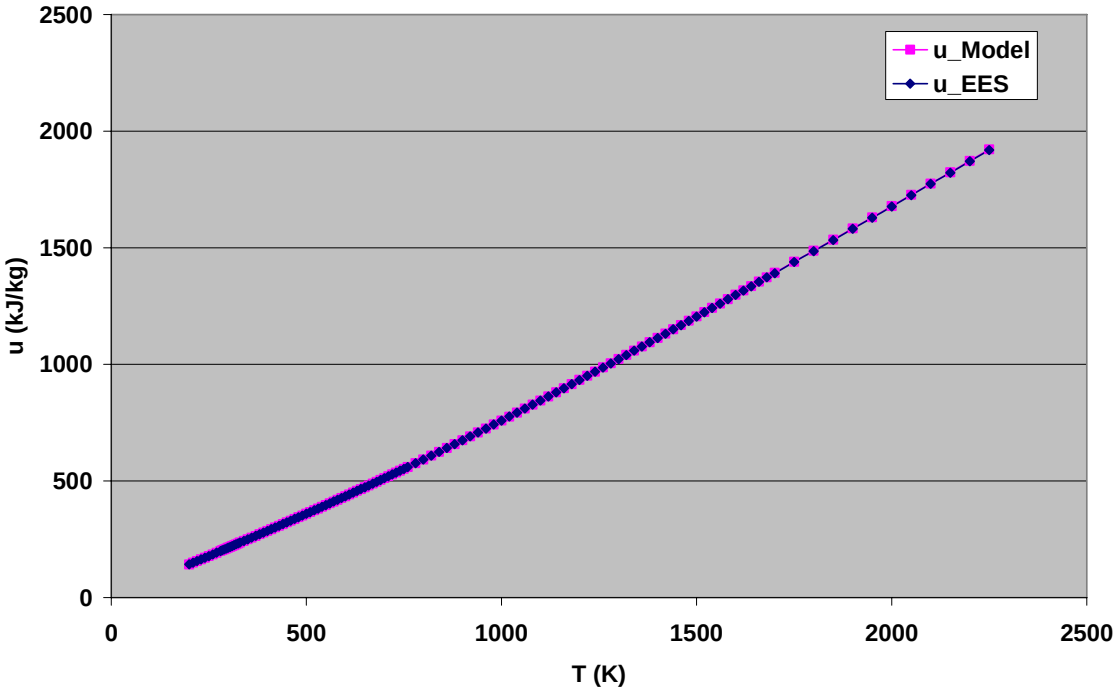

Figure 117: Comparison of u Vs T function for air between Model and EES

It can be seen from Figure 117 that the VB.Net function agrees closely with the one from EES. The equation coded in Visual Basic.Net is a Chebyshev polynomial of order 20 and the curve-fitting was done in Table Curve 2D version 5.01. The deviation between VB. Net and EES is shown in Figure 118 and the deviation was less than ± 0.2 %.

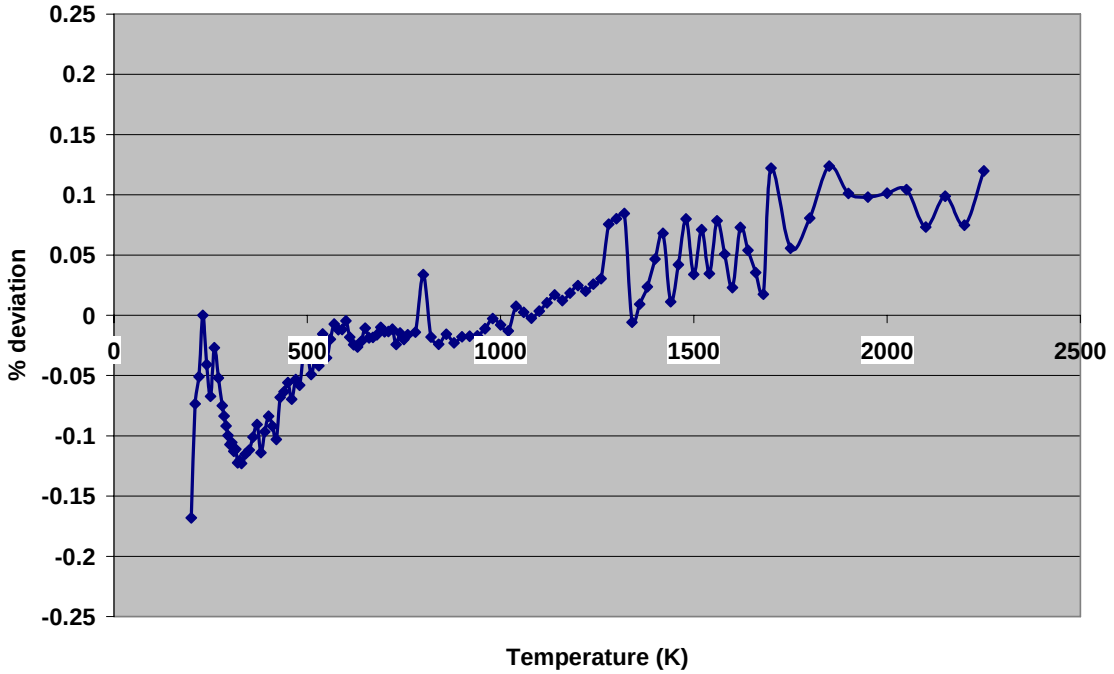

Figure 118: % Deviation for u Vs T function for air between Model and EES

Figure 119 shows the inverse of the above function which is used to calculate the temperature of a state point when the internal energy (u) is known. The curve fitted equation is a Fourier series polynomial of order 10x2. The deviation between VB. Net and EES is shown in Figure 120 and the deviation was less than ± 0.2 %.

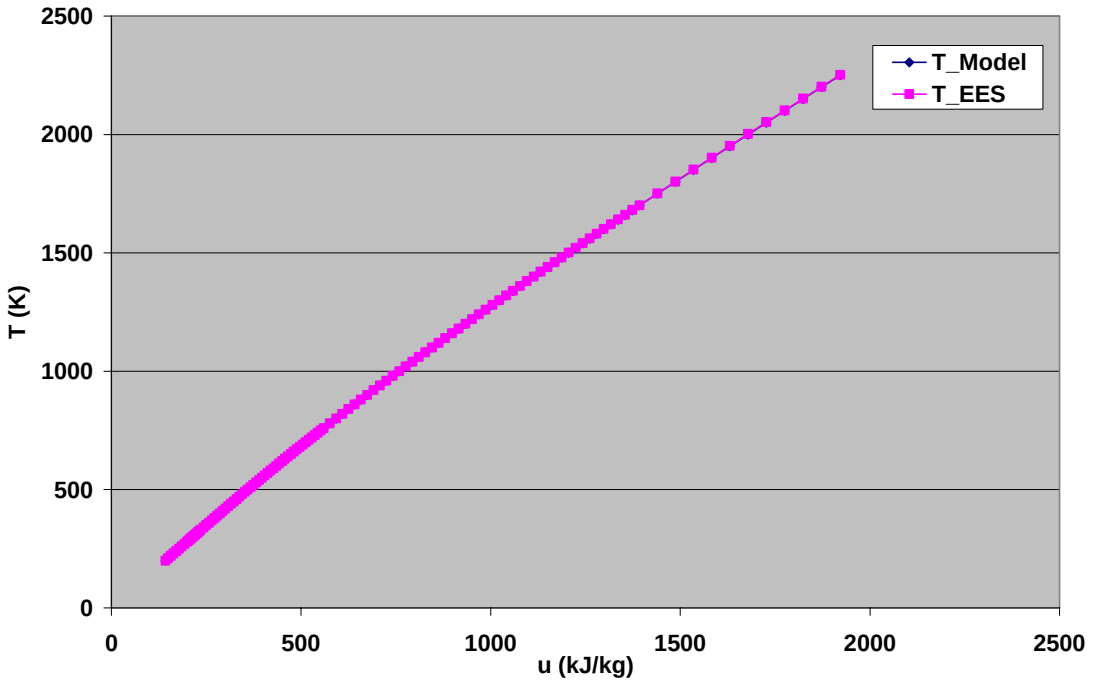

Figure 119: Comparison of T Vs u function for air between Model and EES

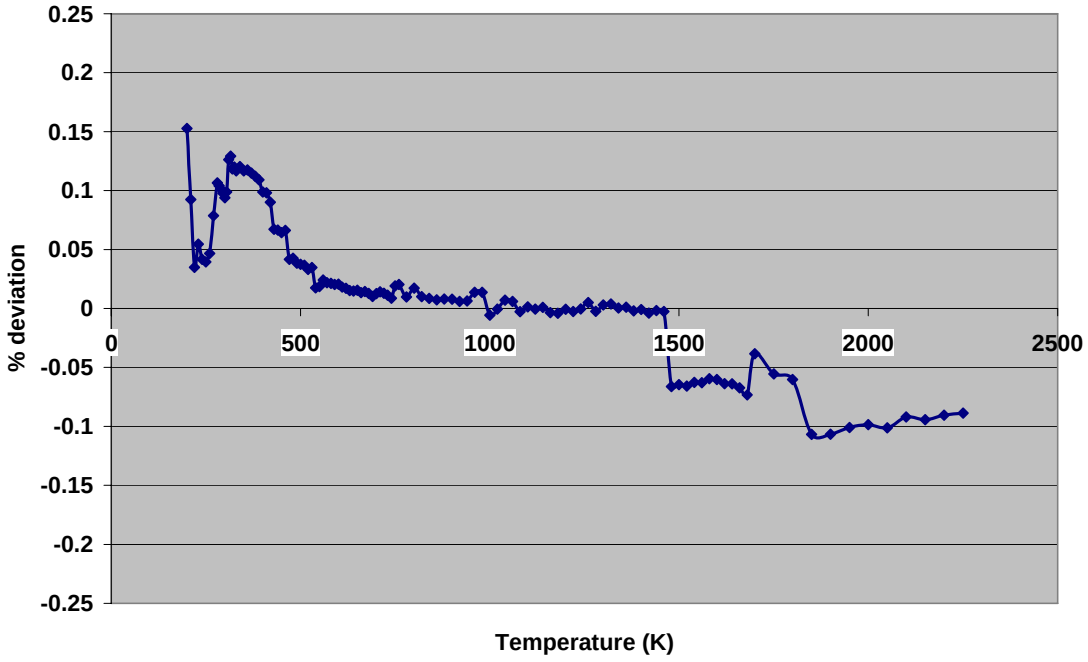

Figure 120: % Deviation for T Vs u function for air between Model and EES

Figure 121 compares the values of specific heat for constant pressure (C_p) of air predicted by the VB.Net function and EES for different temperature values. The C_p Vs T function in VB.Net is a Fourier series polynomial of order 6x2.

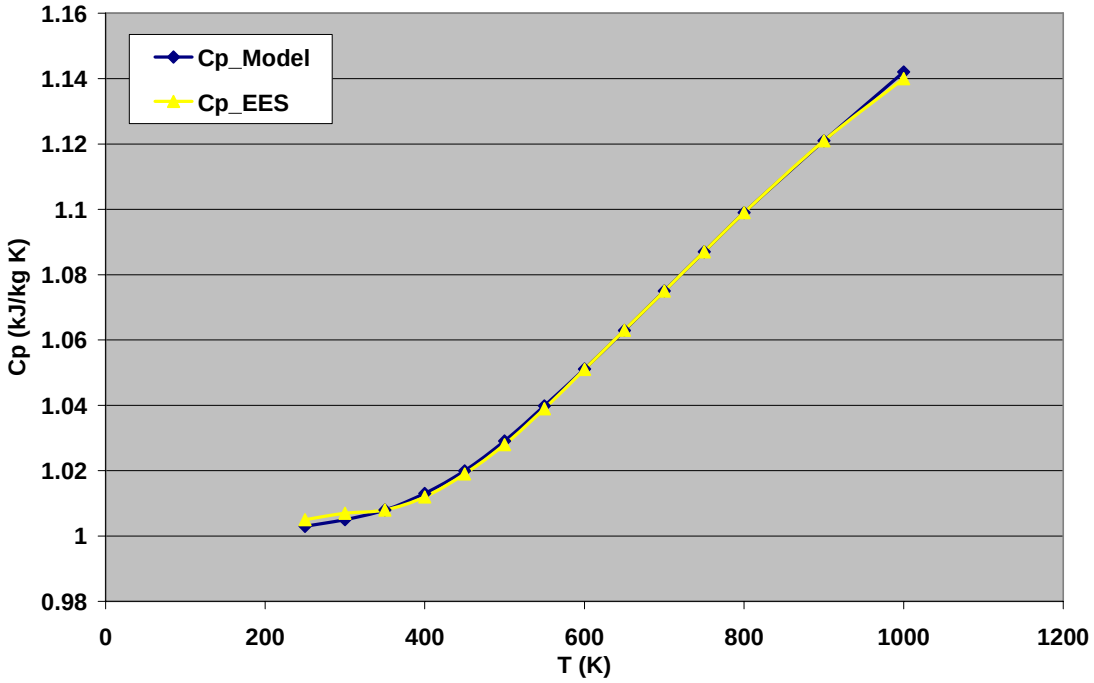

Figure 121: Comparison of Cp Vs T function for air between Model and EES

From Figure 121 it can be observed that the values of C_p predicted by VB.Net and EES match pretty well. The deviation between VB. Net and EES is shown in Figure 122 and the deviation was within ± 0.25 %.

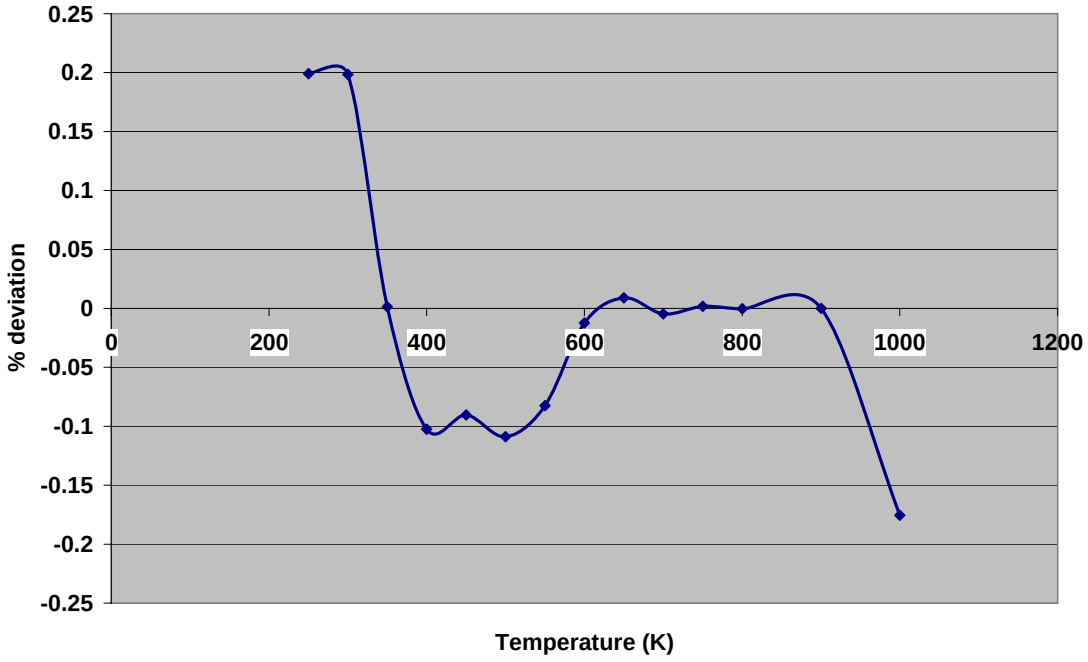

Figure 122: % Deviation for Cp Vs T function for air between Model and EES

The comparison of specific heat at constant volume (C_v) of air over a range of temperature between VB.Net and EES is shown in Figure 123. The curve fitted equation coded in VB.Net is a Fourier series polynomial of order 6x2. The deviation between VB. Net and EES is shown in Figure 124 and the deviation was within ± 0.25 %.

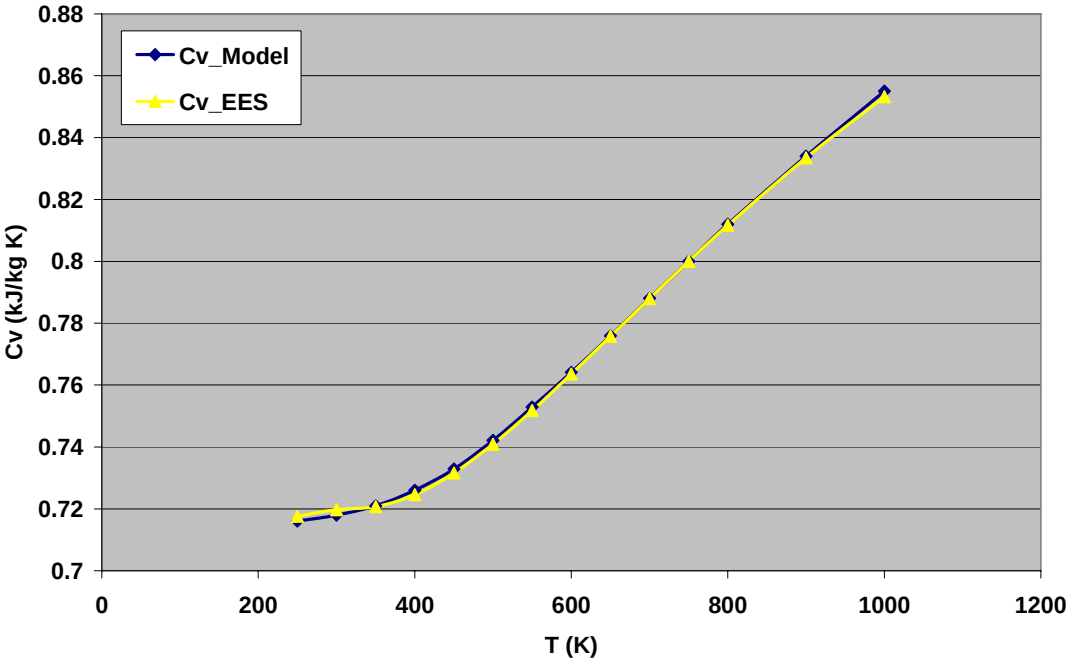

Figure 123: Comparison of Cv Vs T function for air between Model and EES

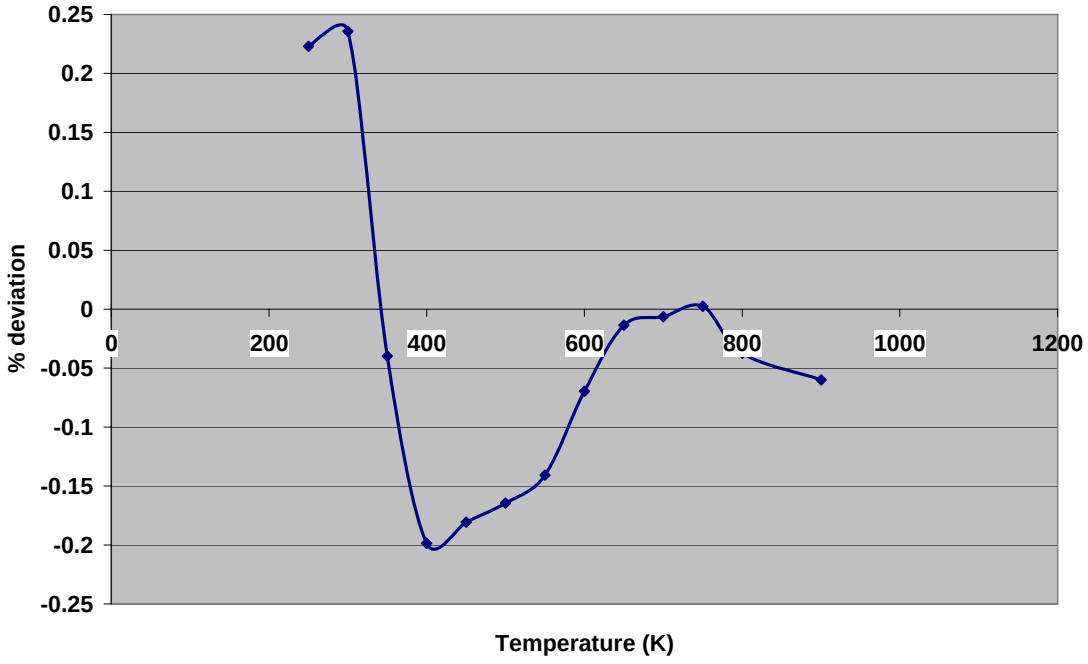

Figure 124: % Deviation for Cv Vs T function for air between Model and EES

6.7.2 Moist air

The property routines for moist air were coded in Visual Basic.Net using thermodynamic data and equations from the ASHRAE Fundamentals Handbook. These thermodynamic property functions were then compared with the functions for air-water mixture fluid described in EES Version 7.183-3D. In EES, air-water vapor mixture (psychrometric) properties use the thermodynamic data from Hyland and Wexler, "Formulations for the Thermodynamic Properties of the Saturated Phases of H2O from 173.15 K to 473.15 K, ASHRAE Transactions, Part 2A,Paper 2793 (RP-216), (1983). Figure 125 shows the comparison of saturated water vapor pressure over a range of temperatures between VB.Net and EES property function. The deviation between VB. Net and EES is shown in Figure 126 and the deviation was less than 0.7 % and -0.1 %.

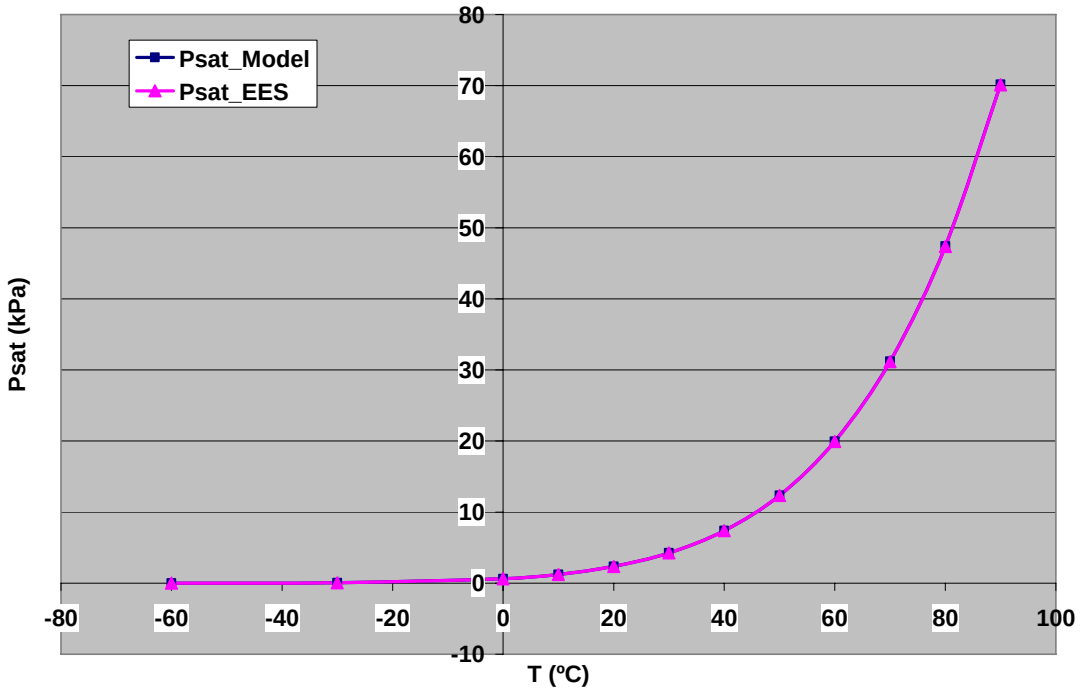

Figure 125: Comparison of saturated vapor pressure of moist air between Model and EES

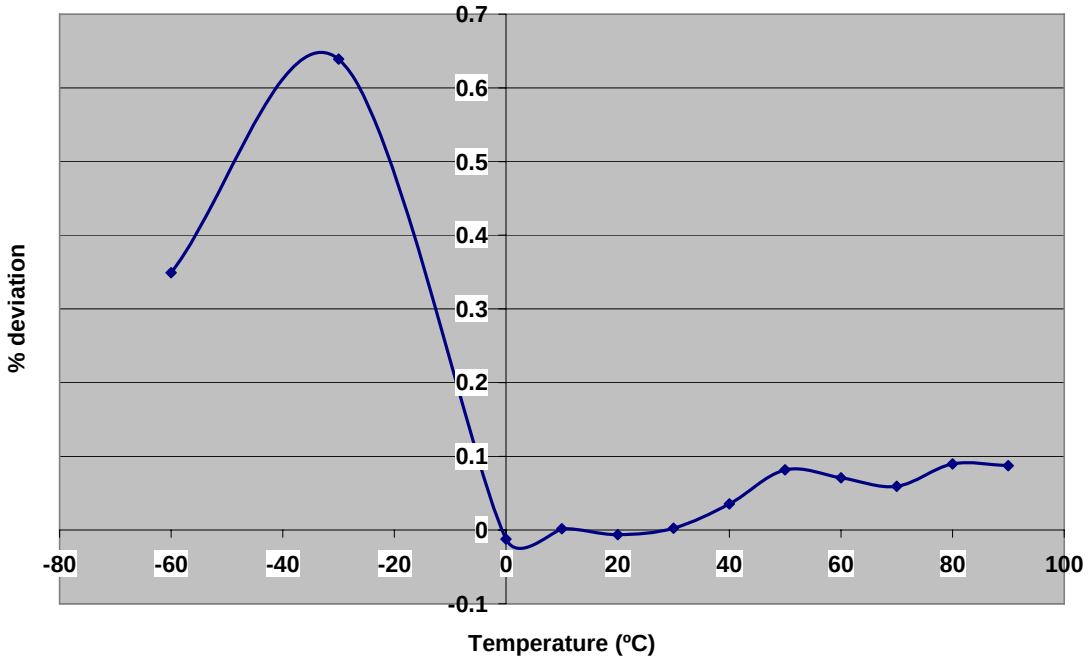

Figure 126: % Deviation for saturated vapor pressure of moist air between Model and EES

Comparison of the enthalpy of moist air predicted by EES and the VB.Net function for different temperatures is depicted in Figure 127.

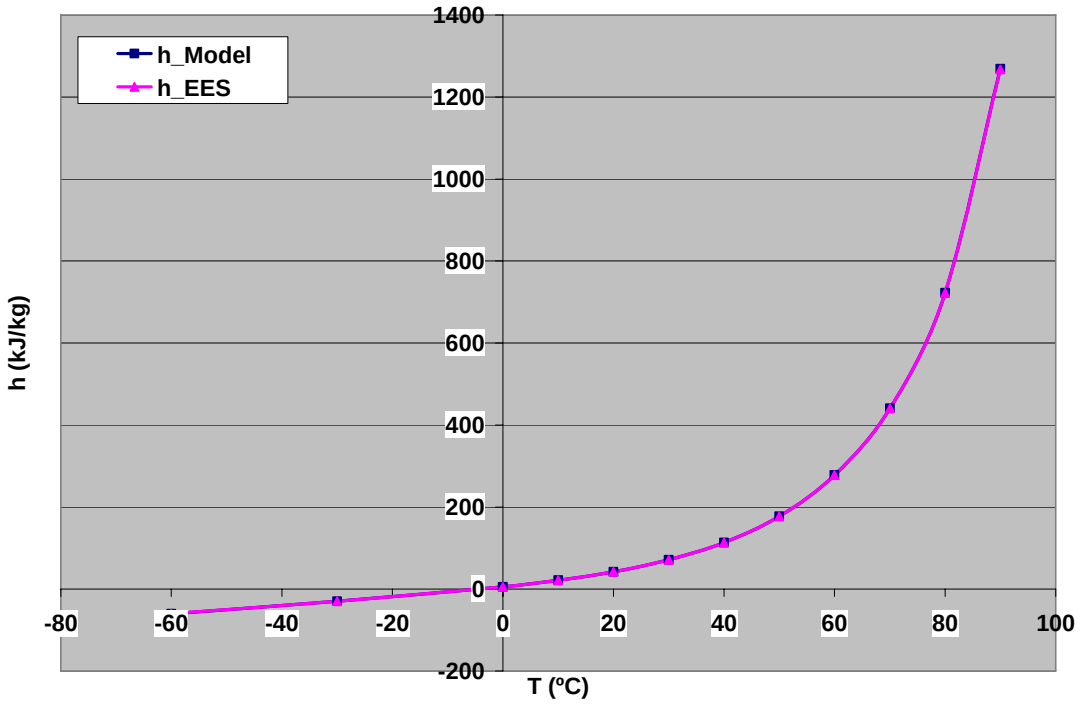

Figure 127: Comparison of enthalpy of moist air between Model and EES

It can be observed from Figure 127 that the enthalpy of moist air predicted by VB.Net function (ASHRAE) agrees pretty well with EES. The deviation between VB. Net and EES is shown in Figure 128 and the deviation was found to be less than 0.35 %.

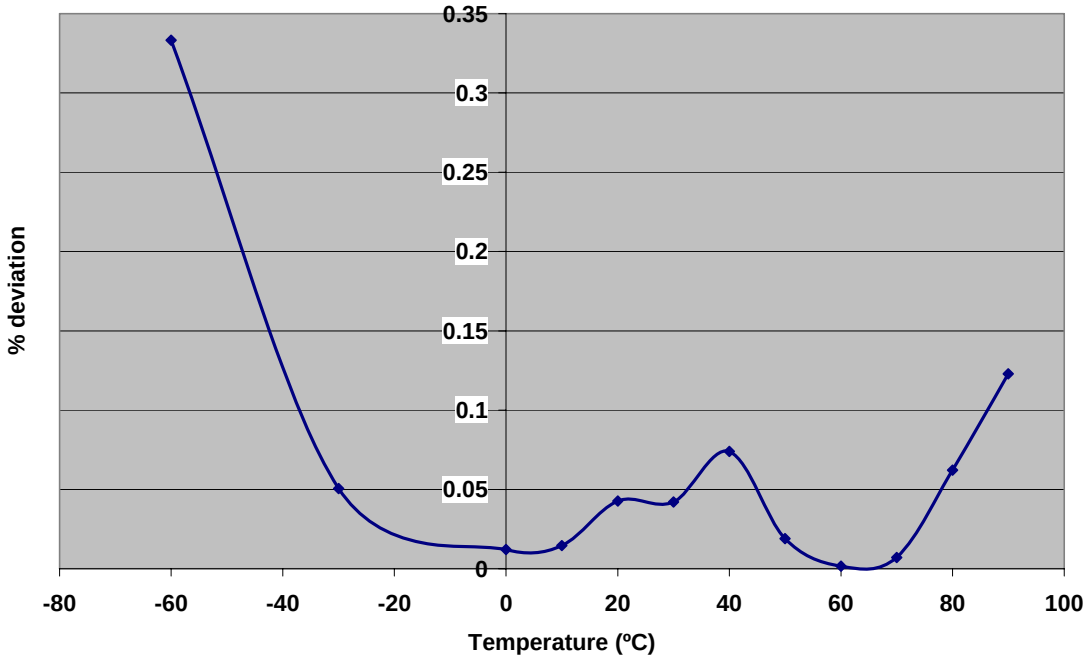

Figure 128: % Deviation for enthalpy of moist air between Model and EES

Figure 129 compares the specific volume (v) of the moist air between EES and Visual Basic.Net. The deviation between VB. Net and EES is shown in Figure 130 and the deviation was less than 0.04 %.

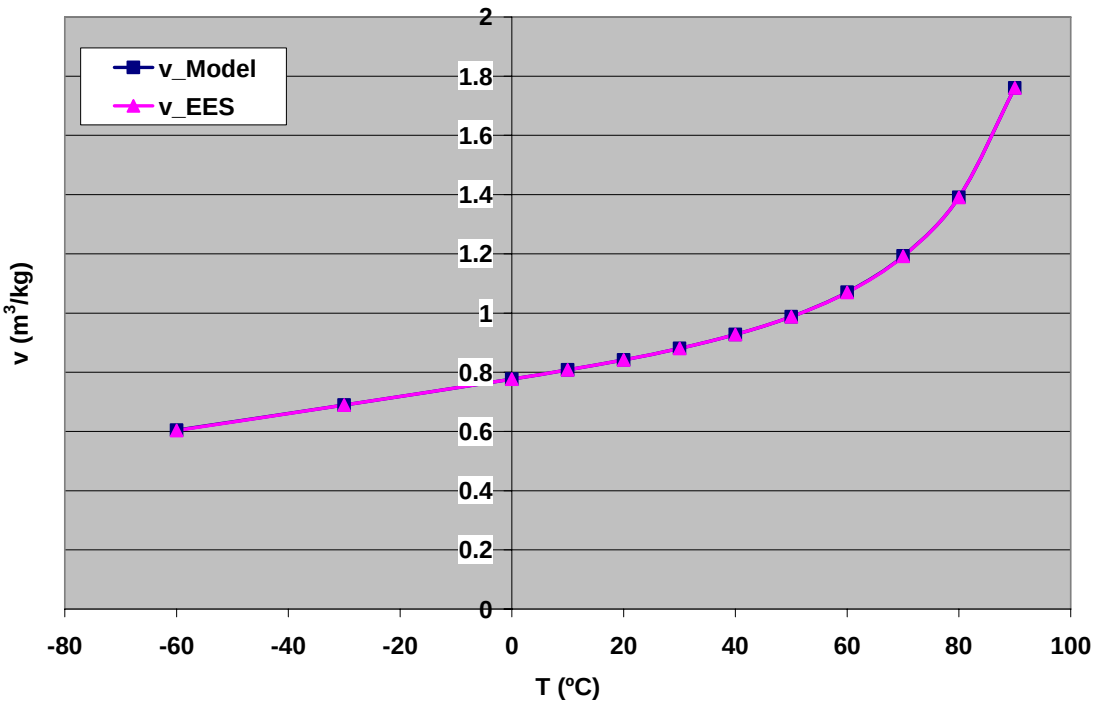

Figure 129: Comparison of specific volume of moist air between Model and EES

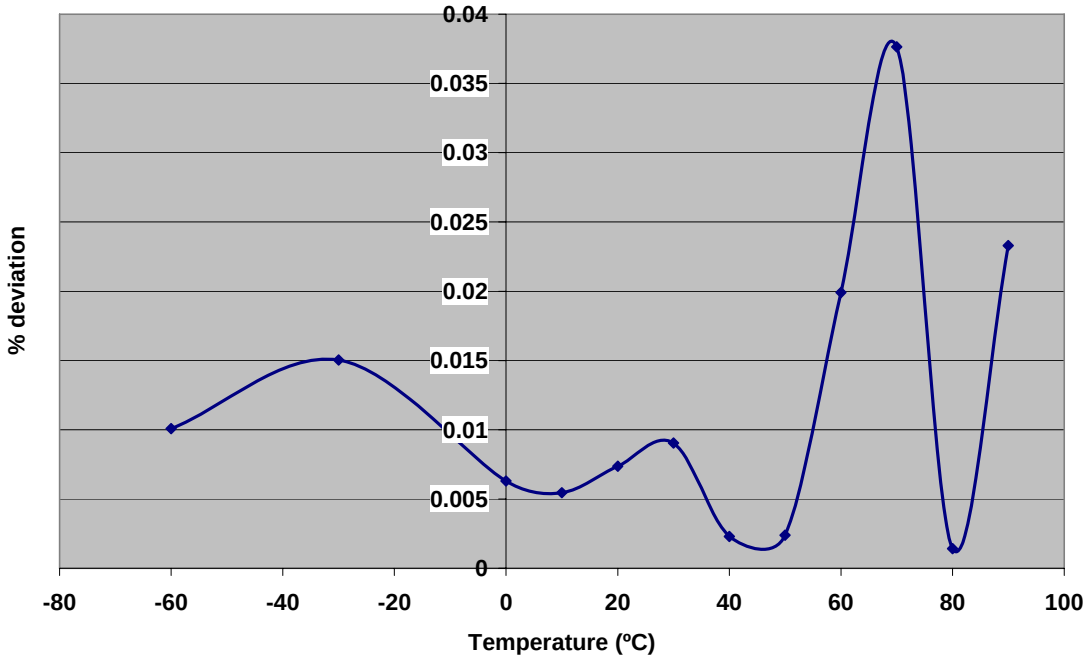

Figure 130: % Deviation for specific volume of moist air between Model and EES

In Figure 131, the humidity ratio of moist air over a range of temperatures predicted by VB.Net function and EES is shown. The two correlations match closely with each other. The deviation between VB. Net and EES is shown in Figure 132 and the deviation was less than 0.7 % and -0.1%.

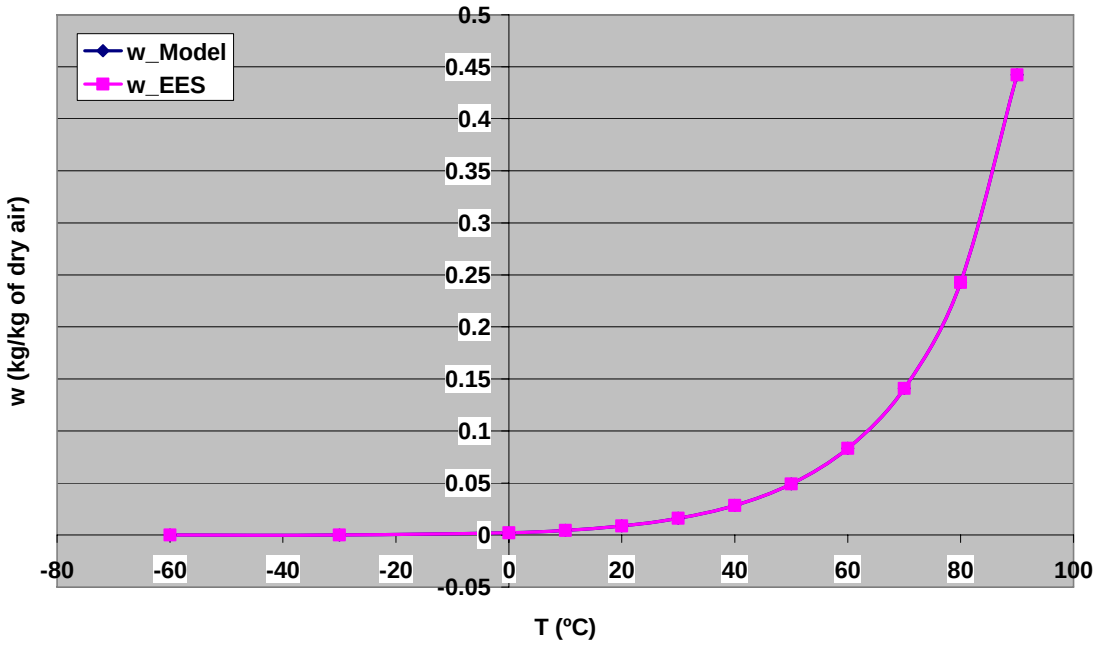

Figure 131: Comparison of humidity ratio of moist air between Model and EES

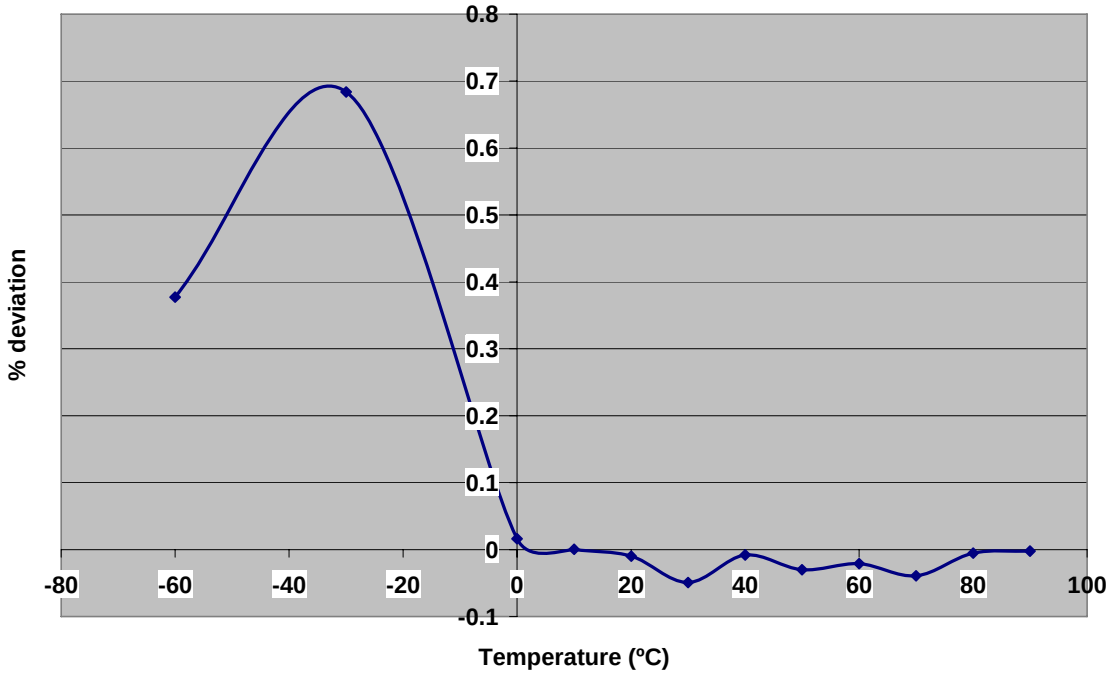

Figure 132: % Deviation for humidity ratio of moist air between Model and EES

Figure 133 shows the comparison of the density of moist air between VB.Net and EES property functions. The two functions almost overlap each other. The deviation between VB. Net and EES is shown in Figure 134 and the deviation was within ± 0.05 %.

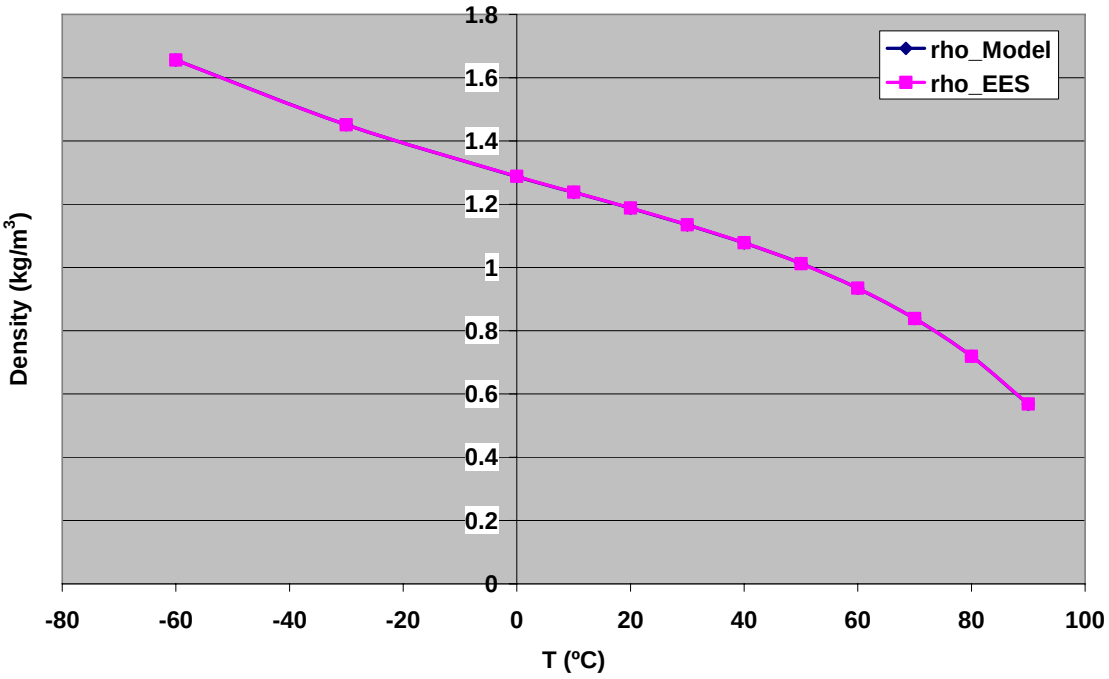

Figure 133: Comparison of density of moist air between Model and EES

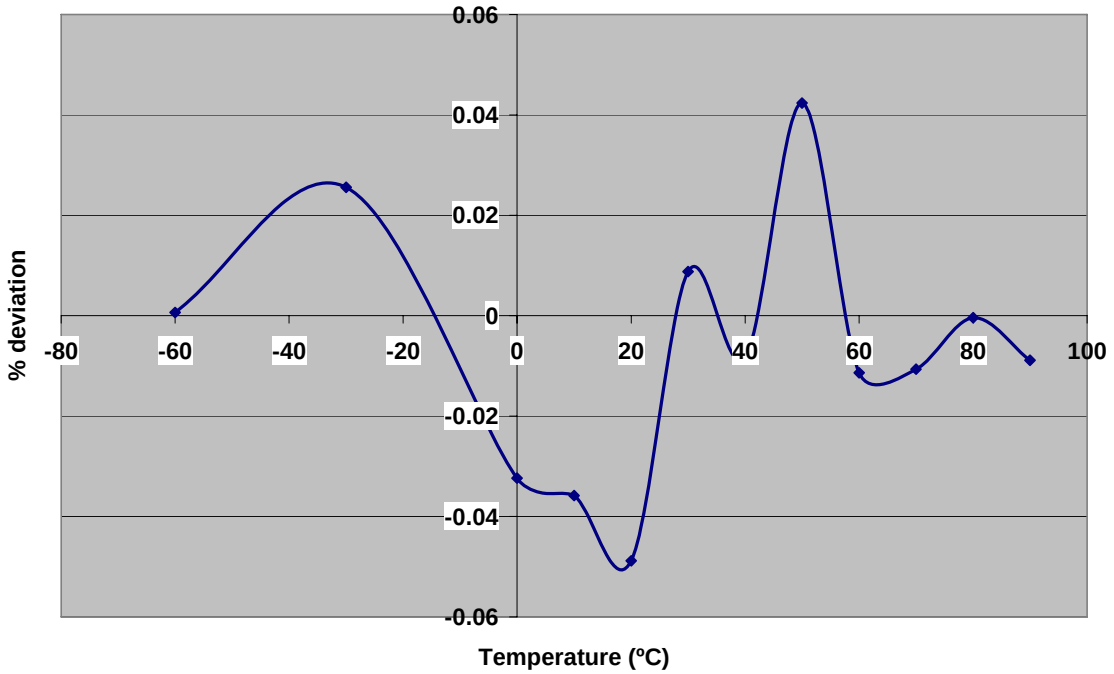

Figure 134: % Deviation for density of moist air between Model and EES

Figure 135 compares the specific heat at constant pressure (C_p) of moist air between Visual Basic.Net and EES. The specific heat at constant pressure was

calculated at a constant humidity ratio of 0.01605 kg/kg air (T=30ºC and RH=60 %) It can be seen from Figure 135 that the values of C_p predicted by EES and VB.Net match pretty closely. The deviation between VB. Net and EES is shown in Figure 136 and the deviation was less than 2.5 %.

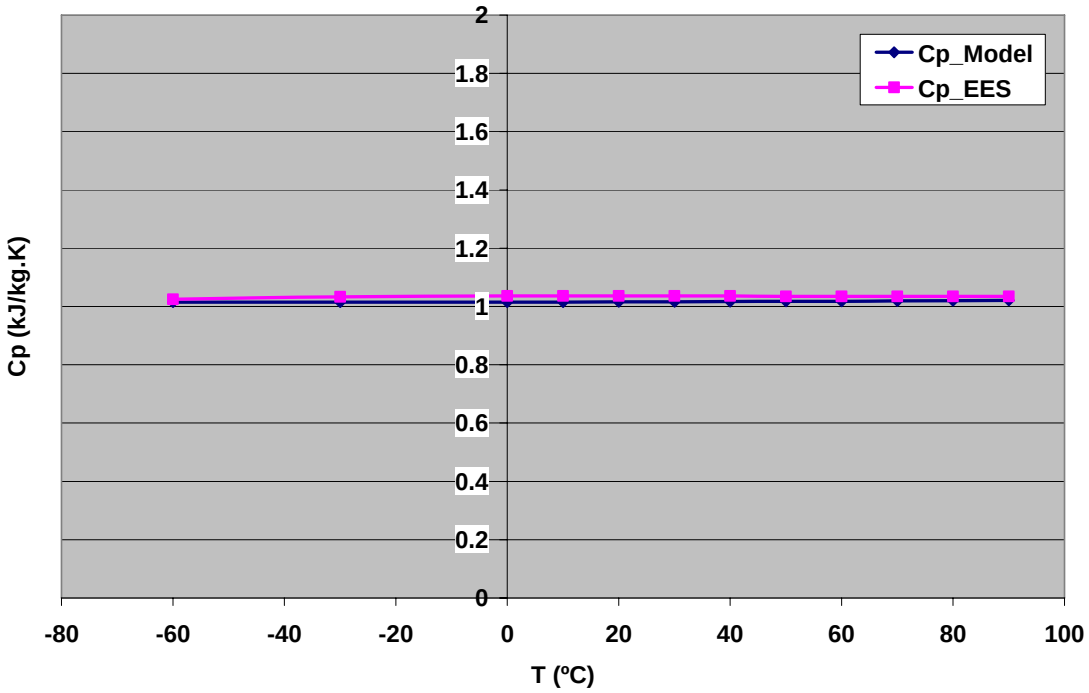

Figure 135: Comparison of specific heat at constant pressure (Cp) and constant humidity ratio of moist air between Model and EES

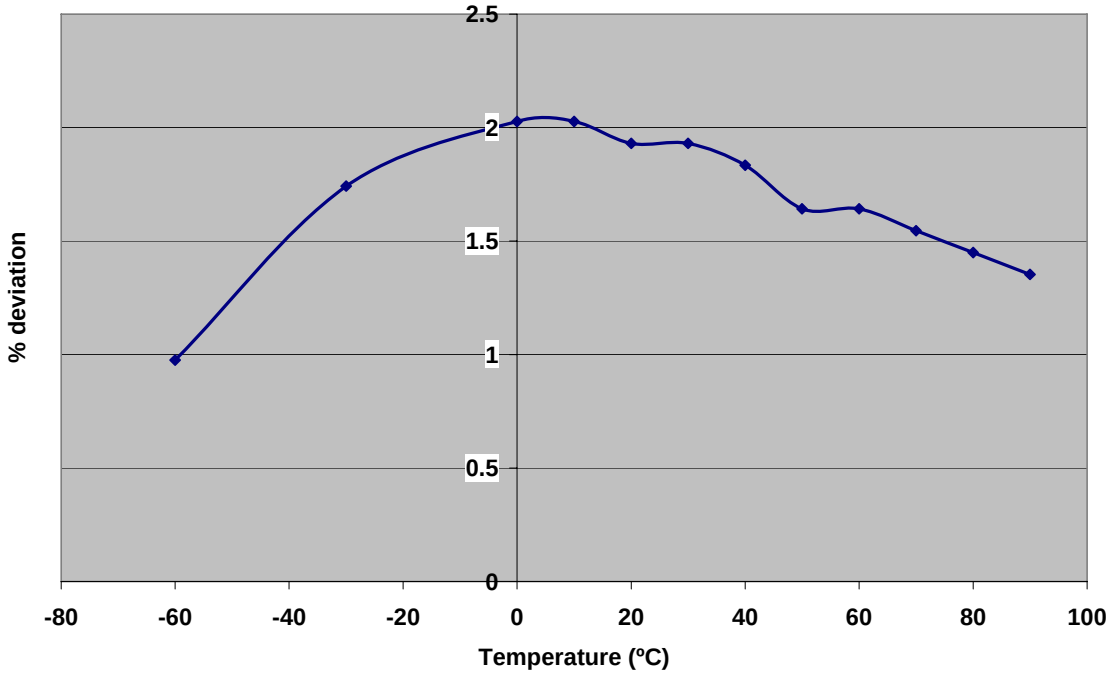

Figure 136: % Deviation for specific heat of moist air between Model and EES

6.7.3 Lithium Chloride – Water Solution

In the CHP system, the liquid desiccant dehumidification system uses lithium chloride water solution as the desiccant medium. Hence it's necessary to model and validate the property functions of lithium chloride water solution to accurately predict the performance of the dehumidification system. Thermodynamic data of vapor pressure, specific heat etc of lithium chloride solution for a wide range of temperature and salt concentration was obtained from AIL Research Inc. The thermodynamic data was then curve fitted in Table Curve 3D version 4.0 to get surface equations and then coded in Visual Basic.Net. The vapor pressure function in Visual Basic.Net is a Chebyshev X, Y bivariate polynomial of order 10. Figure 137 shows the plot of vapor pressure of lithium chloride water solution over a range of solution temperatures for

10 % salt concentration while Figure 138 shows the percentage deviation between the model and different sources in the literature. The percentage deviation at 10 % LiCl salt concentration was found to be within ± 8 %.

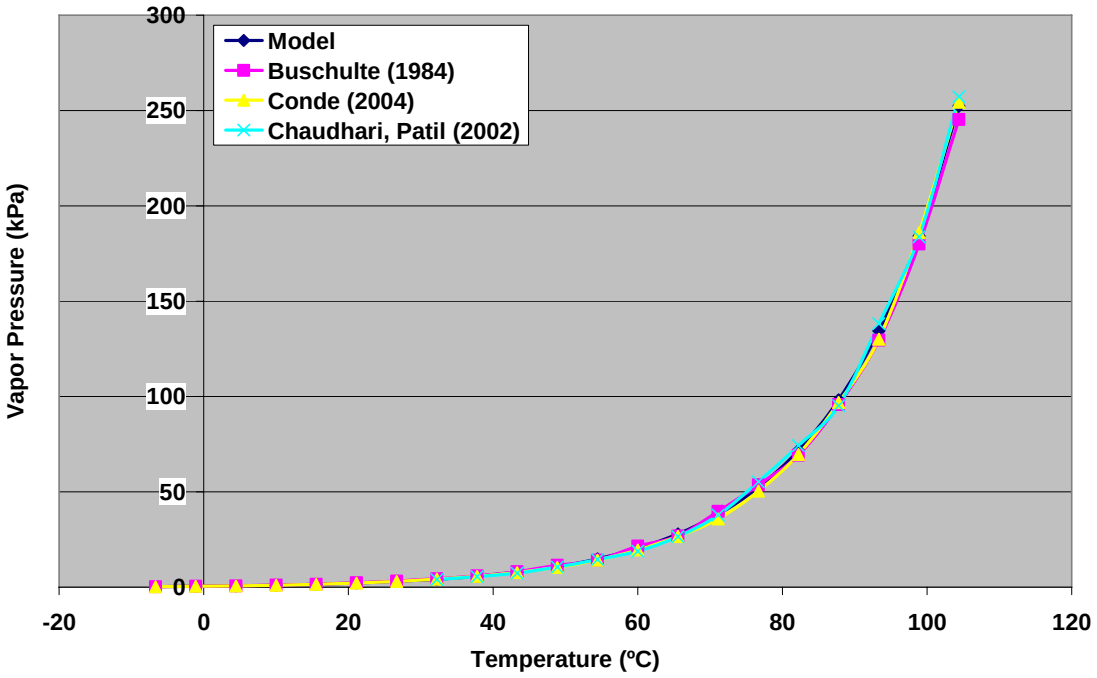

Figure 137: Vapor Pressure of lithium chloride water solution for different temperatures at 10 % salt concentration

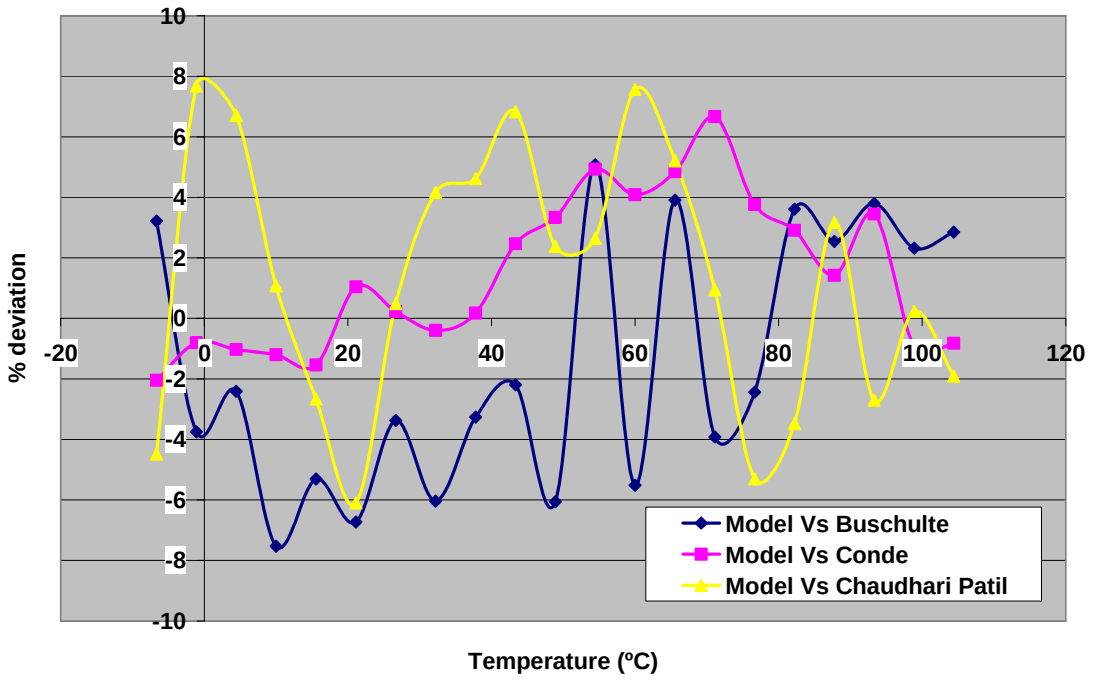

Figure 138: % Deviation in vapor pressure of lithium chloride water solution at 10 % salt concentration

Figure 139 plots vapor pressure of lithium chloride water solution at 15 % salt concentration over different solution temperatures and Figure 140 shows the deviation between model and other literature sources. The deviation in this case was again well below ± 8 %.

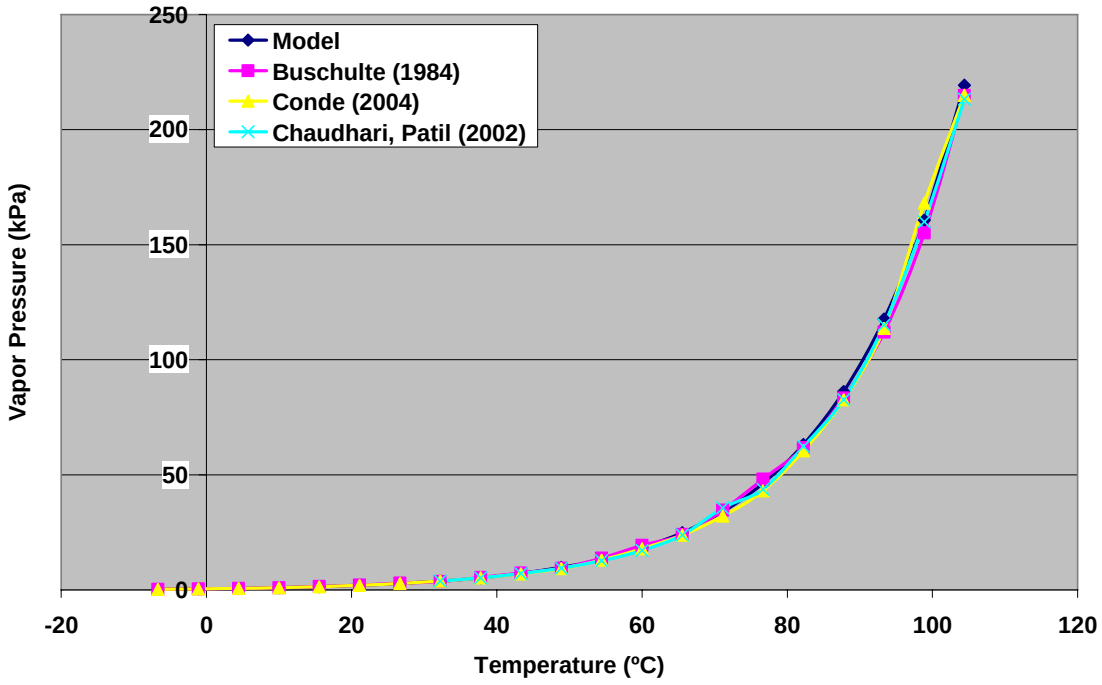

Figure 139: Vapor Pressure of lithium chloride water solution for different temperatures at 15 % salt concentration

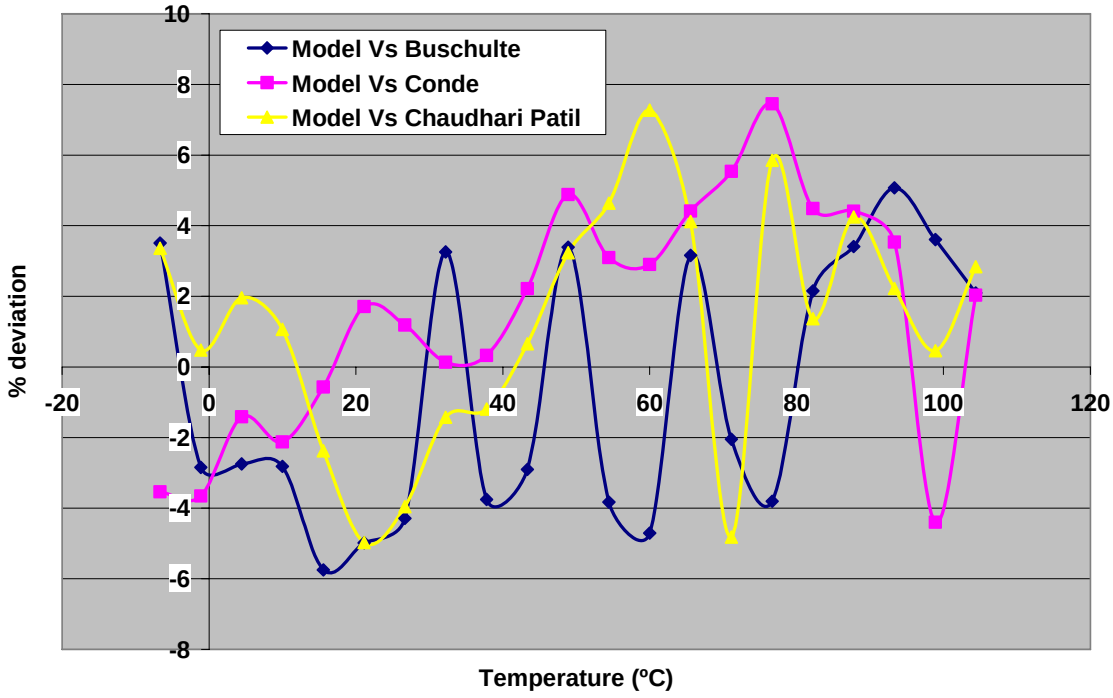

Figure 140: % Deviation in vapor pressure of lithium chloride water solution at 15 % salt concentration

Figure 141 shows the plot of vapor pressure of lithium chloride water solution over a range of solution temperatures for 20 % salt concentration while Figure 142 shows the percentage deviation between the model and different sources in the literature. The percentage deviation at 20 % LiCl salt concentration was found to be less than ± 7 %.

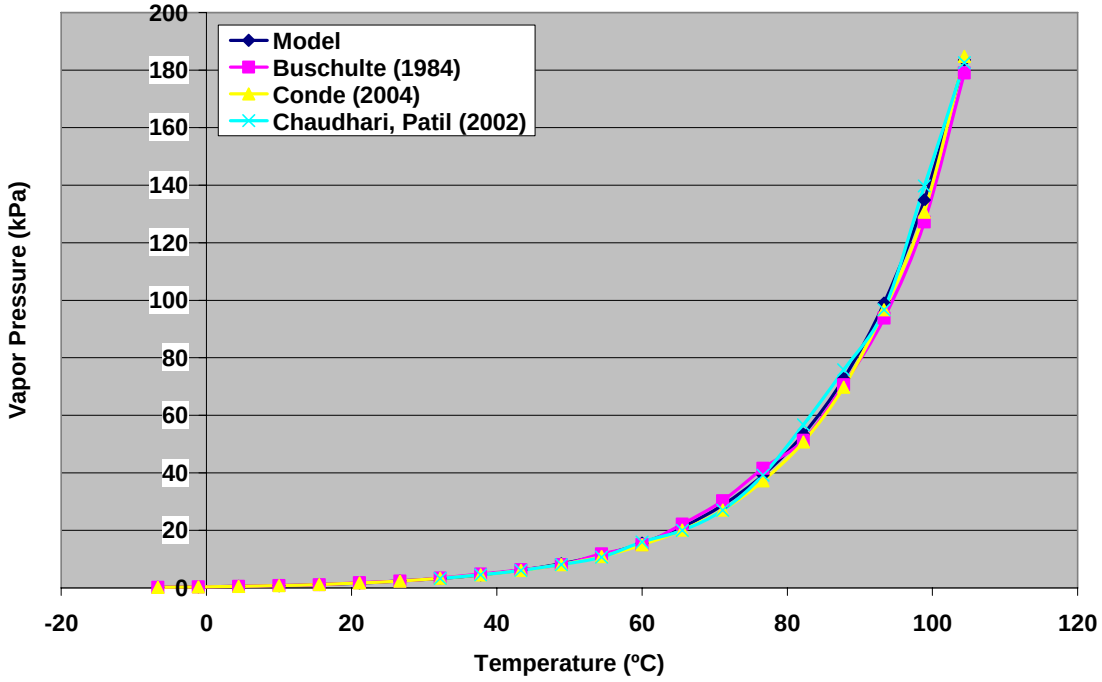

Figure 141: Vapor Pressure of lithium chloride water solution for different temperatures at 20 % salt concentration

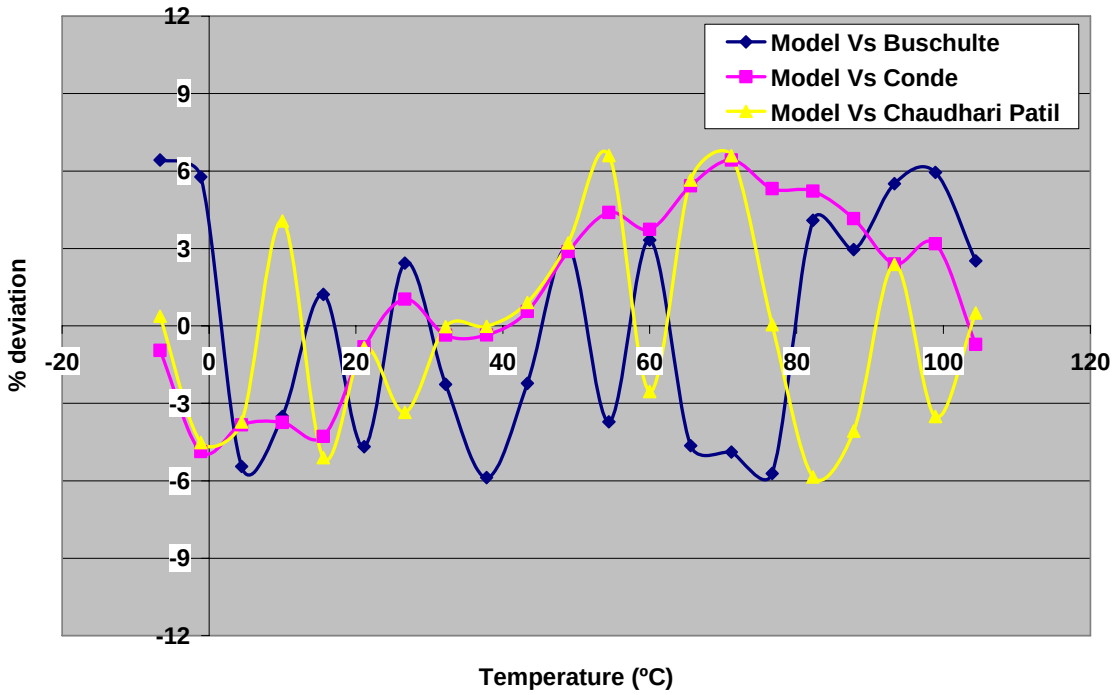

Figure 142: % Deviation in vapor pressure of lithium chloride water solution at 20 % salt concentration

The vapor pressure plot of LiCl – water solution for different solution temperatures at 25 % salt concentration is shown in Figure 143. The deviation in this case was found to be within ± 8 % which is plotted in Figure 144.

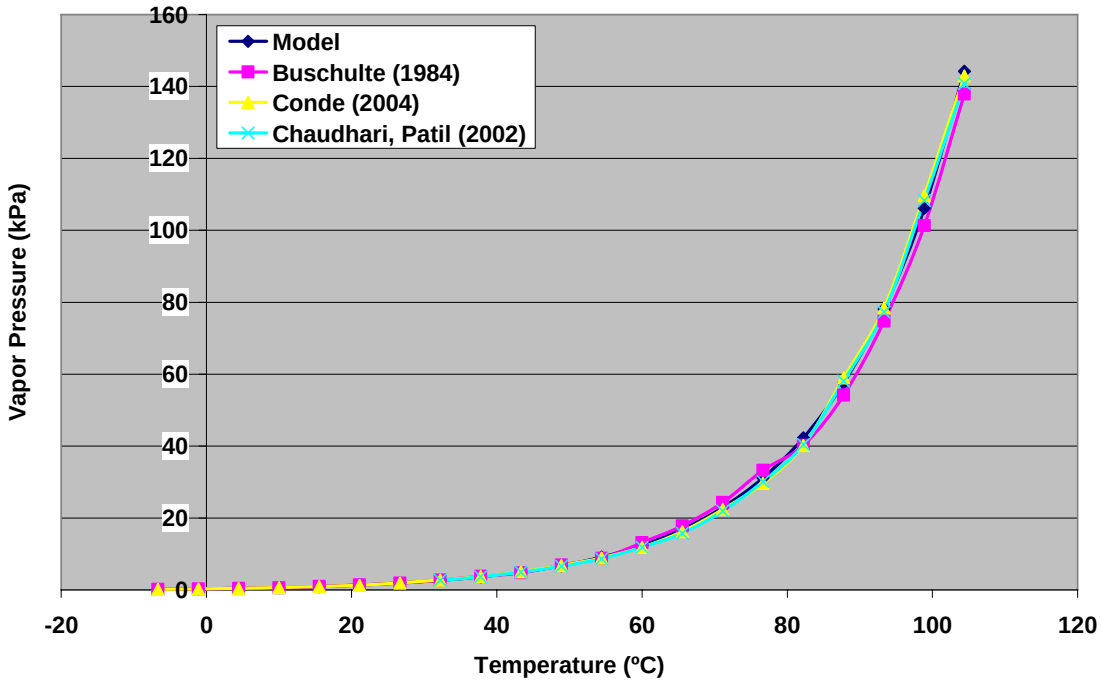

Figure 143: Vapor Pressure of lithium chloride water solution for different temperatures at 25% salt concentration

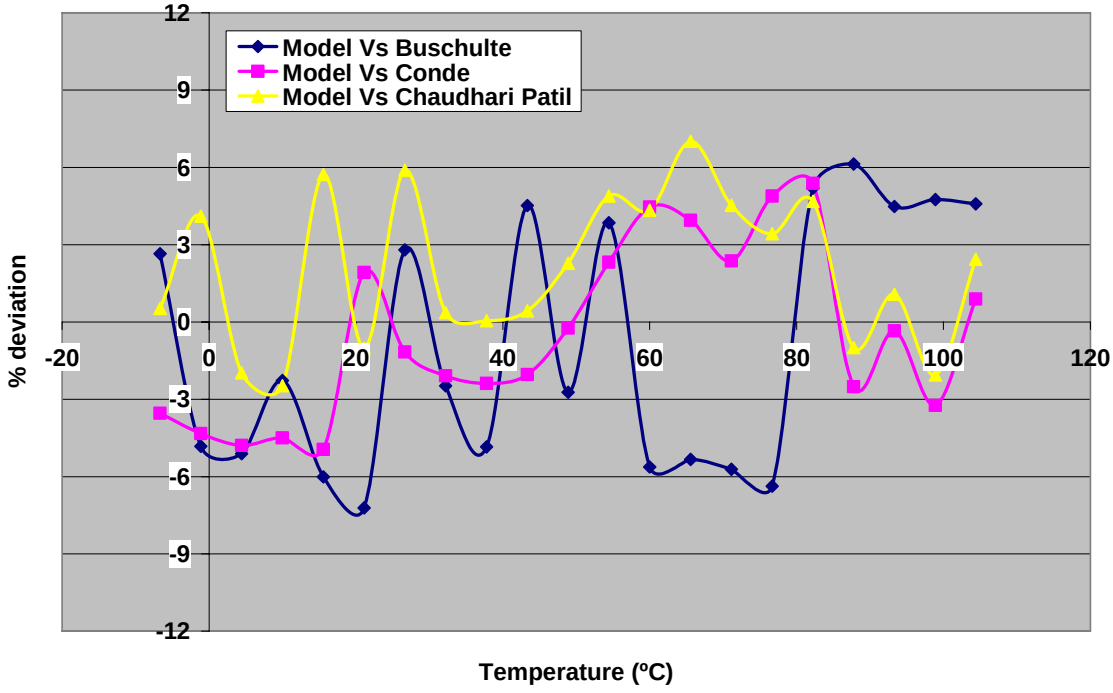

Figure 144: % Deviation in vapor pressure of lithium chloride water solution at 25 % salt concentration

Figure 145 shows the comparison of the vapor pressure function between the model and other literature sources for the salt concentration of 30 %. The percentage deviation at 30 % concentration was well within ± 8 %. The deviation between the model and the literature sources is shown in Figure 146.

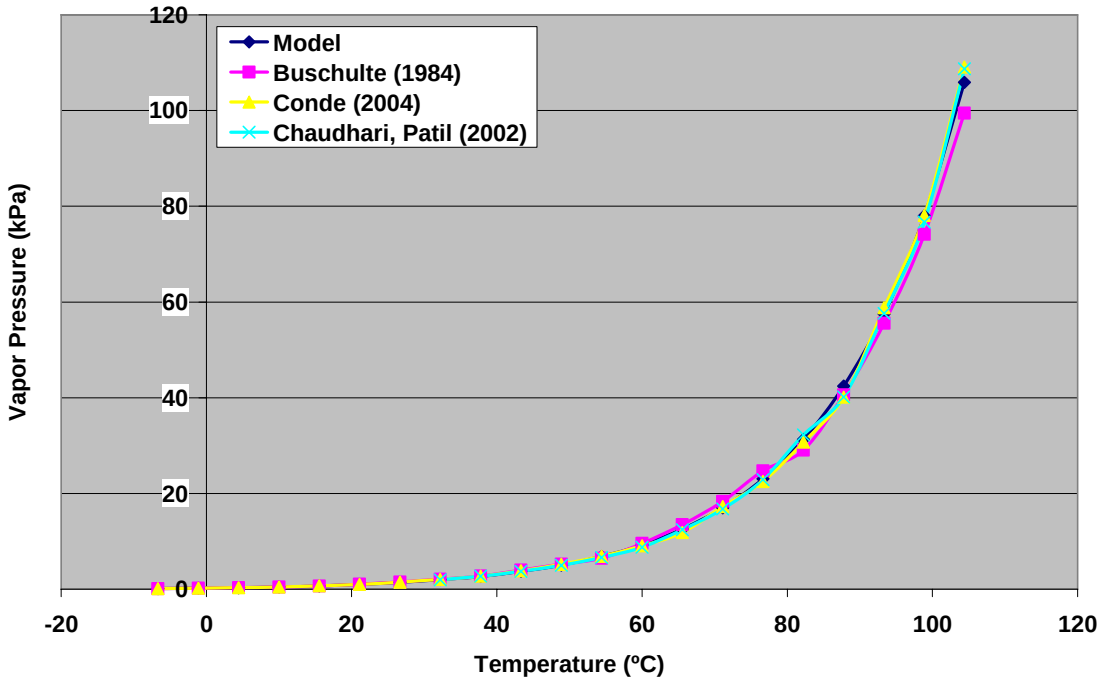

Figure 145: Vapor Pressure of lithium chloride water solution for different temperatures at 30% salt concentration

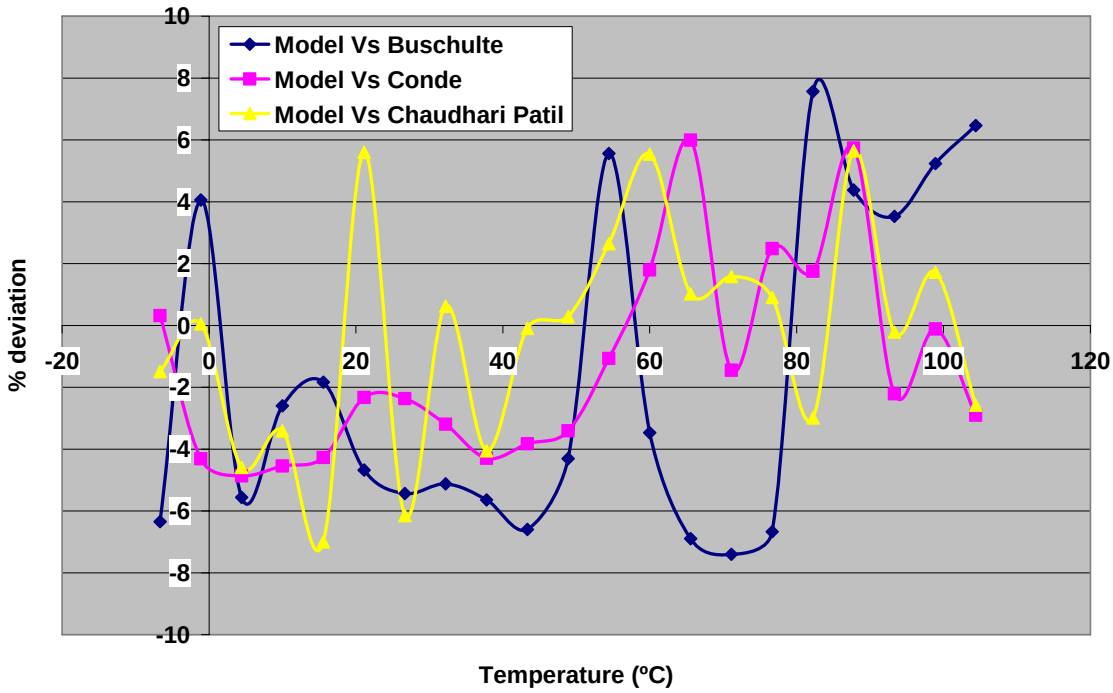

Figure 146: % Deviation in vapor pressure of lithium chloride water solution at 30 % salt concentration

The plot of vapor pressure of lithium chloride water solution at 35 % salt concentration is shown in Figure 147 while the deviation for the 35 % concentration is plotted in figure 32. The deviation as can be seen from Figure 148 was less than ± 8 %.

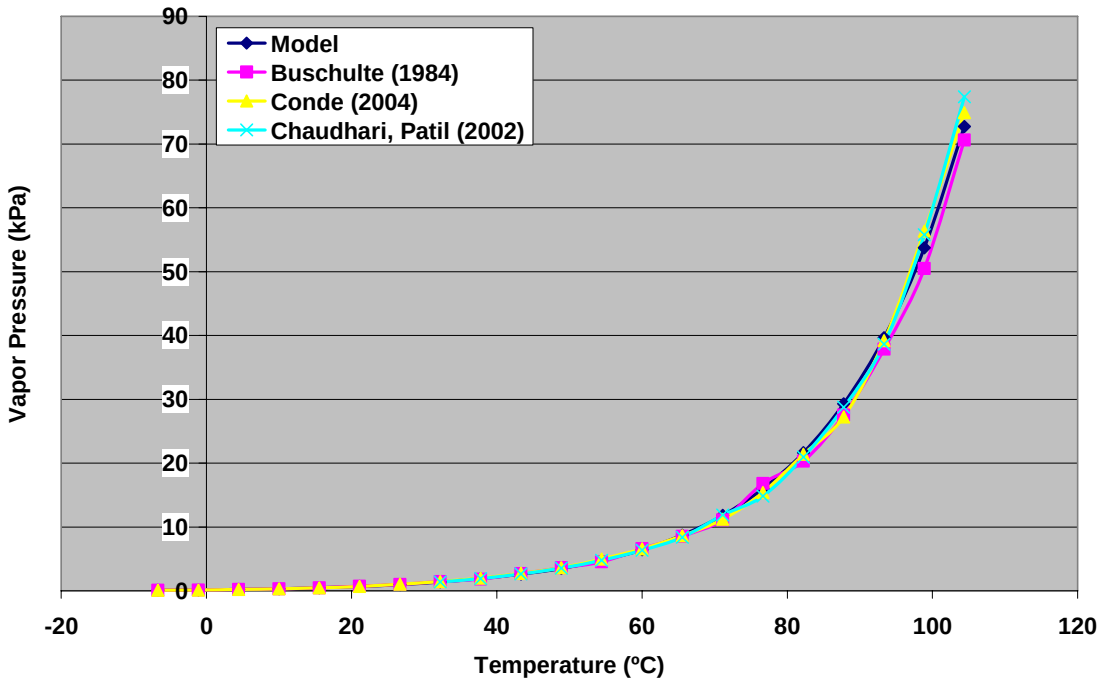

Figure 147: Vapor Pressure of lithium chloride water solution for different temperatures at 35% salt concentration

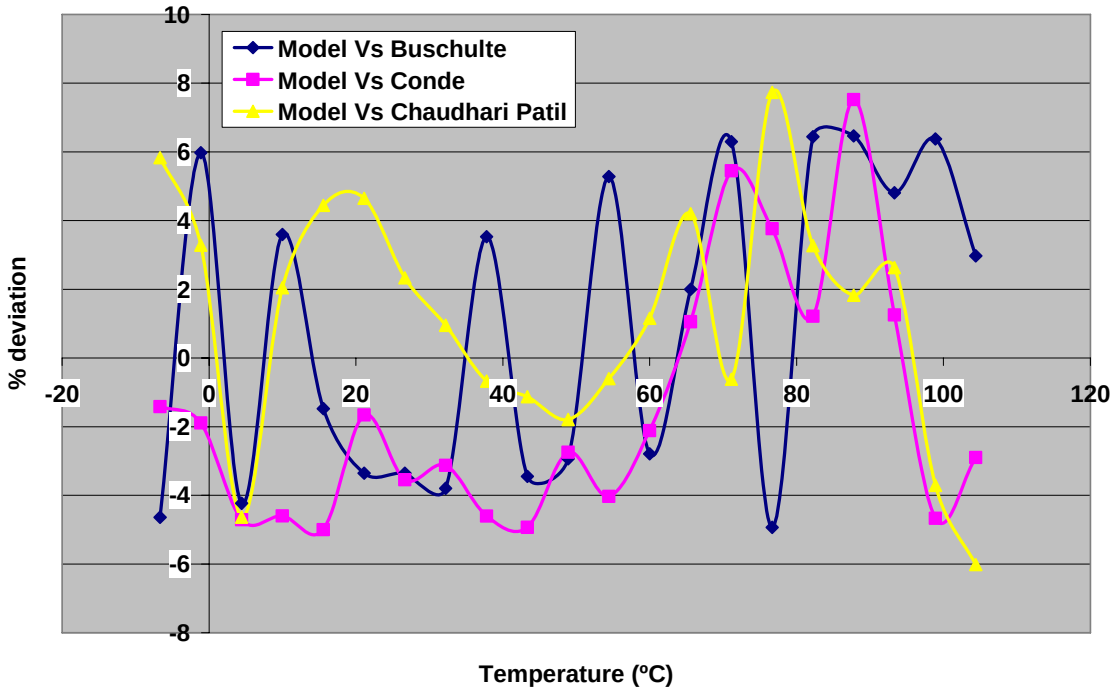

Figure 148: % Deviation in vapor pressure of lithium chloride water solution at 35 % salt concentration

The vapor pressure plot of lithium chloride water solution at 40 % salt concentration is plotted in Figure 149 and the deviation for this case is plotted in Figure 150. The percentage deviation in vapor pressure for 40 % salt concentration was observed to be within ± 8 %.

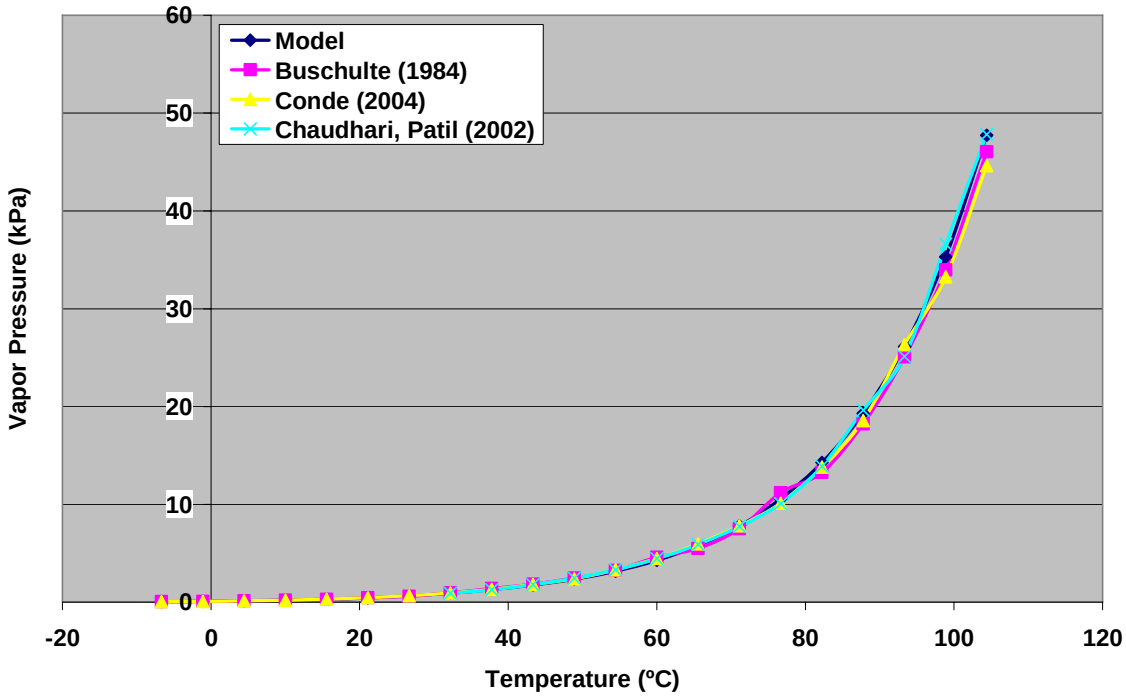

Figure 149: Vapor Pressure of lithium chloride water solution for different temperatures at 40% salt concentration

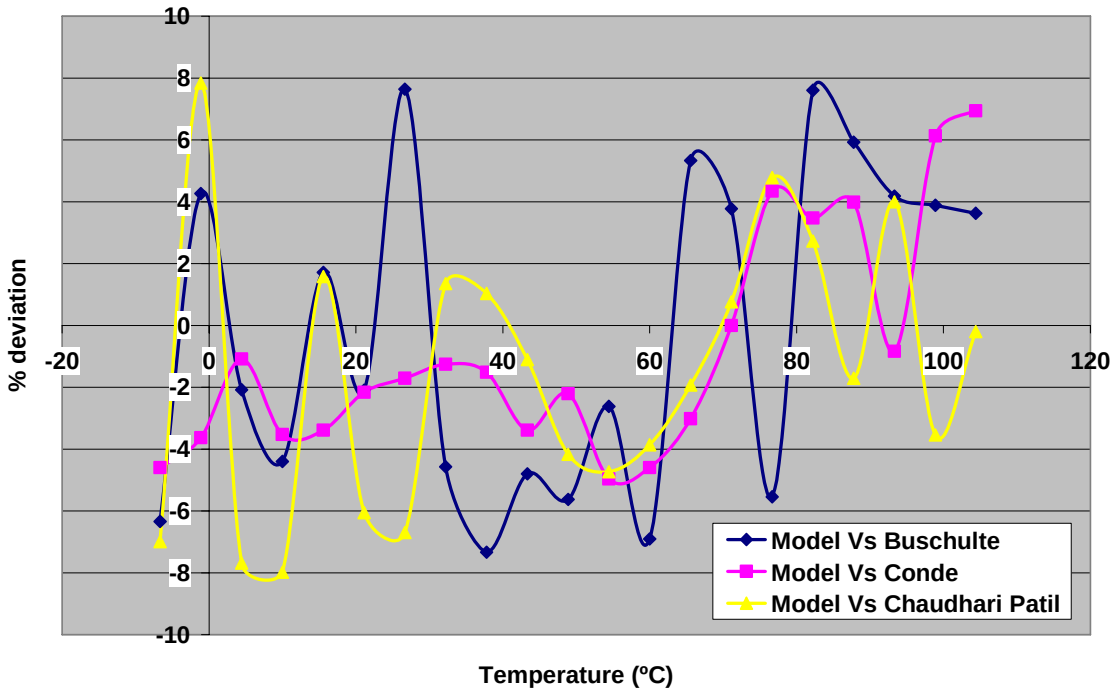

Figure 150: % Deviation in vapor pressure of lithium chloride water solution at 40 % salt concentration

Figure 151 shows the comparison of the vapor pressure of lithium chloride water solution between the model and other literature sources for the salt concentration of 45 %. Figure 152 plots the percentage deviation in vapor pressure for 45 % salt concentration and it is seen that the deviation in this case too was within ± 8 %.

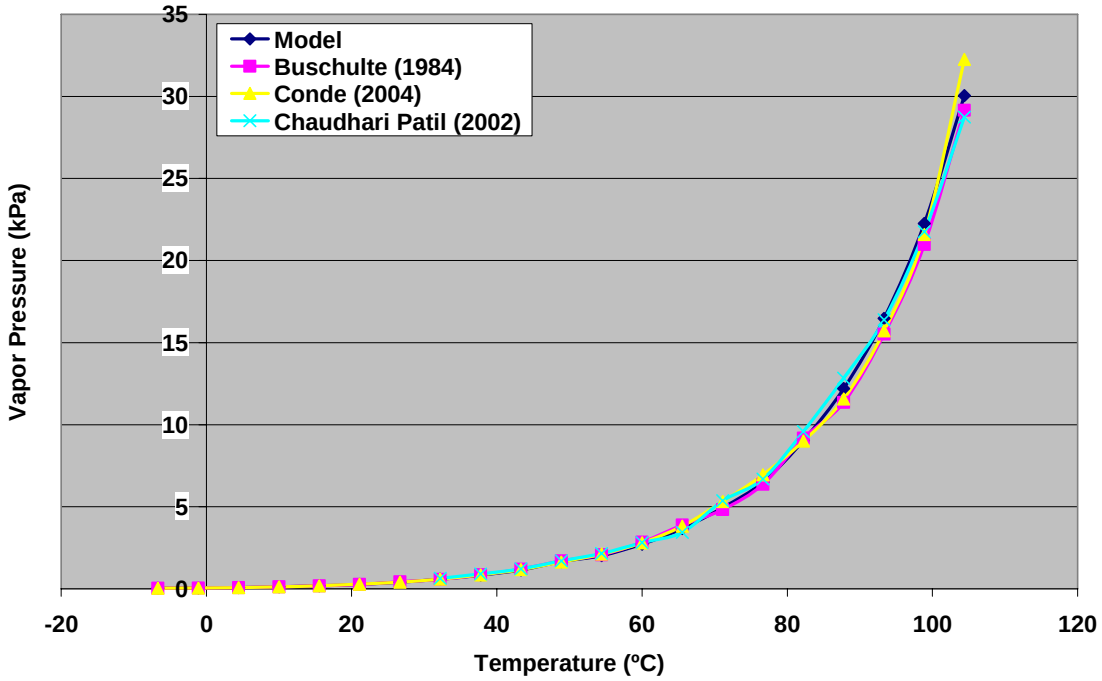

Figure 151: Vapor Pressure of lithium chloride water solution for different temperatures at 45% salt concentration

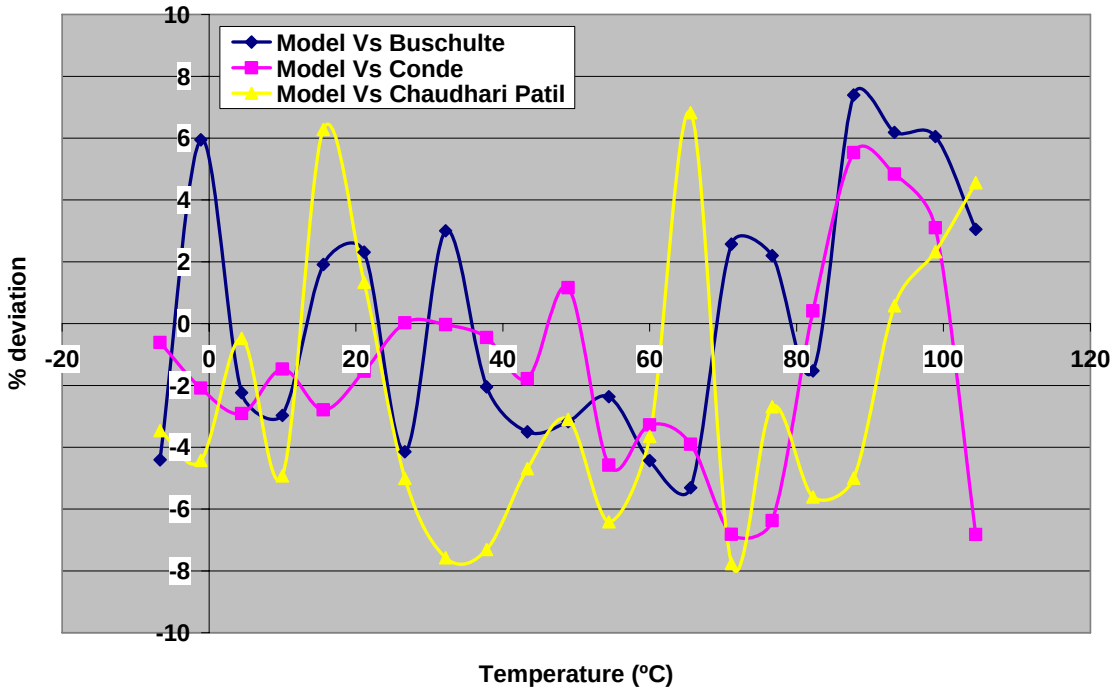

Figure 152: % Deviation in vapor pressure of lithium chloride water solution at 45 % salt concentration

Thus it can be seen from the above plots that the vapor pressure function coded in VB.Net from the thermodynamic data supplied by AIL Research Inc. matches very well with the vapor pressure correlations from the literature for all the concentration levels. Though the deviation in vapor pressure of lithium chloride water solution for individual cases was found to be in the range of ± 8 %, the average percentage deviation between the vapor pressure property function of the model and the ones available in literature was found to be less than ± 5 % over the entire range of concentration as well as solution temperatures. Figure 153 shows the plot of average percentage deviation over a range of LiCl concentrations for different values of solution temperatures while Figure 154 gives the average percentage deviation over the range of solution temperatures for different LiCl concentration levels.

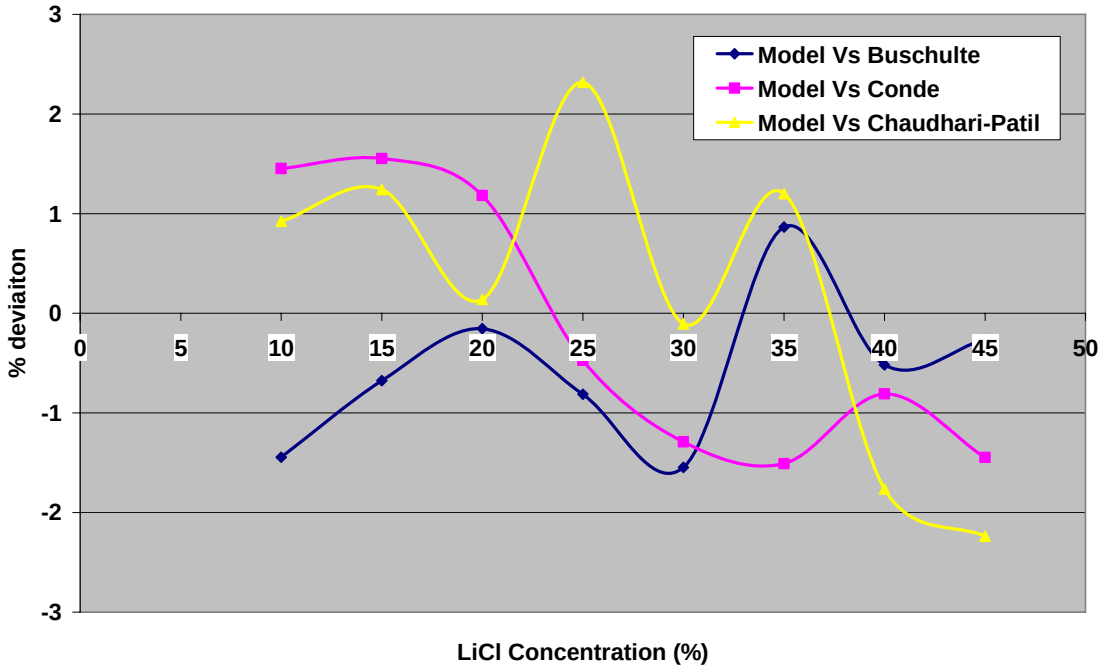

Figure 153: Average % deviation in vapor pressure function over range of LiCl concentrations

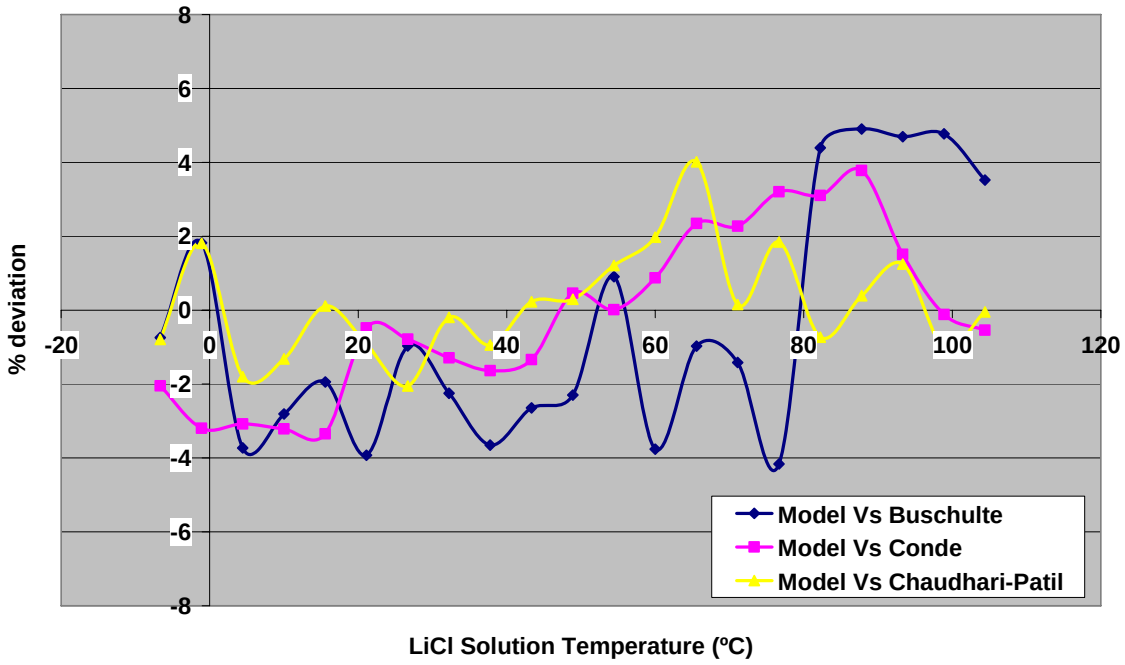

Figure 154: Average % deviation in vapor pressure function over range of LiCl solution temperatures

The vapor pressure of lithium chloride solution in VB.Net was also compared with the vapor pressure data available in Gmelins Handbook of Inorganic Chemistry (Lithium, 1960). Figure 155 shows the comparison of vapor pressure of lithium chloride solution for different concentrations at a solution temperature of 18 ºC between Gmelin and VB.Net while Figure 156 and Figure 157 show the plots of vapor pressure at solution temperatures of 20.28 ºC and 25 ºC respectively. It is seen from the plots that the VB.Net function agrees closely with the vapor pressure data from Gmelins Handbook too.

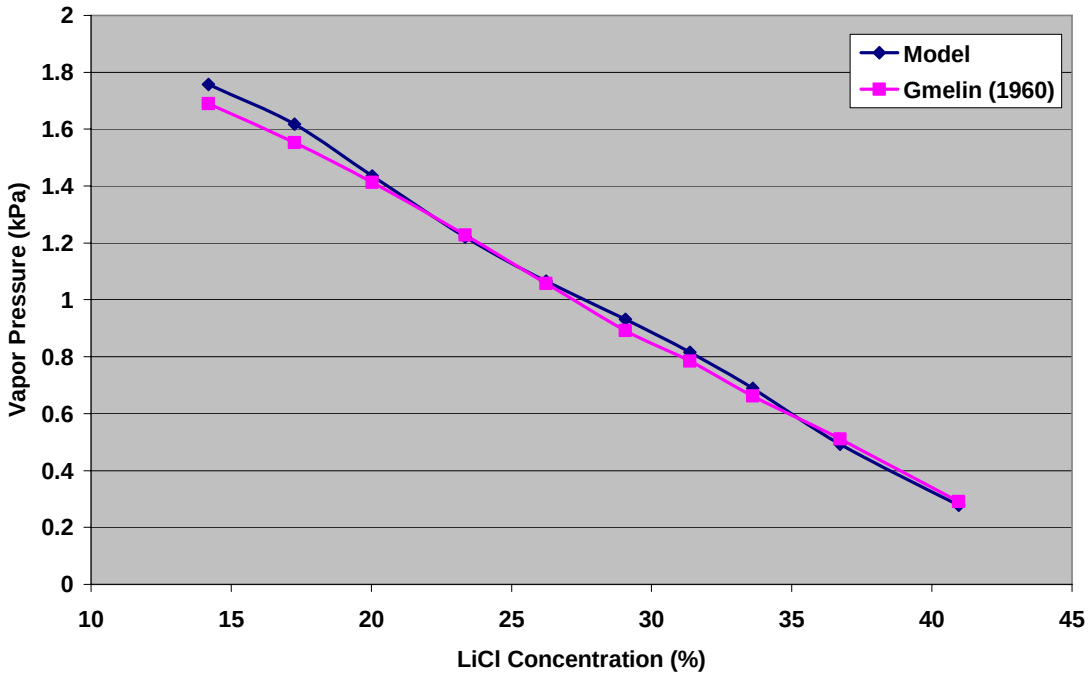

Figure 155: Comparison of vapor pressure of lithium chloride water solution at 18 ºC between Model and Gmelins Handbook

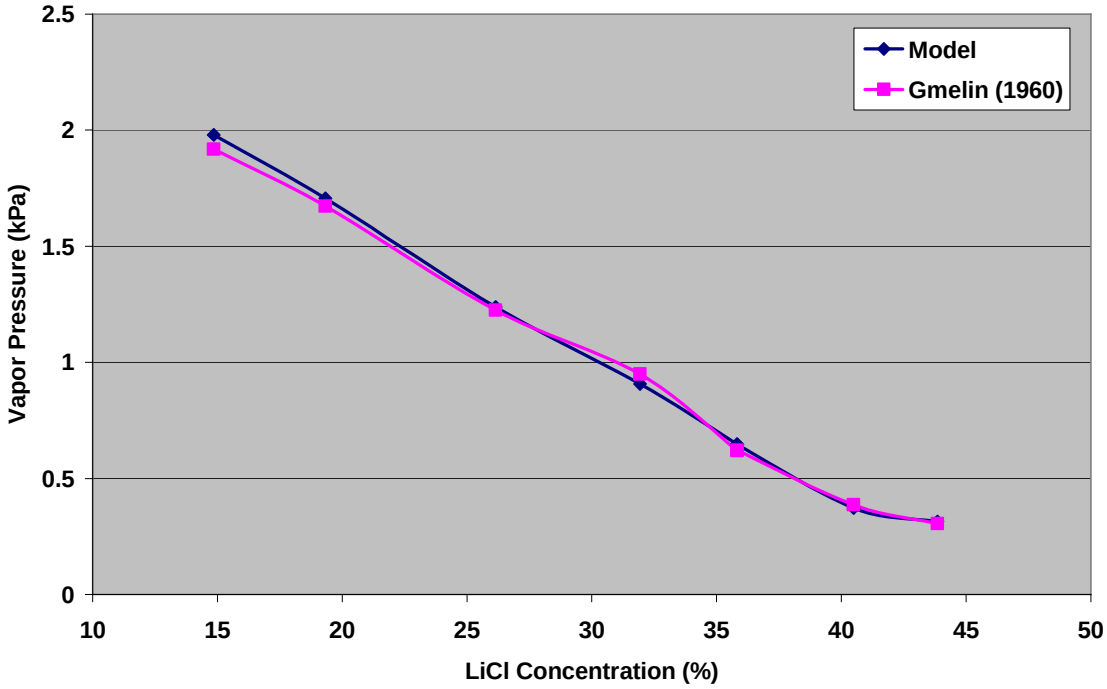

Figure 156: Comparison of vapor pressure of lithium chloride water solution at 20.28 ºC between Model and Gmelins Handbook

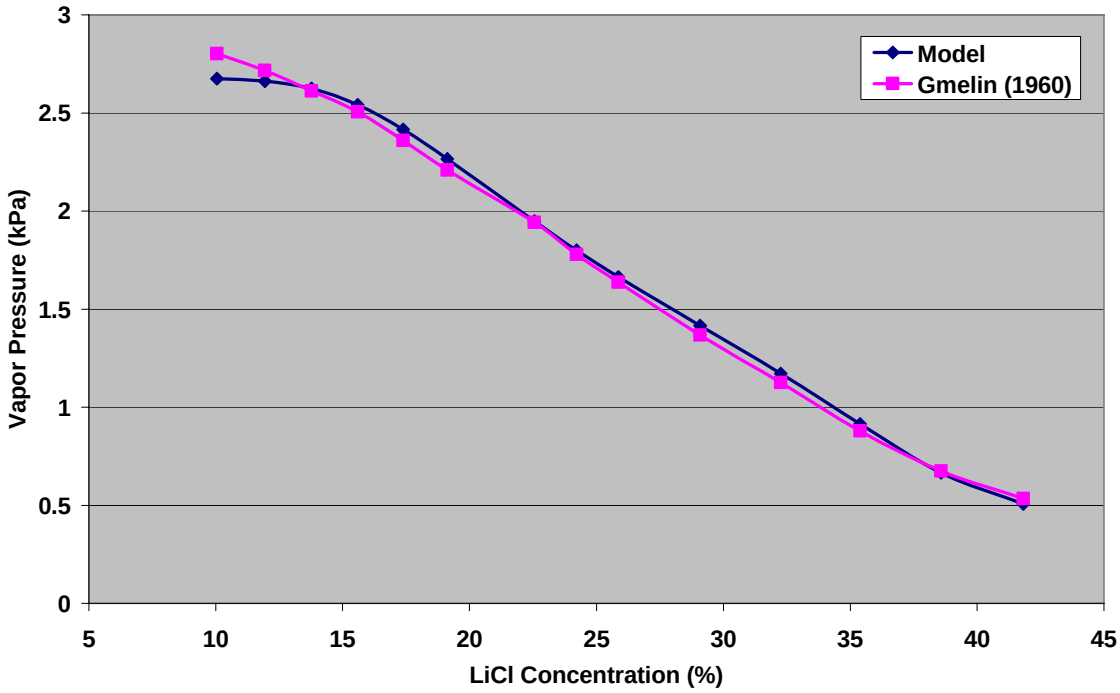

Figure 157: Comparison of vapor pressure of lithium chloride water solution at 25 ºC between Model and Gmelins Handbook

The percentage deviation between the VB.Net vapor pressure function and the Gmelins Handbook at 18ºC, 20.28ºC and 25ºC were plotted and is shown in Figure 158 Figure 159 and Figure 160 respectively. The percentage deviation was found to be less than ± 5 % for all the 3 cases.

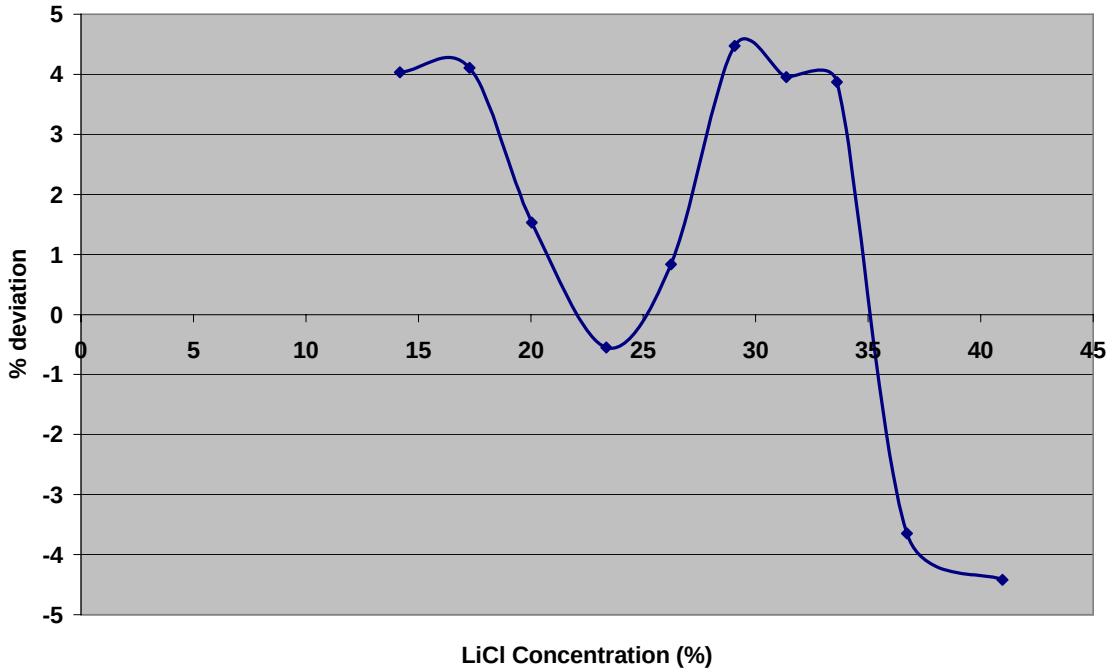

Figure 158: % Deviation between Model and Gmelins Handbook for vapor pressure at 18°C

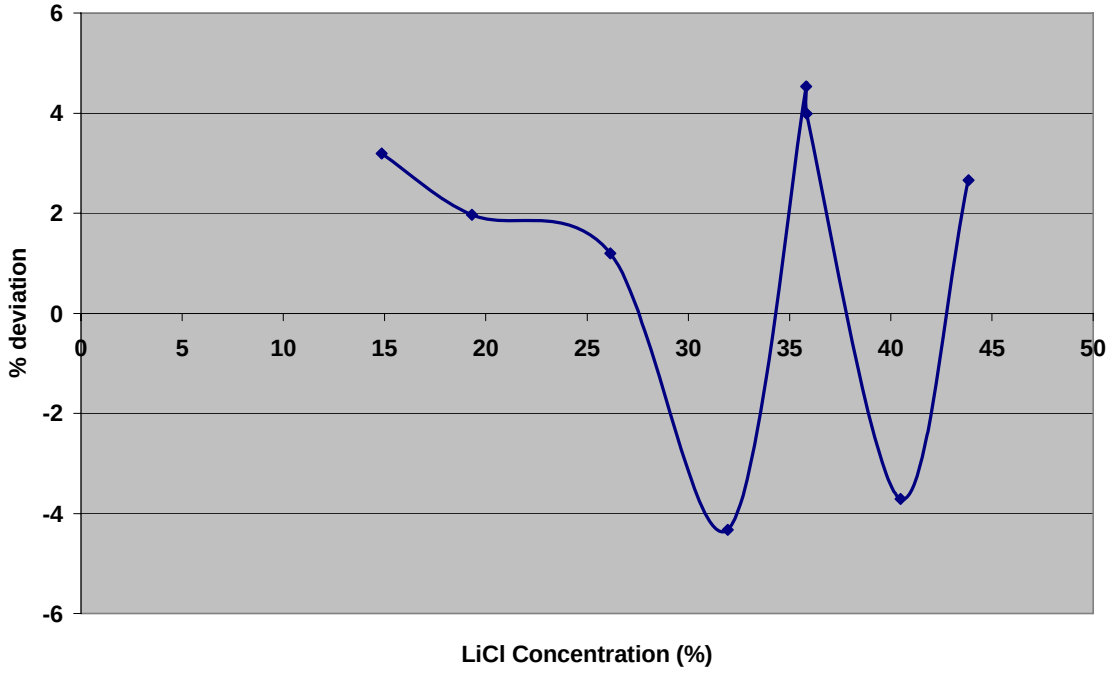

Figure 159: % Deviation between Model and Gmelins Handbook for vapor pressure at 20.28°C

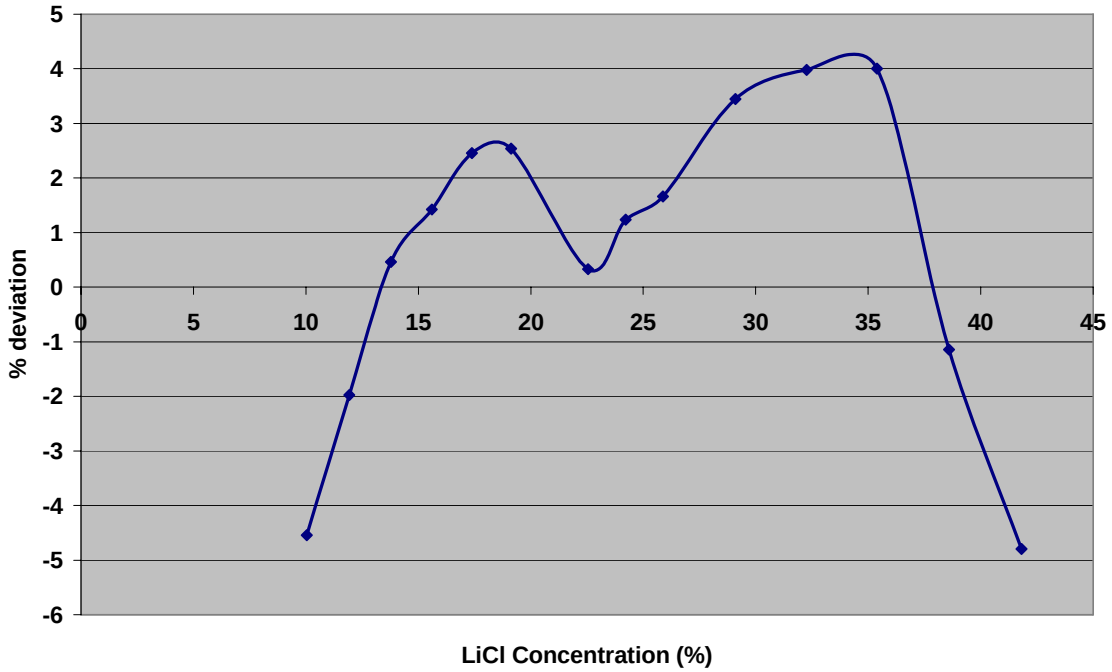

Figure 160: % Deviation between Model and Gmelins Handbook for vapor pressure at 25ºC

The specific heat function for lithium chloride water solution given by the company and coded in Visual Basic.Net is based on data and formula published in the paper by Tadashi Uemura titled "Studies on the Lithium-Chloride Water Absorption Refrigeration Machine" (1967). Figure 161 shows the plot of specific heat at constant pressure of the lithium chloride water solution over a range of solution temperatures for salt concentration of 10 %. It can be observed from Figure 161 that the specific heat relation in VB.Net agrees closely with the ones available in literature. The deviation in specific heat at 10 % salt concentration is shown in Figure 162 and it is seen from Figure 162 that the deviation was well under ± 1.5 %.

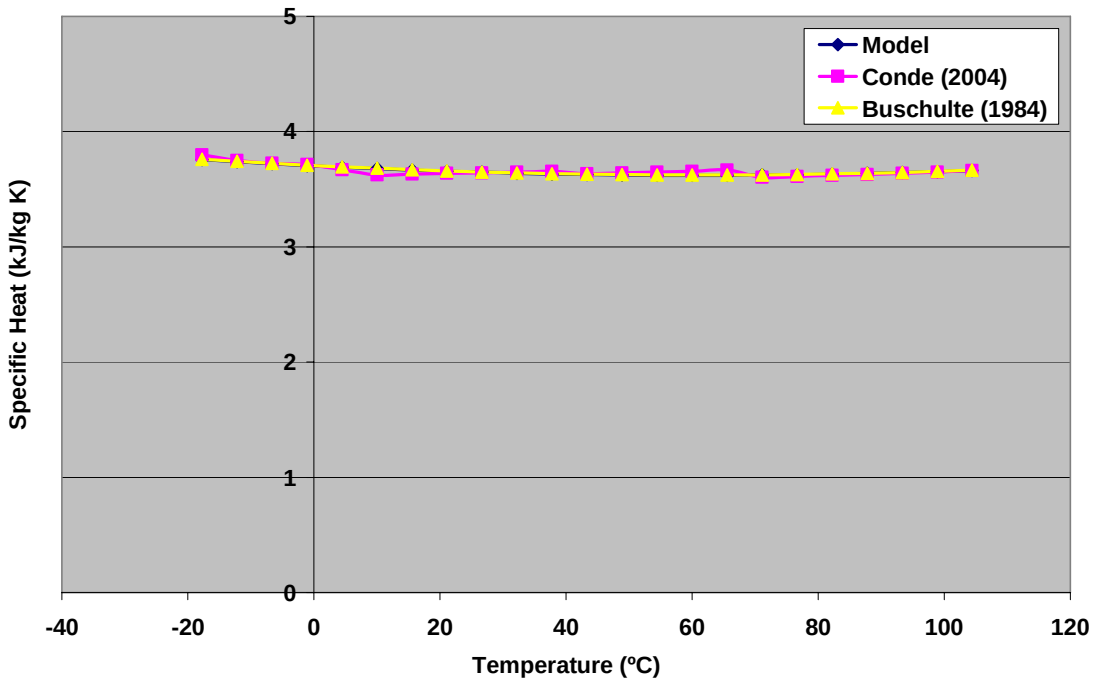

Figure 161: Specific Heat of lithium chloride water solution for different temperatures at 10 % salt concentration

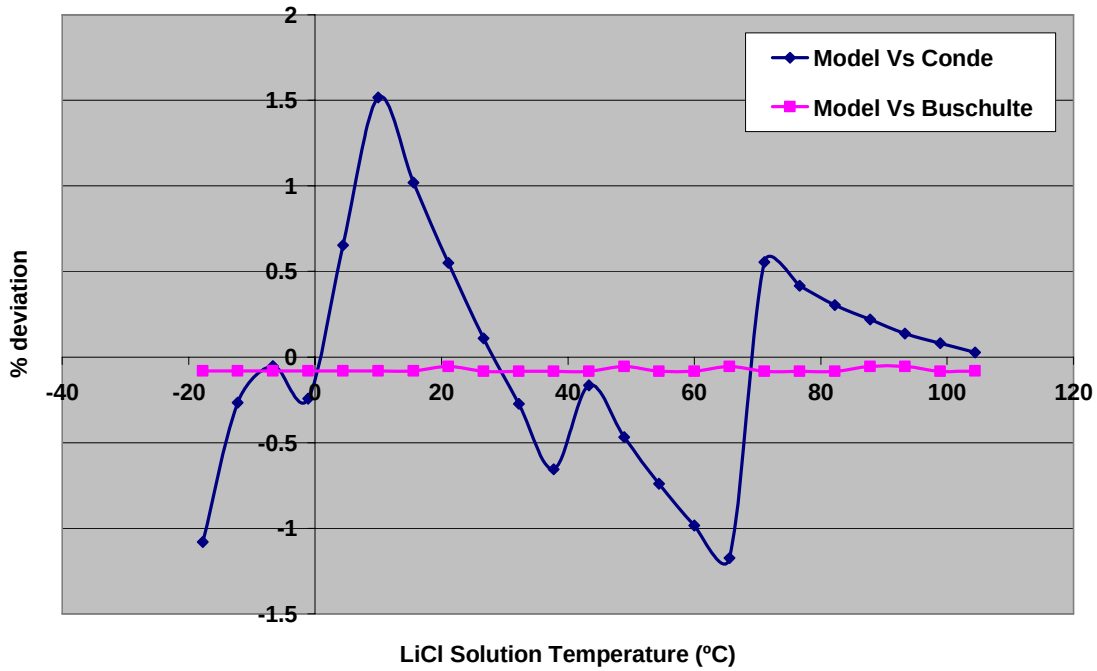

Figure 162: % Deviation in specific heat of lithium chloride water solution at 10 % salt concentration

The plot of specific heat of lithium chloride water solution at 15 % concentration as per the model and the literature sources is shown in Figure 163 while the deviation at 15 % concentration is plotted in Figure 164. The percentage deviation in this case was less than 1.5 %.

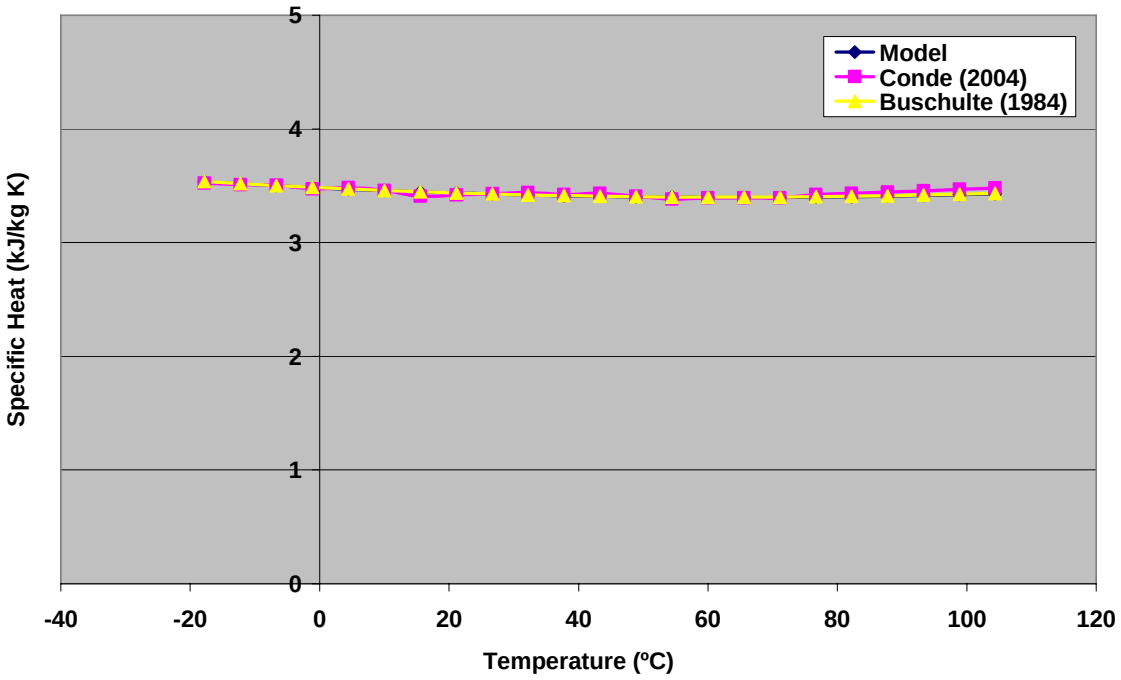

Figure 163: Specific Heat of lithium chloride water solution for different temperatures at 15 % salt concentration

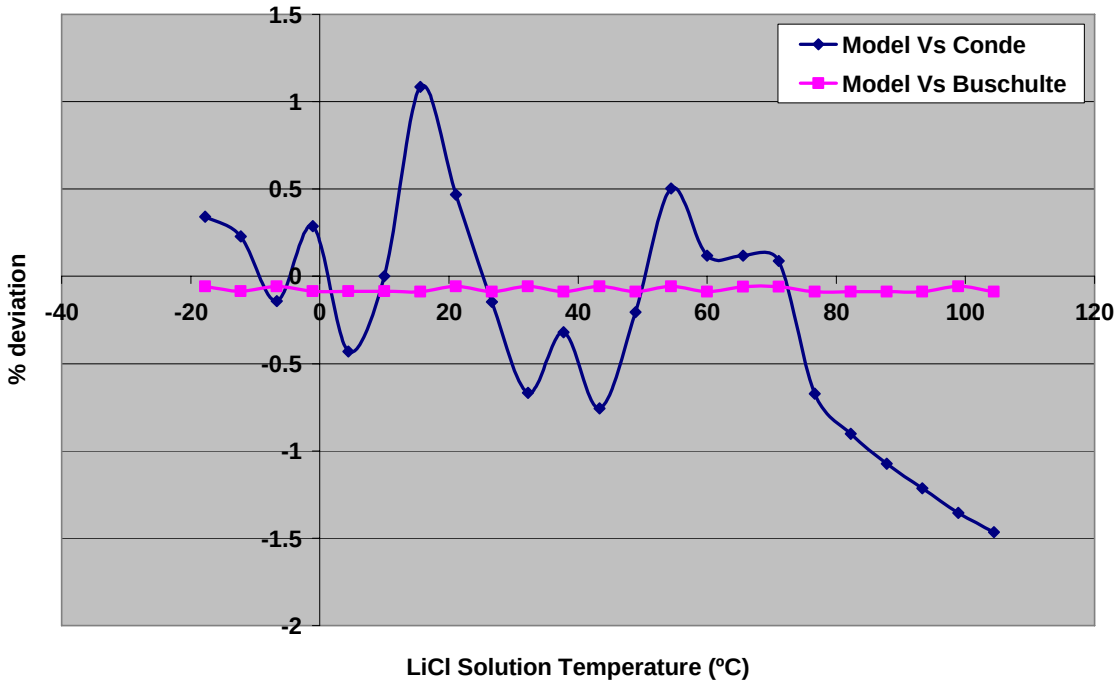

Figure 164: % Deviation in specific heat of lithium chloride water solution at 15 % salt concentration

Figure 165 shows the comparison of specific heat of lithium chloride water solution between the model and literature at 20 % salt concentration and it is seen that the specific heat predicted by the model in VB.Net agrees quite well with the ones from the literature. Figure 166 shows the percentage deviation in specific heat at 20 % concentration between the model and the literature sources. It is observed that the deviation was within ± 1 %.

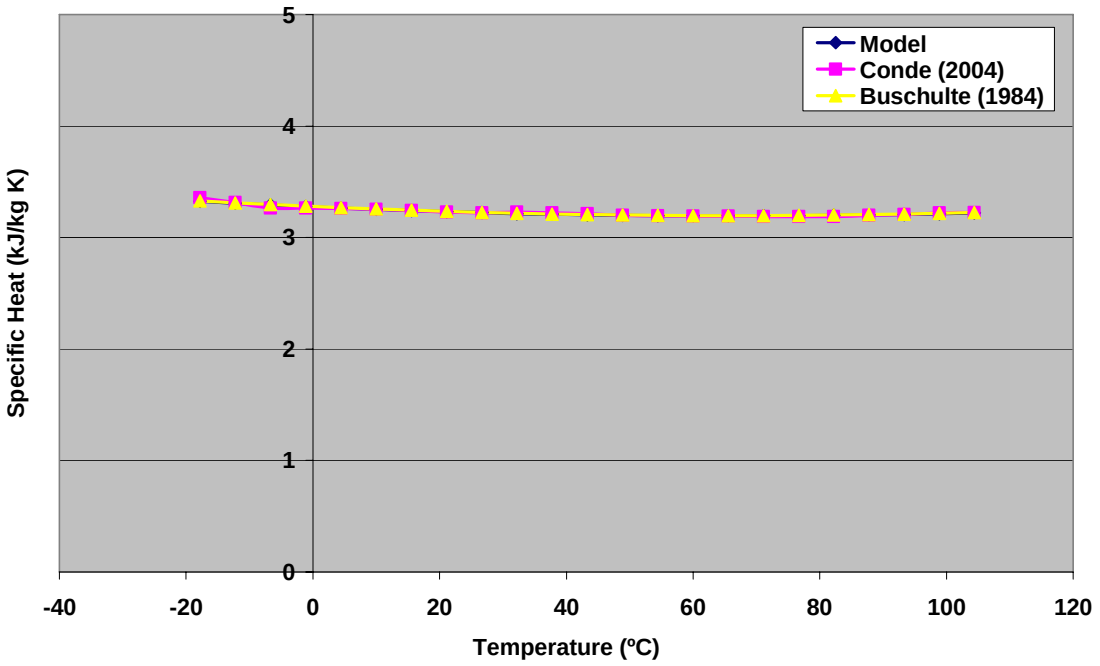

Figure 165: Specific Heat of lithium chloride water solution for different temperatures at 20 % salt concentration

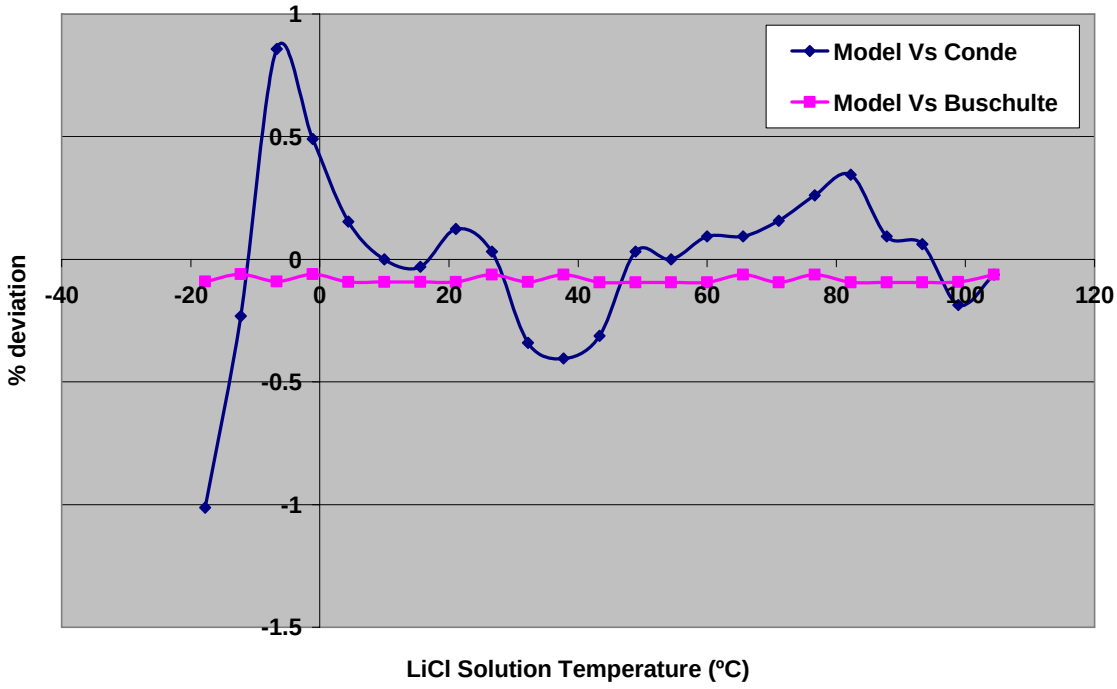

Figure 166: % Deviation in specific heat of lithium chloride water solution at 20 % salt concentration

Figure 167 shows the specific heat of lithium chloride water solution at 25 % salt concentration while the percentage deviation is plotted in Figure 168 for the 25 % concentration. The deviation in this case was found to be within ± 1.2 %.

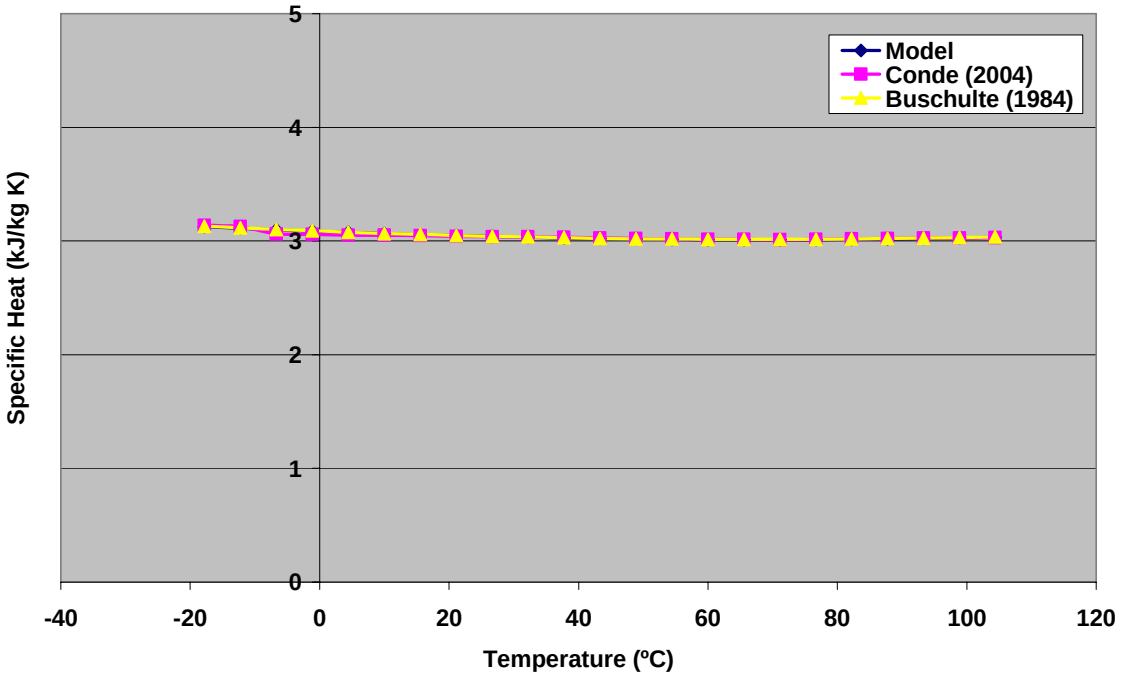

Figure 167: Specific Heat of lithium chloride water solution for different temperatures at 25 % salt concentration

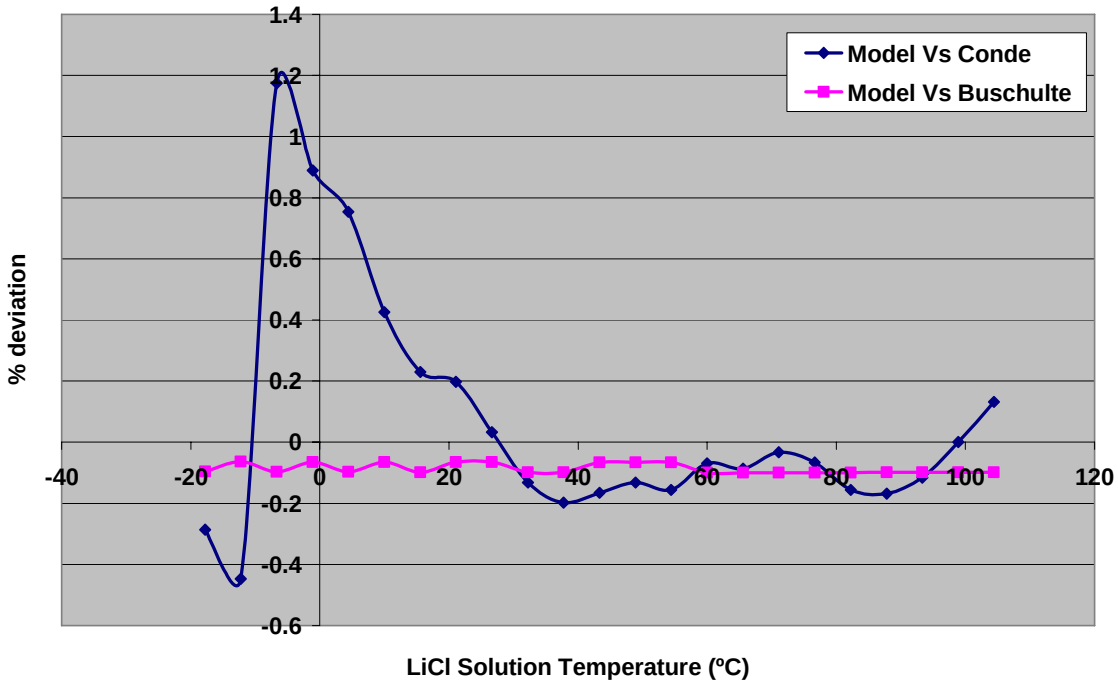

Figure 168: % Deviation in specific heat of lithium chloride water solution at 25 % salt concentration

The comparison of specific heat of the lithium chloride water solution between the model and literature for salt concentration of 30 % is shown in Figure 169 and the percentage deviation in this case was less than ± 0.5 % which is plotted in Figure 170.

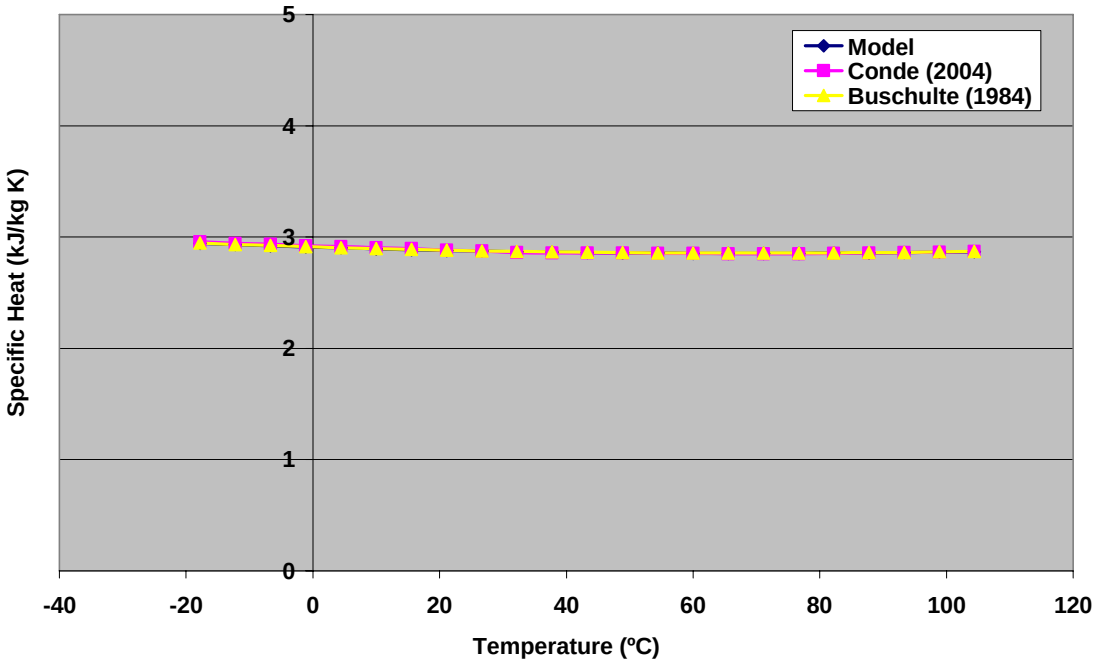

Figure 169: Specific Heat of lithium chloride water solution for different temperatures at 30 % salt concentration

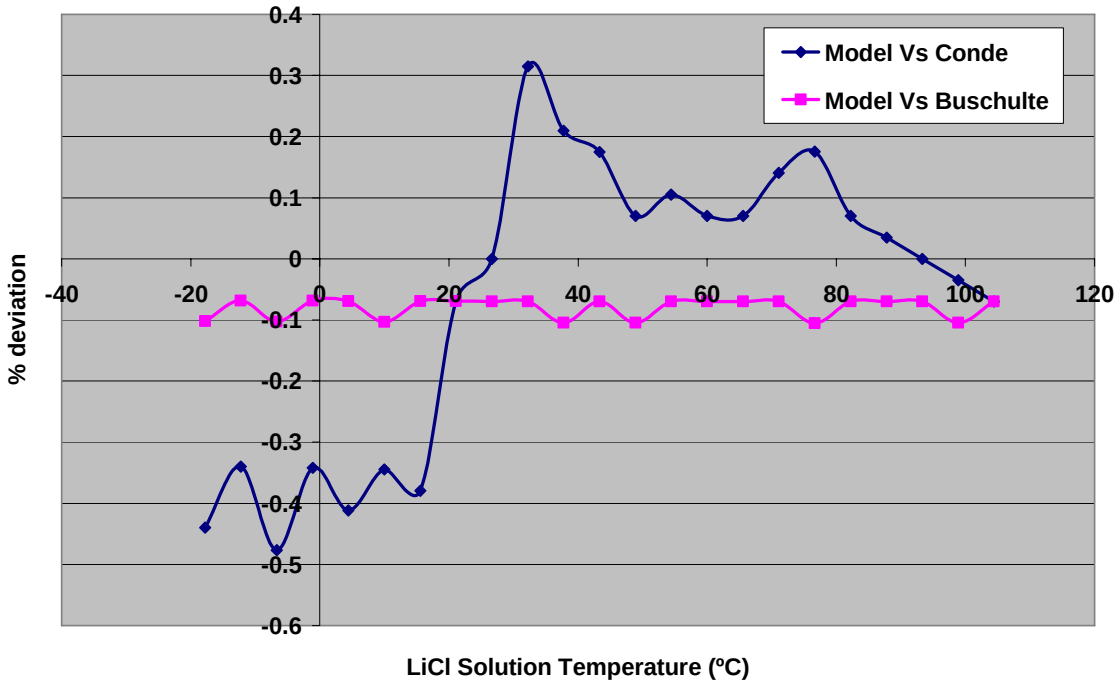

Figure 170: % Deviation in specific heat of lithium chloride water solution at 30 % salt concentration

Figure 171 and Figure 172 show the plots for specific heat of lithium chloride water solution and the percentage deviation at 35 % salt concentration respectively. It is seen from Figure 172 that the deviation was within ± 0.3 %.

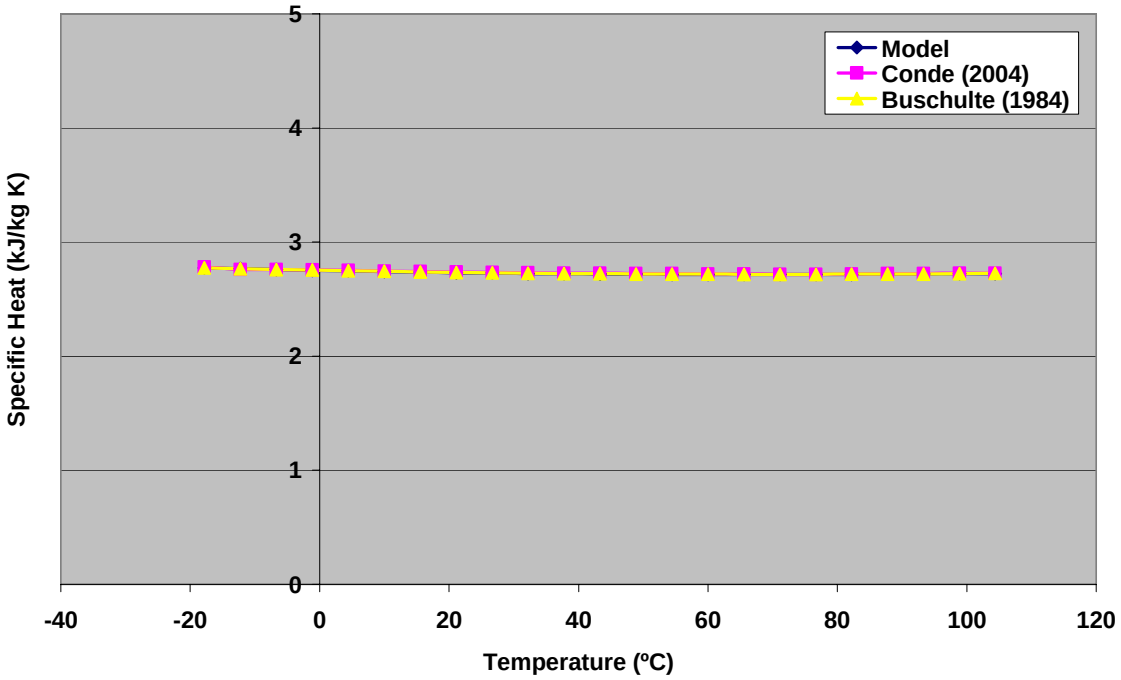

Figure 171: Specific Heat of lithium chloride water solution for different temperatures at 35 % salt concentration

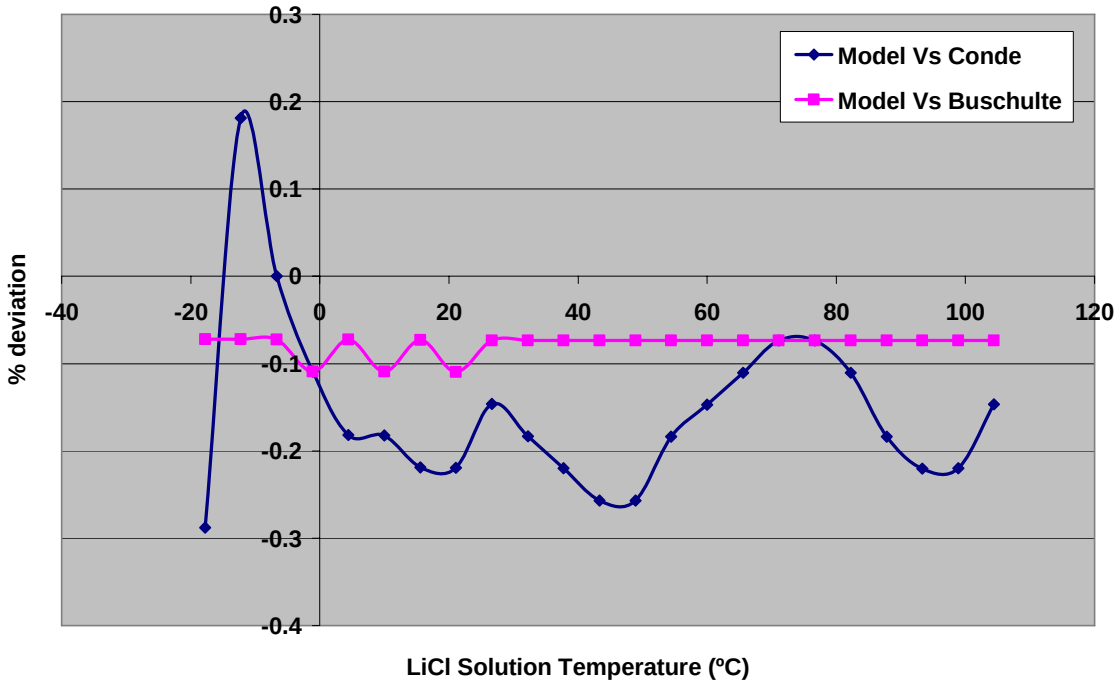

Figure 172: % Deviation in specific heat of lithium chloride water solution at 35 % salt concentration

Figure 173 plots the specific heat of lithium chloride water solution at 40 % salt concentration while the percentage deviation is shown in Figure 174. The deviation at 40 % salt concentration was found to be within ± 0.3 %.

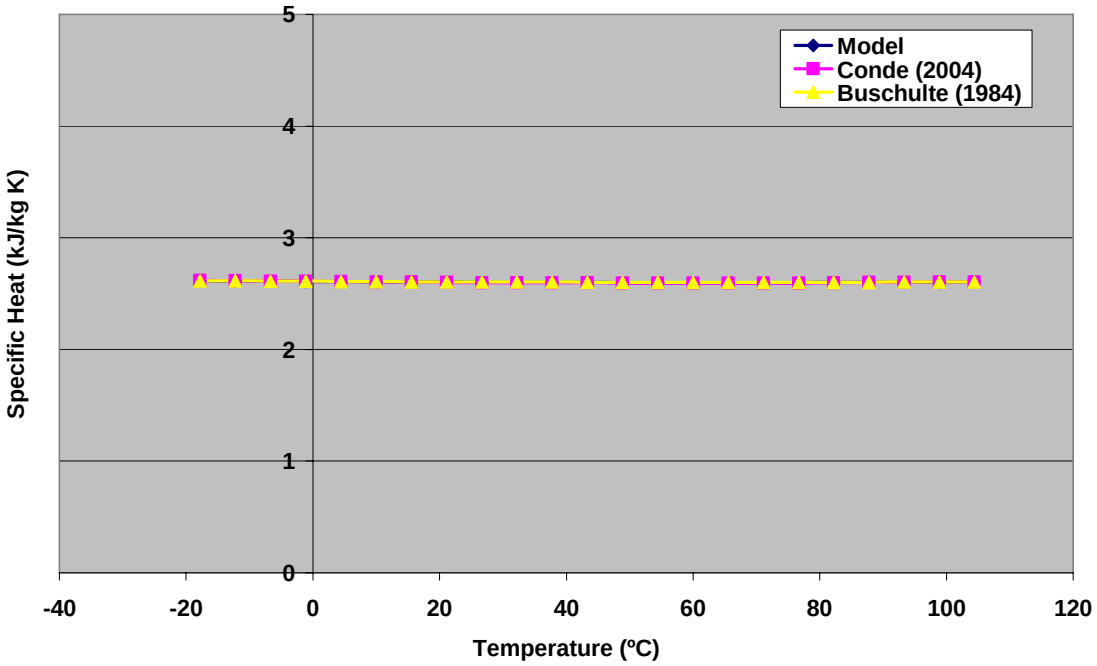

Figure 173: Specific Heat of lithium chloride water solution for different temperatures at 40 % salt concentration

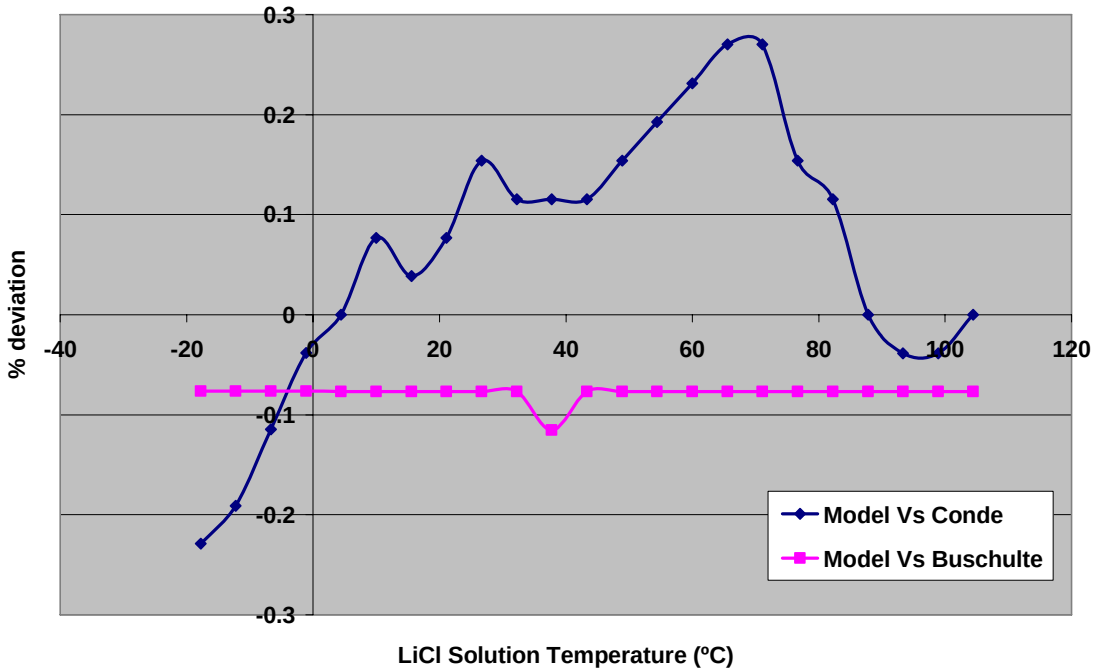

Figure 174: % Deviation in specific heat of lithium chloride water solution at 40 % salt concentration

The plot of specific heat of lithium chloride water solution at 45 % salt concentration is shown in Figure 175. The percentage deviation in this case was less than ± 0.3 % and is plotted in Figure 176.

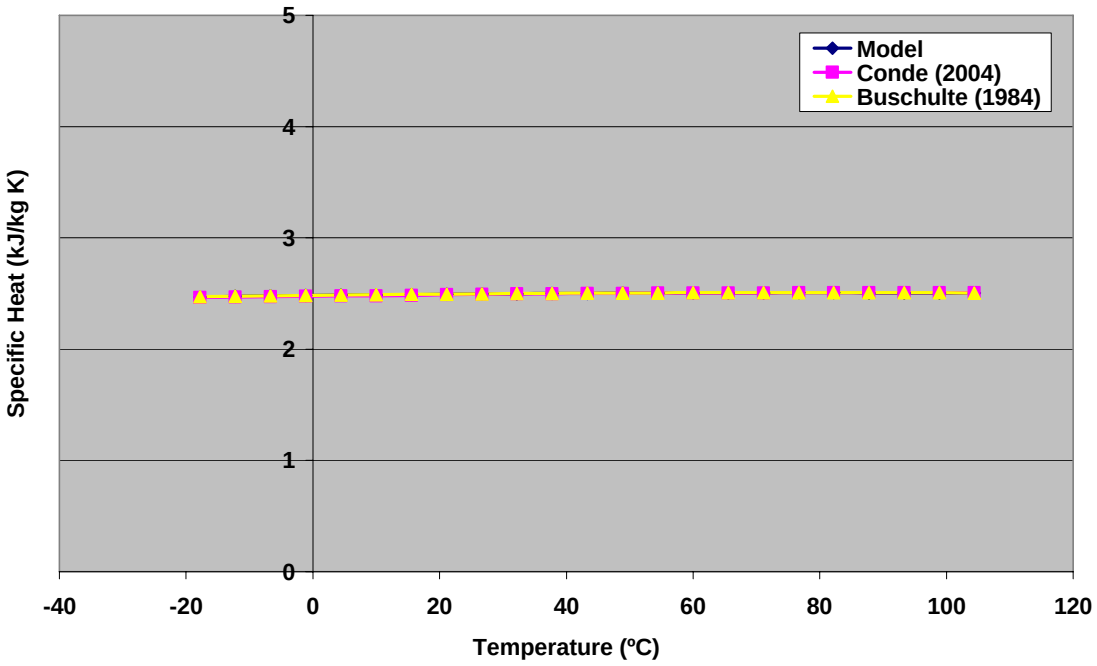

Figure 175: Specific Heat of lithium chloride water solution for different temperatures at 45 % salt concentration

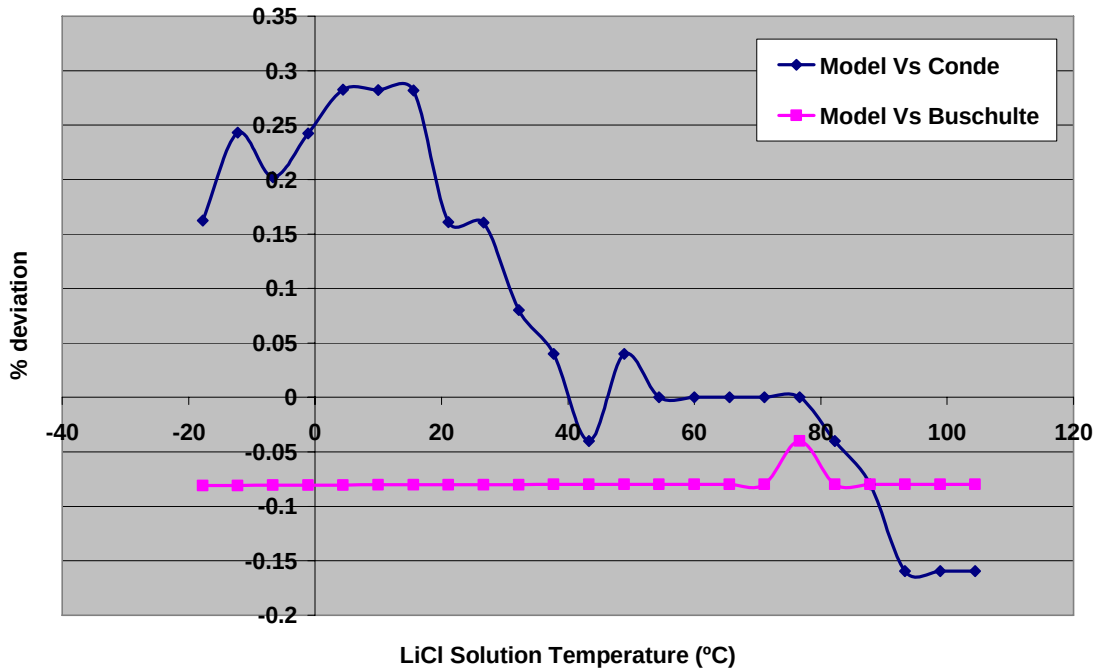

Figure 176: % Deviation in specific heat of lithium chloride water solution at 45 % salt concentration

The average percentage deviation between the VB.Net specific heat (C_p) property function and the ones available in literature was found to be less than ± 0.4 % over the entire range of concentration as well as solution temperatures. Figure 177 shows the plot of average percentage deviation over a range of LiCl concentrations for different values of solution temperatures while Figure 178 gives the average percentage deviation over the range of solution temperatures for different LiCl concentration levels.

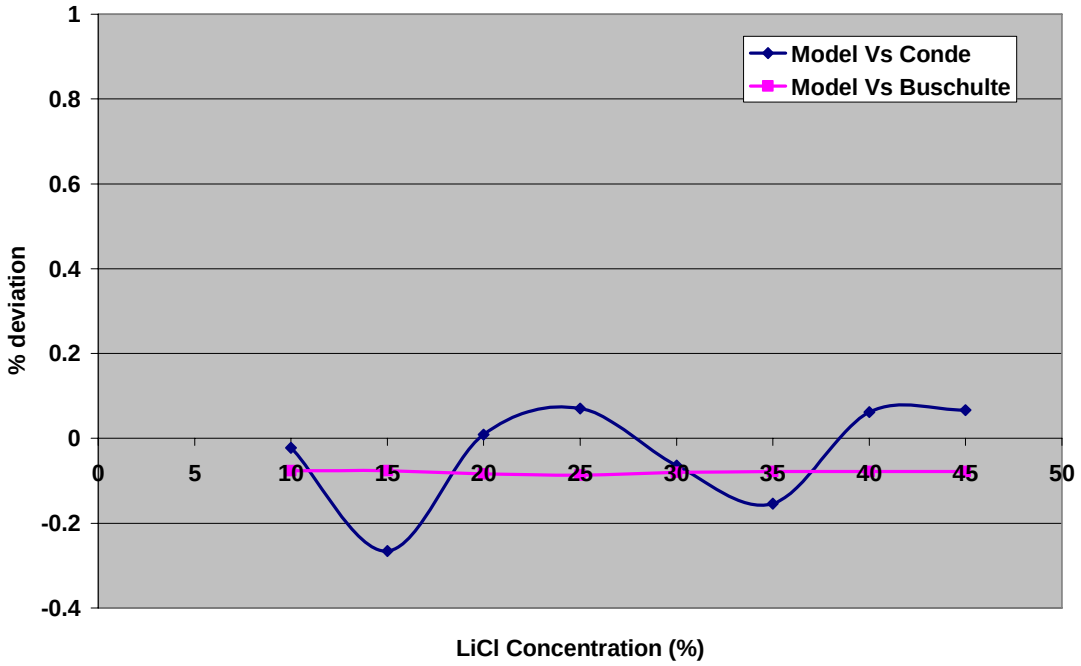

Figure 177: Average % deviation in Cp function over range of LiCl

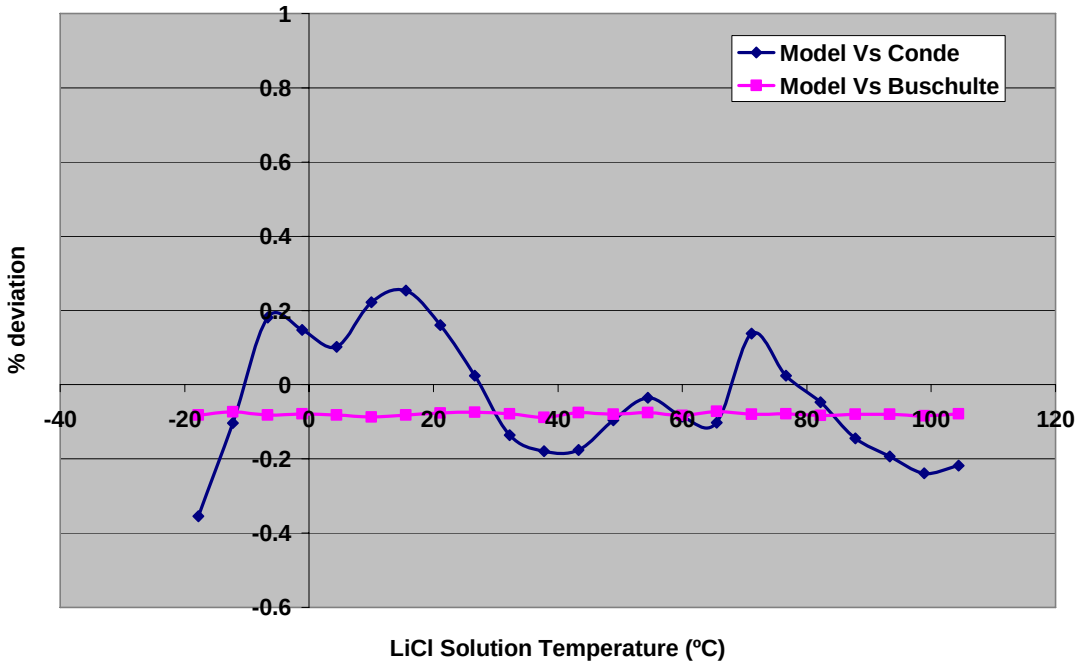

Figure 178: Average % deviation in Cp function over range of LiCl

The specific heat at constant pressure of lithium chloride solution in VB.Net was also compared with the specific heat data available in Gmelins Handbook of Inorganic Chemistry (Lithium, 1960). Figure 179 shows the comparison of specific heat of lithium chloride solution for different concentrations at a solution temperature of 20 ºC between Gmelin and VB.Net while Figure 180 shows the plots of specific heat at a solution temperature of 25 ºC. It is seen from the Figure 179 and Figure 180 that the VB.Net function matches closely with the specific heat data from Gmelins Handbook.

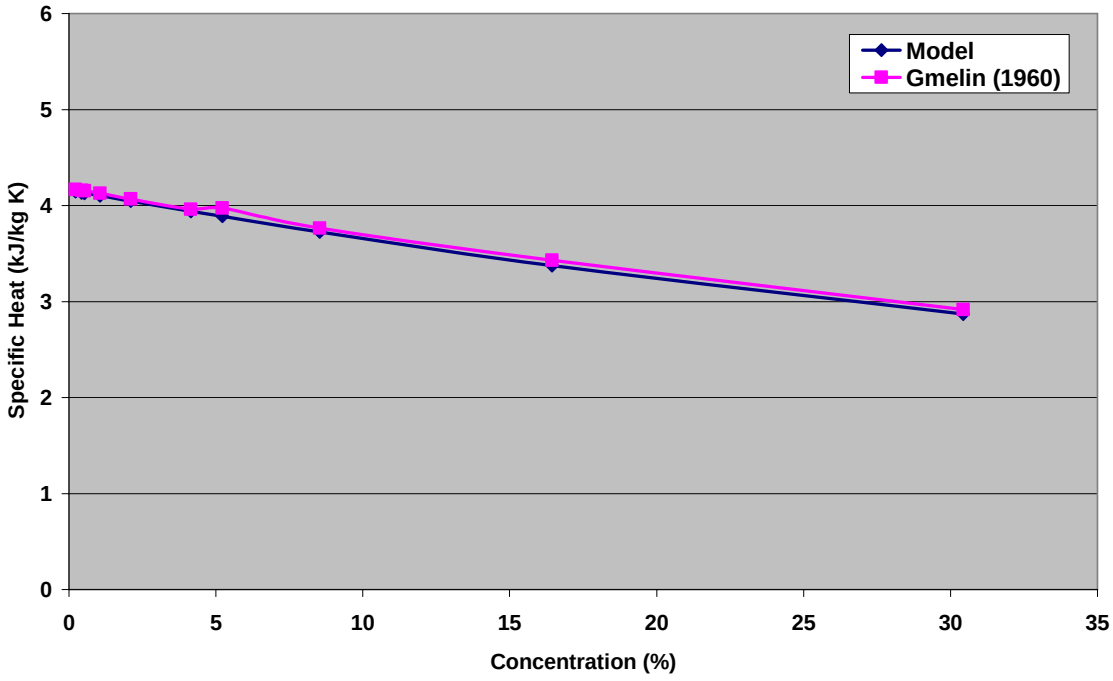

Figure 179: Comparison of specific heat of lithium chloride water solution at 20 ºC between Model and Gmelins Handbook

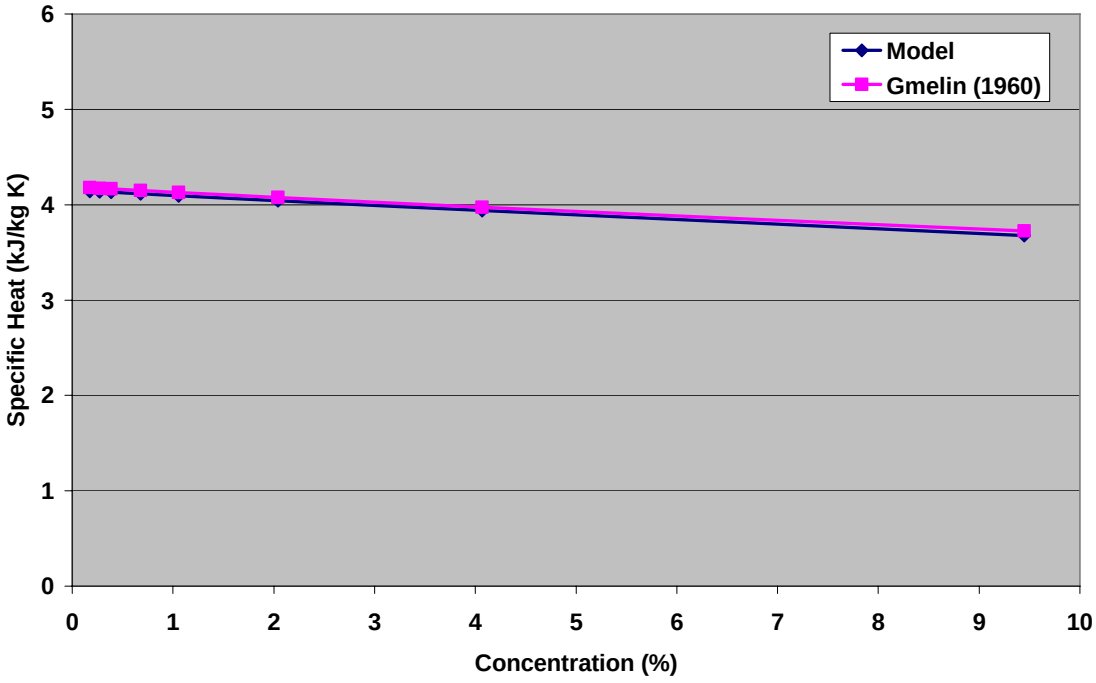

Figure 180: Comparison of specific heat of lithium chloride water solution at 25 ºC between Model and Gmelins Handbook

The percentage deviation between the VB.Net specific heat (C_p) function and the Gmelins Handbook at 20ºC and 25ºC were plotted and is shown in Figure 181 and Figure 182 respectively. The percentage deviation was within – 2.5 % in the case of C_p at 20ºC while it was within – 1.4 % for C_p at 25ºC.

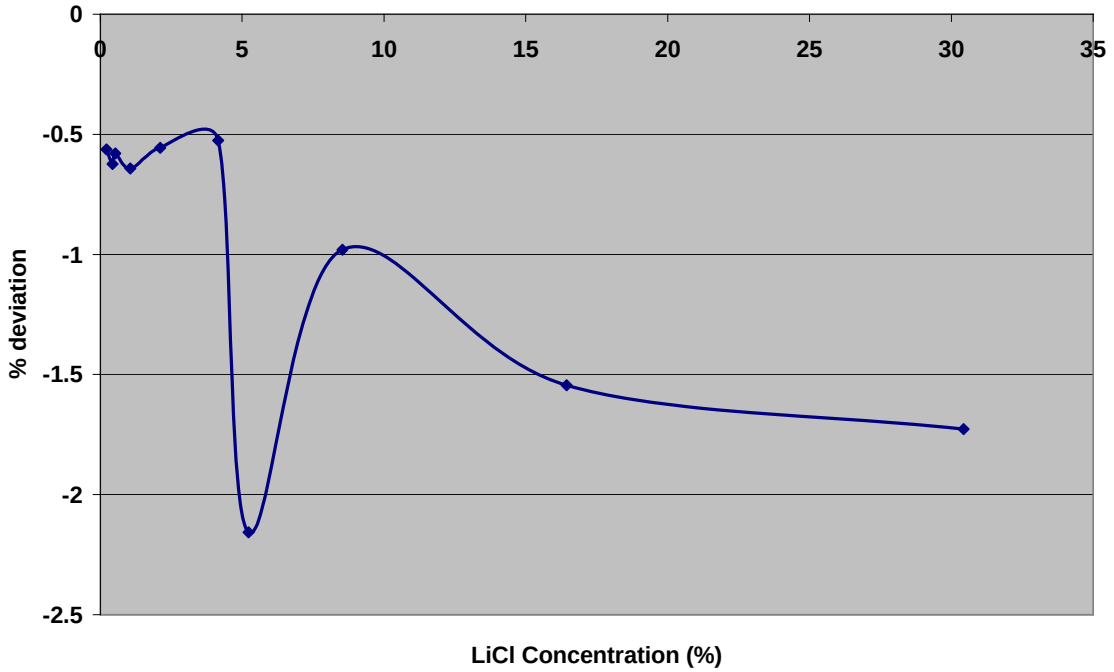

Figure 181: % Deviation between Model and Gmelins Handbook for specific heat at 20ºC

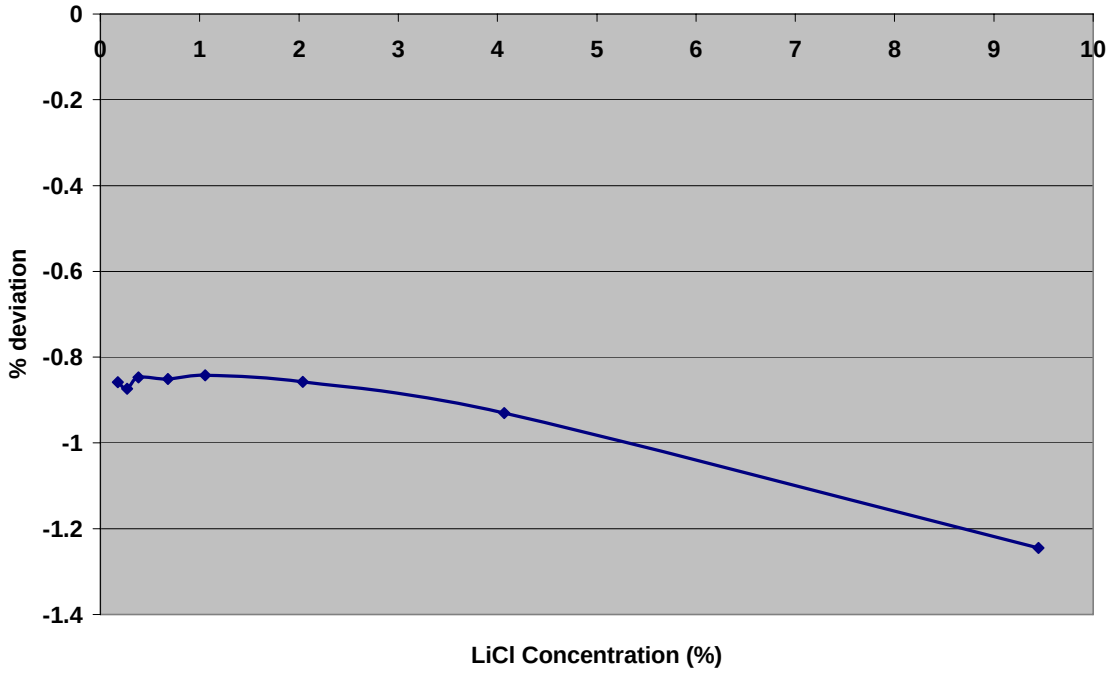

Figure 182: % Deviation between Model and Gmelins Handbook for specific heat at 25ºC

Figure 183 shows the plot of the enthalpy of lithium chloride water solution over a range of solution temperatures for salt concentration of 20 %. The enthalpy of solution function in Visual Basic.Net is a Chebyshev X, Y bivariate polynomial of order 10. The deviation in the enthalpy function is plotted in Figure 184. It can be seen from Figure 184 that the deviation was within ± 6 % for enthalpy at 20 % concentration.

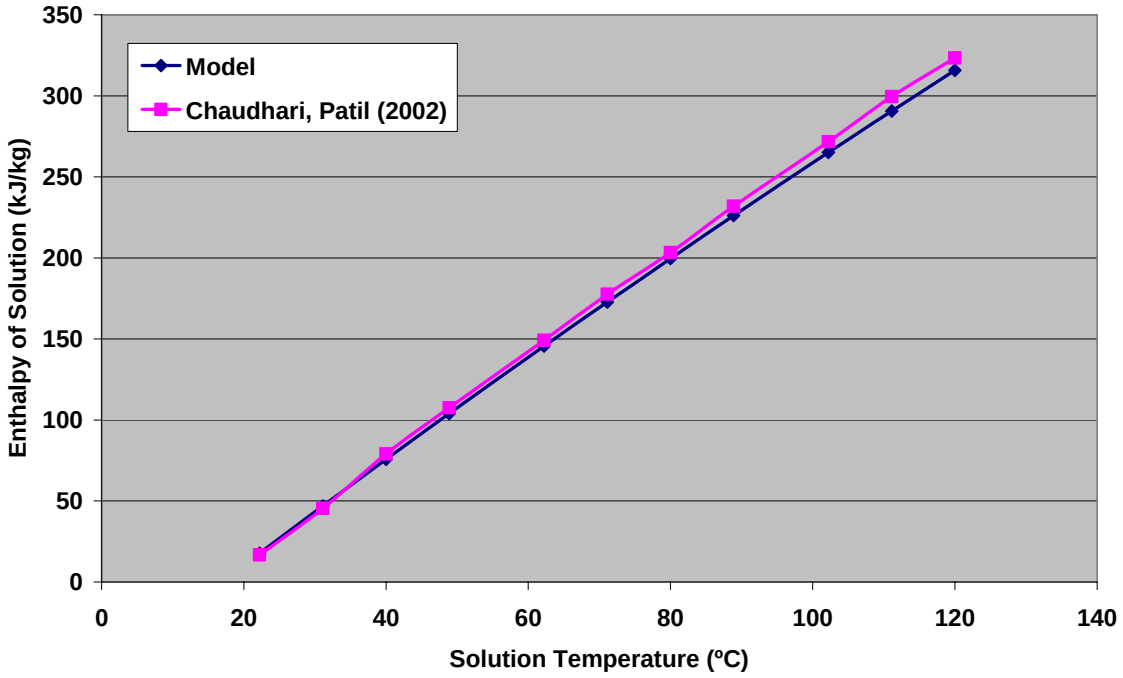

Figure 183: Enthalpy of lithium chloride water solution for different temperatures at 20 % salt concentration

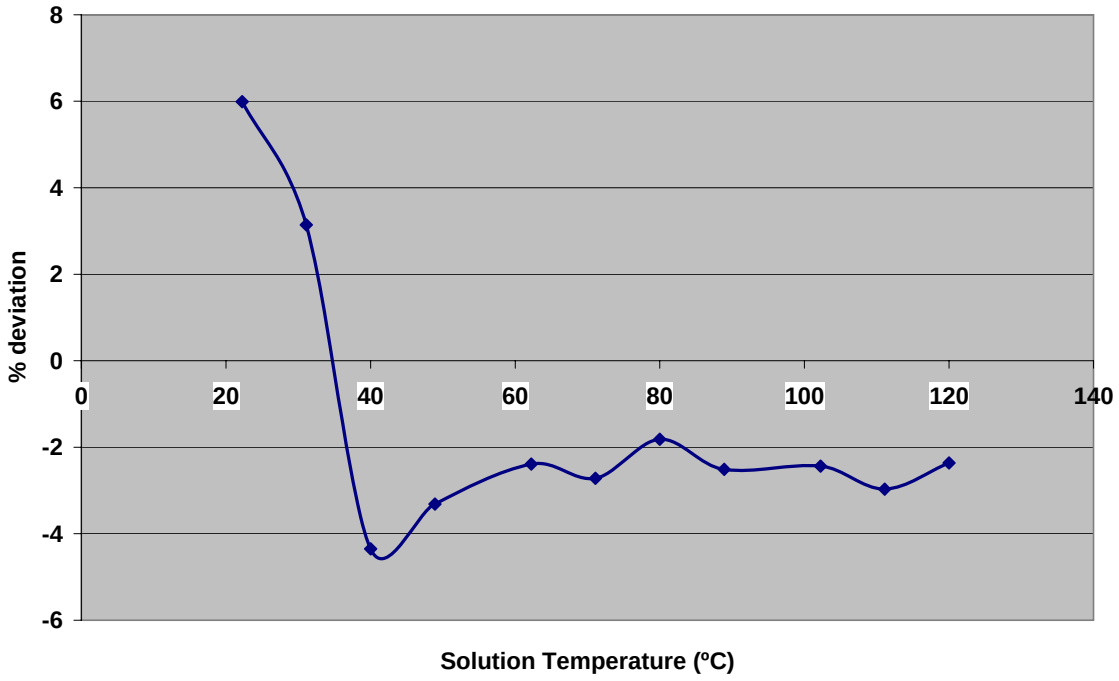

Figure 184: % Deviation in enthalpy of lithium chloride water solution at 20 % salt concentration

The plot of enthalpy for 25 % salt concentration is shown in Figure 185 while the percentage deviation is plotted in Figure 186. The deviation in enthalpy of lithium chloride water solution at 25 % concentration was less than ± 6 % as can be seen from Figure 186.

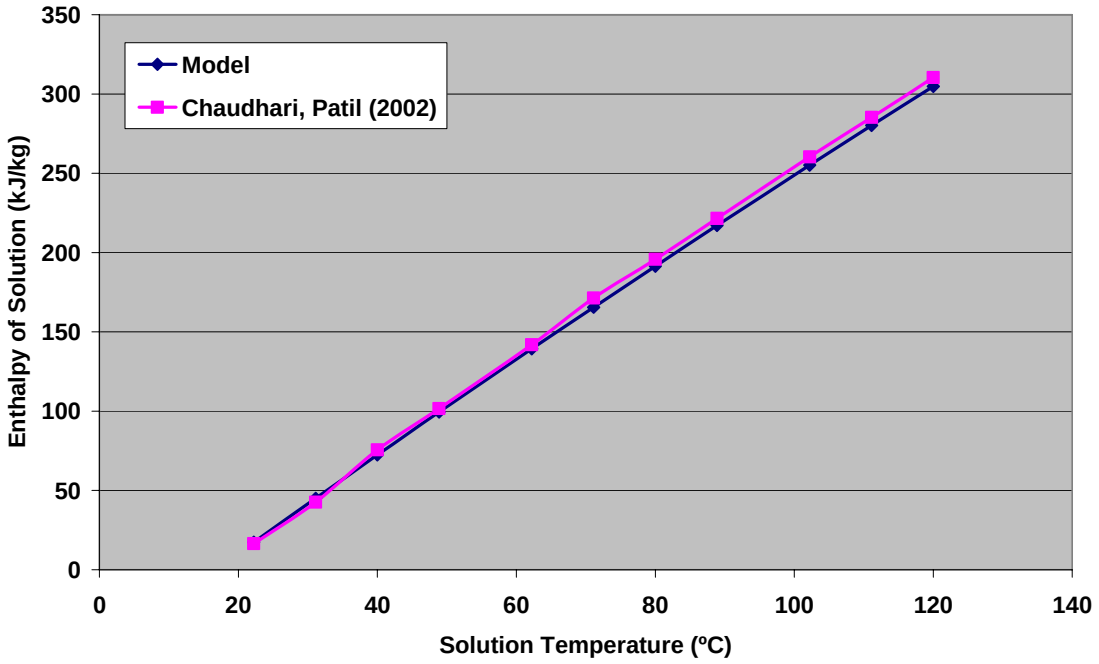

Figure 185: Enthalpy of lithium chloride water solution for different temperatures at 25 % salt concentration

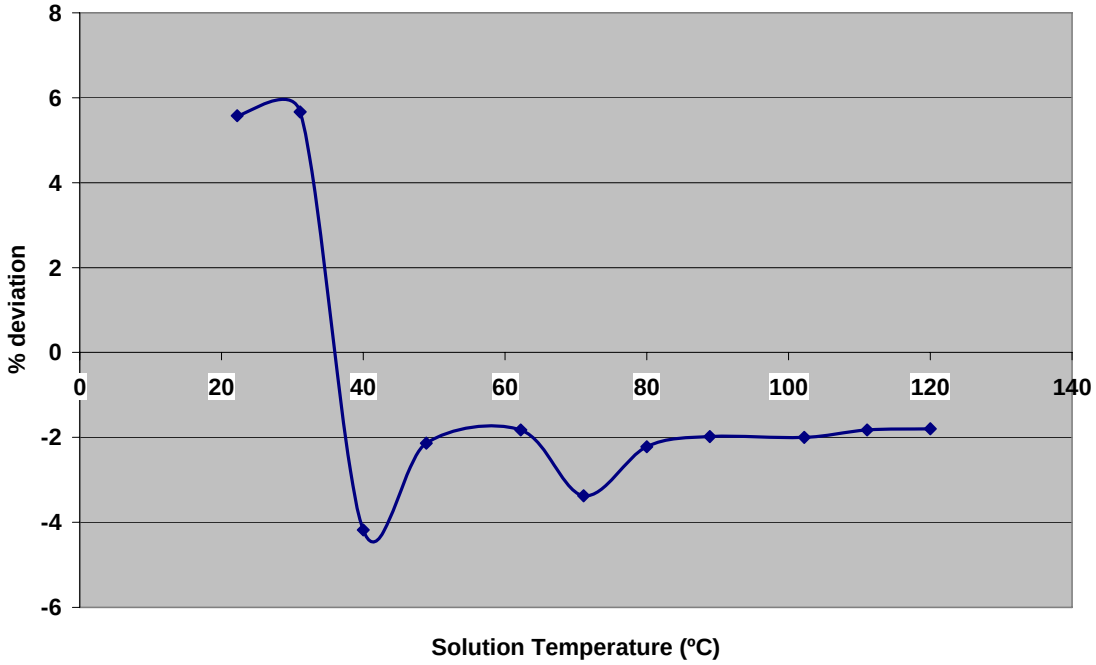

Figure 186: % Deviation in enthalpy of lithium chloride water solution at 25 % salt concentration

Figure 187 and Figure 188 show the plots of enthalpy of lithium chloride water solution and the percentage deviation in enthalpy for salt concentration of 30 %. It is observed from Figure 188 that the deviation was less than ± 4 %.

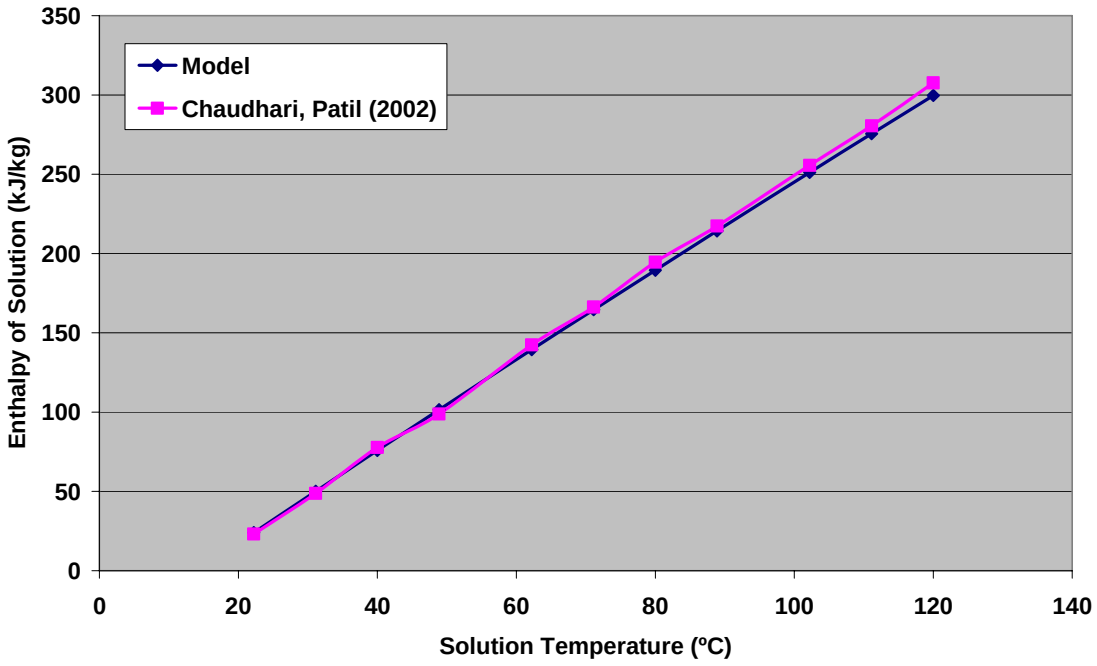

Figure 187: Enthalpy of lithium chloride water solution for different temperatures at 30 % salt concentration

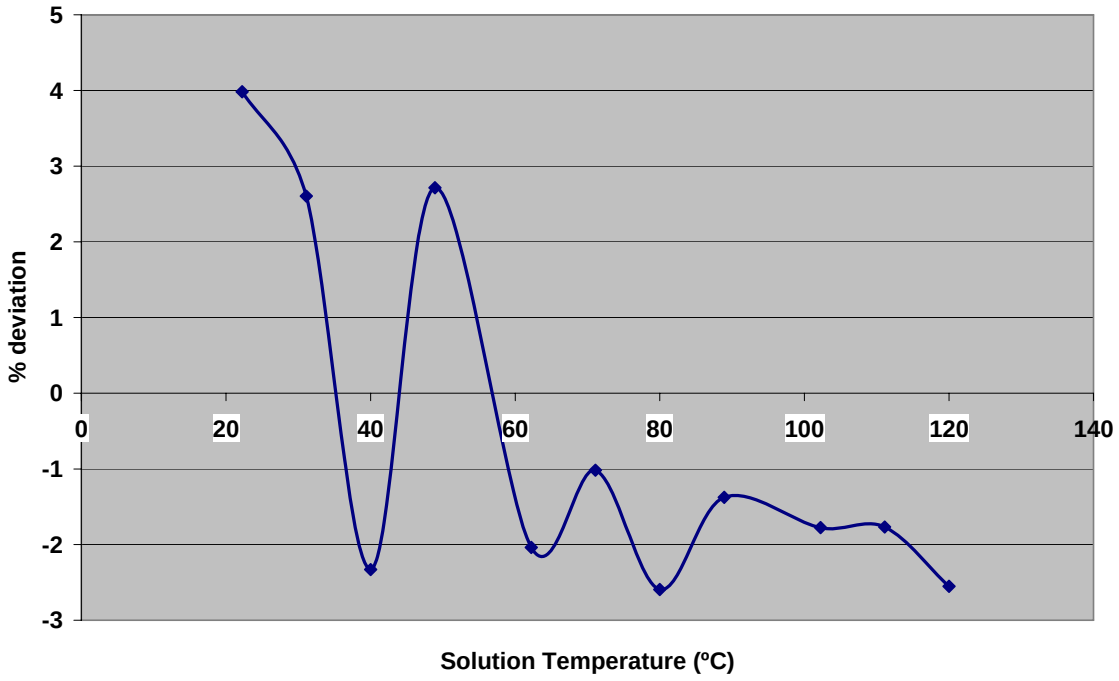

Figure 188: % Deviation in enthalpy of lithium chloride water solution at 30 % salt concentration

Figure 189 shows the comparison of enthalpy of lithium chloride water solution between model and literature at 35 % salt concentration while Figure 190 shows the deviation in enthalpy between them. It is seen from Figure 190 that the deviation was within ± 4 %.

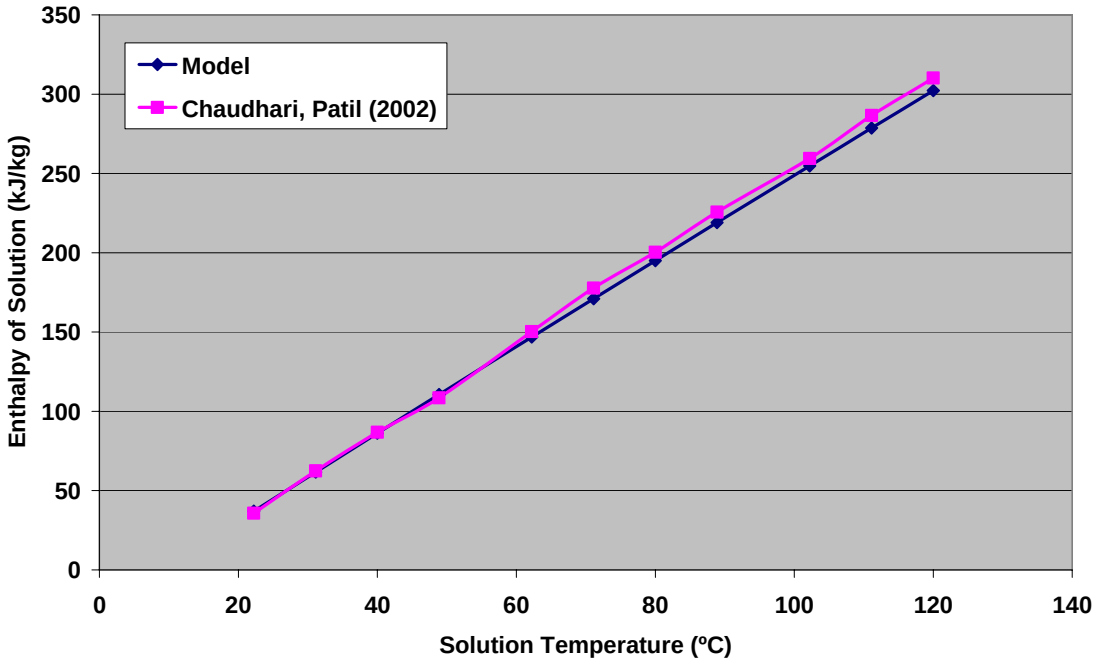

Figure 189: Enthalpy of lithium chloride water solution for different temperatures at 35 % salt concentration

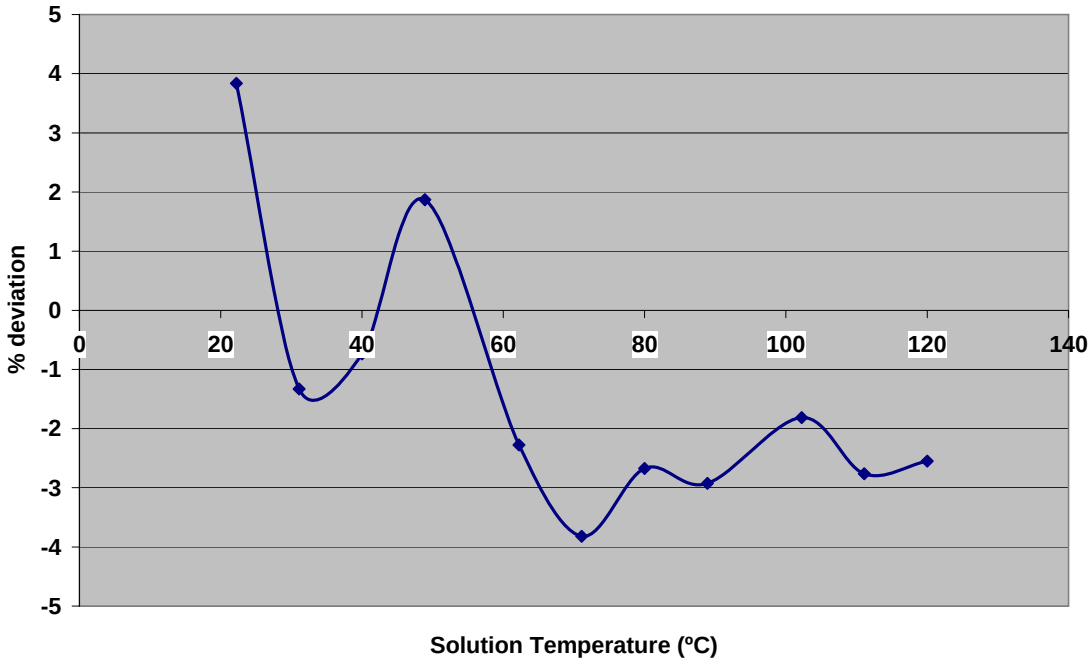

Figure 190: % Deviation in enthalpy of lithium chloride water solution at 35 % salt concentration

Figure 191 shows the plot of enthalpy of lithium chloride water solution at 40 % salt concentration and it can be seen that the enthalpy function from the model agrees closely with the one available in literature. The deviation in this case was found to be within – 5 % and is plotted in Figure 192.

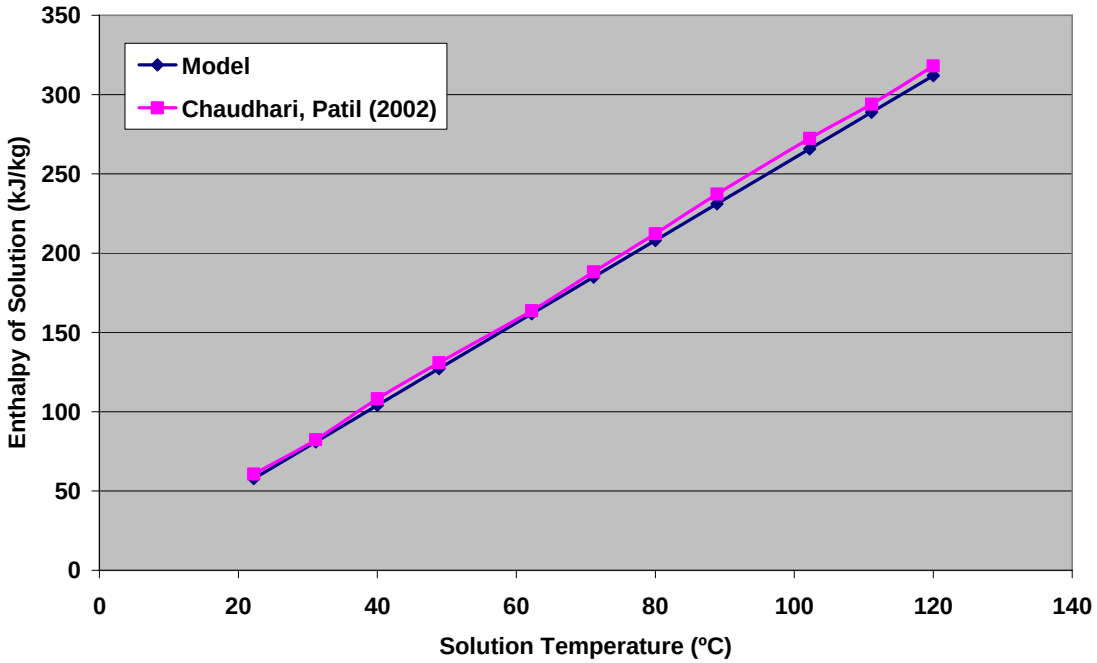

Figure 191: Enthalpy of lithium chloride water solution for different temperatures at 40 % salt concentration

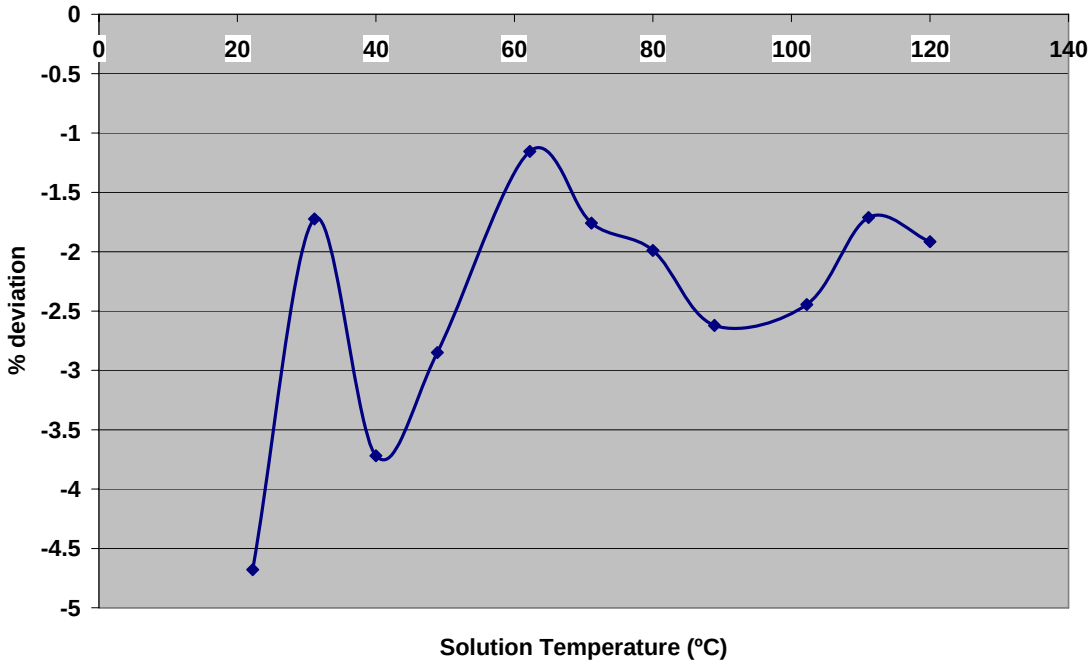

Figure 192: % Deviation in enthalpy of lithium chloride water solution at 40 % salt concentration

The plot of enthalpy of lithium chloride water solution at 45 % salt concentration is shown in Figure 193 while the percentage deviation for 45 % salt concentration is plotted in Figure 194. The deviation in this case was within – 3.5 % as can be observed from Figure 194.

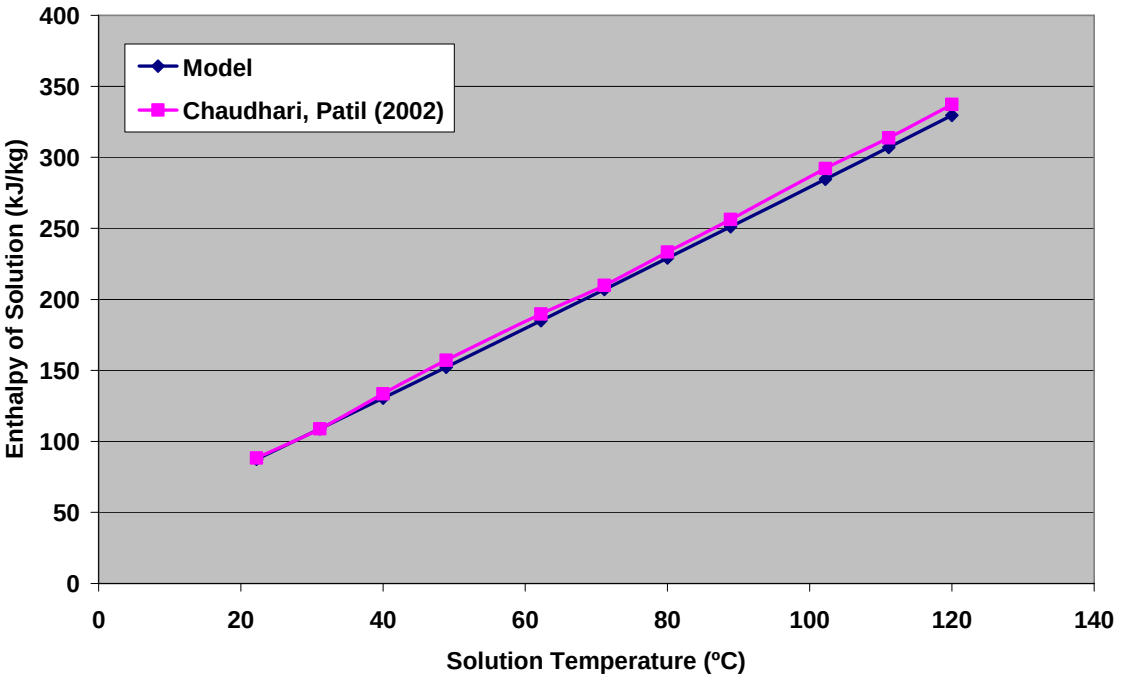

Figure 193: Enthalpy of lithium chloride water solution for different temperatures at 45 % salt concentration

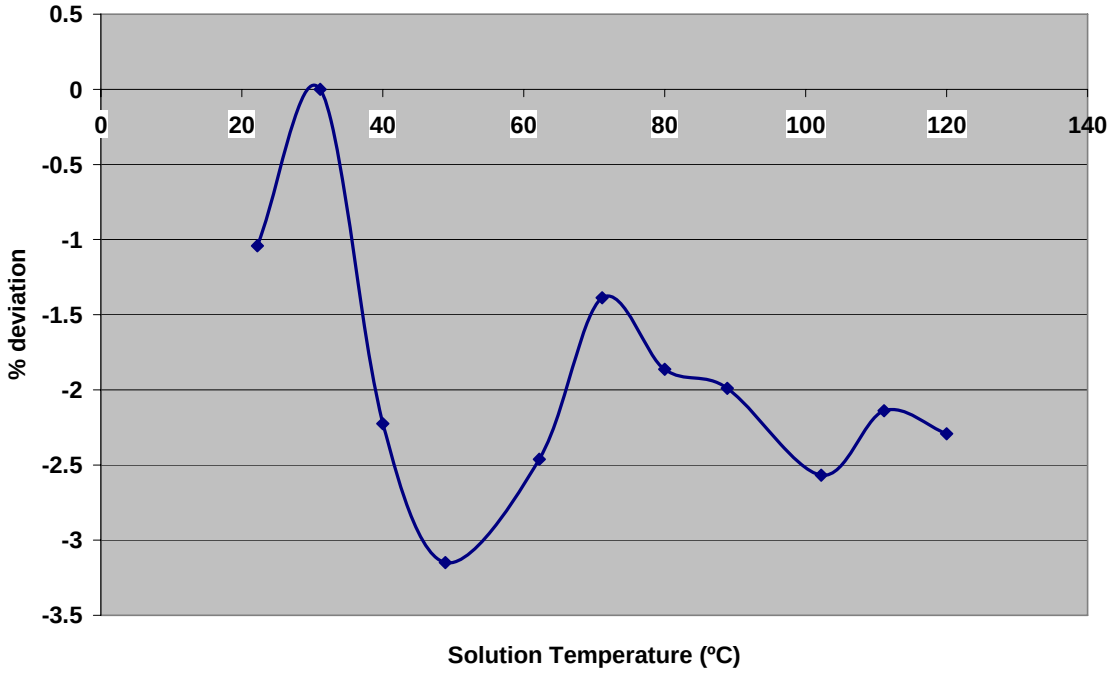

Figure 194: % Deviation in enthalpy of lithium chloride water solution at 45 % salt concentration

Figure 195 shows the plot of enthalpy of lithium chloride water solution at salt concentration of 50 %. The deviation in enthalpy for the 50 % salt concentration was found to be within ± 3.5 % as can be seen in Figure 196.

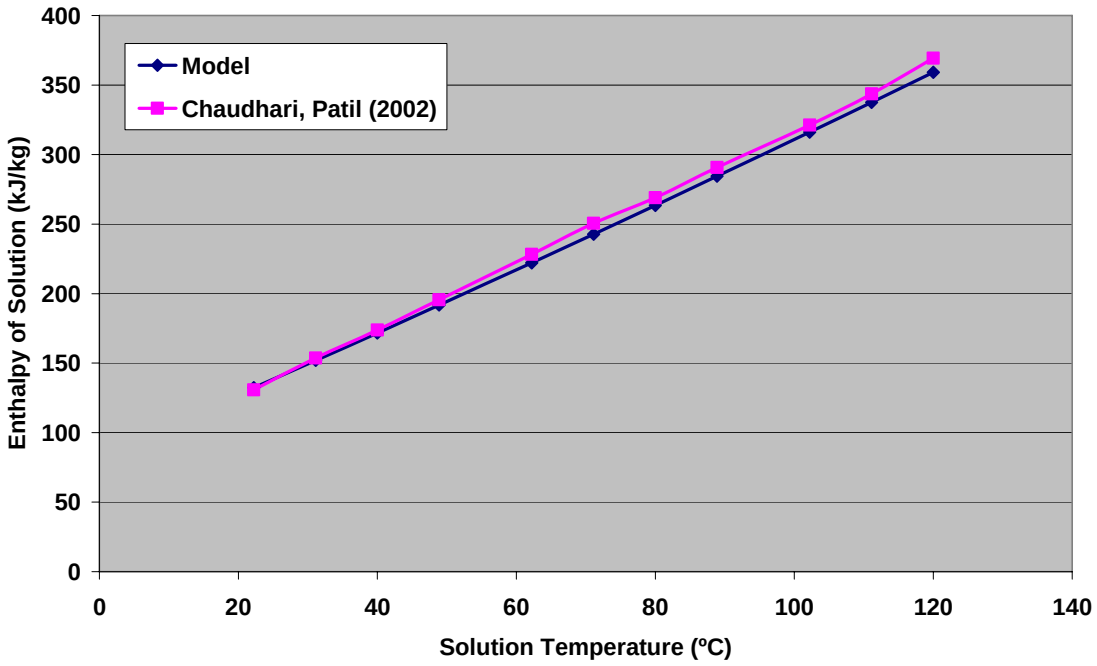

Figure 195: Enthalpy of lithium chloride water solution for different temperatures at 50 % salt concentration

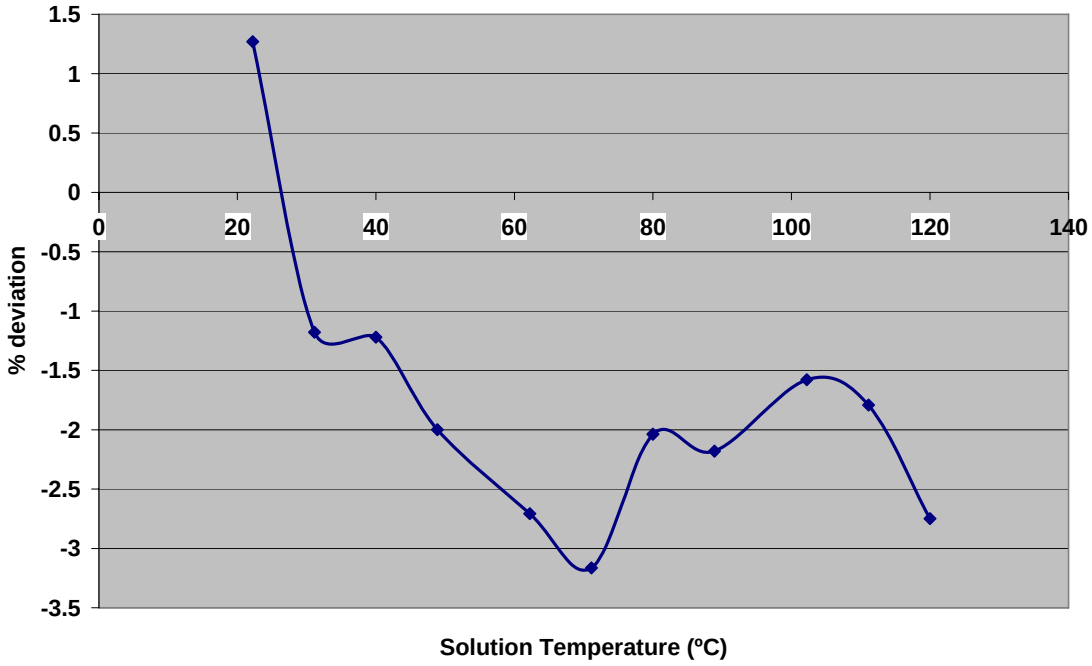

Figure 196: % Deviation in enthalpy of lithium chloride water solution at 50 % salt concentration

It can be seen from the above plots that the enthalpy of solution function coded in VB.Net from the thermodynamic data supplied by the company matches very well with the enthalpy correlation available from the literature for all the concentration levels. The individual percentage deviations in the enthalpy function were plotted in the figures shown above. The average percentage deviation between the VB.Net enthalpy property function and the one available in literature (Chaudhari, Patil, 2002) was found to be within ± 3 % over the entire range of concentration as well as solution temperatures. Figure 197 shows the plot of average percentage deviation over a range of LiCl concentrations for different values of solution temperatures while Figure 198 gives the average percentage deviation over the range of solution temperatures for different LiCl concentration levels.

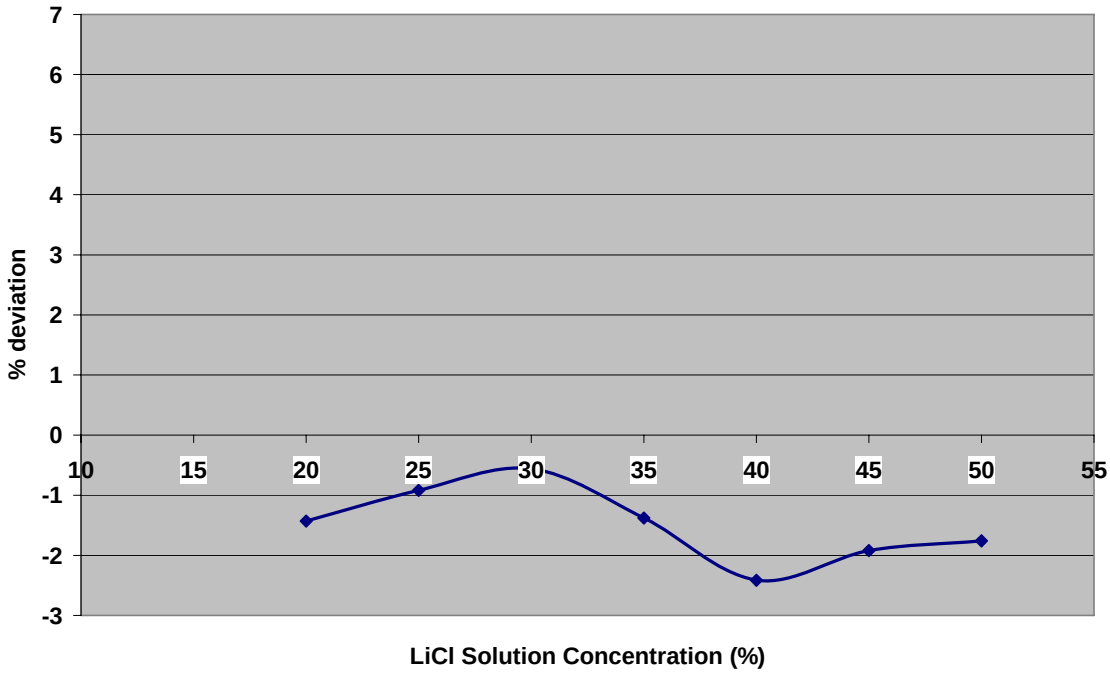

Figure 197: Average % deviation in enthalpy function over range of LiCl concentrations.

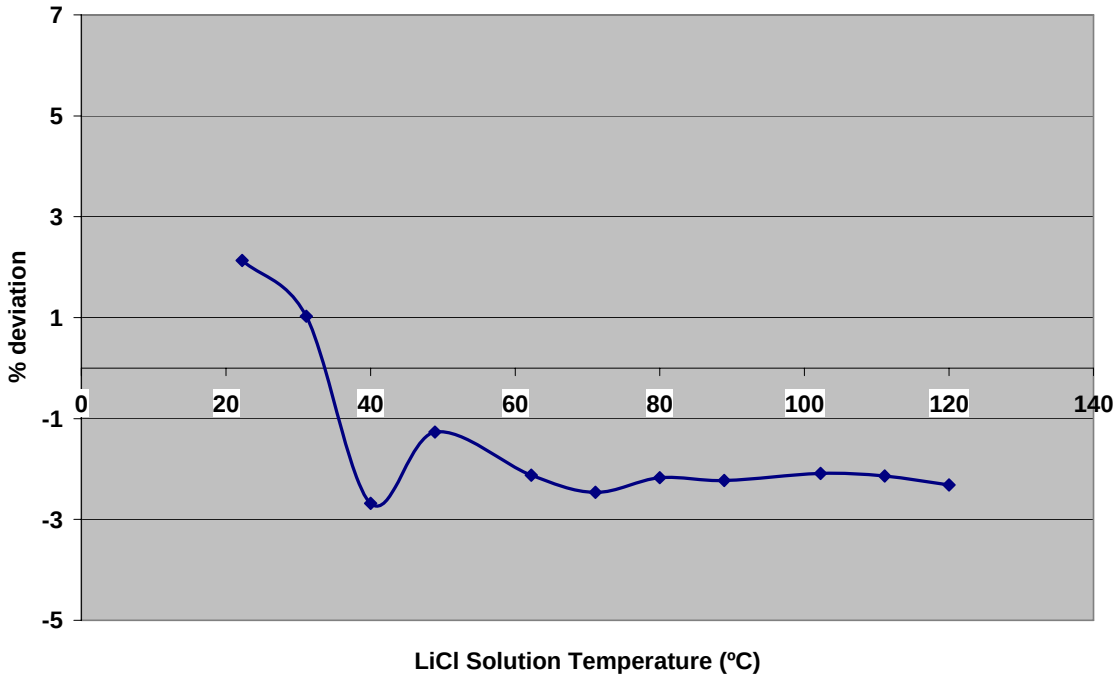

Figure 198: Average % deviation in enthalpy function over range of LiCl solution temperatures

6.8 Validation of Model with Experimental Results

In this section, the computational results obtained from the thermodynamic model are compared with the experimental data. Figure 199 shows the comparison between experiment and simulation of the process air supplied by the liquid desiccant unit to mixed air chamber of RTU 1. The experimental data was recorded in summer 2005 over a range of ambient air temperatures from 25 ºC to 32 ºC.

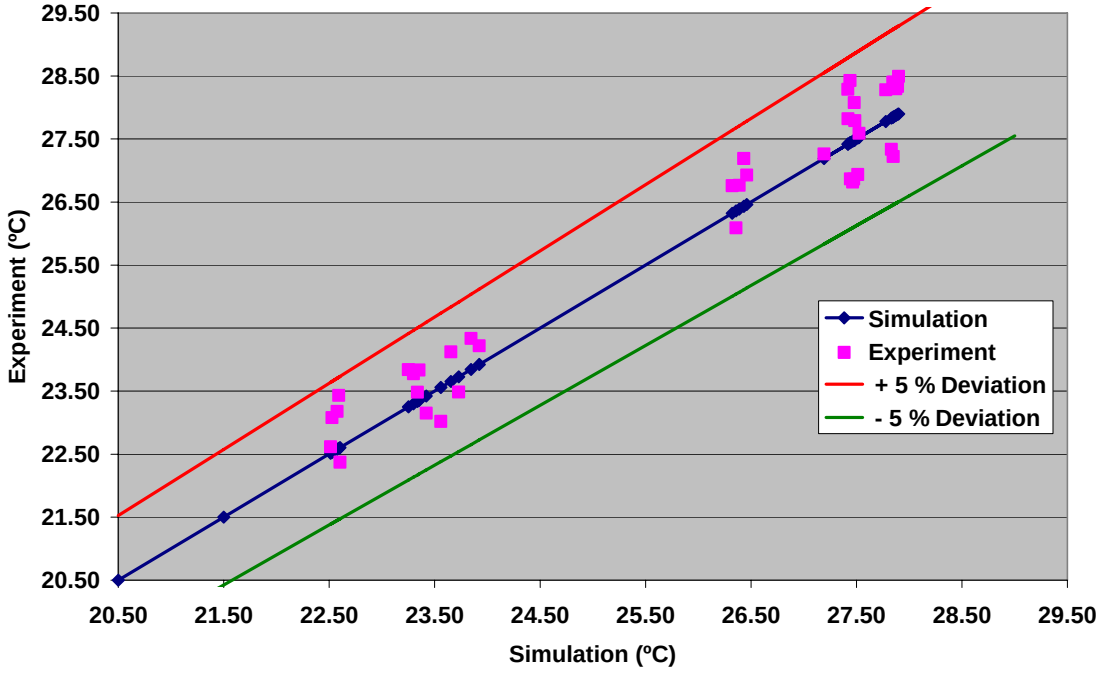

Figure 199: Comparison of Process Air Temperature between Experiment and Simulation

It is observed from Figure 199 that there is good agreement between the experimental and simulation results for process air temperature. The deviation between the computational and experimental result for process air temperature is found to be within ± 5 % or the difference between the experimental and predicted process air temperature was within ± 1 ºC.

The comparison between experimental data and the results from the simulation for process air humidity ratio is plotted in Figure 200.

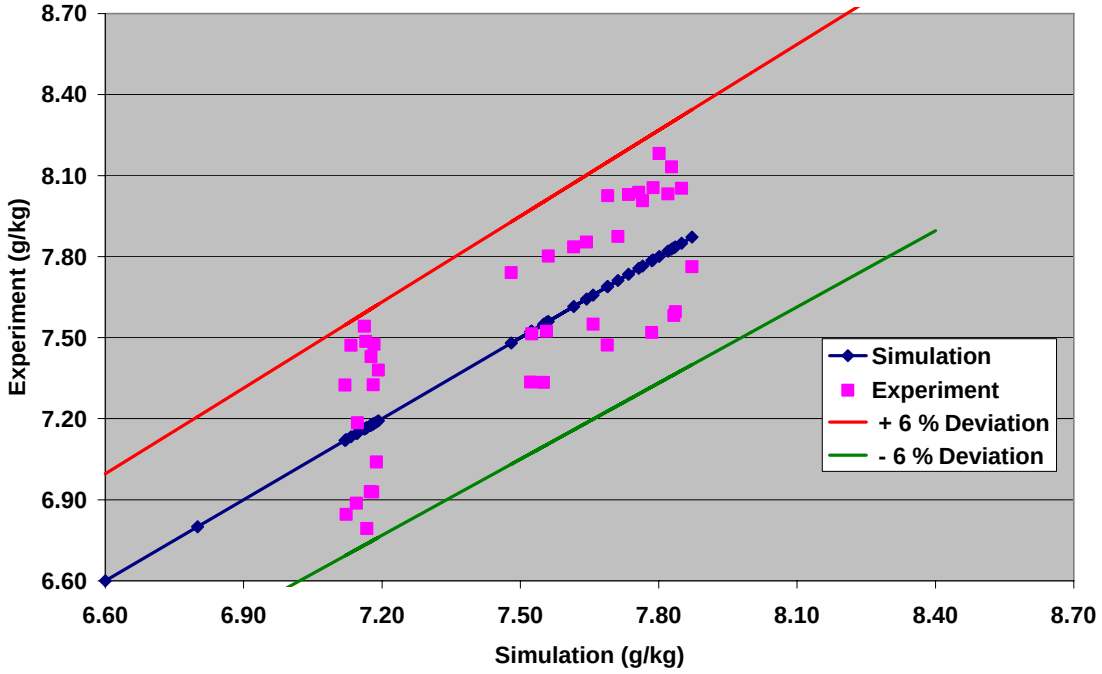

Figure 200: Comparison of Process Air Humidity Ratio between Experiment and Simulation

It is seen from Figure 200 that the process air humidity ratio found from experimental results falls within ± 6 % of the predictions from the simulation.

The heat recovery loop was also modeled and integrated along with the engine and liquid desiccant unit models. Figure 201 shows the comparison of the glycol temperature at the outlet of the exhaust gas heat exchanger between experimental result and that predicted by simulation. The heat recovery loop temperature graphs have more number of points than the process air temperature and humidity ratio since the engine generator was run both in winter and summer season while the liquid desiccant unit was run only in summer. The cooling tower for the liquid desiccant unit needs to be drained every winter and hence the LDU is run only in summer

season. The heat recovery loop temperatures were validated over a wide range of outdoor air temperature varying from -10 ºC to 36 ºC.

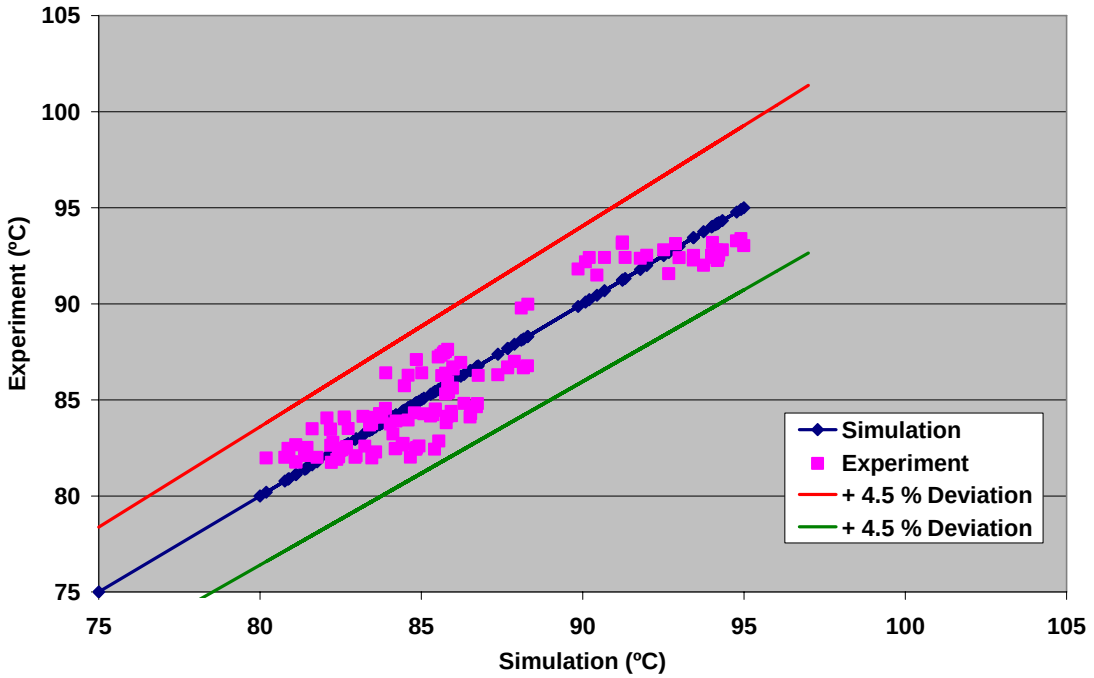

Figure 201: Comparison of Exhaust Gas HX Outlet Temperature between Experiment and Simulation

It is seen from Figure 201 that the simulation result for the exhaust gas heat exchanger outlet temperature matches pretty well with the experimental data. The deviation between the experimental and simulation result is within ± 4.5 %. The experimental and computational result for the glycol temperature at the outlet of the jacket water heat exchanger is shown in Figure 202.

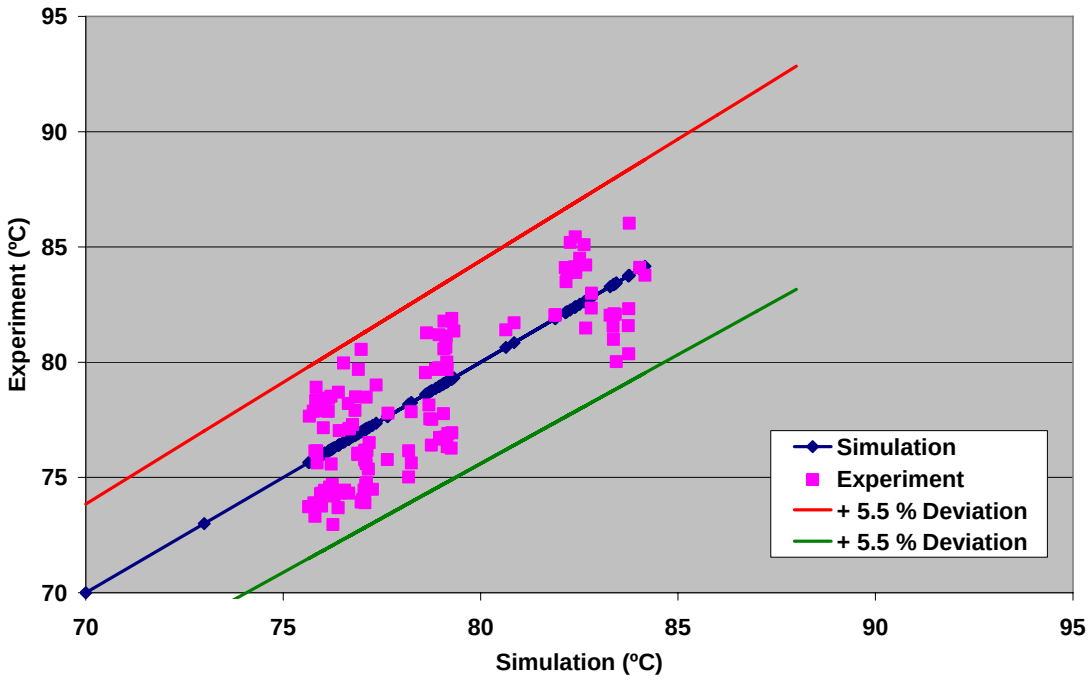

Figure 202: Comparison of Jacket Water HX Outlet Temperature between Experiment and Simulation

It is observed from Figure 202 that the percentage deviation between simulation and experimental results for the jacket water heat exchanger outlet temperature is within ± 5.5 %.

A comparison of the net electrical efficiency of the engine generator at base load of 75 kW, between the experimental and simulation results was also done over a range of ambient air enthalpies and is shown in Figure 203.

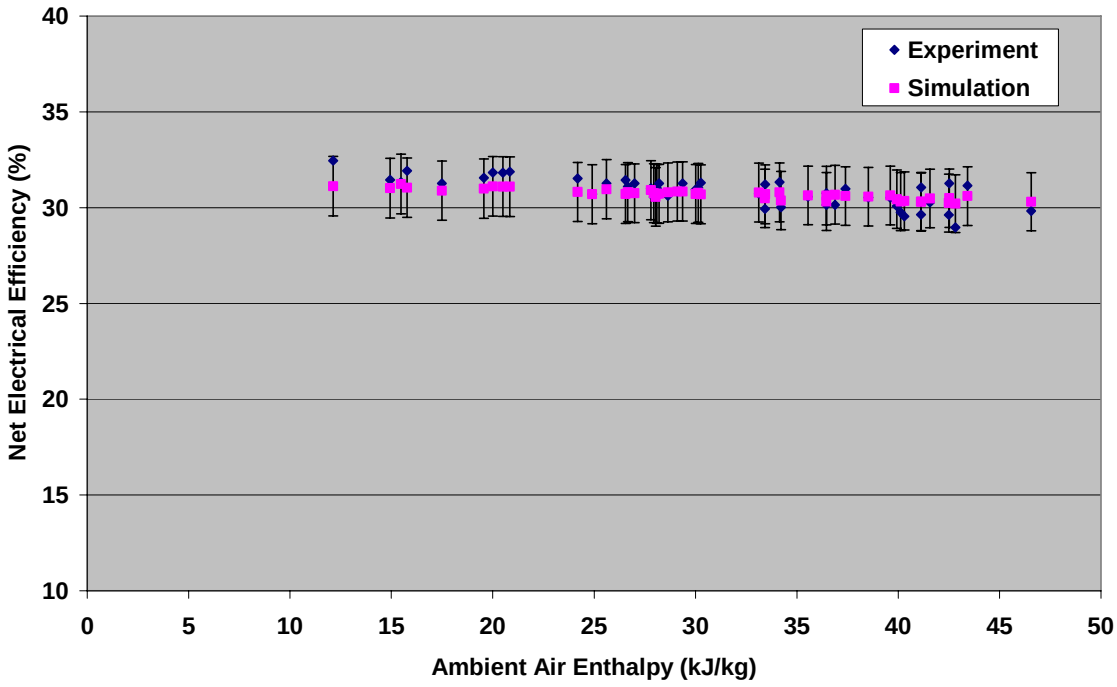

Figure 203: Comparison of Net Electrical Efficiency of Engine Generator at 75 kW between Experiment and Simulation

There is a good agreement between the simulation and experiment in this case and it is seen from Figure 203 that the net electrical efficiency of the engine at 75 kW predicted by the model is within ± 5 % of the experimental data.

Based on figures 198-202, it is seen that the simulation results reflect the overall experimental trend quite accurately even though the individual experimental points fall within ± 6% in some cases. The model accuracy obtained here is enough to predict the performance of the integrated CHP system under various conditions reasonably.

6.9 Integration of Liquid Desiccant with Roof Top Unit

The liquid desiccant dehumidifier can be used to dehumidify the different air streams of the roof top unit such as the outdoor air, return air or mixed air. Figure 204 shows the schematic of a typical roof top unit (RTU) and the different options by which a liquid desiccant unit can be integrated or retrofitted with an existing RTU.

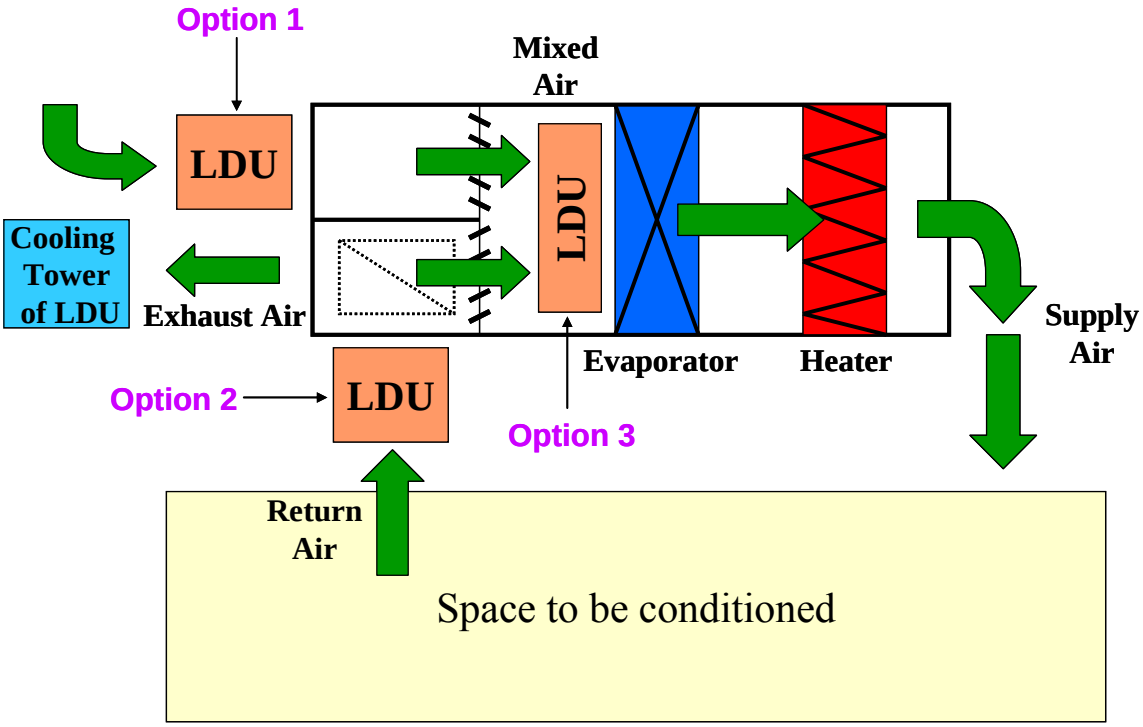

Figure 204: Different options to integrate the liquid desiccant system with roof top unit

As shown in Figure 204, option 1 is the method in which the liquid desiccant unit is integrated with the RTU 1 at the Chesapeake building where the liquid desiccant system dehumidifies the outdoor air, which is usually around 20 - 30 % of the total air supplied to the conditioned space. Option 2 would result in the

dehumidification of the return air from the conditioned space. The return air is also a little humid and warmer as compared to the supply air temperature and humidity since it picks up the moisture from the room and the occupants in the room. Also the return air forms the larger part of the total air supplied to the room which is around 70 - 80 % depending on the quantity of fresh outdoor air drawn in by the RTU. In the third option the liquid desiccant dehumidifies the mixed air after both the outdoor and return air streams mix in the mixed air chamber of the RTU.

Figure 205 and Figure 206 show the plot of return air temperature and humidity ratio recorded experimentally from 8:00 am – 5:00 pm at the Chesapeake building on two typical summer weekdays in the year 2005.

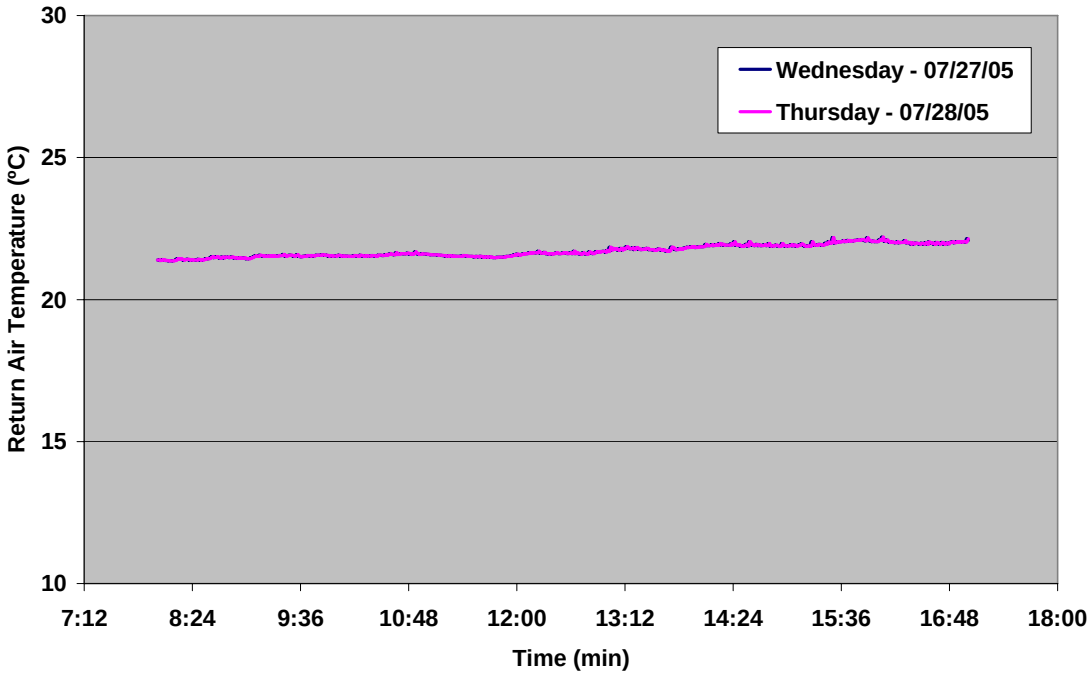

Figure 205: Typical return air temperature at Chesapeake building in summer

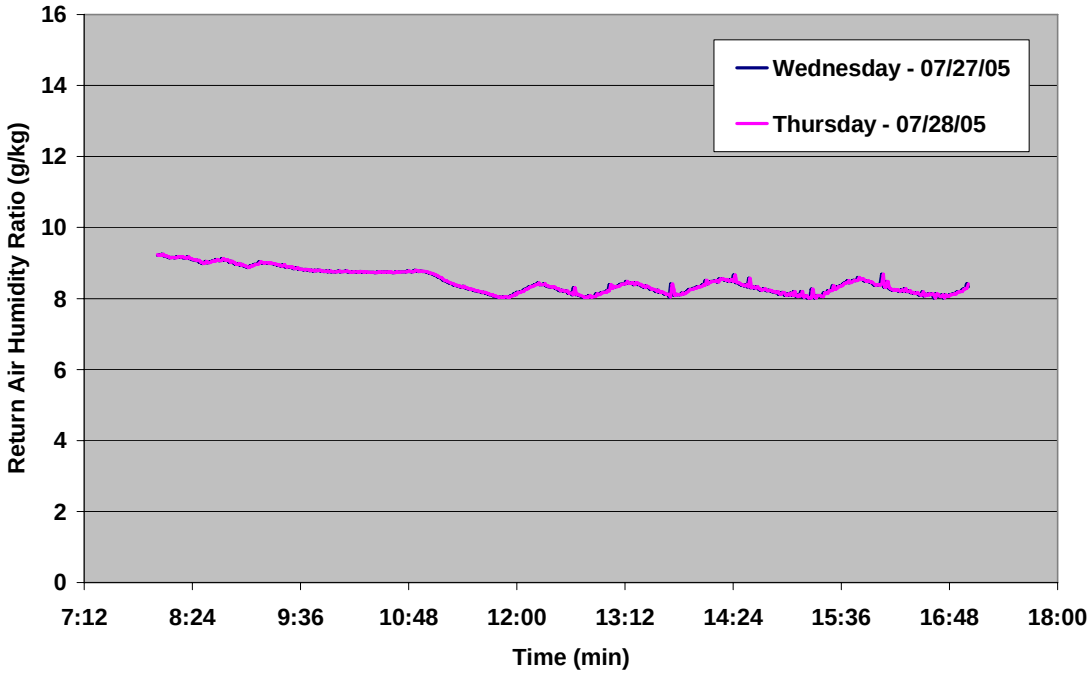

Figure 206: Typical return air humidity ratio at Chesapeake building in summer

It can be seen from Figure 205 and Figure 206 that the return air conditions do not vary too much over the course of operation of the roof top unit. The average return air temperature was about 21.7 ºC while the average humidity ratio was around 8.5 g/kg. Hence it was found from experiments that the return air is neither too hot nor as humid as the outdoor air conditions.

The outdoor and return air are mixed in the mixed air chamber and hence the temperature and humidity ratio of the mixed air depend on the conditions of both the return air as well as the outdoor air. It was shown in the previous discussion that the return air stream is not very hot or humid. Hence the mixed air conditions really depend on the temperature and humidity ratio of the outdoor air. Also the volume flow rate of the mixed air is around 20,000 cfm while the outdoor air is only 3000 cfm. Thus if the liquid desiccant unit is used to process the mixed air stream of the

RTU, then the size of the LDU would be much larger than the existing liquid desiccant unit that handles 3000 cfm of air. This would result in increased capital cost for the liquid desiccant system as well. The roof top unit is usually located on the roof and hence additional costs need to be incurred for structural reinforcement if the LDU is used to process the 20,000 cfm of mixed air. Thus the most economical option to integrate the liquid desiccant unit with the RTU is option 1 where it handles the outdoor air stream and also the outdoor air has the highest humidity ratio of all the three air streams.

The above analysis showed that the best option to integrate this CHP system for a commercial office building is to use the liquid desiccant unit to dehumidify the outdoor air stream. However this may not be true for all the other applications in the commercial sector. For instance for a building or a hotel with a swimming pool, the return air stream would be much more humid than the return air from an office building. In such a case it would be more economical and beneficial to integrate the liquid desiccant system to process the return air stream rather than the outdoor air which implies that employing the liquid desiccant unit in the most humid air stream is the best option since that would provide the largest benefit. Also in cases where 100 % outdoor air is required, the savings achieved by using the integrated CHP system would be much higher resulting in lower payback periods.

Figure 204 also shows that the cooling tower of the liquid desiccant system can utilize the building air that is exhausted as the fresh outdoor air is drawn in for heat exchange since the return air is both cooler and drier than the outdoor air. This arrangement has been adopted in the current experimental setup where the exhaust air

is drawn from the return air section of the RTU 1 through ducting that was retrofitted onto the top of RTU 1. Outdoor air could have been used for this application, but having an available stream of much cooler and drier air allows the LiCl solution to be cooled down much further than would be possible with outdoor air. The end result is process air that is both cooler and less humid than outdoor air. It would be advantageous to use the outdoor air in place of the building return air only when the outdoor air enthalpy is less than the return air stream. However it was found that even for the state of California which has the mildest weather of all the seven states analyzed, the number of hours when the outdoor air enthalpy was lower than the return air was only 73 in the entire cooling season from May to October. Thus it is beneficial to make use of return air that would otherwise be exhausted, in the cooling tower of the liquid desiccant system.

The above integration design guidelines are formulated for the case of a retrofit installation such as the Chesapeake building which was already designed and built along with the HVAC equipment. However for a new installation, the situation might be a little different. For instance, if for a new building, the HVAC unit is on the ground instead of the roof, then the structural reinforcement required at the Chesapeake building would be completely eliminated. However the controls for the capture and utilization of the waste heat in the heat recovery loop would still be the same. Also the cost of electrical interconnection needed to connect the engine generator to the grid would be lower in the new installation as the necessary wiring and conduits can be integrated with the building electrical infrastructure along with the other electrical loads of the building.

6.10 Discussion of Simulation Results

After the validation of the simulation model with experimental data was completed, the thermo-economic model was run for all the cases of ambient air conditions and electricity and gas prices for the seven states described in previous sections. This section discusses in detail the energy saving potential of the integrated CHP system in comparison to a conventional system under the various scenarios.

6.10.1 Cooling Season

In this analysis, the cooling season is considered to comprise of six months from May to October. The roof top unit is assumed to be operating from 5:00 am – 10:00 pm, seven days a week. It is assumed that the roof top unit is equipped with an economizer cycle and does not need any mechanical cooling when the outside air temperature is less than or equal to 18 ºC.

Figure 207 shows the total electricity consumption in terms of kWh per month for the different states for the baseline system. In the baseline system all the cooling is done by the RTU alone and the CHP system is not operated at all. The total kWh of electrical consumption is the summation of the cooling as well as the reheat energy required by the RTU at the various ambient air conditions for the different states.

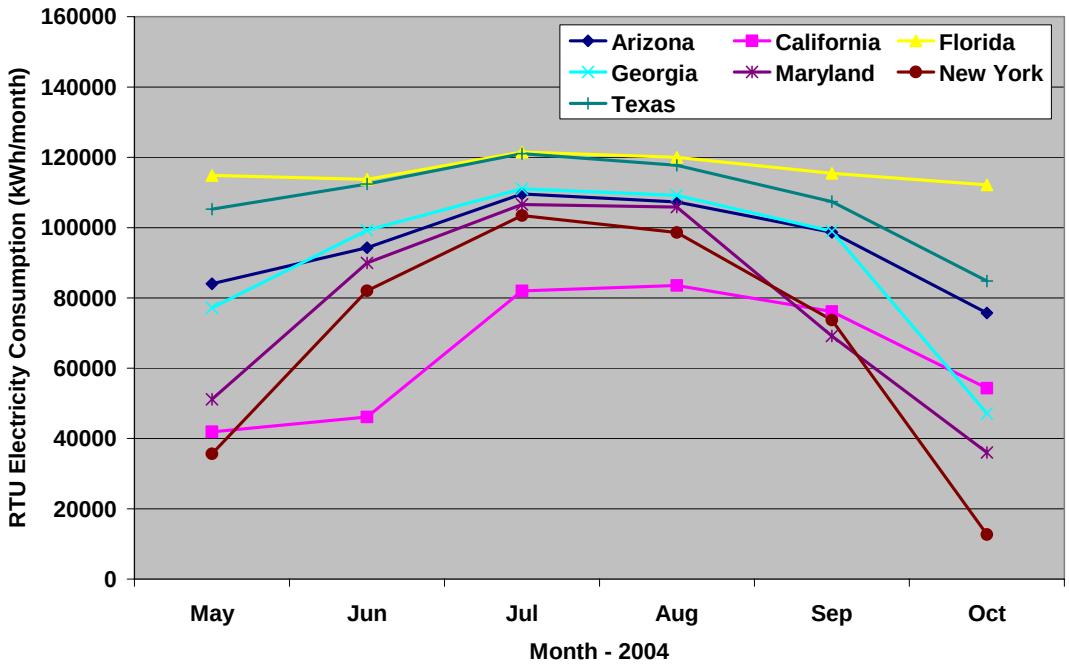

Figure 207: Total kWh of electricity consumption by RTU for different states for the baseline system

It can be observed from Figure 207 that the total electricity consumption is higher for the states of Florida, Texas and Arizona owing to their very hot and humid weather conditions as was shown in the previous sections. On the other hand, California and New York have somewhat mild ambient weather and hence consume less electricity as can be seen in Figure 207. Also the total number of operating hours during which mechanical cooling is provided by the roof top unit differs for each month from state to state. This fact is evident for the month of October where Florida still has more number of hours with higher temperatures and humidity levels as compared to New York. Therefore the total electricity consumption for New York in October was only 12,671 kWh while for Florida it was much higher at around 112,190 kWh.

Figure 208 plots the net electricity consumption in kWh of the RTU when the CHP system is in operation. The roof top unit in this case is still controlled based on supply temperature and not humidity ratio. Hence the RTU would still cool the air up to 13 ºC to remove the moisture from the air and hence requiring the reheat energy to heat the air back to supply temperature. This scenario is currently very much like the way the roof top unit is controlled and operated at the Chesapeake building. The data shown in Figure 208 represents the net electrical kWh required by the RTU after subtracting the net electrical power supplied by the engine generator. The engine generator was considered to be base loaded providing 75 kW of power for the data plotted in Figure 208.

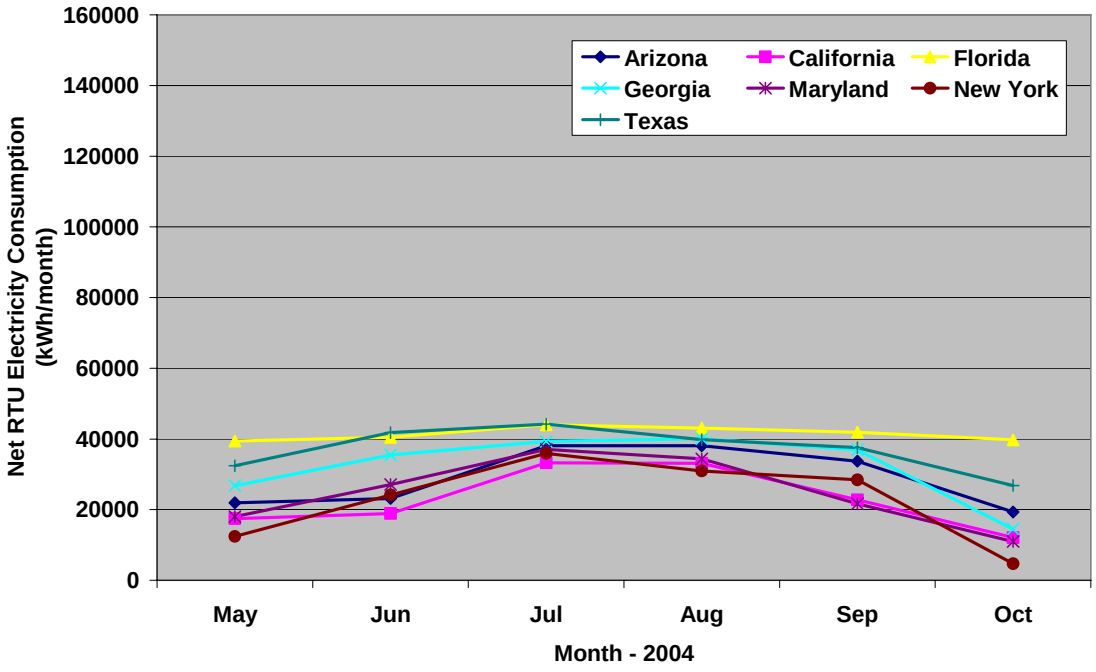

Figure 208: Net kWh of electricity consumption by RTU without humidity ratio control with CHP system at 75 kW

It can be seen from Figure 208 that the net electrical consumption of the RTU reduces when used along with a CHP system. The reduction in the electrical

consumption is on account of two reasons; firstly the liquid desiccant system takes care of a part of the cooling load of the roof top unit by providing both latent as well as sensible cooling and secondly the engine supplies 75 kW of power at the same time. Thus the electrical power drawn from the grid by the roof top unit decreases as can be seen from Figure 208. It can be further observed from comparing Figure 207 and Figure 208 that the maximum electrical consumption was around 121,496 kWh for Florida state in the month of July for the baseline system while the highest electrical consumption when the RTU was operated with the CHP system at 75 kW was for Texas at around 44,190 kWh in the month of July.

The net electrical consumption by the roof top unit from the grid when it was operated with the CHP system, similar to the above case except that the engine generator was run at part load of 40 kW is plotted in Figure 209. It is seen from Figure 209 that the net electrical consumption increases in comparison to the 75 kW case. The net electrical consumption was around 63,720 kWh for Texas in the month of July when the engine was run at 40 kW as compared to 44,190 kWh when the engine was base loaded at 75 kW.

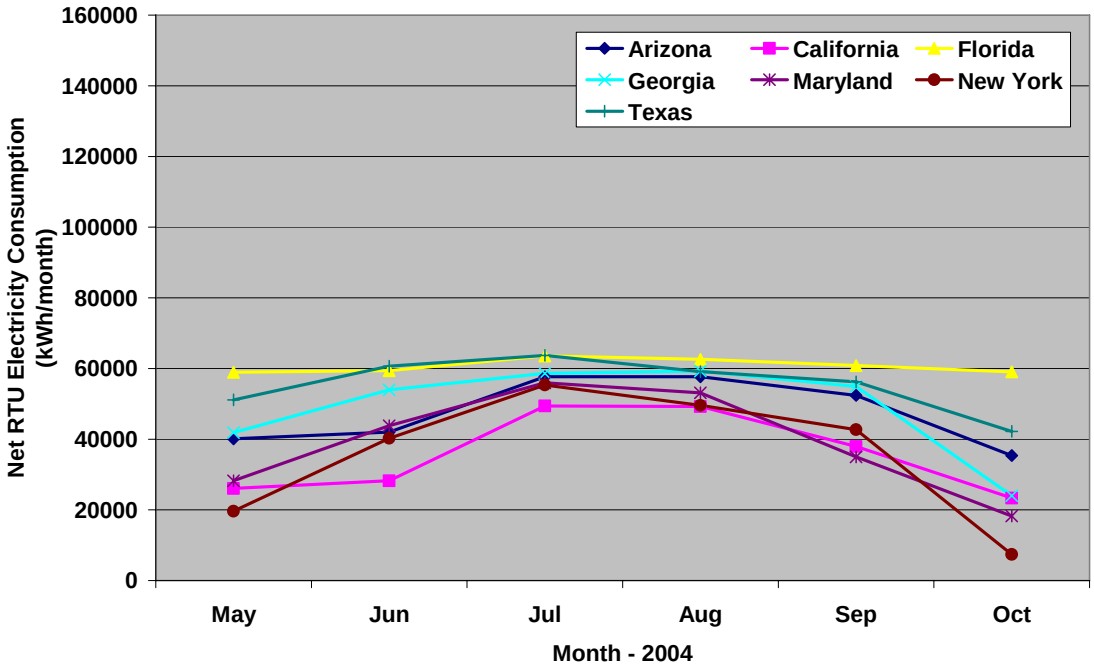

Figure 209: Net kWh of electricity consumption by RTU without humidity ratio control with CHP system at 40 kW

The last case considered in the analysis is when the RTU is run along with the CHP system and the roof top unit is controlled by humidity ratio of the supply air rather than its temperature. In such a situation, the roof top unit would cool the air up to 13 ºC only when the humidity ratio of the mixed air is greater than 8.5 g/kg of dry air (corresponding to supply air humidity ratio). At all other conditions, the roof top unit only provides the sensible cooling while the liquid desiccant unit takes care of the entire latent load. This also saves on the reheat energy required to heat the air since the air will be cooled only to the room set point temperature. Figure 210 shows the net electrical kWh consumption when the roof top unit was run with humidity control along with the CHP system where the engine generator was run at full load of 75 kW. It is observed from Figure 210 that the net electrical consumption is negative for some of the months in the state of New York, California and Maryland because

the amount of kWh produced by the engine generator is higher than the electrical kWh required by the roof top unit. Hence the net difference is negative which means that this extra amount of electricity is supplied to the building for its other electrical loads rather than deriving it from the electrical grid.

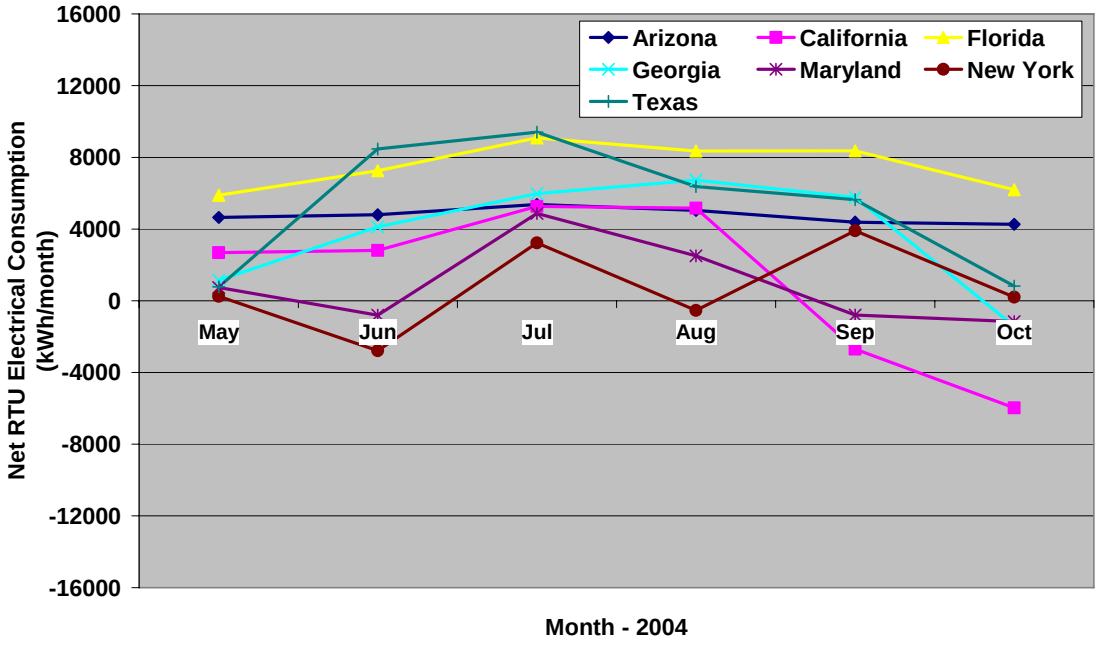

Figure 210: Net kWh of electricity consumption by RTU with humidity ratio control with CHP system at 75 kW

Figure 211 shows the results of the net electrical consumption for a similar case as above except that the engine generator was run at part load of 40 kW.

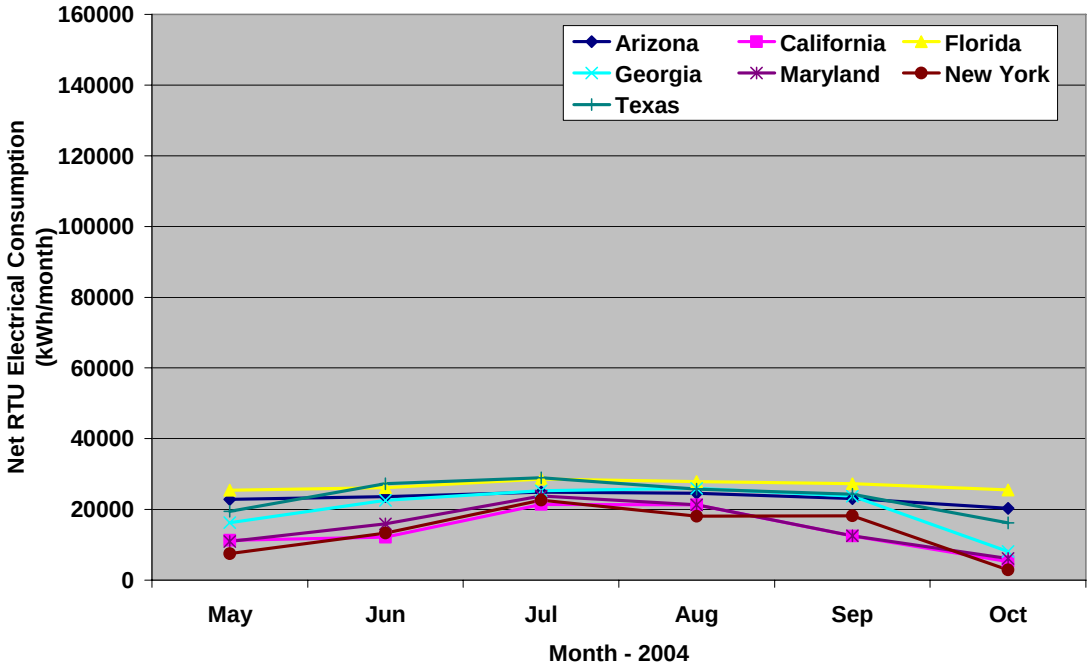

Figure 211: Net kWh of electricity consumption by RTU with humidity ratio control with CHP system at 40 kW

By comparing Figure 210 and Figure 211 it is observed that the amount of kWh of electricity produced by the engine at part load of 40 kW is not enough to satisfy the total energy requirement of the roof top unit for any of the states and hence the RTU still consumes a portion of electricity from the grid. However the amount of electrical consumption from the utility in this case is still less than the electrical consumption in the baseline system as well as when the RTU is operated with CHP system but is controlled by temperature.

The cost of electricity incurred per month for operating the roof top unit in the baseline system is given by the following equation,

$$Cost_{elec} = \left(Power_{cool} + Power_{reheat}\right) X \left(\frac{hours}{month}\right) X \left(\frac{cents}{kWhX100}\right)$$

Where,

$Cost_{elec}$ = Cost of electricity in dollars per month

$Power_{cool}$ = Electrical power consumed by the RTU to cool the air

$Power_{reheat}$ = Electrical power consumed by the RTU to reheat the supply air back to it's set point temperature.

The net cost of electricity paid to the utility per month when the roof top unit is operated along with the CHP system is calculated as,

$$Cost_{elec} = \left[\left(Power_{cool} + Power_{reheat}\right) - \left(Power_{eng}\right)\right] X \left(\frac{hours}{month}\right) X \left(\frac{cents}{kWhX100}\right)$$

Where,

$Power_{eng}$ = Net engine power produced by the engine generator of the CHP system.

Figure 212 shows the cost of electricity per month for the seven different states when the roof top unit is operated alone without the CHP system in the baseline system.

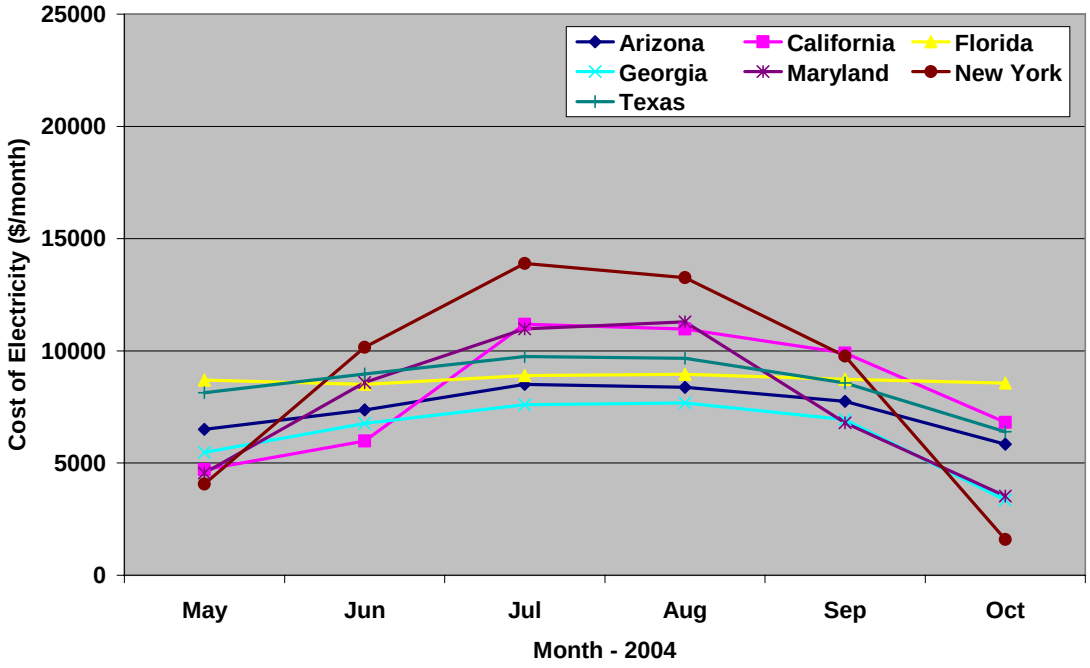

Figure 212: Cost of electricity for operating RTU for different states for the baseline system

It can be observed from Figure 212 that the cost of electricity was the highest in the state of New York, especially for the months of July and August followed closely by the states of California and Maryland. These states have such high costs of electricity owing to their higher cents/kWh of electricity even when the weather conditions are not as extreme as those found in the states of Florida and Arizona. The highest cost of electricity was in the state of New York at around $13,891 for the month of July as can be seen from Figure 212. The cost of electricity when the RTU was assisted by the operation of the CHP system but without humidity ratio control is shown in Figure 213. The engine generator in the CHP system was run at 75 kW and the cost reflects the price paid for the portion of electricity purchased from the utility after utilizing all the electrical power produced by the engine generator at 75 kW.

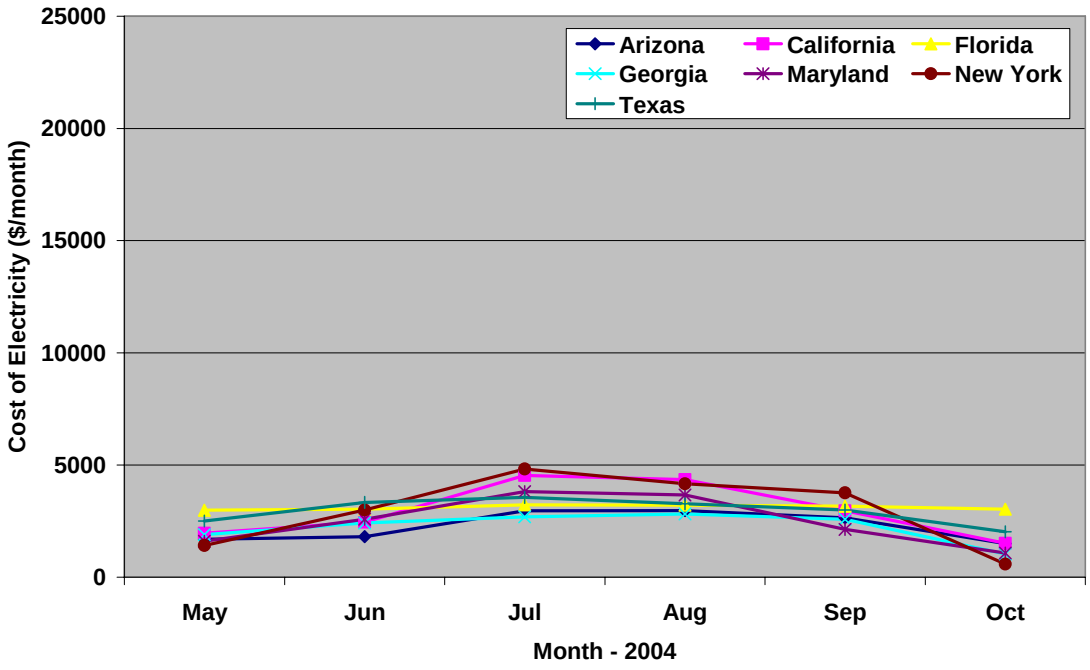

Figure 213: Cost of electricity for operating RTU without humidity ratio control with CHP system at 75 kW

It can be seen from Figure 213 that as compared to the baseline system, the cost of electricity is reduced as a result of operating the CHP system. The highest cost of electricity again is for the state of New York in the month of July at around $4827 as compared to $13,891 for the same month and state for the baseline system which is a reduction of $9064 for the month of July alone. For the same case of operating the RTU without humidity ratio control with CHP system as above, Figure 214 shows the cost of electricity purchased from the utility when the engine generator was run at 40 kW.

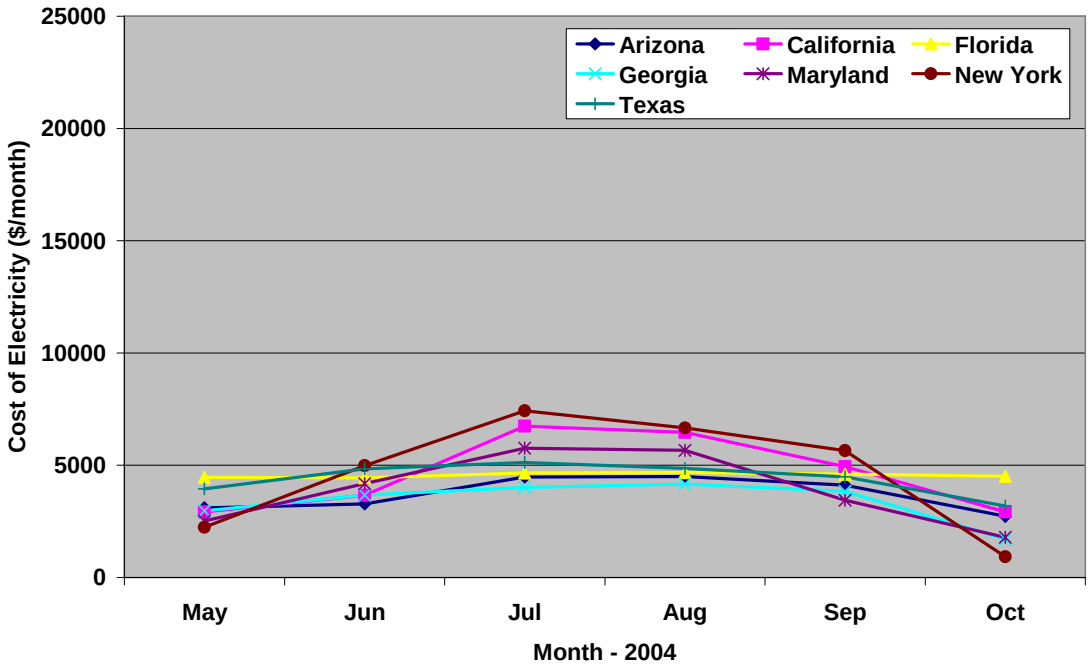

Figure 214: Cost of electricity for operating RTU without humidity ratio control with CHP system at 40 kW

Comparing Figure 213 and Figure 214 it is found that the cost of electricity purchased from the grid is more when the engine is run at 40 kW than at 75 kW. Considering the state of New York for the month of July, it is observed that the cost of electricity for the amount purchased from the utility increases to $7432 at 40 kW as compared to $4827 when the engine is run at 75 kW. The cost of electricity when the RTU is operated along with the CHP system at 75 kW and the RTU is controlled by humidity ratio of supply air rather than it's temperature is plotted in Figure 215.

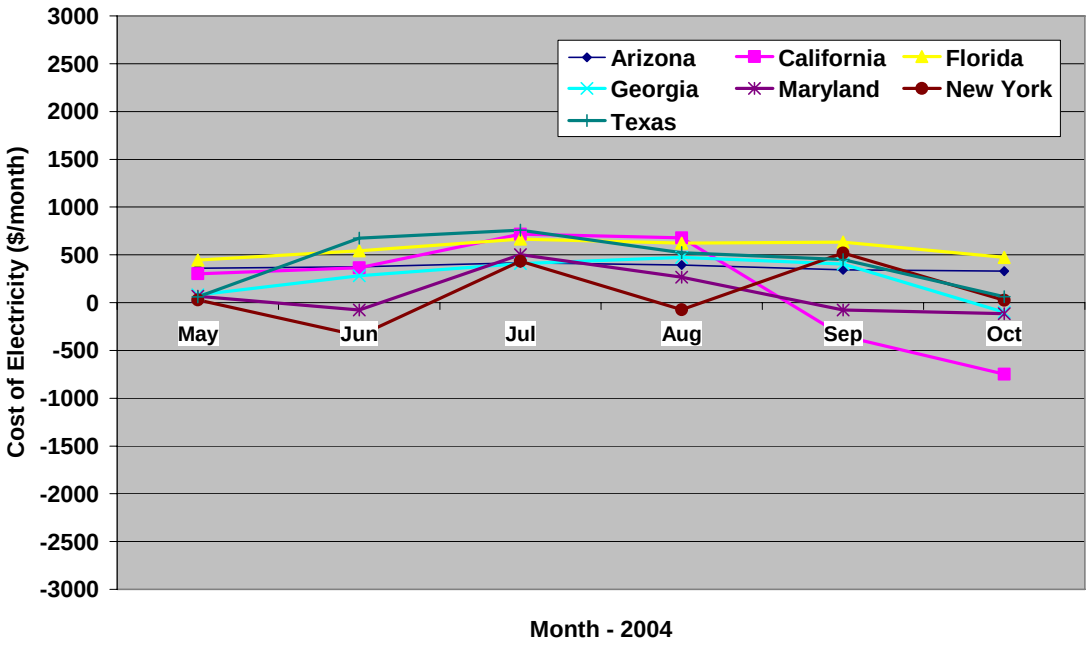

Figure 215: Cost of electricity for operating RTU with humidity ratio control with CHP system at 75 kW

The negative values of the cost of electricity shown in Figure 215 signify the cost of electricity saved as a result of operating the CHP system. It is seen from Figure 215 that the states of California, New York and Maryland have their cost of electricity as negative and hence their cost of electricity represents the cost of the excess amount of electricity that is still available from the engine generator after satisfying all the electrical power requirement of the roof top unit. As this excess amount of electricity is supplied to the building to cater to its other electrical loads, it displaces the electrical costs otherwise needed from the electrical utility. For the similar case of operating the RTU with humidity ratio control with CHP system as above, Figure 216 shows the cost of electricity purchased from the utility when the engine generator was run at 40 kW.

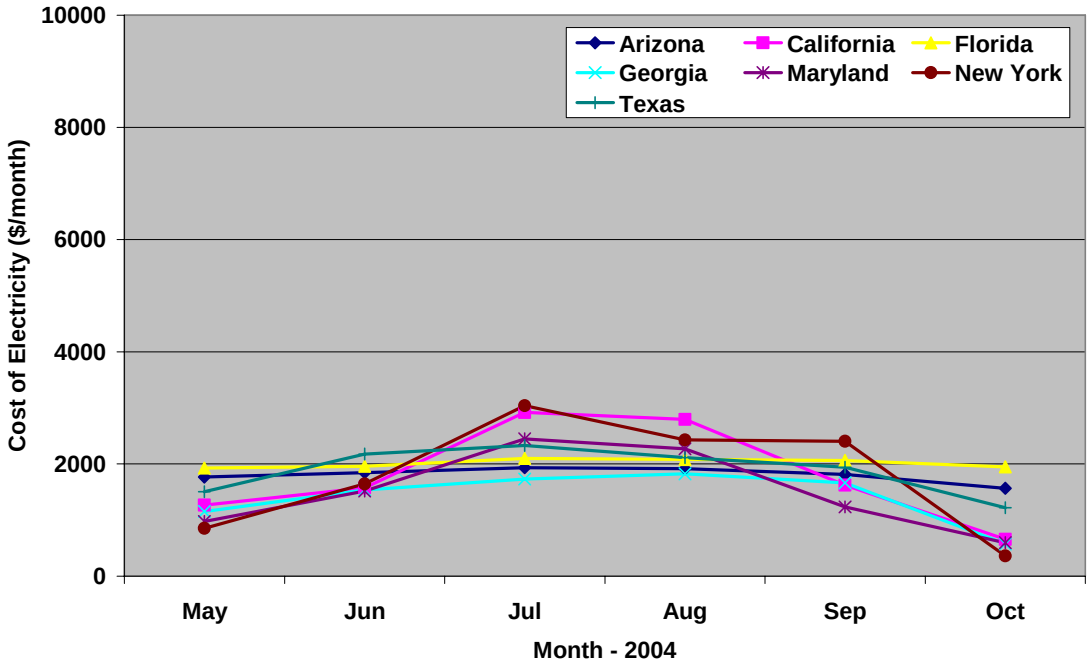

Figure 216: Cost of electricity for operating RTU with humidity ratio control with CHP system at 40 kW

In comparison to Figure 215, it is seen from Figure 216 that the cost of electricity per month is positive for the states which mean that the building still has to pay a certain amount for the electricity drawn from the utility. However the cost of electricity paid to the utility in this case is still less than the electrical cost in the baseline system as well as when the RTU is operated with CHP system but is controlled by temperature. The maximum cost of electricity paid to the utility in this case was for the state of New York at around $3037 for the month of July 2004.

The above sections described the kWh of electrical consumption and the cost of electricity for operating the roof top unit and the CHP system. However to run the engine generator of the CHP system, natural gas fuel needs to be combusted in order to realize the savings in electrical costs shown above. The cost of natural gas fuel depends upon the geographical location as well as whether the engine generator is run

at full load or part load. The cost of natural gas incurred per month in operating the CHP system is calculated by the following equation,

$$Cost_{NG} = Q_{NG} X 3414.425 X \left(\frac{1}{LHV_{NG}} \right) X \left(\frac{hours}{month} \right) X \left(\frac{\$}{1000\, ft^3} \right)$$

Where,

$Cost_{NG}$ = Cost of natural gas fuel in dollars per month

Q_{NG} = Amount of natural gas fuel combusted in the engine generator in kW

LHV_{NG} = Lower heating value of natural gas = 910 Btu/ft^3.

The amount of natural gas fuel combusted (Q_{NG}) is multiplied by 3414.425 to convert kW to Btu/hr (1 kW = 3414.425 Btu/hr).

Figure 217 shows the cost of natural gas fuel per month for the seven different states when the engine generator is run at 75 kW while Figure 218 plots the natural gas cost when the engine generator is run at 40 kW. From Figure 217 and Figure 218 it can be observed that the cost of natural gas is much higher in the state of Georgia followed by Florida owing to higher natural gas costs as well as more number of operating hours. It is interesting to note that the natural gas cost is lower in the states of New York and California while the cost of saved electricity is higher in these states, thus providing favorable economic conditions for the operation of a CHP system. The maximum cost of natural gas was found to be for the state of Georgia at around $7373 in the month of July for the year 2004 when the engine was run at 75 kW while it was around $4710 for the same state and month when the engine generator was operated at part load of 40 kW.

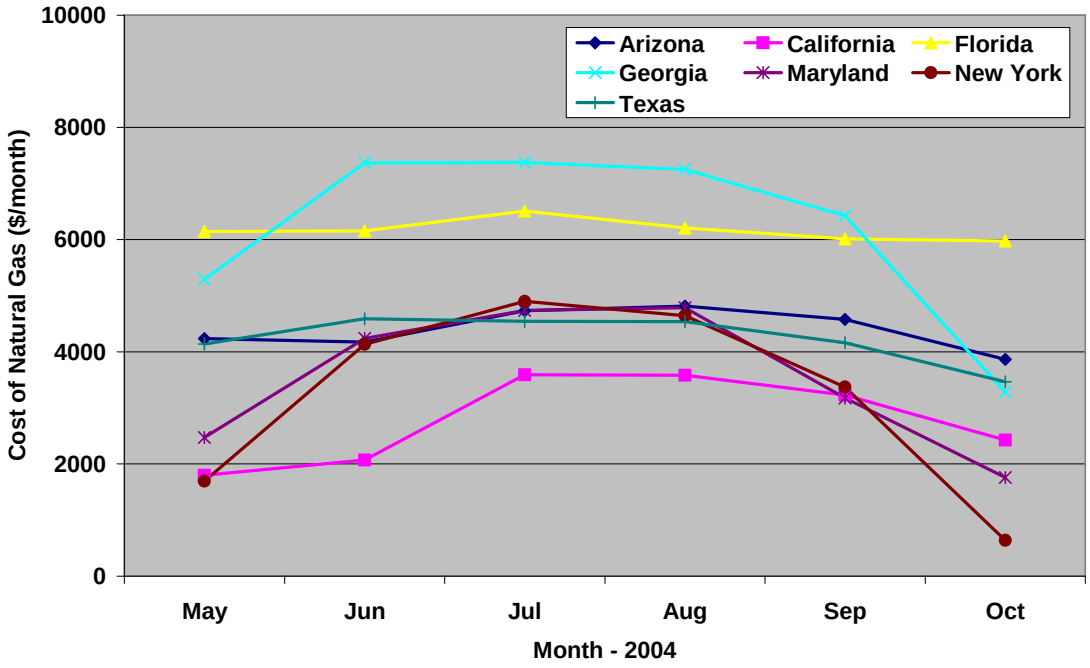

Figure 217: Cost of natural gas in summer for different states when the engine generator is run at 75 kW

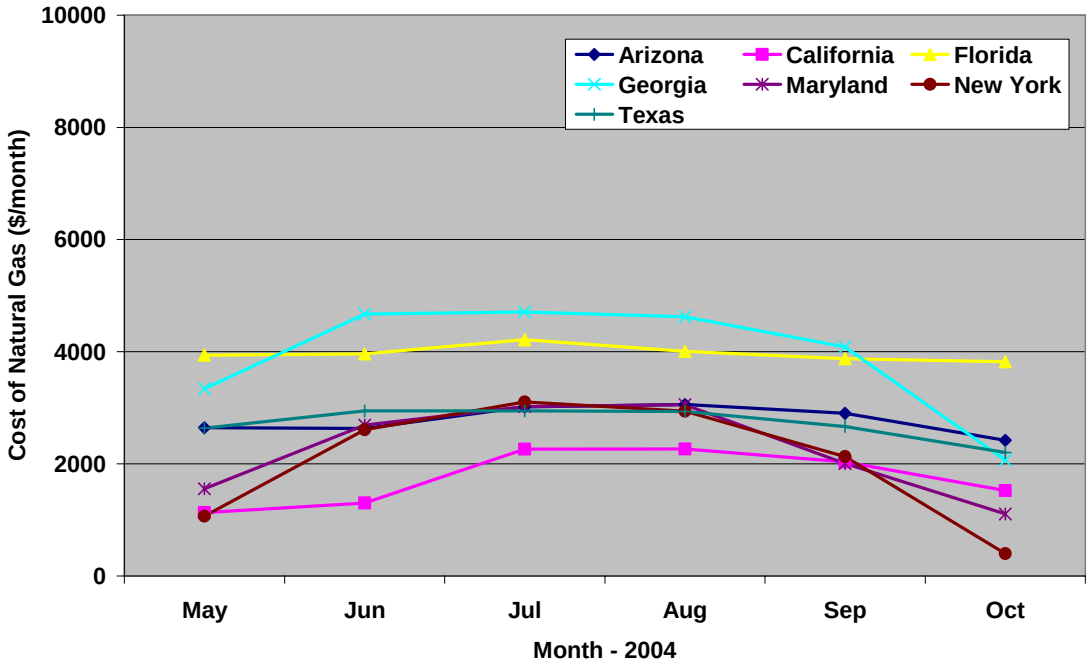

Figure 218: Cost of natural gas in summer for different states when the engine generator is run at 40 kW

The total cost of operating the roof top unit alone in the baseline system was plotted in Figure 212. The total cost involving the operation of both the roof top unit along with the CHP system is given by the following equation,

$$Cost_{total,op} = Cost_{net,elec} + Cost_{NG}$$

Where,

$Cost_{total,op}$ = Total operational cost of the CHP system combined with the roof top unit

$Cost_{net,elec}$ = Net cost of electricity purchased from the utility

$Cost_{NG}$ = Cost of natural gas fuel combusted in the engine generator of the CHP system.

The total operational cost for the case when the roof top unit was controlled based on supply air temperature and was operated along with the CHP system with the engine generator base loaded at 75 kW is shown in Figure 219. The total operational cost for the state of New York in the month of July was around $9727 while the operational cost in the baseline system was about $13,891 which is a net savings of $4164 in the month of July itself for New York by operating the CHP system at 75 kW and without modifying any controls on the roof top unit. The maximum operational cost in this case was for the state of Georgia in the month of August 2004 at around $10,067.

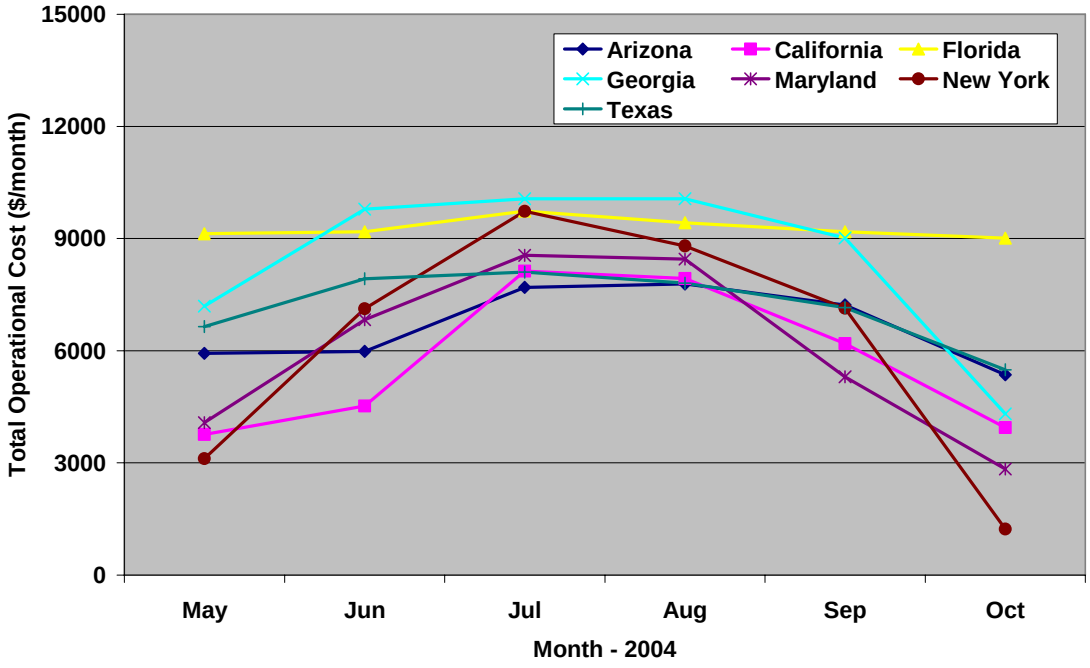

Figure 219: Total operational cost of operating RTU without humidity ratio control with CHP system at 75 kW

Figure 220 shows the operational cost for the same case as above except that the engine generator is run at part load of 40 kW. It can be observed from Figure 220 that the operational cost of the system increased for New York in the month of July to around $10,537 as compared to the previous case when the engine is run at full load of 75 kW. However for the state of Georgia, the operational cost at 75 kW was $ 10,067 in the month of August while it is reduced to around $8788 at 40 kW. This is because of the higher electricity prices and lower natural gas prices in New York as compared to lower electricity prices and higher natural gas prices in Georgia.

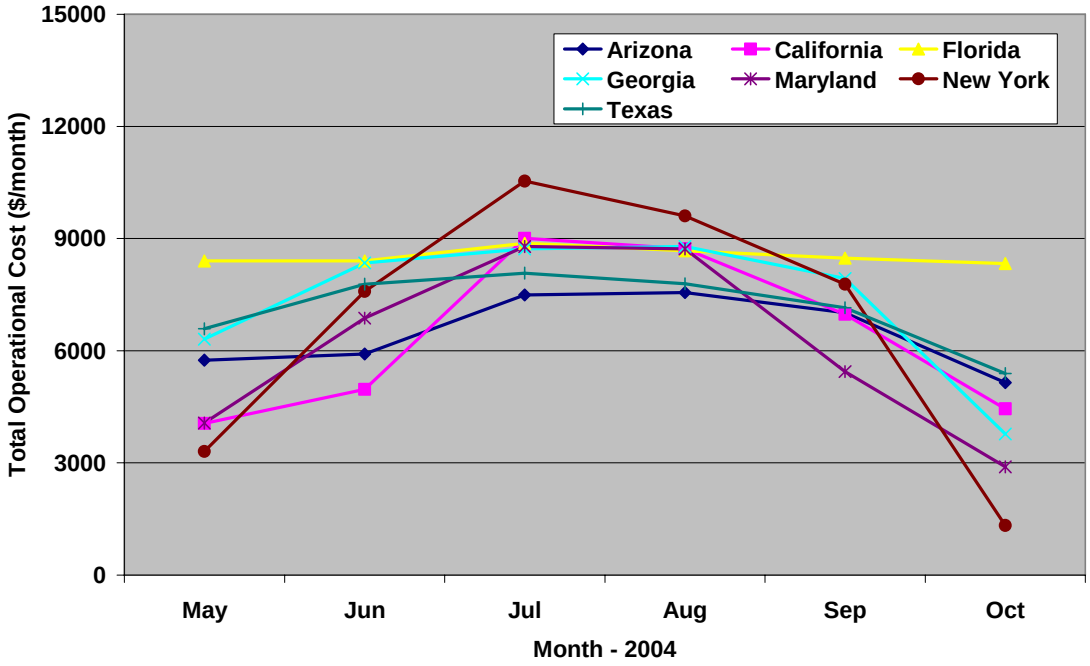

Figure 220: Total operational cost of operating RTU without humidity ratio control with CHP system at 40 kW

The total operational cost of running the RTU along with the CHP system when the RTU is controlled by the humidity ratio of the supply air is shown in Figure 221. The engine generator was assumed to run at full load of 75 kW in this case. It is seen that the operational cost is quite lower as compared to the previous case where the RTU was controlled by supply air temperature. In this case, it is found that the operational cost is much higher for the state of Georgia followed closely by Florida as compared to the other states due to their high cost of natural gas as was indicated in Figure 217. The maximum operational cost was found to be around $7782 for the state of Georgia in the month of July 2004.

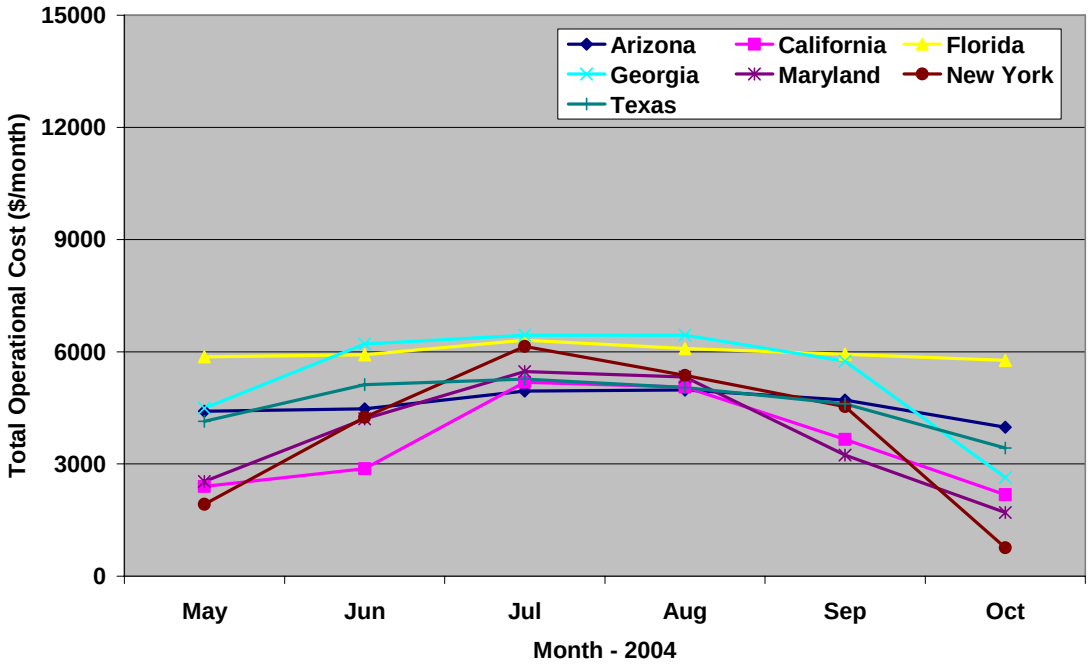

Figure 221: Total operational cost of operating RTU with humidity ratio control with CHP system at 75 kW

Figure 222 plots the operational cost of operating the RTU with humidity ratio control and the CHP system with the engine generator being at part load of 40 kW. It is observed from Figure 222 that the operational cost of the system reduces for the state of Georgia to around $6440 in the month of July as compared to $7782 when the engine generator was run at 75 kW. However the total cost for operating the system in New York for the month of July increases to about $6142 at 40 kW as compared to $5332 when the engine generator was base loaded at 75 kW.

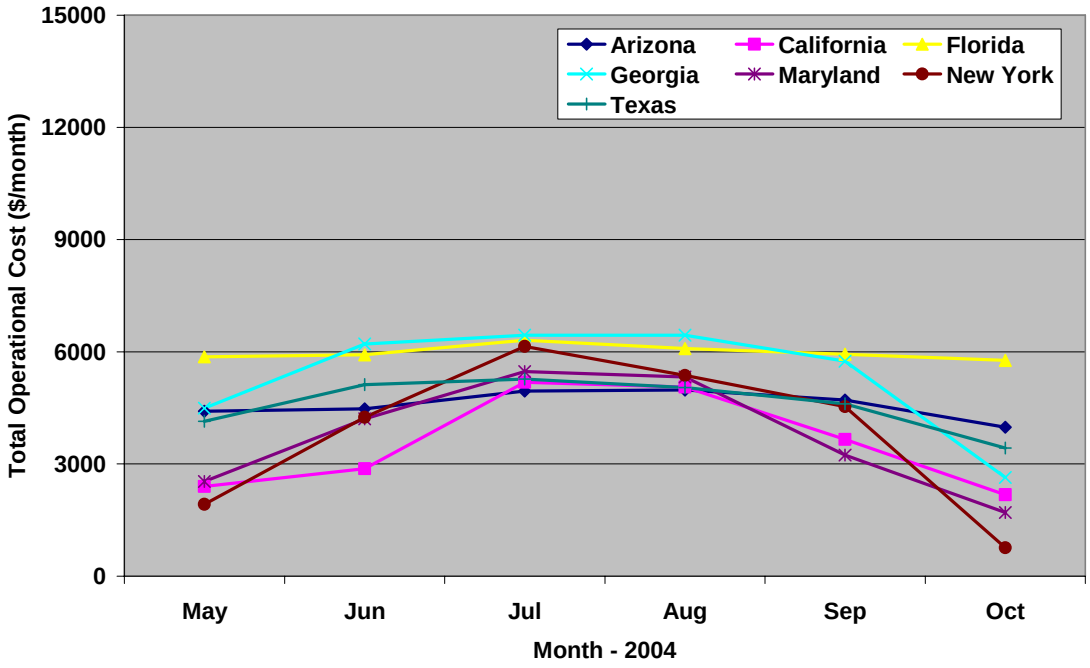

Figure 222: Total operational cost of operating RTU with humidity ratio control with CHP system at 40 kW

6.10.2 Heating Season

In this analysis, the heating season is considered to last for six months from November to April. The roof top unit is assumed to be operating from 5:00 am – 10:00 pm, seven days a week, similar to the cooling season. It is assumed that the building does not need any kind of heating when the outside air temperature is greater than or equal to 25 ºC. Space heating currently in the Chesapeake building is achieved through electric resistance heaters in the VAV boxes. However if there was an hydronic loop for heating the building rather than electric resistance heaters then the hot water generated from the waste heat of the engine generator could very well be used in the winter season for space heating. This would result in higher operating hours for the engine generator resulting in lower payback periods. This aspect of the

CHP system is investigated in this section and energy savings due to use of waste heat for space heating has been quantified in detail.

Figure 223 shows the total waste heat recovered in kWh from the jacket water and the exhaust gas heat exchangers at 75 kW that can be used for space heating of the building for the different months in the various states.

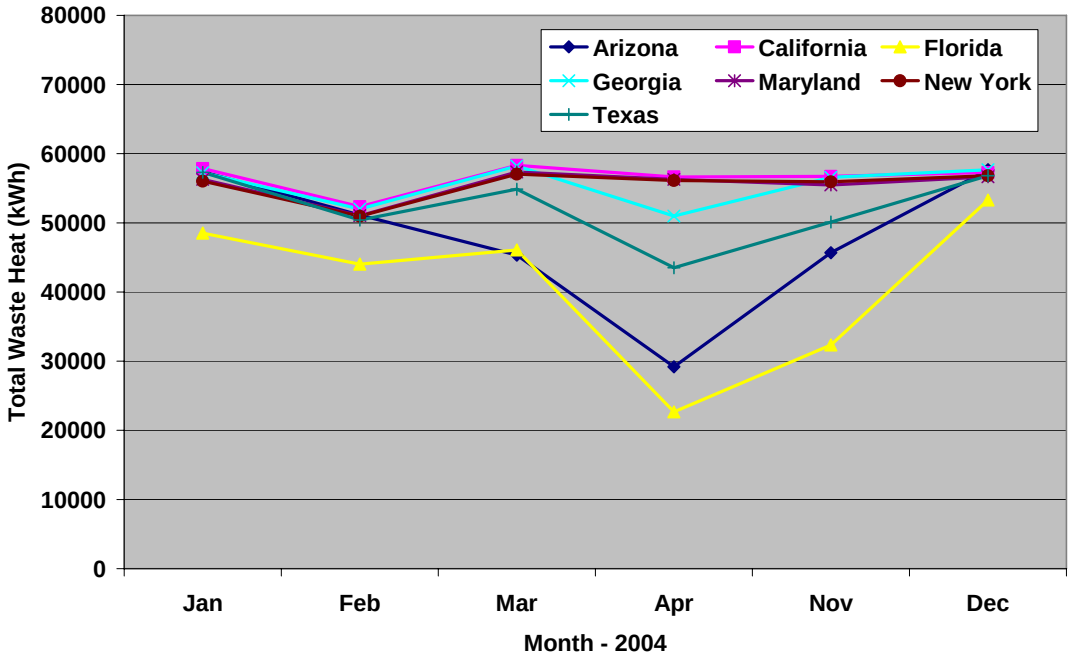

Figure 223: Total waste heat at 75 kW available for space heating for different states

It is observed from Figure 223 that the maximum kWh of waste heat produced by the engine generator at 75 kW was around 58,332 kWh in the month of April for the state of California. The total amount of waste heat available for space heating was lower in the month of April for the states of Arizona and Florida compared to other states due to lower number of operating hours. Figure 224 plots the total waste heat available to the building for space heating in the different months from November to April for the various states when the engine generator was run at 40 kW.

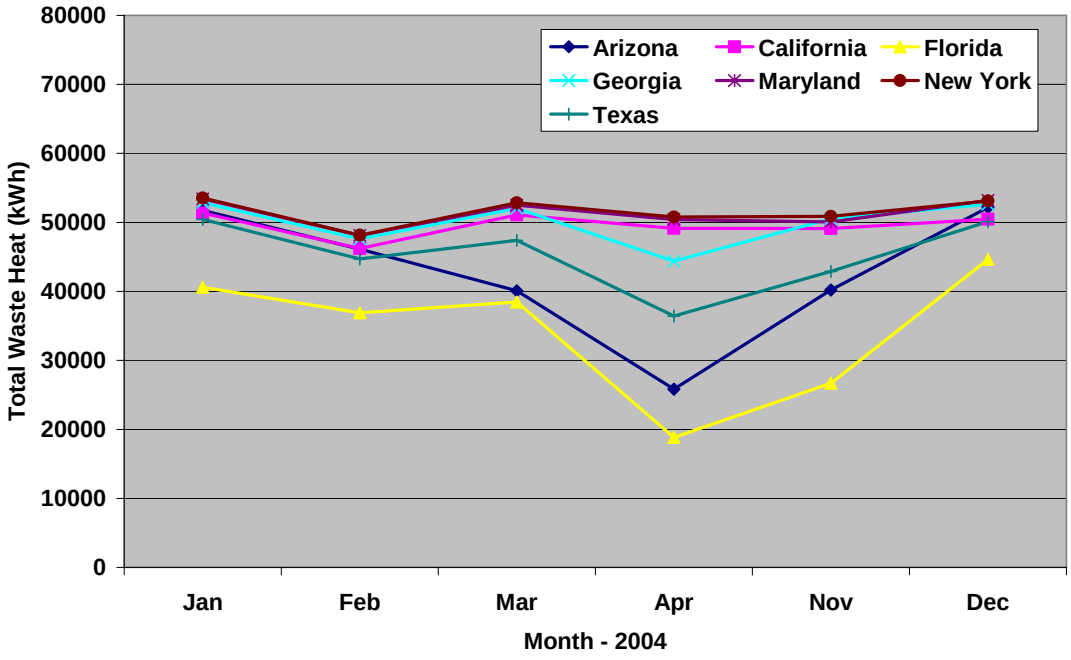

Figure 224: Total waste heat at 40 kW available for space heating for different states

At part load of 40 kW, the total waste heat recovered from the engine generator is less than that available at full load of 75 kW as can be seen from Figure 224. The maximum kWh of waste heat available for space heating of the building at 40 kW was around 53,524 kWh for the state of New York in the month of January.

By operating the CHP system in winter, not only the waste heat can be used to displace the electricity used for space heating but also the electrical power produced by the engine generator can be utilized in the building to take care of certain electrical loads. Figure 225 shows the total savings in dollars per month in terms of electricity by the building as a result of the waste heat available for heating purposes and the electrical power supplied by the engine generator at 75 kW that otherwise would have been purchased from the utility for the various states.

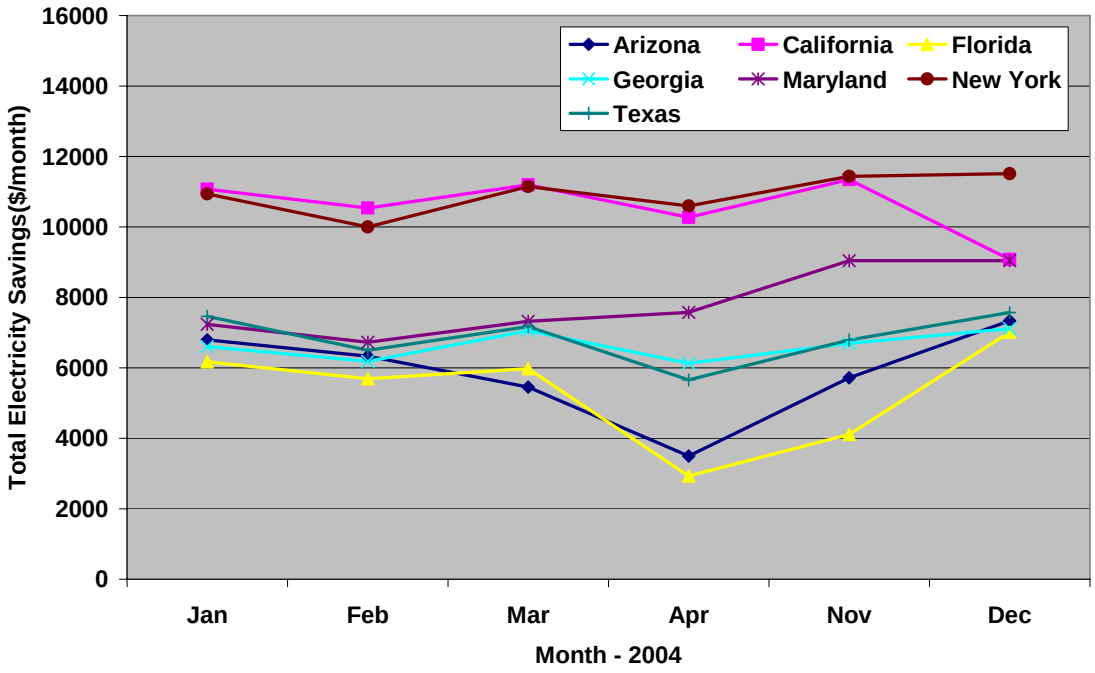

Figure 225: Total Electricity Savings for different states at 75 kW

From Figure 225, it is found that the savings in electrical costs were quite significant and higher for New York and California owing to their high electricity rates and the maximum savings in electrical costs at around $11,515 were realized for the state of New York in the month of December 2004.

The total savings in electrical costs when the engine generator was run at 40 kW is plotted in Figure 226 for the different states. The maximum electrical savings in this case was around $8801 in the month of December for the state of New York.

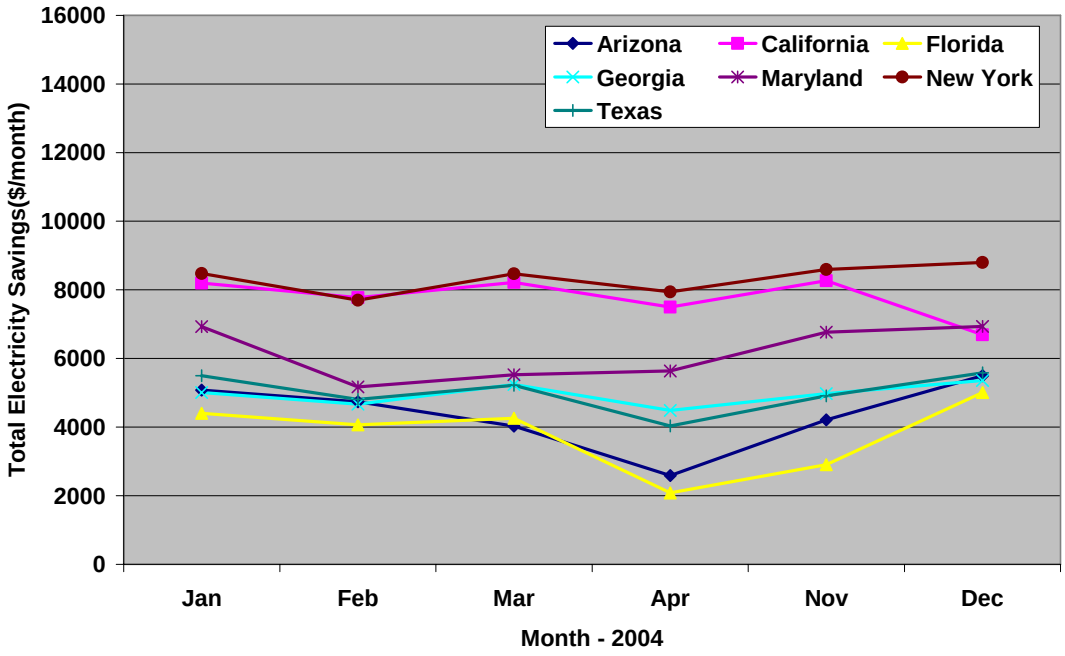

Figure 226: Total Electricity Savings for different states at 40 kW

The cost of operating the engine generator in the CHP system in winter which is actually the cost of the natural gas fuel is shown in Figure 227 when the engine generator was run at full load of 75 kW while Figure 228 plots the natural gas cost when the engine was run at part load of 40 kW. It is found from the plots shown in Figure 227 and Figure 228 that the maximum cost for operating the engine generator was for the state of Georgia in the month of November 2004 owing to high natural gas prices in that state. The cost of natural gas for Georgia in November was around $6028 when the engine was run base loaded at 75 kW while it was about $3703 when engine generator was operated at part load of 40 kW.

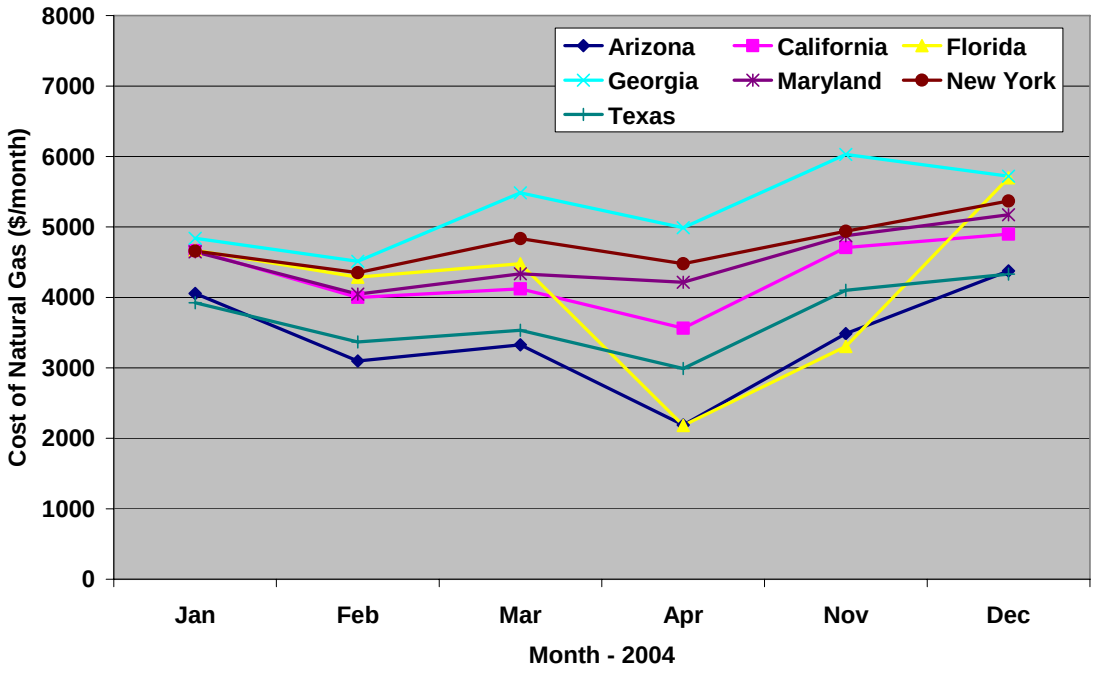

Figure 227: Cost of natural gas in winter for different states when the engine generator is run at 75 kW

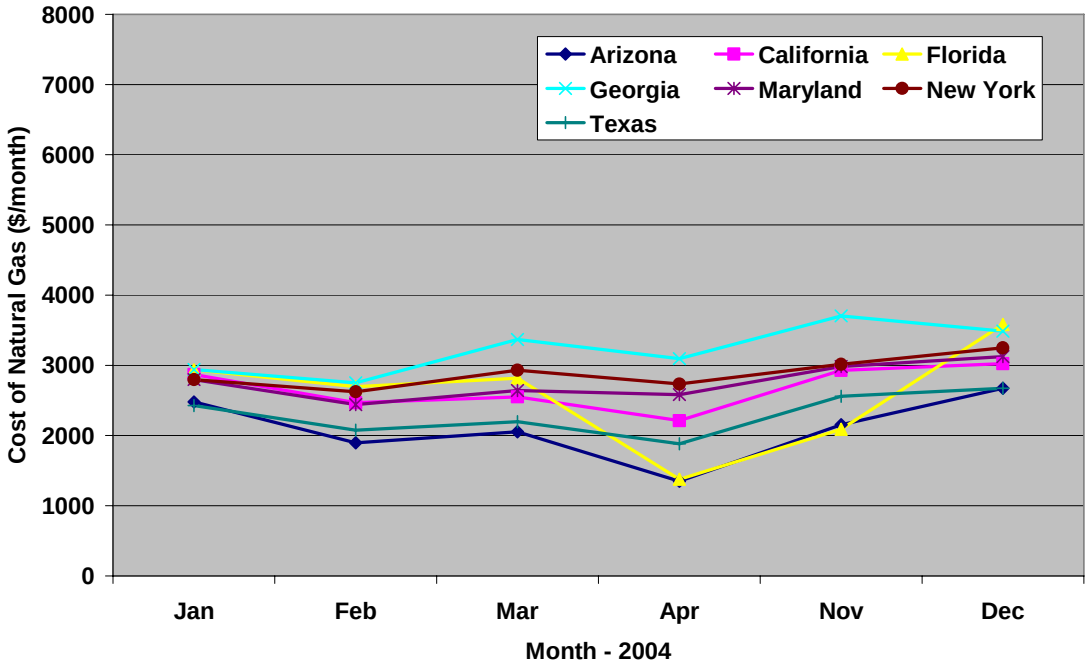

Figure 228: Cost of natural gas in winter for different states when the engine generator is run at 40 kW

6.10.3 Return on Investment (ROI)

This section explains in detail the net savings achieved in the cooling and heating season by operating the roof top unit along with the CHP system for all the different scenarios that were discussed in previous sections. Based on the savings and initial capital cost, the return on investment and payback period is then calculated for each case.

Figure 229 shows the net savings realized in the cooling season when the RTU is controlled with supply air temperature and operated along with the CHP system with the engine base loaded at 75 kW. The net savings is calculated by subtracting the cost of electricity in operating the RTU in the baseline system from the total operational cost of running the RTU along with the CHP system.

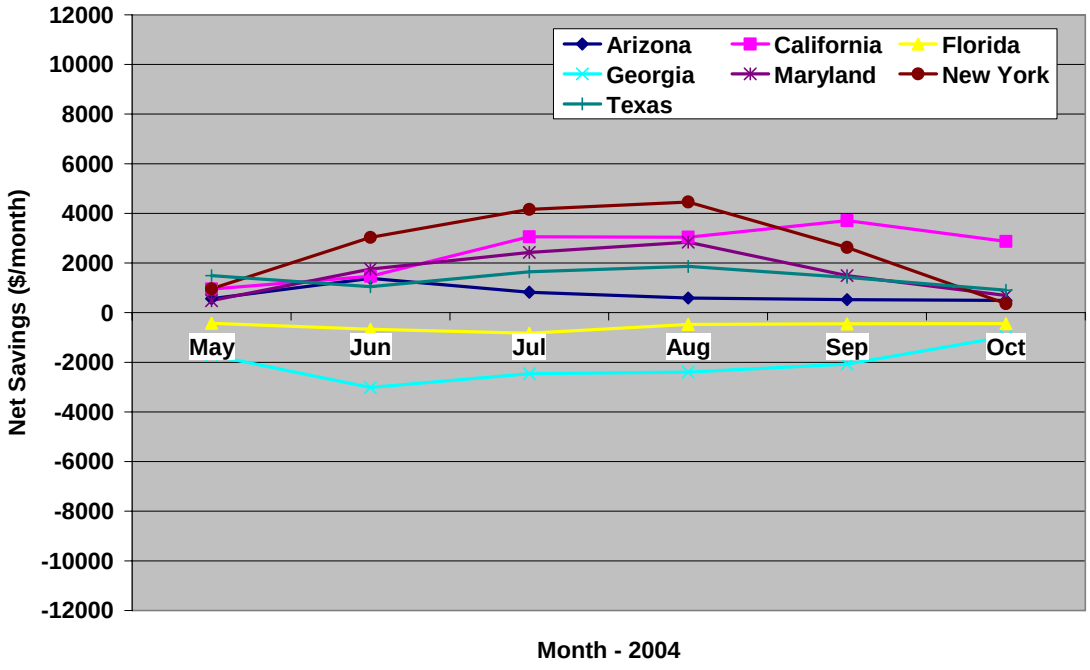

Figure 229: Net Savings realized by operating RTU without humidity ratio control with CHP system at 75 kW in the cooling season

It can be observed from Figure 229 that there is some net savings when the RTU is temperature controlled and is operated along with the CHP system at 75 kW in the states of New York and California. However in this configuration, the net savings is negative for the states of Florida and Georgia throughout the cooling season implying that the cost to operate the combined system of CHP and RTU is higher than the baseline system of running the RTU alone on electricity. This is due to the rather higher price of natural gas in these states as compared to their electrical rates, making it cheaper to run the system on electricity. Similar characteristics in net savings are noted when the engine is run at part load of 40 kW in the same configuration as above as can be seen from Figure 230.

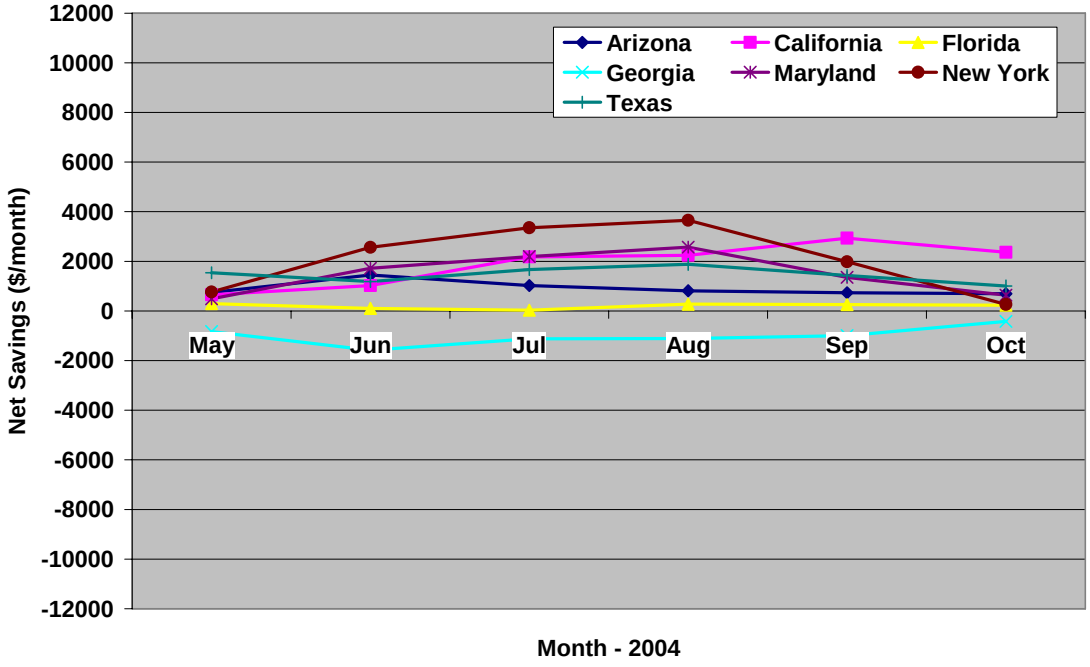

Figure 230: Net Savings realized by operating RTU without humidity ratio control with CHP system at 40 kW in the cooling season

The net savings achieved when the roof top unit was controlled by the supply air humidity ratio rather than its temperature and was operated along with the CHP system with the engine generator running at 75 kW in the summer season is plotted in Figure 231.

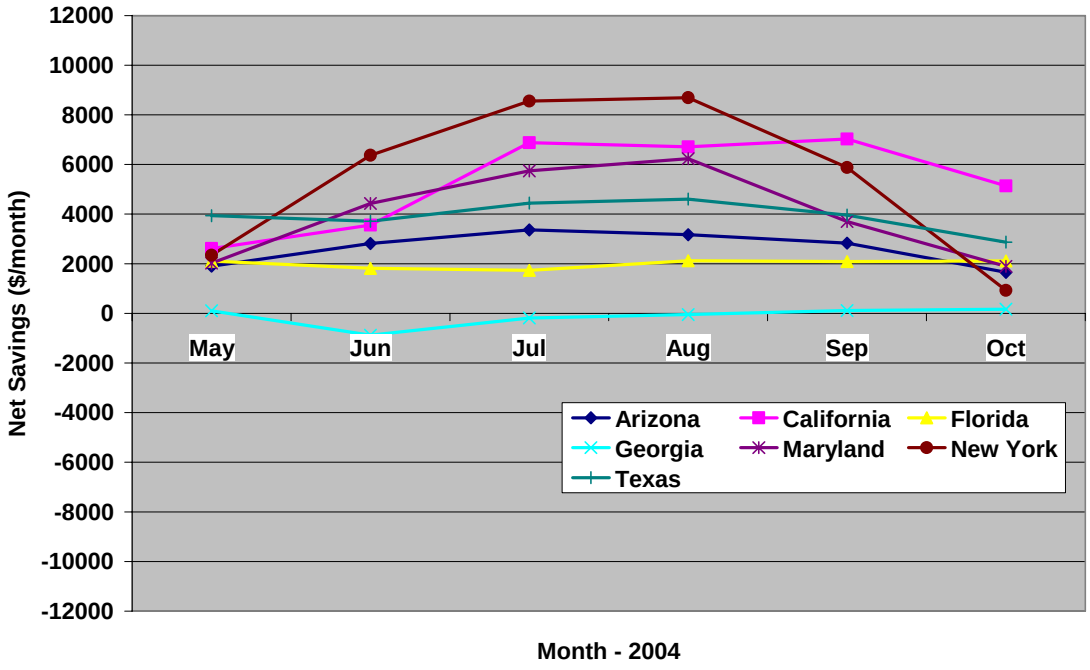

Figure 231: Net Savings realized by operating RTU with humidity ratio control with CHP system at 75 kW in the cooling season

As can be seen from Figure 231, the net savings in this case was positive for all the states except for Georgia as compared to the previous case where the RTU was controlled by the supply air temperature. The net savings were quite significant in the state of New York as well as California due to their high electricity prices and comparatively lower natural gas prices while the net savings achieved were less in states with high natural gas prices such as Georgia and Florida. In fact for the state of Georgia the net savings were found to be negative for the months of June, July and August of 2004. The maximum net savings in the cooling season was observed in the

state of New York at around $8691 in the month of August 2004. Figure 232 plots the net savings in the cooling season for the same configuration as above except that the engine was run at part load of 40 kW.

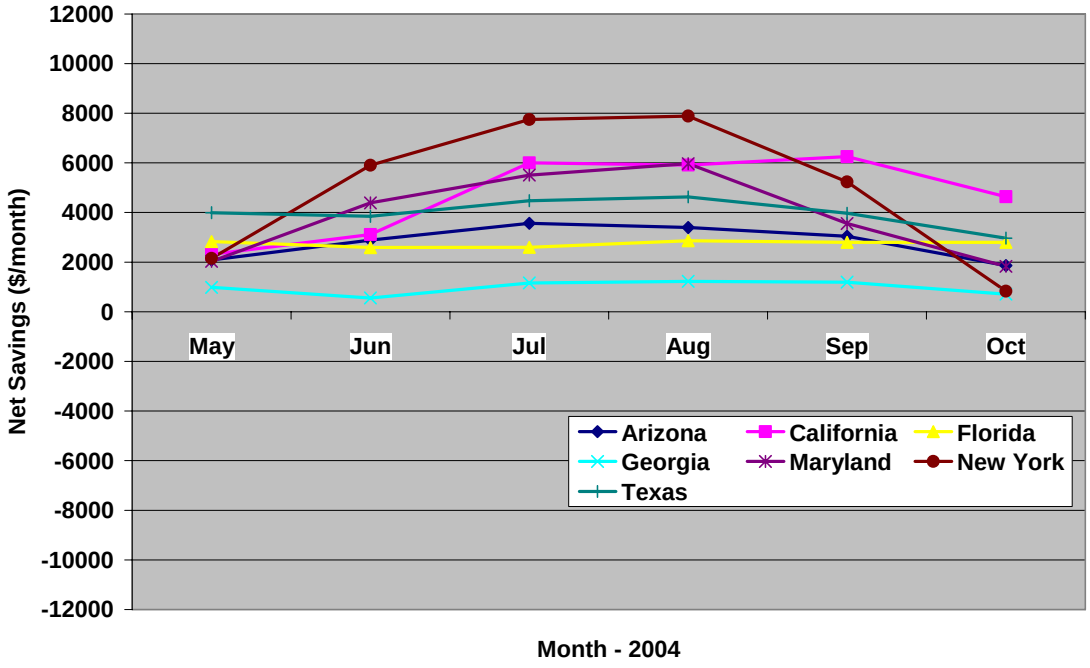

Figure 232: Net Savings realized by operating RTU with humidity ratio control with CHP system at 40 kW in the cooling season

It is observed from Figure 232 that the net savings for states like New York and California decreases when the engine generator is run at 40 kW as compared to 75 kW while it actually increases in the state of Georgia and Florida at 40 kW in comparison with the 75 kW. The maximum net savings in this configuration was again for the state of New York at around $7890 in the month of August 2004.

The net savings achieved by operating the engine generator in the heating season at 75 kW and utilizing the waste heat for space heating is shown in Figure 233.

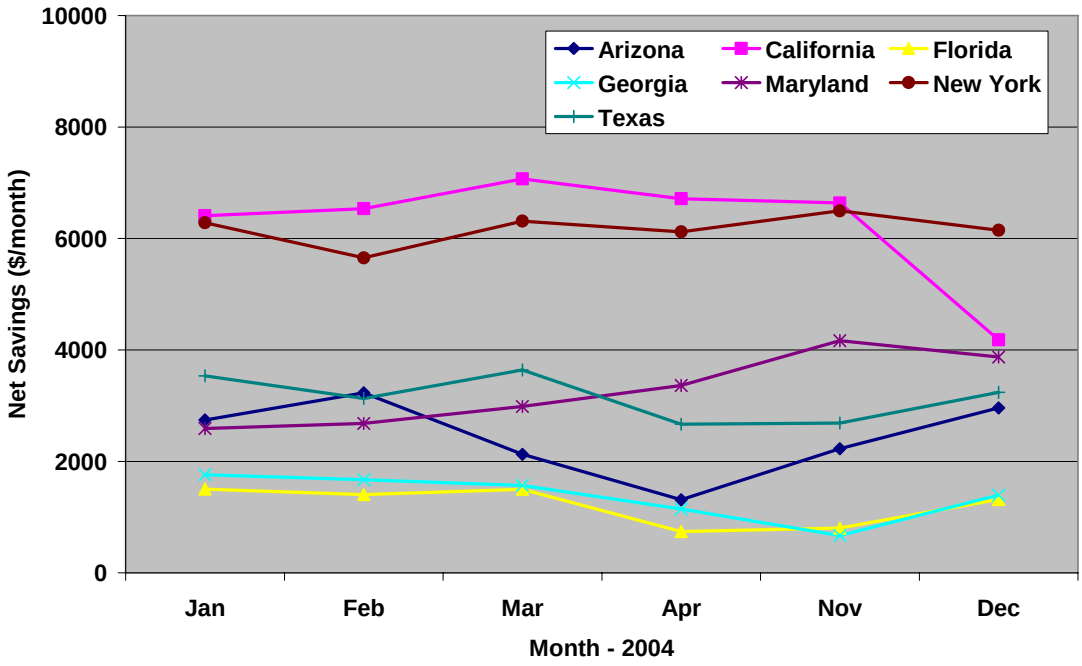

Figure 233: Net Savings for different states in the heating season at 75 kW

It can be seen from Figure 233 that the net savings in the heating season were significantly higher in New York and California due to high electricity prices as compared to Florida and Georgia where the net savings get reduced owing to high natural gas prices. The maximum net savings at around $7069 was obtained in the month of March 2004 in California. Figure 234 plots the net savings in the heating season when the engine generator was run at part load of 40 kW.

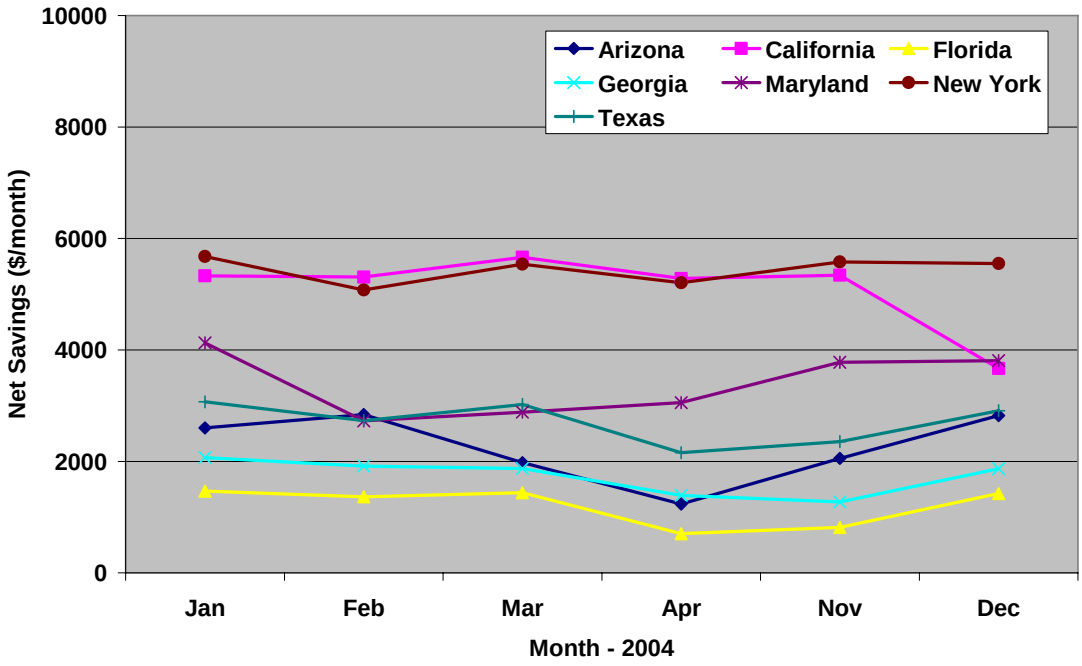

Figure 234: Net Savings for different states in the heating season at 40 kW

The net savings for the 40 kW case are a little higher for the states of Florida and Georgia while they are lower in California and New York as compared to the case when the engine generator was run at full load of 75 kW. The maximum net savings in the case of 40 kW was around $5678 in the month of January 2004 for the state of New York.

The total net savings achieved in the entire cooling season for the different states is obtained by adding up the net savings in every month from May to October. Figure 235 shows the net savings for the complete cooling season of 2004 for the various states when the RTU was controlled based on supply air temperature and was run along with the CHP system.

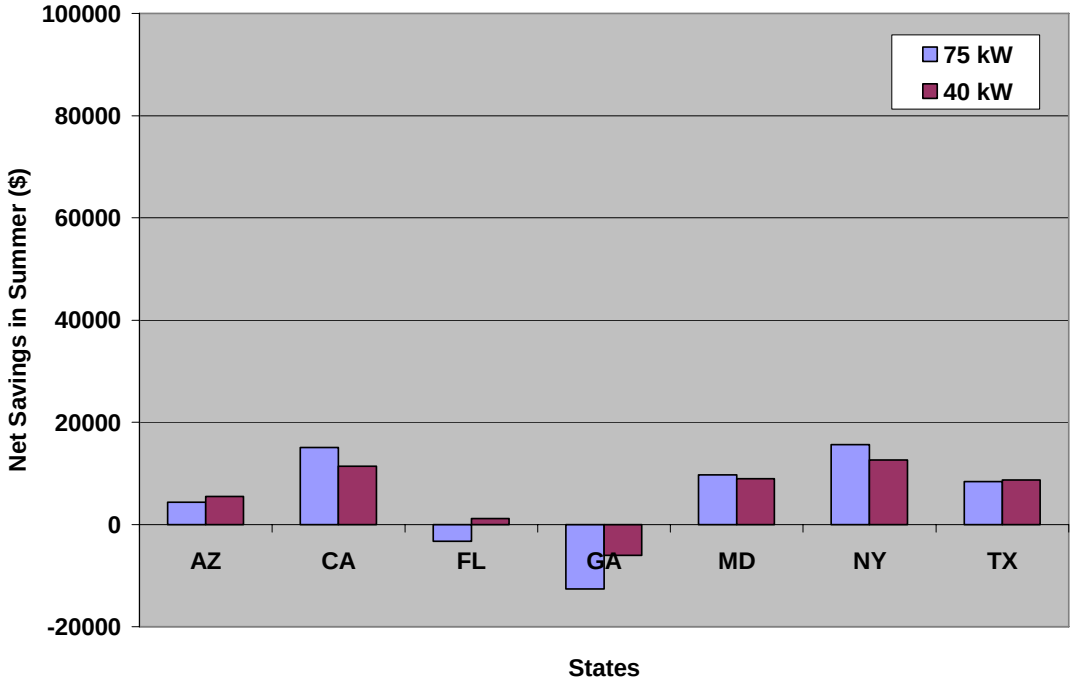

Figure 235: Total net savings for different states in summer with RTU without humidity ratio control and CHP system

It is found from Figure 235 that there is not any savings obtained in the state of Georgia when the RTU is controlled by the supply air temperature and is operated along with the CHP system either at 75 kW or 40 kW implying that its more expensive to use a CHP system as compared to operating the RTU alone in the baseline system. There is some savings in this type of configuration for Florida only when the engine generator is run at part load of 40 kW. The maximum savings of around $15,598 for this case was achieved in the state of New York for the entire cooling season. Figure 236 plots the net savings in the cooling season realized when the roof top unit was controlled by the humidity ratio of supply air and was run along with the CHP system with the engine generator producing 75 kW and 40 kW of electrical power.

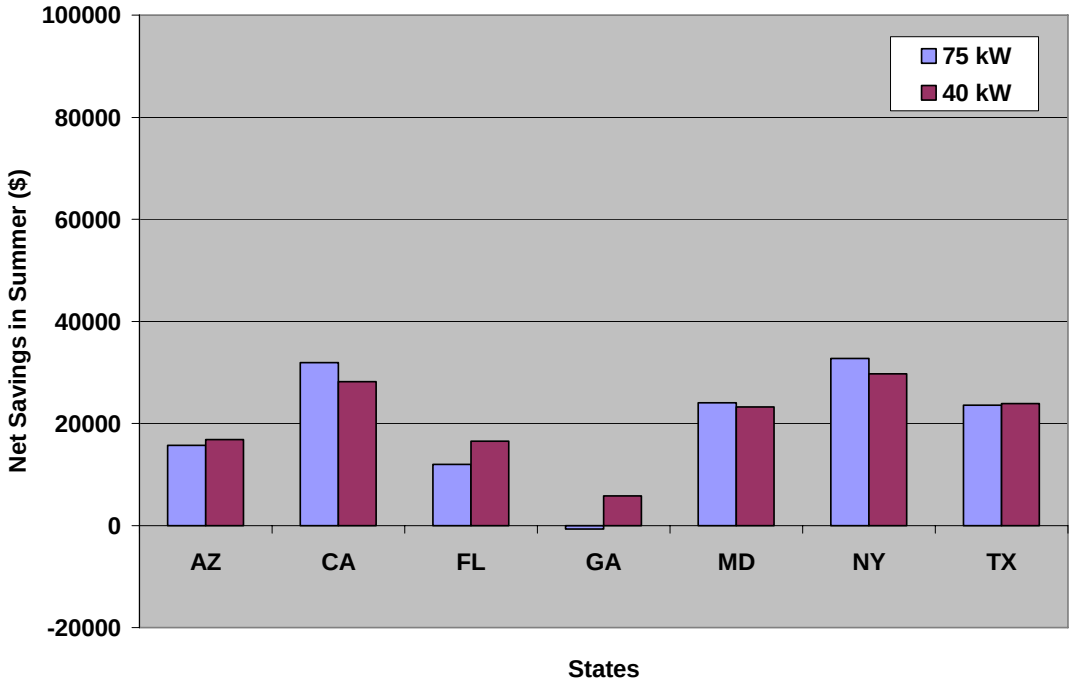

Figure 236: Total net savings for different states in summer with RTU with humidity ratio control and CHP system

It can be observed from Figure 236 that the total savings achieved in this configuration is higher than the previous case where the RTU is controlled by supply air temperature. For the state of Georgia, operating the engine generator at 75 kW still does not give any savings while operating it at 40 kW is a little cheaper than the baseline system. The maximum total savings for this configuration was found to be about $32,771 for New York for the entire summer season.

The net savings achieved in the heating season for the various states when the engine generator was run at 75 kW and 40 kW and the waste heat was used for space heating in the building is shown in Figure 237.

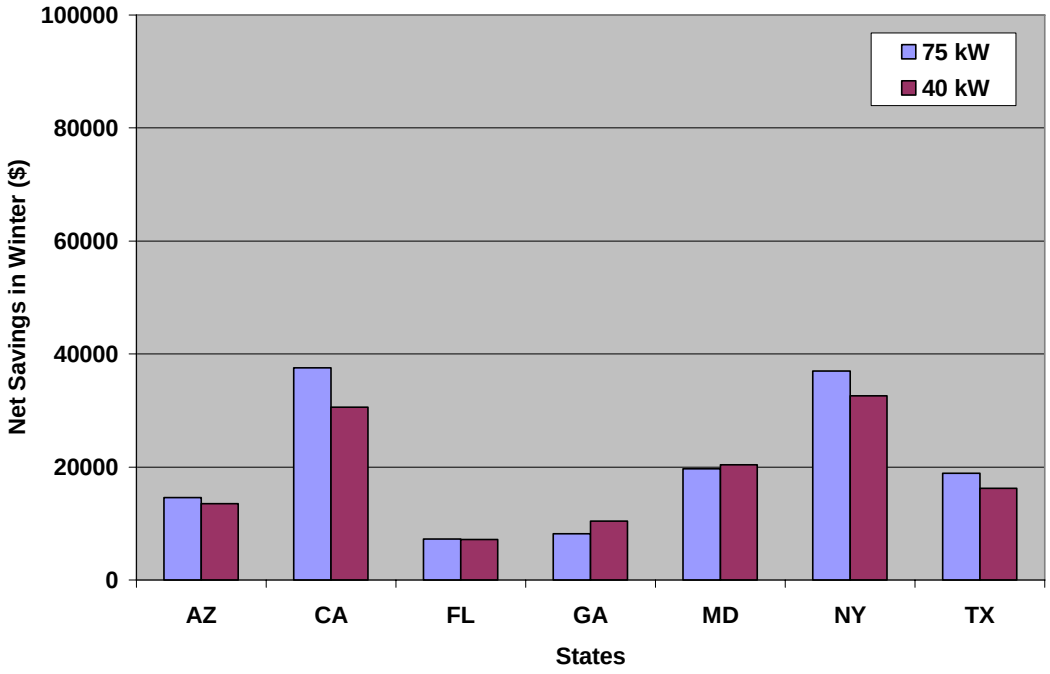

Figure 237: Total net savings for different states in the winter season

From Figure 237, it can be seen that higher amount of savings was realized in the states of California and New York when the engine generator was run at full load of 75 kW while it was more beneficial and cheaper to run the engine at part load of 40 kW for Georgia owing to higher natural gas prices as compared to electricity rates. The maximum savings in the heating season was about $37,550 in the state of California followed closely by New York.

Figure 238 shows the net savings achieved in the winter season for the different states when a natural gas fired boiler was used to supply the hot water for space heating instead of using the waste heat from the engine generator. The combustion efficiency of the boiler was assumed to be around 80 %. In this analysis it was assumed that the boiler would produce the same amount of hot water as the engine generator produces at 75 kW and 40 kW to have an even comparison between the two

cases and these have been labeled as NG boiler – 75 and NG boiler – 40 respectively in Figure 238.

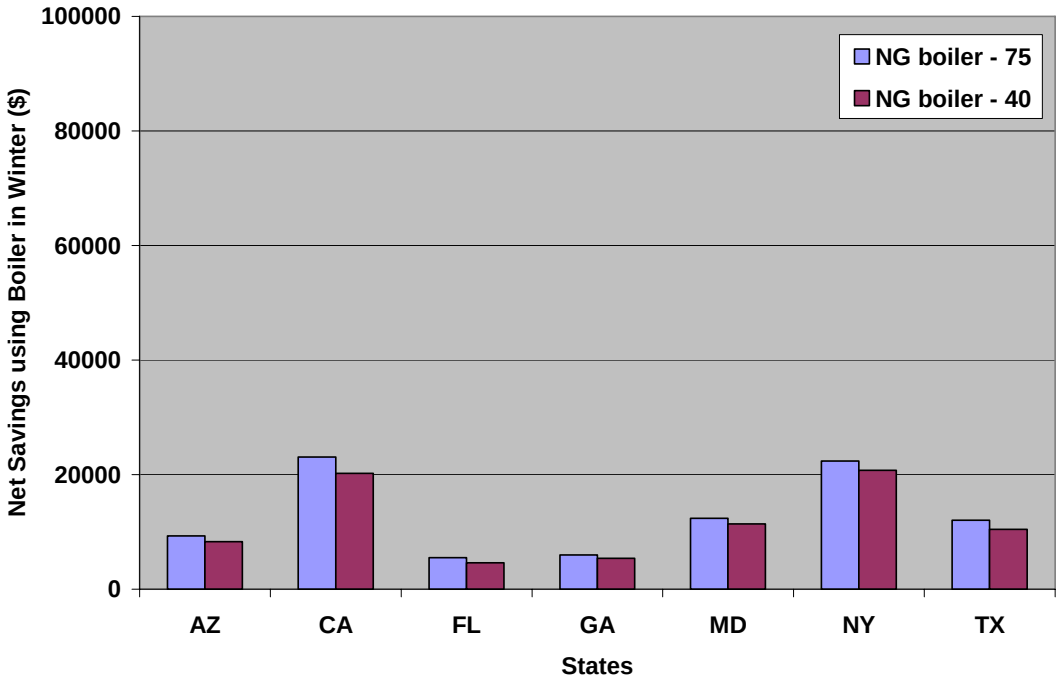

Figure 238: Net Savings for different states using natural gas fired boiler in the winter season

By comparing Figure 237 and Figure 238, it is found that the net savings realized by using the engine generator is always higher than that obtained by using the natural gas boiler since the CHP system provides two useful outputs, the electricity that can be used in the building and the waste heat that can be used for space heating.

Thus it can be concluded from above figures that the net savings achieved varies not only from state to state but also from summer to winter season. Also there can be various ways of operating the CHP system such as running the engine generator at 75 kW in the summer season and 40 kW in the winter season to maximize the total savings in the entire year. Figure 239 shows the total savings achieved in the entire

year 2004 for the different combinations of running the engine generator for the case when the RTU was controlled based on the temperature of the supply air.

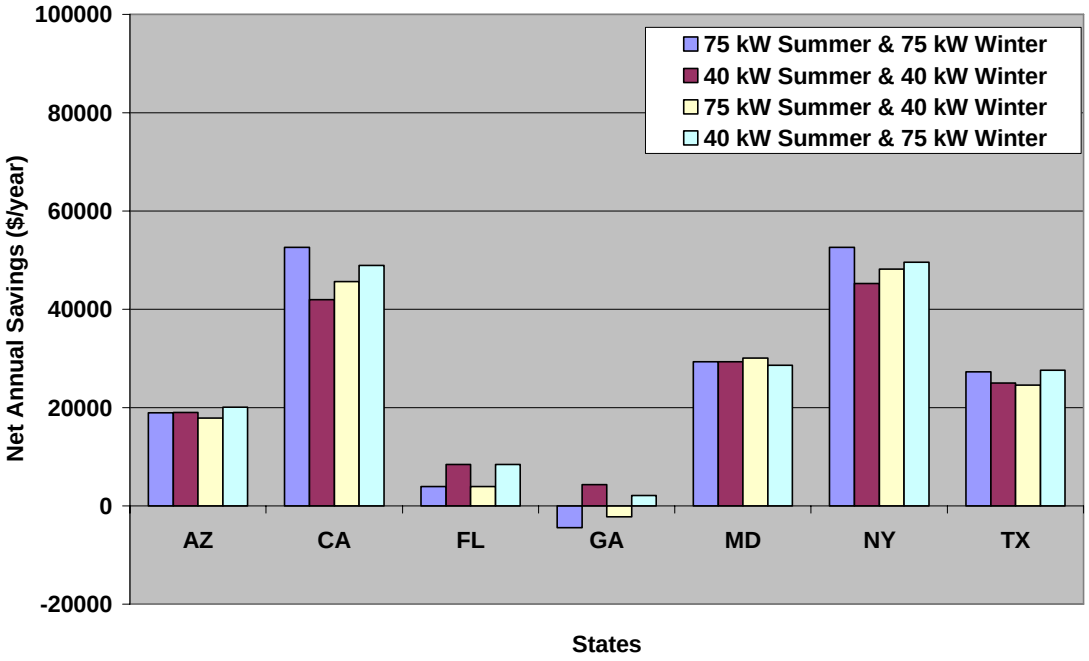

Figure 239: Total Savings achieved in the year 2004 for different engine loads with no humidity ratio control for RTU

By looking at the different combinations in Figure 239, it is found that for the case when the RTU is not controlled by supply air humidity ratio, the combination of running the engine generator at 75 kW both in summer and winter yields more savings in the state of California and New York while in the case of Georgia, the condition where the engine is run at part load of 40 kW in summer and winter is more beneficial. The maximum total savings in this configuration was around $52,633 in the state of California. Figure 240 plots the total annual savings for the year 2004 similar to Figure 239 except that the roof top unit was in this case controlled based on the humidity ratio of the supply air.

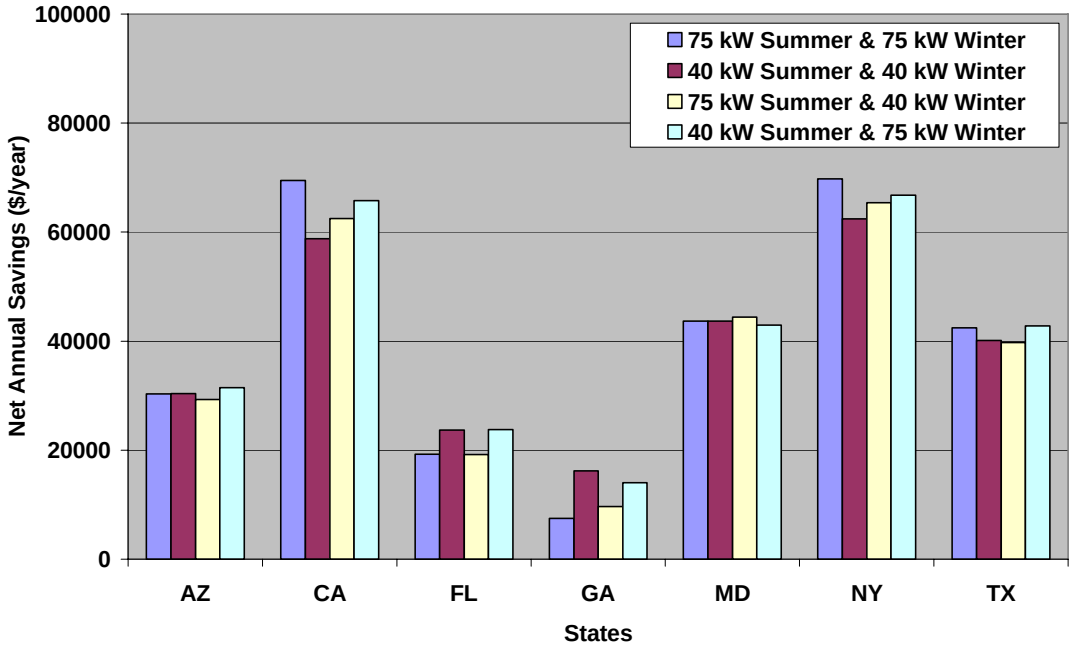

Figure 240: Total Savings achieved in the year 2004 for different engine loads with humidity ratio control for RTU

By comparing Figure 239 and Figure 240, it is seen that the operating the roof top unit based on humidity ratio control along with the CHP system results in significant savings as compared to the case where RTU is controlled by temperature. In this configuration it is found that the maximum savings for the annual year of 2004 was around $69,781 for New York when the engine was run at full load of 75 kW both in summer and winter season as compared to maximum savings of $52,633 in the state of California for the previous case shown in Figure 239.

Based on the total savings obtained in the year 2004 and the capital cost of individual equipments of the CHP system, a simple return on investment (ROI) analysis was done to calculate the payback period for the CHP system in the different states. The payback period for the different states was found out using the following equation,

$$Period_{payback} = \frac{Cost_{CHPSystem}}{Savings_{total}}$$

Where,

$Period_{payback}$ = Payback period for investment in CHP system in years

$Cost_{CHPSystem}$ = Total capital cost of the CHP system

$Savings_{total}$ = Total annual savings

The capital cost of individual equipments was obtained from the respective manufacturers. The capital cost of the engine generator used in the calculations is $65,000 while the cost of the liquid desiccant unit is $60,000. Figure 241 shows the payback periods for the different states and various combinations of engine loads for the case when the RTU is controlled by supply air temperature.

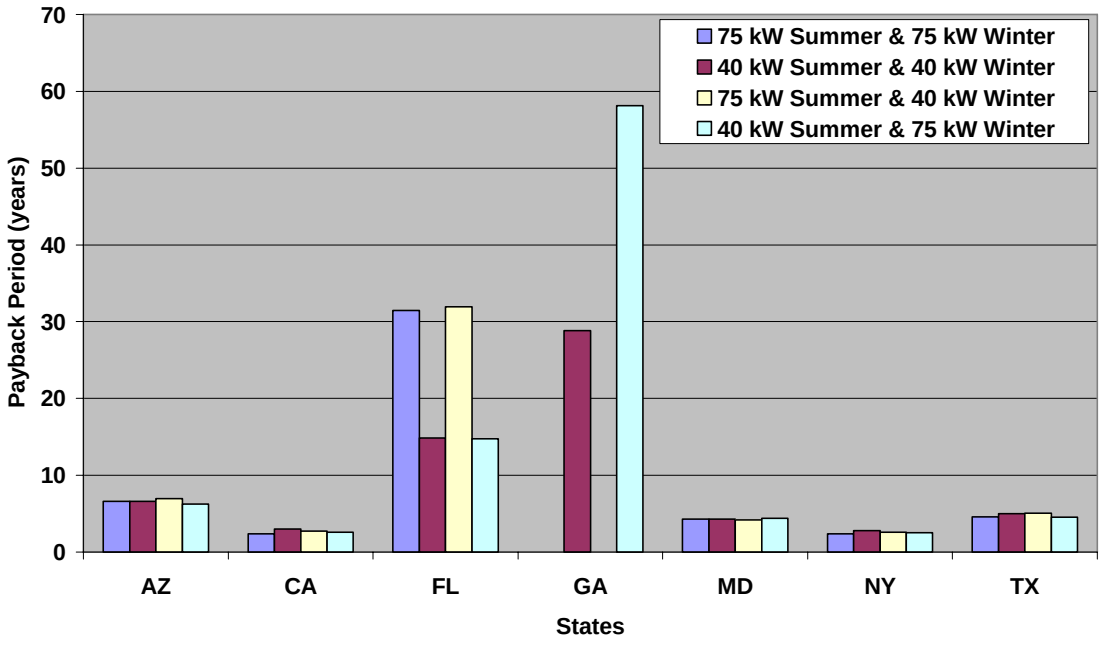

Figure 241: Payback period for different states for RTU without humidity ratio control

It can be seen from Figure 241 that the payback period in this case is around 2 – 3 years in New York and California while the payback period for the state of Georgia is a lot higher. There is no payback periods shown for Georgia for the cases when the engine generator was run at full load of 75 kW in the summer and winter as well as for the case of running the engine at 75 kW in summer and 40 KW in winter due to the fact that there is no savings for those combinations of engine loads since it is much more expensive to run the CHP system and the RTU as compared to running the RTU alone in the baseline system. Table 25 summarizes the payback periods for the different states for all the combinations of operating the engine generator when the RTU does not have humidity ratio control.

Table 25: Payback period for different states for RTU without humidity ratio control and various engine loads

States	75 kW Summer & 75 kW Winter	40 kW Summer & 40 kW Winter	75 kW Summer & 40 kW Winter	40 kW Summer & 75 kW Winter
Arizona	6.59	6.58	6.98	6.23
California	2.37	2.98	2.74	2.55
Florida	31.45	14.86	31.95	14.75
Georgia	-	28.86	-	58.16
Maryland	4.26	4.26	4.16	4.37
New York	2.38	2.76	2.59	2.52
Texas	4.58	5.01	5.08	4.53

The payback period for the various states when the roof top unit was controlled based on the humidity ratio of supply air is shown in Figure 242.

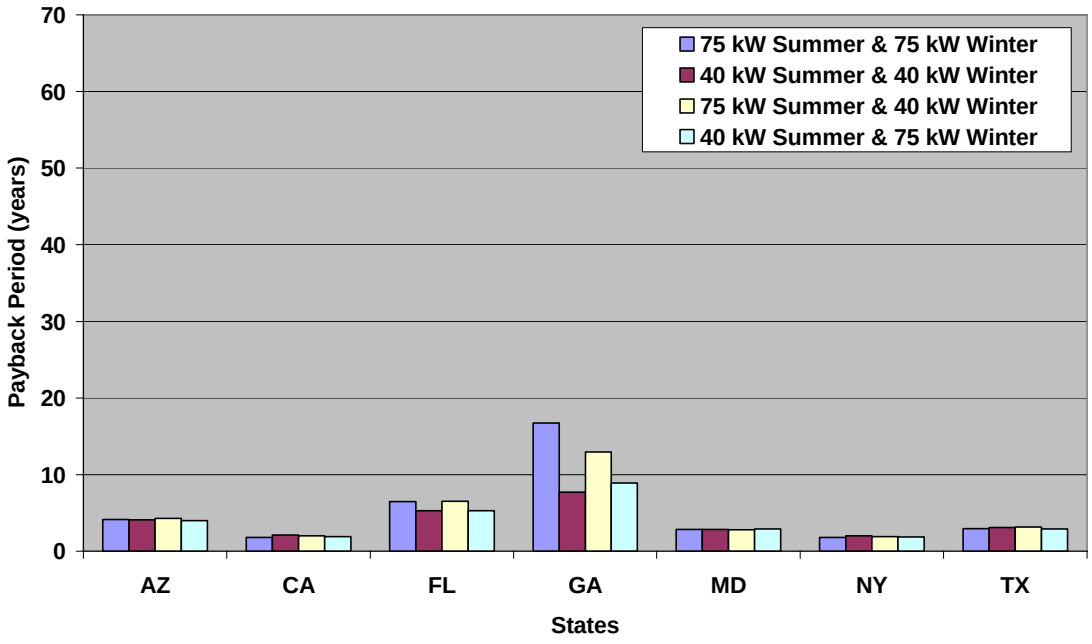

Figure 242: Payback period for different states for RTU with humidity ratio control

It is observed from Figure 242 that minimum payback period is around 1.8 years for the states of New York and California when the engine generator is base loaded at 75 kW in summer and winter season. The minimum payback period in this case for Georgia was found to be around 7.7 years when the engine generator is run at part load of 40 kW for both the heating and cooling season. Table 26 gives the payback period for all the states at different engine loads for the case when RTU is controlled by humidity ratio of supply air.

Table 26: Payback period for different states for RTU with humidity ratio control and various engine loads

States	75 kW Summer & 75 kW Winter	40 kW Summer & 40 kW Winter	75 kW Summer & 40 kW Winter	40 kW Summer & 75 kW Winter
Arizona	4.12	4.12	4.27	3.98
California	1.80	2.13	2.00	1.90
Florida	6.49	5.28	6.51	5.26
Georgia	16.70	7.70	12.93	8.90
Maryland	2.86	2.86	2.82	2.91
New York	1.79	2.00	1.91	1.87
Texas	2.95	3.12	3.14	2.92

Thus it can be concluded from the analysis of the simulation results that for the year 2004, the states of California and New York offered the most favorable conditions for operating the CHP system. Though the CHP system saves some money in the state of Georgia, the payback period is quite higher as compared to New York and California.

The above payback analysis was based on only the capital cost of the equipment. A more detailed economic analysis can be conducted if needed that would include the installation as well as the maintenance costs of the integrated CHP system. The installation cost of the CHP system would vary from region to region

especially the cost of the electrical interconnection since some regions may not require all the relays that were used in this case, at the Chesapeake building.

Chapter 7: Design Guidelines

Based on exhaustive experimental analysis, detailed computer simulation and hands on experience gained through installation, operation and maintenance of the integrated system, valuable design guidelines on the integration and operation of the engine generator – liquid desiccant system are developed and presented in this section.

7.1 Installation and Integration Guidelines

The lessons learned during the installation and setting up of the experimental CHP system is discussed in this section.

The piping between the engine generator heat recovery system and the liquid desiccant system should be kept at a minimum to avoid heat losses in the pipes. As the roof top unit to which the liquid desiccant dehumidification unit was connected was on the roof, the liquid desiccant unit was also installed on the roof. Thus in order to reduce the heat losses in the pipes, the best place for the engine generator was as close to the liquid desiccant unit as possible. However in achieving all the above requirements it is important to do a detailed structural analysis of the existing roof columns as well as the platform on which the engine generator and liquid desiccant unit would be placed. In the case of the Chesapeake building, a structural analysis of the existing platform was done and additional structural beams were welded to the platform for reinforcement.

The design of the heat recovery loop is another key aspect that needs to be addressed during the integration of the engine generator with the liquid desiccant unit. The controls for the heat recovery loop should be designed in such a way that the modifications to the existing equipment are kept at a minimum without compromising the performance of the entire CHP system. Different factors that need to be resolved while finalizing the controls of the heat recovery loop are:

1. The return temperature of the ethyl glycol solution to the engine generator is set at 82 ºC (179 F). This is a critical parameter and this temperature should not be allowed to go too much below 82 ºC (179 F), otherwise there is a possibility of running the engine too cold and eventually damaging the engine.
2. The liquid desiccant unit accepts or rejects heat based on the level of lithium chloride solution in the regenerator. At reduced moisture loads the regenerator cannot use all the heat that the engine supplies it with and care needs to be taken to see that the unit does not over regenerate, otherwise it would result in crystallization of the lithium chloride solution when the outside air humidity falls below design.
3. The maximum pressure drop across the regenerator heat exchanger on the ethyl glycol side needs to be maintained below 2.3 psi according to engine manufacturer's requirements.

Hence the controls of the heat recovery loop are based on the liquid level in the regenerator and the inlet temperature of the ethyl glycol solution to the dump radiator while satisfying the maximum pressure drop requirement.

The operation of the dampers in the outdoor air and exhaust air ducts have to be coordinated such that when the liquid desiccant system is running, the dampers in the process air and return air duct to the cooling tower are open while the respective dampers on the roof top unit are closed and vice versa to maintain the designed amount of air flow through the roof top equipment.

Issues with electrical interconnection to the grid also contribute greatly to the complexity of the CHP installation. The electrical interconnection process was one of the most rigorous, expensive and time consuming part of the experimental installation. Although the Institute of Electronic and Electrical Engineers (IEEE) is examining interconnection standards to facilitate safe and easy connection of CHP to the grid, currently there is no national uniform technical standard for grid interconnection. Typically, grid interconnection is controlled by the utilities and varies from state to state, so CHP installations at one facility may not be the same for another. In addition, interconnection is by and large expensive and often requires additional interconnect studies to be performed prior to commencing the installation such as the short circuit and interconnection study that was conducted before connecting the engine generator parallel to the grid. The disagreements over interconnection requirements result in delays, additional costs and timing uncertainties. For the current CHP system, designing the electrical interconnection was complex and had to include a lot of protective relays and functions in order to meet:

1. Safety of the occupants of the building which was foremost since the system is operated in a real office building with real people working in it.

2.Safety of the existing building electrical infrastructure and the switchgear.

3.Safety of the engine generator and other CHP equipment.

Several important lessons were learnt during the electrical interconnection process that is crucial for safety of the occupants of the building and the building electrical infrastructure, as well as the protection of the engine generator and microturbine. Taking cognizance of the lessons learnt during the installation will considerably reduce the time and expenses for future building engineers and system integrators and help in developing uniform interconnection standards. Some of the aspects that need to be taken care of during the electrical interconnection are:

1. Can one just tap into the main bus bar? The bus bar should be checked for its maximum capacity before connecting additional loads and generators on it.
2. Can the existing switchgear handle two generators that are both connected in parallel?
3. Can two different types of generators run simultaneously at the same time? This was true in this case since both the microturbine and engine generator sense frequency and voltage levels of the utility and then delivers power after matching those levels. So it's important that the two generators don't interfere with each other's operation.
4. A short circuit and interconnection study should be done in advance before material purchase to avoid lead time in procurement of circuit breakers and other essential components. This was done in the current research to find out the interrupting capacities of the two circuit breakers connected to the main

switchboard and to check whether the selected circuit breakers faulted at the right fault levels of current and voltage.

During the installation of the engine generator, all of the above issues were resolved together with the university facilities management personnel, the utility company, switchgear supplier and microturbine and engine generator manufacturers.

7.2 Operation Guidelines

There are different possible options of operating the integrated engine generator – liquid desiccant system that depend on various factors like ambient conditions as well as on fluctuating electricity and natural gas prices. The operation guidelines outlined in this section are based on the results obtained through extensive computer simulation.

The roof top unit should be operated and controlled based on the humidity ratio of the supply air rather than its temperature since it's the most energy efficient way and results in maximum savings.

For states like California and New York which have moderate weather and higher electricity prices as compared to natural gas rates, the engine generator should be base loaded throughout the year during the summer and winter season to get maximum savings and higher return on investment.

In states where the natural gas prices are quite high such as the state of Georgia, the engine generator should not be base loaded since it is actually cheaper to run the roof top unit on electricity. In such an event, the engine generator should be operated

at part load of 40 kW both in summer and winter season and the savings would be realized in the cooling season only when the RTU is controlled by supply air humidity ratio.

If a commercial office building already has a hydronic water loop for heating purposes in place, then it becomes much easier for retrofitting and integrating the CHP system at lower initial costs. This also facilitates the use of the engine generator waste heat for space heating resulting in higher number of operating hours for the engine generator and hence more savings. In the heating season too, for states like California and New York, where the electricity prices are high, the engine generator should be run at full load of 75 kW to get higher heat output and lower payback periods. In states where the price of natural gas is very high like Georgia, it is more economical to run the engine generator at part load of 40 kW in the heating season to get higher return on investment.

Chapter 8: Conclusions

8.1 Summary of Accomplishments

The major accomplishments and distinguishing contributions of this research are as follows:

1. A complete first-of-its-kind CHP system consisting of a 75 kW reciprocating engine generator and a 3000 cfm liquid desiccant dehumidification system was designed, built and integrated into a fully occupied commercial office building infrastructure.
2. A novel method of integrating the liquid desiccant dehumidification with conventional building HVAC equipment along with the required damper controls was presented in this research for the first time.
3. The efficient application of combined waste heat recovered from jacket water as well as exhaust gases from reciprocating engines for regeneration of liquid desiccants was demonstrated.
4. A comprehensive thermodynamic and economic model that was validated with experimental results was developed which can be used as an evaluation or screening tool by facility owners, equipment operators or design engineers to assess the viability of the integrated CHP system under different scenarios of varying weather conditions and fluctuating energy prices.
5. Based on exhaustive experimental analysis, detailed computer simulation and hands on experience gained through installation, operation and maintenance of

the integrated system, valuable design guidelines on the integration and operation of the integrated engine generator – liquid desiccant system are formulated and presented in this research.

6. Key areas for performance improvement of the integrated CHP system were identified through this research. One of the improvements suggested is the increase in the net electrical efficiency of reciprocating engine generators. It was found that the CHP system 1 consumes more in terms of primary energy consumption as compared to the combined cycle power plant and this is because the electrical efficiency of the engine generator was only around 31 % as compared to a combined cycle power plant efficiency of 41 %. This electric efficiency has to be increased for engine generator based CHP systems to compete with combined cycle power plants in the future. There is significant research currently being sponsored by the US Department of Energy (US DOE) in this direction through the Advanced Reciprocating Engine System (ARES) program. Launched in 2001, the ARES' goals for advanced gas engines include a thermal efficiency of 50 %, NO_x emissions of 0.1 g/bhp-hr, installed capital cost of US $400 to $450 per kWe and maintenance costs of $0.01 per kWe-hr while maintaining the current engine reliability. The other area by which performance of the system can be improved is through the reduction of parasitic electrical power. If the parasitic electrical power consumption is reduced, then the net electrical power available from the engine generator would be more for the same amount of natural gas combusted resulting in greater benefits from the integrated CHP system.

7. Finally this research provides a great deal of useful information for promotion of the integrated CHP system in commercial market based on
    a. Valuable operating experience and integration challenges in a real office building.
    b. Performance characterization of the integrated CHP system through extensive data analysis.

8.2 Conclusions

The research presented here investigates the integrated engine generator – liquid desiccant CHP system in commercial building applications by designing and building a fully integrated CHP system installed in a fully occupied commercial office building. A comprehensive characterization of the performance of the CHP system consisting of the engine generator and liquid desiccant system was conducted through extensive data analysis. It was found that the electrical efficiency of the engine generator was affected by ambient air temperatures though not as severely as in the case of a gas turbine. It was seen from experimental results that the electrical efficiency of the engine generator at full load of 75 kW decreased from about 32 % to around 30 % as outdoor air enthalpy increased from 12 kJ/kg to 46 kJ/kg. The engine generator was also tested at different part loads both in summer and winter season and engine performance curves were developed through experimental analysis (page no. 130). It was found that the net electrical efficiency decreased from about 32 % at 75 kW to around 24 % at 40 kW. An interesting aspect of the integrated CHP system that was observed from experimental results was that the CHP efficiency of the system

actually is higher at part load than at full load as compared to the electrical efficiency which is greater at base load than part load. The CHP efficiency varied from 66 % at 75 kW to about 75 % at 40 kW. Following the performance characterization, a comparison based on primary energy consumption between the CHP system, conventional power plant and state of the art combined cycle power plant was done. It was found that the integrated CHP system consumes 16.3 % less in primary energy as compared to a conventional power plant. However it consumed 15.3 % more in primary energy than a combined cycle power plant.

A comprehensive thermodynamic and economic model was built using Visual Basic.Net and was validated using the experimental data. The simulation results were found to be in good agreement with the experimental data and the deviation was within ± 6 %. Based on simulation results it was observed that in places like California and New York, maximum savings can be achieved when the engine generator is base loaded at 75 kW while in states like Georgia where the natural gas prices are too high, the engine generator should be run at part load of 40 kW. Various integration options of the liquid desiccant unit with the roof top unit were analyzed and it was observed that the most economic and energy efficient option for a commercial office building was to use the liquid desiccant system to dehumidify the outdoor air since it's the most humid of all the three air streams. Also the liquid desiccant unit has to handle a lower air flow rate that reduces the size and cost of the LDU. From simulation results, it was found that the most energy efficient way to operate the roof top unit is to control its operation based on the humidity ratio of supply air rather than its temperature. Lower payback periods were realized when the

waste heat of the engine was utilized to displace electricity for space heating in the building. Finally design guidelines for the integration and operation of the integrated CHP system are developed from the experimental and simulation analysis that would allow future building design engineers and system integrators to make better decisions about installing CHP systems.

8.3 Future Work

The following items are suggested to be addressed in a continuation of the work presented in this research.

To gain a comprehensive understanding of the energy and economic benefits of the integrated CHP system in commercial facilities, a similar investigation should be undertaken in facilities other than office buildings such as hospitals and hotels. This is important since the heating and cooling load profiles are vastly different depending on the use of each facility.

Besides providing energy savings and possible cost savings, the integrated CHP system can provide a reduction in emissions as compared to conventional coal burning power plants. An investigation of the environmental effects of the CHP system can be worthwhile especially when coupled with incentives or programs that offer emission credits.

It was observed from experimental performance measurements that the parasitic electrical power consumed by the auxiliaries such as the pumps and fans in the integrated CHP system is quite high. A study of the different ways to reduce the parasitic electrical consumption would be useful since the net electrical power

available from the engine generator would be more for the same amount of natural gas combusted resulting in greater benefits from the integrated CHP system.

A new low flow conditioner was retrofitted to the existing liquid desiccant unit in late summer 2005. The new conditioner is completely different in design and has a much lower flow rate of liquid desiccant solution than the original conditioner. A performance comparison between the old and new conditioner can be evaluated in the next cooling season.

An investigation into the transient effects of CHP components can provide a better insight into how different components behave and interact with each other in an integrated system.

Appendix A: Uncertainty Analysis

This section describes the magnitude of uncertainty for experimental results presented in this dissertation arising from uncertainties in the sensors used in the experimental setup. Table 27 shows the instrumentation used in the experimental work along with the associated error for each sensor.

Table 27: Instrumentation and Sensor Error

Measurement/Sensor	Error
Heat recovery loop glycol temperature sensor (Minco)	± 1 ºC
Glycol mass flow rate sensor (Omega)	± 2 %
Natural gas flow rate sensor (American Meter Company)	± 1 %
Air temperature sensor (Vaisala)	± 0.3 ºC
Air relative humidity sensor (Vaisala)	± 2 %

Precision Error

The total uncertainty of a measurement due to the uncertainty of individual parameters is referred to as the propagation of uncertainty (Beckwith et al. 1993). Also referred to as precision, the total uncertainty of any function may be calculated using the Pythagorean summation of uncertainties which is defined as (Kline et al. 1959):

$$u_F = \sqrt{\left(\frac{\partial F}{\partial v_1} * u_1\right)^2 + \left(\frac{\partial F}{\partial v_2} * u_2\right)^2 + \left(\frac{\partial F}{\partial v_3} * u_3\right)^2 + \ldots + \left(\frac{\partial F}{\partial v_n} * u_n\right)^2}$$

Where,

u_F = uncertainty of the function

u_n = uncertainty of the parameter

F = function

v_n = parameter of interest (measurement)

n = number of variables

The partial derivatives of each independent measurement in the parameters were calculated using the uncertainty propagation function in the Engineering Equation Solver (EES) and applied within the program to the root mean square outcome.

Figure 243 shows the plot of the electrical efficiency of the engine generator at 75 kW along with the uncertainty involved in its calculation due to the uncertainties of measured variables. It is found that calculated value of electrical efficiency has an uncertainty of ± 0.2887 %.

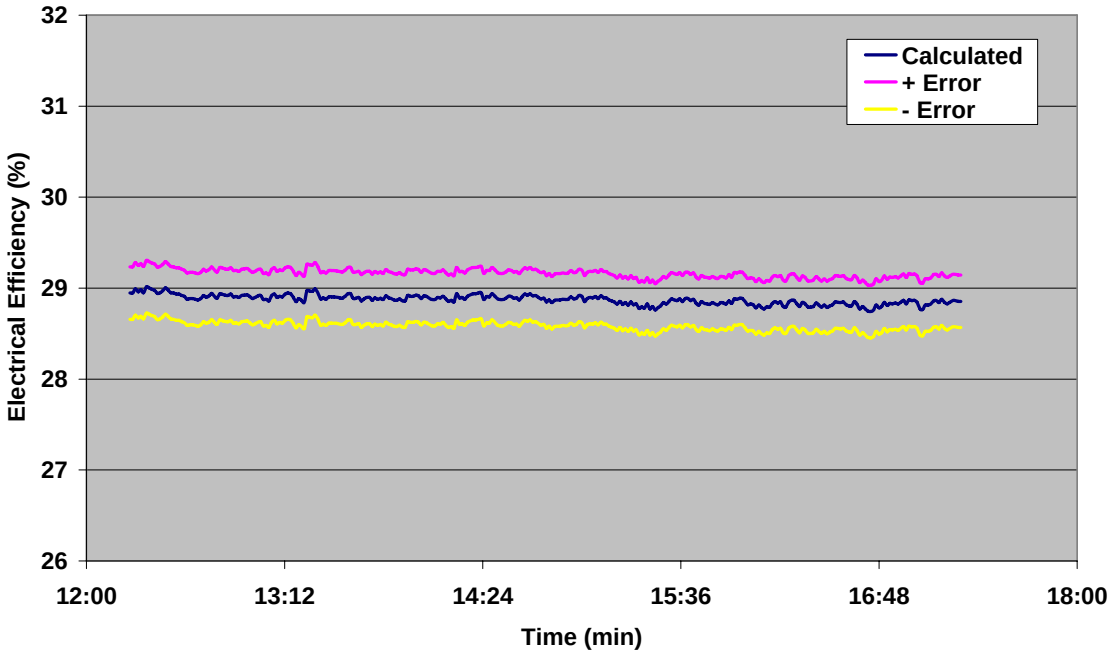

Figure 243: Uncertainty in calculated electrical efficiency of engine generator at 75 kW

Figure 244 plots the calculated value of the total thermal COP of the liquid desiccant system along with its uncertainty based on the accuracy of the different sensors used in measuring the temperature, relative humidity of air etc. It is seen from Figure 244 that the uncertainty in the total thermal COP of the liquid desiccant system is ± 0.06855.

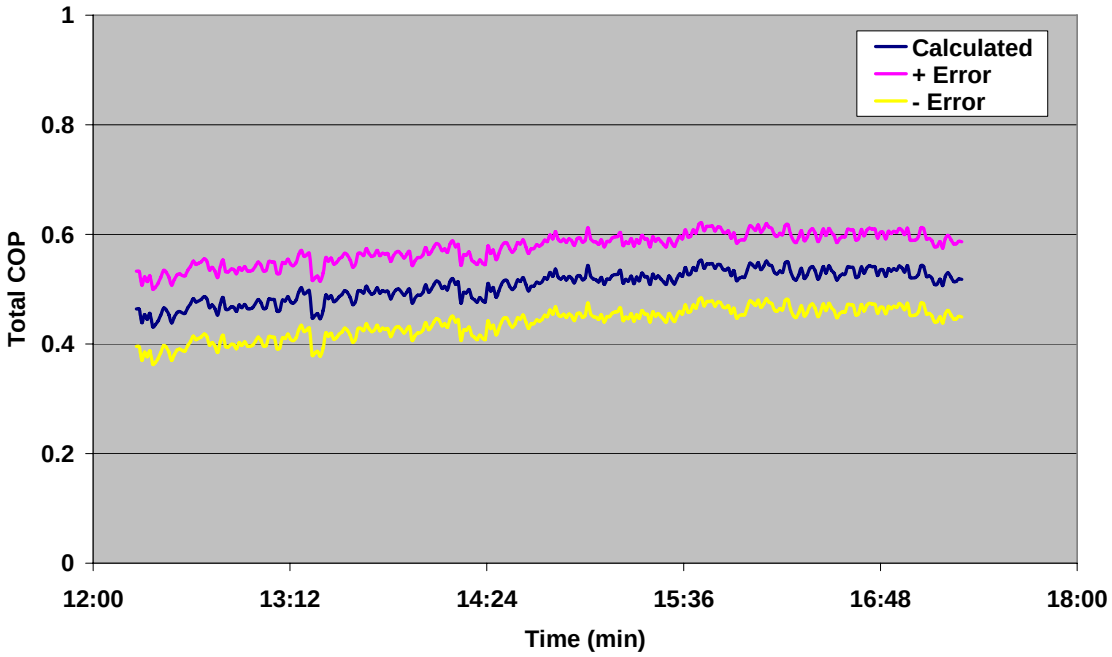

Figure 244: Uncertainty in calculated total thermal COP of liquid desiccant system

Appendix B: CHP Efficiency Definitions

The following different types of CHP efficiency definitions were covered by Petrov, A et al in their paper titled "Evaluation of Different Efficiency Concepts of an Integrated Energy System (IES)".

The first category of CHP efficiency is called as the overall efficiency which is defined as the ratio of the sum of net electrical power output and total useful heating/cooling/latent output from thermally activated technology (TAT) devices to the fuel input (based on HHV or LHV of the fuel such as natural gas):

$$\eta_{overall} = \frac{W_{el} + \sum Q}{Q_{in}}.100$$

or including electrical parasitics of all TAT devices of the current IES arrangement by adding them to the heat input:

$$\eta_{overall} = \frac{W_{el} + \sum Q}{Q_{in} + \sum W_{par}}.100$$

or subtracting them from the net electrical output:

$$\eta_{overall} = \frac{\left(W_{el} - \sum W_{par}\right) + \sum Q}{Q_{in}}.100$$

Where,

η = efficiency of IES

Q = fuel or energy input, TAT useful output

W = electrical power output, parasitics

The second type of CHP efficiency is the fuel utilization efficiency which is defined as the ratio of the net electrical power output to the net fuel input. The net fuel input is obtained by subtracting the fuel input that is used to produce useful heating/cooling/latent output, at a given TAT device efficiency, from the total fuel input:

$$\eta_{fuel-ut} = \frac{W_{el}}{Q_{in} - \Sigma\left(\frac{Q}{\eta}\right)}.100$$

or including electrical parasitics of all TAT devices of the current IES arrangement by adding them to the heat input:

$$\eta_{fuel-ut} = \frac{W_{el}}{Q_{in} + W_{par} - \Sigma\left(\frac{Q}{\eta}\right)}.100$$

or subtracting them from the net electrical output:

$$\eta_{fuel-ut} = \frac{\left(W_{el} - \Sigma W_{par}\right)}{Q_{in} - \Sigma\left(\frac{Q}{\eta}\right)}.100$$

Another way of expressing the CHP efficiency of an IES is through fuel energy savings efficiency which reflects fuel savings associated with IES power generation as compared to the use of separate heating/cooling/latent and electric power sources:

$$\eta_{fuel-sav} = \left(1 - \frac{Q_{in}}{\frac{W_{el}}{\eta_{typ-el}} + \Sigma\left(\frac{Q}{\eta_{typ-th}}\right)}\right).100$$

Where,

η_{typ-el} = typical average electric grid efficiency

η_{typ-th} = typical average TAT device efficiency

or including electrical parasitics of all TAT devices of the current IES arrangement by adding them to the heat input:

$$\eta_{fuel-sav} = \left(1 - \frac{Q_{in} + \sum W_{par}}{\frac{W_{el}}{\eta_{typ-el}} + \sum \left(\frac{Q}{\eta_{typ-th}} \right)} \right) .100$$

or subtracting them from the net electrical output:

$$\eta_{fuel-sav} = \left(1 - \frac{Q_{in}}{\frac{\left(W_{el} - \sum W_{par} \right)}{\eta_{typ-el}} + \sum \left(\frac{Q}{\eta_{typ-th}} \right)} \right) .100$$

The CHP efficiency can also be defined as economic efficiency which is the modified version of the overall efficiency to account for economic values of fuel input ($\$_{in}$), net electrical power output ($\$_{el}$) and useful heating/cooling/latent output ($\$_{th}$):

$$\eta_{econ} = \frac{W_{el}.\$_{el} + \sum (Q.\$)}{Q_{in}.\$_{in}} .100$$

or including electrical parasitics of all TAT devices of the current IES arrangement by adding them to the heat input:

$$\eta_{econ} = \frac{W_{el}.\$_{el} + \sum(Q.\$)}{Q_{in}.\$_{in} + \sum\left(W_{par}.\$_{el}\right)}.100$$

or subtracting them from the net electrical output:

$$\eta_{econ} = \frac{\left[\left(W_{el} - \sum W_{par}\right).\$_{el}\right] + \sum(Q.\$)}{Q_{in}.\$_{in}}.100$$

References

1. Peng, S., 1982, “Analysis and Simulation of an Efficient Liquid Desiccant System for Warehouse Dehumidification”, ASHRAE Transactions, Vol. 88, pp. 1097 – 1112.
2. Szklo, S., Scares, B. and Tolmasquim, T., 2004, “Energy consumption indicators and CHP technical potential in the Brazilian hospital sector”, Energy Conversion and Management, Vol. 45, No.13-14, pp. 2075 - 2091.
3. Ahmed, S., Gandhidasan, P. and Al-Farayedhi, A., 1998, “Thermodynamic Analysis of Liquid Desiccants”, Solar Energy, Vol. 62, No. 1, pp. 11 – 18.
4. Nayak, S. Ray, S. and Radermacher, R., 2004, “Second Generation Integrated Combined Heat and Power Engine Generator and Liquid Desiccant System”, Proceedings of 2004 ASME International Mechanical Engineering Congress, Anaheim, California, USA.
5. Marantan, A., Popovic, P. and Radermacher, R., 2002, “The Potential of BCHP Technology in Commercial Buildings – Characterizing the BCHP Demonstration Building”, ASHRAE symposium on CHP Technologies for the New Century, ASHRAE Transactions, Vol.108, Pt.1.
6. Burdon, P., 1998, “CHP planning for Newcastle upon Tyne”, Engineering Science and Education Journal, Vol. 4, pp. 171 – 176.
7. Williams, M., Griffiths, J. and Knight, P., 1996, “Combined heat and power: sizing plant for new hospitals”, Proceedings of the Chartered

Institution of Building Services Engineers (Building Services Engineering Research and Technology), Vol.17, No.3, pp. 147 - 152.

8. Cowie, M., Marantan, A., Garland, P. and Radermacher, R., 2002. "CHP for Buildings – The Challenge of Delivering Value to the Commercial Sector", Proceedings of the International Mechanical Engineering Congress and Exposition Emerging and New Technologies for Heat Pump and Refrigeration Cycles and CHP (Combined Cooling, Heating and Power), New Orleans, LA.
9. Hanitsch, R. and Bleyl, W., 1995, "CHP combined heat and power-a way to improve energy efficiency", Proceedings of 30th Universities Power Engineering Conference, London, UK, Vol.1, pp. 33 – 36.
10. Nayak, S. and Radermacher, R., 2004, "CHP for Buildings: Integration of a 75 kW Engine Generator with Liquid Desiccant System", Improving Energy Efficiency in Commercial Building Conference (IEECB'04), Frankfurt, Germany.
11. Jackson, T., 1988, "Small-scale CHP: a test case for private generation", Proceedings of Renewable Energy Sources for the 21st Century International Conference, Bristol, UK, pp. 87 - 94.
12. Alton, J., 1987, "Hospitals take on combined heat and power in the energy battle", Electrical India, Vol. 27, No. 20, pp. 15 - 17.
13. Jackson, T., 1987, "Non-stop running gives CHP an edge", Heating and Air Conditioning Journal, No. 661, pp. 23 - 24.

14. Jafari, R., 2002, “Cogeneration plant for National Institutes of Health”, 2002 IEEE Industrial and Commercial Power Systems Technical Conference, NJ, USA, pp. 14-16.
15. Evans, B., 1995, “CHP for Small Schemes: Design Considerations”, H & V Engineer, Vol.62, pp. 13 - 18.
16. Kuehn, E., 1993, “Technology advances boost reciprocating engine efficiency”, Power Engineering, Vol. 97, No. 2, pp. 30 - 33.
17. Lee, H., 1987, “A sample of cogeneration system in a hospital”, Refrigeration, Vol. 62, pp. 274 - 292.
18. Leijendeckers, H., Peters, M., and Liebeek, A., 1971, “The first 420-bed total energy hospital”, Proceedings of conference on total energy, London, UK, pp. 263 - 278.
19. Schaaf, H., 1998, “Gas Engines for Bank Building (CHP)”, Diesel & Gas Turbine Worldwide, Vol. 30, pp. 40 – 42.
20. Marantan, A., 2002, “Optimization of Integrated Microturbine and Absorption Chiller Systems in CHP for Buildings Applications”, Ph.D. Thesis, University of Maryland, College Park, Maryland, USA.
21. Smith, M., Few, P. and Twidell, J., 1995, “Technical and Operational Performance of a Small – Scale, Combined Heat and Power (CHP) Plant”, Energy, Vol. 20, No. 12, pp. 1205 – 1214.
22. Packer, J. and Woodworth, M., 1991, “Advanced Package CHP Unit for Small Scale Operation”, Power Engineering Journal, pp. 135 – 142.

23. Maidment, G. and Prosser, G., “The use of CHP and absorption cooling in cold storage”, Applied Thermal Engineering, Vol. 20, No.12, pp. 1059 - 1073.
24. Tassou, A. and Leung, K., 1992, “Energy conservation in commercial air conditioning through ice storage and cold air distribution design”, Heat Recovery Systems & CHP, Vol.12, No.5, pp. 419 - 425.
25. Epler, K., 2004, “Distributed Generation Systems to the Rescue”, Distributed Energy.
26. Babus'Haq, F., Pearson, P., Probert, D. and O'Callaghan, W., 1990, “Economics of mini-combined heat and power packages for use in hotels”, Heat Recovery Systems & CHP, Vol.10, No.3, pp. 269 - 275.
27. Nakazaki, Y., Mizuguchi, K., Okada, R. and Shimizu, R., 1991, “Co-generation System Using a Gas Engine Generator for Telecommunications Power Plants”, Proceeedings of INTELEC’91, pp. 374 – 378.
28. Brown, S., 1996, “Single-site and industrial-scale schemes [CHP]”, Applied Energy, Vol.53, pp. 149 - 155.
29. Lahdelma, R. and Hakonen, H., 2003, “An efficient linear programming algorithm for combined heat and power production”, European Journal of Operational Research, Vol. 148, pp. 141 – 151.
30. Uszkat, M. and Szargut, J., 2004, “Simulation analysis of a repowered double fuel CHP plant including a nonevaporative heat recovery boiler”, International Journal of Energy Research, Vol.28, No.8, pp. 661 - 682.

31. Marbe, A., Harvey, S. and Berntsson, T., 2004, “Biofuel gasification combined heat and power-new implementation opportunities resulting from combined supply of process steam and district heating”, Energy, Vol.29, No.8, pp. 1117 - 1137.
32. Casten, R., 2003, “Combined heat and power: recycling energy”, Power Engineering, Vol.107, No.9, pp. 26 - 30.
33. Ashmore, C., 2003, “Roche chemical adding turbomach 32MW combined cycle cogen plant”, Gas Turbine World, Vol.33, No.3, pp. 20 - 24.
34. Liszka, M., Manfrida, G. and Ziebik, A., 2003, “Parametric study of HRSG in case of repowered industrial CHP plant”, Energy Conversion and Management, Vol.44, No.7, pp. 995 - 1012.
35. Cormio, C., Dicorato, M., Minoia, A. and Trovato, M., 2003, “A regional energy planning methodology including renewable energy sources and environmental constraints”, Renewable & Sustainable Energy Reviews, Vol.7, No.2, pp. 99 - 130.
36. Mouri, K., 2003, “Overview of the recent Japanese power industries and distributed resources”, Proceedings of the ICOPE-03, International Conference on Power Engineering - 03, Tokyo, Japan, pp. 1 - 30.
37. Hepbasli, A. and Ozalp, N., 2002, “Co-generation studies in Turkey: an application of a ceramic factory in Izmir, Turkey”, Applied Thermal Engineering, Vol.22, No.6, pp. 679 - 691.
38. Hepbasli, A. and Ozalp, N., 2002, “Development of cogeneration in Turkey”, Energy Sources, Vol.24, No.3, pp. 195 - 204.

39. Liao, X., 2004, “The Development of an Air-Cooled Absorption Chiller Concept and its Integration in CHP Systems”, Ph.D. Thesis, University of Maryland, College Park, Maryland, USA.
40. Hepbasli, A. and Ozalp, N., 2002, “Present status of cogeneration applications in Turkey”, Energy Sources, Vol.24, No.2, pp. 169 - 177.
41. Bonilla, D., Akisawa, A. and Kashiwagi, T., 2002, “The adoption of cogeneration in the Japanese manufacturing sector: technological, economic and institutional determinants”, International Journal of Energy Technology and Policy, Vol.1, pp. 181 - 196.
42. Donne, S., Pike, W. and Savry, R., 2001, “Application of modern methods in power plant simulation and control”, Computing & Control Engineering Journal, Vol.12, No.2, pp. 75 - 84.
43. Soares, B., Szklo, S. and Tolmasquim, T., 2001, “Incentive policies for natural gas-fired cogeneration in Brazil's industrial sector-case studies: chemical plant and pulp mill”, Energy Policy, Vol.29, No.3, pp. 205 - 215.
44. Sengul, M., Ozturk, S. and Yorukeren, N., 2001, “Modeling and simulation of the combined heat and power plant of a real industrial system”, Proceedings of the IASTED International Conference Modeling, Identification, and Control. Anaheim, CA, USA, pp. 615 - 619.
45. Axelsson, H., Asblad, A. and Berntsson, T., 1999, “A new methodology for greenhouse gas reduction in industry through improved heat exchanging and/or integration of combined heat and power”, Applied Thermal Engineering, Vol.19, No.7, pp. 707 - 731.

46. Illerhaus, W. and Verstege, F., 1999, “Optimal operation of industrial CHP-based power systems in liberalized energy markets”, Proceedings of 1999 PowerTech Conference. Budapest, Hungary.
47. Varley, J., 1998, “All together now at the MIDER refinery power plant”, Modern Power Systems, Vol.18, No.6, pp. 37 - 39.
48. Rogers, S., 1998, “Grid connection of embedded CHP plants”, Proceedings of IEE Colloquium on Developments in Combined Heat and Power into the Millennium, Glasgow, UK, pp. 1 - 11.
49. Puigjaner, L., 1997, “Process integration with combined heat and power (CHP)”, Applied Thermal Engineering, Vol.17, pp. 1015 - 1034.
50. Grewal, S., Konowalec, W. and Hakim, M., 1997, “Optimization of load shedding scheme in an integrated process plant”, Proceedings of 1997 IEEE Industrial and Commercial Power Systems Technical Conference, Philadelphia, PA, USA, pp. 96 - 101.
51. Dubois, J. and Jolivot, D., 1997, “Combined heat and power production. Industrial development”, Proceedings of 14th Biennial International Conference and Exhibition on Electricity Distribution (Distributing Power for the Millennium). Birmingham, UK, Vol.5, pp. 1 – 5.
52. Mansour, M. and Davidson, C., 1996, “A unique cogeneration application in a large pulp mill electrical system”, Annual Pulp and Paper Industry Technical Conference. Birmingham, AL, USA, pp. 256 - 262.
53. Fulton, K., 1996, “New Czech and Slovak designs from 1000 to 4100 kW in power output”, Gas Turbine World, Vol.26, No.4, pp. 26 - 30.

54. Mathis, R., 1996, “Construction and operation of a biomass-fired combined heat and electric power plant”, Elektrotechnik und Informationstechnik, Vol.113, No.9, pp. 616 - 623.
55. Mohanty, B. and Panda, H., 1995, “Integrated energy system for industrial complexes. Part II. A case study using the LP model”, Applied Energy, Vol.51, No.1, pp. 19 - 38.
56. Nayak, S., Radermacher, R., Moran, D. and Garland, P., 2005, “Performance Evaluation of a Reciprocating Engine Based CHP System for Commercial Office Building”, Proceedings of International Sorption Heat Pump Conference, Denver, Colorado, USA.
57. Stromberg, J. and Franck, A., 1994, “Gas turbines in industrial CHP applications-assessment of economics”, Heat Recovery Systems & CHP, Vol.14, No.2, pp. 129 - 141.
58. Brandemuehl, M. and Katejanekarn, T., 2000, “Dehumidification Characteristics of Commercial Building Applications”, Interim Report submitted to ASHRAE 1121-RP.
59. Hedman, B., 2000, “The Market and Technical Potential for Combined Heat and Power in the Commercial/Institutional Sector”, Onsite Sycom Energy Corporation Report.
60. Hedman, B., 2000, “The Market and Technical Potential for Combined Heat and Power in the Industrial Sector”, Onsite Sycom Energy Corporation Report.

61. Cowie, M. Liao, X. and Radermacher, R., 2003. “Performance Comparison of Waste-Heat Driven Desiccant Systems”, ASHRAE Annual Meeting, Kansas City, Kansas, USA.
62. Blok, K. and Turkenburg, C., 1994, “CO_2 emission reduction by means of industrial CHP in the Netherlands”, Energy Conversion and Management, Vol.35, No.4, pp. 317 - 340.
63. Stromberg, J., Franck, A. and Berntsson, T., 1993, “Consequences of recent gas turbine developments for industrial CHP applications”, Heat Recovery Systems & CHP, Vol.13, No.3, pp. 219 - 231.
64. Lowenstein, A., Slayzak, S., Ryan, J. and Pesaran, A., 1998, “Advanced Commercial Liquid-Desiccant Technology Development Study”, National Renewable Energy Laboratory Report.
65. Mahi, P., 1993, “Environmental assessment of combined heat and power projects”, IEE Proceedings A (Science, Measurement and Technology), Vol.140, No.1, pp. 29 - 39.
66. Rossiter, P., 1990, “Criteria for integration of combined cycle cogeneration systems in the process industries”, Heat Recovery Systems & CHP, Vol.10, No.1, pp. 37 - 48.
67. Haywood, D., 1989, “Large-scale combined heat and power”, Proceedings of the Institution of Mechanical Engineers, Part A (Journal of Power and Energy), Vol.204, No. A1, pp. 67 - 75.

68. Cowie, M., 2002, “Characterizing Combined Cooling, Heating and Power for Buildings Systems through Theory and Testing”, Masters Thesis, University of Maryland, College Park, Maryland, USA.
69. Backlund, L and Karlsson, G., 1988, “Cogeneration versus industrial waste heat”, Heat Recovery Systems & CHP, Vol.8, No.4, pp. 333 - 341.
70. Evans, H., 1986, “The application of small-scale CHP units for reducing the energy costs of industrial systems”, International Conference on Industrial Power Engineering, pp. 65 - 67.
71. Chellini, R., 1984, “CHP meets energy demand of a large papermill”, Diesel & Gas Turbine Worldwide, Vol.16, No.6, pp. 36 - 37.
72. Stambler, I., 1985, “See 3-year payback for 8-MW CHP peaking plant”, Gas Turbine World, Vol.15, No.1, pp. 23 - 26.
73. Nash, F., 1983, “NEI-A.P.E. develops a diesel engine CHP system”, APE Engineering, pp. 5 - 11.
74. Wollacott, G., 1983, “Industrial CHP: prospects and developments”, Proceedings of Local Heat and Power Generation: A New Opportunity for British Industry, St. Helier, Jersey, UK, pp. 11 - 38.
75. Pagano, R., Sgandurra, F. and Delpiano, R., 1981, “TOTEM (total energy module). A high efficiency system for generating electricity and heat”, International Conference on Control of Industrial Processes. Milan, Italy, pp. 199 - 215.
76. Klingenberger, U., 2002, “Modeling and Analysis of Solid and Liquid Desiccant Systems in CHP for Buildings Applications”, Masters Thesis,

University of Applied Sciences Offenburg, Germany, University of Maryland, College Park, Maryland, USA.

77. Cleugh, B., 1980, "Economics of commercial and industrial CHP-a simplified approach", Proceedings of IEE Colloquium on Combined Heat and Electrical Power-the Way Forward, London, UK, pp. 1 - 14.
78. Rodrigues, M. and Cavanna, J., 1979, "Optimisation of combined heat and power schemes on industrial sites with complex energy patterns", Energy for industry, Oxford, UK, Pergamon, pp. 207 - 222.
79. Kathabar Systems Inc., "Application Manual for Kathapac Dehumidification".
80. Jansen, A., 1979, "Combined electricity and heat generation in dairy industry", Energy Meeting on Industrial Processes-Energy Conservation R&D, Brussels, Belgium, pp. 507 - 519.
81. Maidment, G., Zhaob, X, and Riffatb, S., 2001, "Combined cooling and heating using a gas engine in a supermarket", Applied Energy, Vol. 68, No. 4, pp. 321 – 335.
82. Maidment, G. and Tozer, M., 2002, "Combined cooling heat and power in supermarkets", Applied Thermal Engineering, Vol.22, No.6, pp. 653 - 665.
83. Maidment, G., Zhao, X., Riffat, B. and Prosser, G., 1999, "Application of combined heat-and-power and absorption cooling in a supermarket", Applied Energy, Vol.63, No.3, pp. 169 - 190.

84. Lazzarin, R., Gasparella, A. and Longo, G., 1999, "Chemical Dehumidification by Liquid Desiccants: Theory and Experiment", International Journal of Refrigeration, Vol.22, pp. 334 – 346.
85. DTE Energy Technologies Inc., "ENI 75 Installation and Operation Manual".
86. Aringhieri, R., 2003, "Optimal Operations Management and Network Planning of a District Heating System with a Combined Heat and Power Plant", Annals of Operation Research, Vol. 120, pp. 173 – 199.
87. Martin, V. and Goswami, D., 2000, "Effectiveness of heat and mass transfer processes in a packed bed liquid desiccant dehumidifier/regenerator", International Journal of Heating, Ventilating, Air-Conditioning and Refrigerating Research, Vol 6, No.1, pp. 21 – 39.
88. Martin, V. and Goswami, D., 1999, "Heat and mass transfer in packed bed liquid desiccant regenerators - an experimental investigation", ASME Journal on Solar Energy Engineering, Vol.121, No.3, pp. 162 – 170.
89. Jain, S., Dhar, P. and Kaushik, S., 2000, "Optimal Design of Liquid Desiccant Cooling Systems", ASHRAE Transactions, Vol.106, pp. 1 – 8.
90. Cengel, Y. and Boles, M., 1994, "Thermodynamics: An Engineering Approach", McGraw-Hill, Second Edition, pp. 455 – 464.
91. Gandhidasan, P. and Alfarayedhi, A., 1994, "Solar Regeneration of Liquid Desiccants suitable for Humid Climates", Energy, Vol.19, pp. 831 – 836.

92. Chung, W., Ghosh, K. and Hines, L., 1993, "Dehumidification of air by aqueous lithium-chloride in a packed-column", Separation Science and Technology, Vol. 28, pp. 533 – 550.
93. McQuiston, F. and Parker, J., 1988, "Heating, Ventilating and Air Conditioning – Analysis and Design, John Wiley & Sons, Third Edition, pp. 70 – 88.
94. Wilkinson, H., 1991, "Evaporative cooling trade-offs in liquid desiccant systems", ASHRAE Transactions, pp. 642 – 649.
95. Trane, 2004, "Packaged Rooftop Air Conditioners Product Catalog".
96. Griffiths, C., 1987, "Desiccant-based environmental control systems", Proceedings of the 9th World Energy Engineering Congress, Atlanta, GA, USA, pp. 65 – 68.
97. Acker, W., 1999, "Industrial dehumidification: Water vapor load calculations and system descriptions, Journal of Heating, Piping, Air Conditioning, Vol.71, No. 3.
98. Grosso, S., Fowler, E. and Pearce, L., 1980, "Dehydration of natural and industrial gas streams with liquid desiccants", IEE Conference on Development in Drying, pp. 468 – 474.
99. Griffiths, W., 1996, "Enhancing ammonia refrigeration", Engineered Systems, Vol.13, No.8.
100. Anon, 2004, "Precise humidity control", Plant Engineering, Vol.58, No.8, pp. 2 – 4.

101. ASHRAE, 1989, “ASHRAE Handbook of Fundamentals”, Atlanta, Georgia.

102. Holzhauer, R., 1979, “Industrial Dehumidification”, Plant Engineering, Vol.33, No.14, pp. 86 – 93.

103. Taylor, C. and Taylor, E., 1948, “The Internal Combustion Engine”, International Textbook Company, First Edition.

104. Gill, P., Smith, J. and Ziurys, E., 1959, “Fundamentals of Internal Combustion Engines as applied to Reciprocating, Gas Turbine and Jet Propulsion Power Plants”, U.S. Naval Institute, Fourth Edition.

105. Kline, S., and McClintock, F., 1959, “Describing Uncertainties in Single-Sample Experiments” Mechanical Engineering.

106. Kinsara, A., Rabghi, O. and Elsayed, M., 1997, “Parametric Study of an Energy Efficient Air Conditioning System Using Liquid Desiccant”, Applied Thermal Engineering, Vol. 18, No. 5, pp. 327 – 335.

107. Fumo, N. and Goswami, D., 2002, “Study of an Aqueous Lithium Chloride Desiccant System: Air Dehumidification and Desiccant Regeneration”, Solar Energy, Vol. 72, No. 4, pp. 351 – 361.

108. Ghaddar, N., Ghali, K. and Najm, A., 2003, “Use of desiccant dehumidification to improve energy utilization in air-conditioning systems in Beirut”, International Journal of Energy Research, Vol. 27, pp. 1317 – 1338.

109. Beckwith, T., Marangoni, R. and Lienhard, J., 1993, “Mechanical Measurements”, Addison-Wesley Publishing Company, Fifth Edition.

110. Petrov, A., Zaltash, A., Labinov, S., Rizy, D., Liao, X. and Radermacher, R., 2004, “Evaluation of Different Efficiency Concepts of an Integrated Energy System (IES)”, Proceedings of 2004 ASME International Mechanical Engineering Congress, Anaheim, California, USA.